

For Reference

NOT TO BE TAKEN FROM THIS ROOM

Ex libris
UNIVERSITATIS
ALBERTAENSIS





Digitized by the Internet Archive
in 2020 with funding from
University of Alberta Libraries

<https://archive.org/details/Rajasekaran1971>

THE UNIVERSITY OF ALBERTA

FINITE ELEMENT ANALYSIS OF THIN-WALLED MEMBERS OF OPEN SECTION

by



S. RAJASEKARAN

A THESIS

SUBMITTED TO THE FACULTY OF GRADUATE STUDIES AND RESEARCH
IN PARTIAL FULFILLMENT OF THE REQUIREMENTS FOR THE DEGREE
OF DOCTOR OF PHILOSOPHY

DEPARTMENT OF CIVIL ENGINEERING

EDMONTON, ALBERTA

FALL, 1971

UNIVERSITY OF ALBERTA

FACULTY OF GRADUATE STUDIES AND RESEARCH

The undersigned certify that they have read, and recommend to the Faculty of Graduate Studies and Research for acceptance, a thesis entitled, "FINITE ELEMENT ANALYSIS OF THIN-WALLED MEMBERS OF OPEN SECTION" submitted by S. RAJASEKARAN in partial fulfillment of the requirements for the degree of DOCTOR OF PHILOSOPHY.

Date. *Sept. 28, 1971*

ABSTRACT

A general approach to the elastic and inelastic analysis of thin-walled members of arbitrary open cross section is presented and a finite element formulation is developed.

Using this formulation, the solution for critical loading as well as nonlinear load deflection response for elastic members is obtained.

Numerical results are presented for simple cases when local and member buckling are coupled.

Inelastic beam-column problems are solved using an iterative incremental technique based on an equilibrium balance, and inelastic buckling problems are solved using a standard eigenvalue solution to evaluate the critical length. Numerical examples are presented and compared with available results.

ACKNOWLEDGEMENTS

The author wishes to express his sincere appreciation to Professor D.W. Murray, supervisor of the study, for his guidance, patience and support throughout the course of the research and his constructive criticism during the preparation of the manuscript.

Helpful suggestions resulting from discussion with Professor P.F. Adams are acknowledged with thanks. In addition the author would like to express his appreciation to Professors R.H. Gallagher, J.S. Kennedy and J. Longworth for serving as members of his thesis committee.

The author gratefully acknowledges the financial support of the University of Alberta for providing the Senior Graduate Fellowship in his final year of graduate study.

The author would like to express his appreciation to the staff members and fellow graduate students who contributed, through their discussions, to the development of this work.

Thanks are also due to staff of the computing center, and to the staff of drafting and printing services, whose cooperation is appreciated.

The author wishes to thank Professor G.R. Damodaran, Director, P.S.G. College of Technology, Coimbatore, India, for providing study leave for his graduate study in Canada.

Mrs. Betty Boon typed the manuscript with great care and patience and her cooperation is appreciated.

TABLE OF CONTENTS

	<u>Page</u>
Title Page	i
Approval Sheet	ii
Abstract	iii
Acknowledgements	iv
Table of Contents	v
List of Tables	ix
List of Figures	x
List of Symbols	xiv
 CHAPTER I INTRODUCTION	 1
1.1 Introductory Remarks	1
1.2 Purpose and Scope	2
1.3 Outline of Contents	3
 CHAPTER II FORMULATION OF ELASTIC BEAM EQUATIONS	 5
2.1 Introduction	5
2.2 Governing Equations Derived from Equilibrium	5
2.3 Governing Equations Derived by Virtual Work	10
2.4 Displacement Equations of Equilibrium	15
2.5 Comparison of Equations	18
2.6 Review of Finite Element Beam Formulations	18
2.7 Finite Element Idealization	20
2.8 Assembly of Finite Element Equations	23
2.9 Summary	26

	<u>Page</u>
CHAPTER III SOLUTION OF ELASTIC BEAMS AND BEAM-COLUMNS	35
3.1 Introduction	35
3.2 Solution of First Order Beam Equations	36
3.3 Elastic Buckling Problems	38
3.4 Solution Methods for Beam-Column Problems	43
3.5 Elastic Beam-Column Response	47
3.6 Summary	49
CHAPTER IV LOCAL BUCKLING OF ELASTIC SECTIONS	70
4.1 Introduction	70
4.2 Assumptions	71
4.3 Equilibrium Equations by Virtual Work	
Including Distortion of the Section	71
4.4 Specialization for Elastic WF Sections	76
4.5 Finite Element Model	78
4.6 Illustrative Solutions	82
4.7 Summary	83
CHAPTER V FORMULATION FOR INELASTIC MEMBERS	94
5.1 Introduction	94
5.2 Formulation of Inelastic Incremental	
Equilibrium Equations	95
5.3 Finite Element Idealization	102
5.4 Transformation and Assembly	104
5.5 Tangent Stiffness Properties	112
5.6 Stress Resultants	112
5.7 Summary	114

CHAPTER VI	SOLUTION FOR INELASTIC MEMBERS	124
6.1	Introduction	124
6.2	Inplane Behaviour of Inelastic Beams	124
6.3	Solutions of Typical In-plane Inelastic Problems	127
6.4	Solution of General Beam-Column Problems	129
6.5	Inelastic Buckling	131
6.6	Solution of Inelastic Buckling Problems	135
6.7	Summary and Conclusions	139
CHAPTER VII	SUMMARY AND CONCLUSIONS	168
List of References		172
APPENDIX A	DETAILS OF ELASTIC FORMULATION	179
A-1	Expressions for Torque and Bimoment	180
A-2	Derivation of Stress Resultants in Terms of Displacements	183
A-3	Residual Stress and Strain	187
A-4	Virtual Work Derivation of Equilibrium Equations	188
A-5	Evaluation of M_p for Elastic Response	192
A-6	Evaluation of Element Flexural and Geometric Stiffness Matrices	193
APPENDIX B	COMPARISON OF ELASTIC FORMULATIONS	201
B-1	Introduction	202
B-2	Formulation of Beam-Column Equations	202
B-3	Nonlinear Analysis of Beam-Columns	206
B-4	Numerical Results	208
B-5	Summary and Conclusion	209

APPENDIX C	DERIVATION OF MATRICES FOR LOCAL BUCKLING	223
APPENDIX D	CALCULATION OF SECTION PROPERTIES AND STRESS RESULTANTS FOR THIN-WALLED SECTIONS	231
D-1	Introduction	232
D-2	Determination of Transformed Section	232
D-3	Evaluation Section Properties	234
D-4	Evaluation of Stress Resultants	239
APPENDIX E	DETAILS OF INELASTIC FORMULATION	245
E-1	Introduction	246
E-2	Derivation of Tangent Stiffness and Geometric Stiffness Matrices 'Formulation 1'	246
E-3	Derivation of Tangent Stiffness and Geometric Stiffness Matrices 'Formulation 2'	251

LIST OF TABLES

	<u>Page</u>
TABLE 2-1 Transformation Matrix	27
TABLE 3-1 Comparison of Finite Element Analysis with Timoshenko	50
TABLE 3-2 Torsional Buckling of Symmetrical I-Beam	51
TABLE 3-3 Comparison of Finite Element Analysis with Reported Results	52
TABLE 4-1 Solutions for Uncoupled Local Buckling	85
TABLE 5-1 Transformation Matrix	116
TABLE 6-1 Birnstiel's Procedure for Solution of H-Columns Under Biaxial Bending	141
TABLE 6-2 Algorithm for Determining Inelastic Critical Lengths	142
TABLE 6-3a Particulars of Beam-Column Problems	145
TABLE 6-3b Particulars of Buckling Problems	146
TABLE 6-3c Nomenclature for Loading	147
TABLE A-1 Boundary Conditions	198
TABLE A-2 Coefficient Matrices	199
TABLE B-1 Linear Incremental Formulation	211
TABLE B-2 Comparison of Beam-Column Solution by Virtual Work and Potential Energy Approaches	214
TABLE C-1, C-2	
C-3 and C-4 Matrices for Local and Member Buckling Coupled Analysis	227 228 229 230

LIST OF FIGURES

<u>Figure</u>		<u>Page</u>
2.1	CROSS SECTION OF A THIN-WALLED BEAM	28
2.2	THIN-WALLED BEAM OF OPEN SECTION-A GENERAL SYSTEM OF LOADS IN A TYPICAL BEAM SEGMENT	28
2.3a	DISPLACEMENT OF A FIBRE DURING DEFORMATION	29
2.3b	PROJECTIONS OF A DEFORMED BAR ON YZ&XZ PLANE	29
2.3c	INTERNAL FORCES INDUCED DUE TO SHEARING DEFORMATION	30
2.3d	INPLANE FORCES INDUCED BY NORMAL AND SHEARING STRESSES	30
2.4	ADDITIONAL TORSIONAL MOMENT INDUCED DUE TO SHEAR STRESSES DURING DEFORMATION	31
2.5	STRESS STRAIN AND DISPLACEMENT NOMENCLATURE IN INITIAL AND INCREMENTED CONFIGURATION	32
2.6	REFERENCE AXES, NODAL DISPLACEMENTS AND STRESS RESULTANTS	33
2.7	THIN-WALLED BEAM WITH RESPECT TO LOCAL AND GLOBAL ORIENTATION	34
3.1	NON-UNIFORM TORSION OF WF BEAM	54
3.2	MOMENT OF RESISTANCE BY ST. VENANT AND WARPING SHEAR	55
3.3	NON-UNIFORM TORSION - COMPARISON WITH DIFFERENT ELEMENTS	56
3.4	CONVERGENCE CHARACTERISTICS	57
3.5	NON-UNIFORM TORSION OF TAPERED BEAMS	58
3.6	NOMENCLATURE FOR SUPPORT CONDITION AND BUCKLING MODE	59
3.7	LATERAL BUCKLING OF A BEAM WHEN LOAD IS ACTING AT d ' y FROM SHEAR-CENTER	60
3.8	COLUMNS SUPPORTED Laterally BY SIDE RAILS	61
3.9	ELASTIC BUCKLING OF UNSYMMETRICAL SECTION	62
3.10	BUCKLING OF TAPERED BEAM-COLUMN	63
3.11	INFLUENCE BUCKLING SURFACE FOR WIDE FLANGE BEAM	64

<u>Figure</u>		<u>Page</u>
3.12a	A NEWTON-RAPHSON METHOD	65
3.12b	MODIFIED NEWTON-RAPHSON METHOD	65
3.13	COLUMN WITH INITIAL IMPERFECTION	66
3.14	LOAD DEFLECTION RESPONSE OF AN INITIALLY IMPERFECT COLUMN	67
3.15	BEAM WITH INITIAL IMPERFECTION-UNIFORM MOMENT	68
3.16	COLUMN WITH SINUSOIDAL IMPERFECTION	69
4.1	LOCAL PLATE CO-ORDINATE DIRECTIONS	86
4.2	LOCAL COORDINATE SYSTEM FOR PLATE DEFORMATIONS	87
4.3	DEFLECTED SHAPE OF THE I-SECTION DUE TO UNIT VALUE OF THE GENERALIZED DISPLACEMENT	88
4.4	GENERAL NOTATIONS	89
4.5	LOCAL BUCKLING OF COLUMNS SUBJECTED TO AXIAL LOAD	90
4.6	COLUMN/LOCAL BUCKLING INTERACTION	91
4.7	INTERACTION OF LATERAL AND LOCAL BUCKLING	92
4.8	PLATE ELEMENTS WITH 18 DEGREES OF FREEDOM AT EACH NODE OF THE BEAM ELEMENT	93
5.1	ISOLATED BEAM-COLUMN	118
5.2	CROSS SECTION OF THE COLUMN IN DISPLACED POSITION	119
5.3	CO-ORDINATE TRANSFORMATION	120
5.4	TRANSFORMED SECTION AXES, DISPLACEMENTS AND STRESS RESULTANT INCREMENTS	121
5.5	ELEMENT NODAL PARAMETERS	122
5.6	TRANSFORMATION FOR STRESS RESULTANTS	123
6.1	LOAD VS END DEFLECTION PLOT	148
6.2	MOMENT VS CURVATURE RELATIONSHIP	149
6.3	LOAD VS END DEFLECTION PLOT FOR WF BEAM-COLUMN	150
6.4	MOMENT VS END ROTATION	151

<u>Figure</u>		<u>Page</u>
6.5	MOMENT VS END ROTATION	152
6.6	TORQUE TWIST RELATIONSHIP FOR AN INELASTIC BEAM-COLUMN	153
6.7	LOAD VS MID-SPAN DISPLACEMENTS	154
6.8	MOMENT VS IN AND OUT OF PLANE RESPONSE	155
6.9a	CROSS-SECTION PROPERTIES OF A DOUBLE ANGLE SECTION	156
6.9b	INELASTIC BUCKLING OF DOUBLE ANGLE STRUT	157
6.10a	HAT SECTION (L OF 33)	158
6.10b	NORMALIZED WARPING COORDINATE	158
6.10c	RESIDUAL STRESS DISTRIBUTION	158
6.11	INELASTIC BUCKLING OF A COLUMN (HAT SECTION)	159
6.12	INELASTIC LATERAL BUCKLING OF A WIDE FLANGE BEAM (UNIFORM MOMENT)	160
6.13	INELASTIC LATERAL BUCKLING OF A BEAM (DOUBLE ANGLE SECTION - UNIFORM MOMENT)	161
6.14	INELASTIC LATERAL TORSIONAL BUCKLING OF A BEAM (ANGLE SECTION - UNIFORM MOMENT)	162
6.15	INELASTIC LATERAL-TORSIONAL BUCKLING OF A BEAM OF UN- SYMMETRICAL SECTION (UNIFORM MOMENT)	163
6.16	INELASTIC LATERAL TORSIONAL BUCKLING OF A WIDE-FLANGE BEAM-COLUMN (AXIAL LOAD AND EQUAL ECCENTRICITY)	164
6.17	INELASTIC LATERAL TORSIONAL BUCKLING OF A BEAM-COLUMN WITH MOMENT GRADIENT	165
6.18	INELASTIC LATERAL BUCKLING OF WIDE FLANGE BEAM (CENTRAL LOAD)	166
6.19	INELASTIC BUCKLING OF BIAXIAL BENDING WITH AXIAL LOAD	167
A.1	SHEAR STRESSES IN A THIN-WALLED BEAM	200
B.1	FLEXURAL STIFFNESS (GENERALIZED COORDINATES)	215

<u>Figure</u>		<u>Page</u>
B.2	FIRST ORDER INITIAL DISPLACEMENT MATRIX	216
B.3	SECONDDORDER INITIAL DISPLACEMENT MATRIX	217
B.4	TRANSFORMATION MATRIX RELATING GENERALIZED COORDINATES TO ELEMENT DISPLACEMENTS	218
B.5	FLOW CHART EXPLAINING THE SOLUTION SCHEME FOR BEAM- COLUMN PROBLEMS	219
B.6	EFFECT OF INCREMENTAL MATRICES IN SMALL DISPLACEMENT RANGE	220
B.7	EFFECT OF INCREMENTAL MATRICES IN LARGE DISPLACEMENT RANGE	221
B.8	PRE AND POST BUCKLING BEHAVIOUR OF BEAM-COLUMN	222
D.1a	TRI-LINEAR STRESS-STRAIN DIAGRAM	241
D.1b	ACTUAL RESIDUAL STRAIN DISTRIBUTION	241
D.1c	ASSUMED RESIDUAL STRAIN DISTRIBUTION	241
D.2	TRANSFORMED SECTION OF A PLATE SEGMENT	242
D.3a	ELASTIC SECTION	243
D.3b	ARBITRARY TRANSFORMED SECTION	243
D.3c	REFERENCE POINTS OF ELASTIC AND TRANSFORMED SECTION	243
D.4	TYPICAL REGION	244
D.5	STRESSES IN A TYPICAL PLATE SEGMENT	244

LIST OF SYMBOLS

In this dissertation, the notation generally corresponds with the notation commonly encountered in texts. All symbols are defined where they first appear in the text. However, in certain cases, it has not been possible to maintain uniform symbology throughout.

$\langle \rangle$	row vector
$\{ \}$	column vector
$[]$	matrix
$\ \quad \ $	determinant
u	continuous variable
\underline{u}	nodal vector
$u' = \frac{du}{dz}$	differentiation with respect to z
$u_{,y} = \partial u / \partial y$	partial differentiation u with respect to y
<u>Variables</u>	
A	area of the cross section; point on the contour of thin-walled section (see Fig. 2.1)
A_w	area of the web
A^T	transformed area
b_f	breadth of the flange
B	length of the smaller leg for angle section (Fig. 6.14); sectorial centroid of elastic section (Fig. D.3a)
b	plate segment length
B'	sectorial centroid of inelastic section (Fig. D.3c)

b_x, b_y	coordinates of the instantaneous shear centre with respect to reference axis passing through 'C'
C	arbitrary point on the cross section (Fig. 2.1) (in special cases, C, refers to centroid)
\bar{C}	instantaneous centroid (Fig. D.3b)
C_x, C_y, C_w	properties of the cross section defined in Equation A-53
d_x, d_y	x and y distances of the load point from shear center
d_w	depth of the web
$D = Et^3/12(1 - \nu^2)$	flexural rigidity of the plate
e_x, e_y	coordinates of point S with reference to coordinate axes through C (Fig. 2.1)
\bar{e}_{ij}, E_{ij}	Green's strain tensors in initial and deformed configuration (Fig. 2.5)
e_{ij}	increment in the quantity of strain tensor
E, E_p, E_s	Young's modulus, plastic modulus and strain hardening modulus respectively (Fig. D.1a)
e_ξ, e_η	coordinates of the instantaneous shear center with respect to instantaneous centroid in the principal directions (Fig. 5.3)
f_1, f_2, f_3	linear, quadratic and cubic interpolation functions, respectively
$[g_{uu}] \dots [g_{\phi\phi}]$	submatrices defined in Equation A-57

$[g_{\ell\ell}]$	element geometric stiffness matrix associated with local buckling (Equation 4-23b)
$[g_{u\ell}] \dots [g_{\ell\phi}]$	submatrices which couples the local and beam buckling (Equation 4-23b)
$[G_t], [G_b]$	submatrices defined in Appendix D
G	shear modulus
H_x, H_y, H_w	properties of the section defined in Equation A-53
I_x, I_y	moment of inertia of the reference axes x, y passing through 'C'
I_{x_w}	moment of inertia of the web about x -axis
$I_\omega = \int_A \bar{\omega}_n^2 dA$	principal sectorial moment of inertia
I_ξ, I_η	principal moments of inertia about ξ and η axes passing through \bar{C}
$I_p = I_x + I_y + A(e_x^2 + e_y^2)$	polar moment of inertia about S
$K = \Sigma bt^3/3$	St. Venant's constant
$[k_{uu}] \dots [k_{\phi\phi}]$	submatrices defined in Equation A-57
$[k_S], [k_S^T], [k_G]$	element flexural stiffness, tangent stiffness and geometric stiffness matrices respectively
$[K_S], [K_S^T], [K_G]$	flexural stiffness, tangent stiffness and geometric stiffness matrices respectively
$[\bar{K}_G]$	'initial stress' stiffness matrix corresponding to some nominal stress distribution
k	plate segment index

$$K_1 = \sigma_c b_1^2 t_1 / \pi^2 D$$

$$[k_{\ell\ell}]$$

$$[k_{st}^{mnj}]$$

$$\ell$$

$$L$$

$$\{\underline{\ell}\}$$

$$M_x, M_y, M_\xi, M_\eta$$

$$M_{cr}$$

$$M_t$$

$$M_o$$

$$M_\omega$$

$$M_Y$$

$$m_t$$

$$M_{pc}$$

$$M_\rho = \int_A \sigma_z \rho^2 dA$$

$$M_\alpha, M_\beta \text{ and } M_{\alpha\beta}$$

$$M_{\rho\bar{s}} = M_{\rho\zeta}$$

$$[N_1], [N_2]$$

buckling coefficient

element flexural stiffness matrix corresponding to the degrees of freedom associated with local buckling (Equation 4-23a)

coefficient matrices as defined in Equation A-56

element length

length of the member

degrees of freedom associated with local buckling

moments about respective axes (Fig. 5.6)

critical moment

torsional moment

applied moment

warping torque

yield moment

distributed torque

reduced plastic moment due to presence of axial load

a stress resultant evaluated with respect to S

moments about corresponding coordinate directions of the plate

stress resultant evaluated with respect to \bar{S}

Marcal's first and second order initial displacement matrices

P_Y	yield load
P	axial load; and arbitrary point P as shown in Fig. 5.1
p	nodal number
P_{cr}	critical load
p_x, p_y	distributed loads
$\overline{p}_x, \overline{p}_y$	change in transverse forces
q	nodal number; and distributed loads
Q	length of the longer leg of angle section (Fig. 6.14); and lateral load
r_n, r	projection of ρ on the tangent and perpendicular to the tangent at point A on the contour of the thin-walled beam (Fig. 2.1)
r	plate region index
r_x, r_y	radii of gyration about x and y axes respectively
$\{r_E\}, \{R_E\}$	element displacements and forces respectively
$\{r_o\}$	initial imperfection
$\{\Delta r\}, \{\Delta R\}$	increments in nodal displacements and forces respectively
s	arbitrary point of the cross section (Fig. 2.1) (for special case refers to shear center); and surface area
s_{ij}	Kirchhoff's stress tensor in the deformed configuration
\overline{s}	instantaneous shear center (Fig. D.3b)

$S_{\omega}, S_{\omega x}, S_{\omega y}$	sectorial static moment, linear sectorial static moments about x and y axes respectively
$S_{\omega}^T, S_{\omega x}^T, S_{\omega y}^T$	tangent properties
\bar{t}_i, T_i	surface loads in initial and deformed configuration (Fig. 2.5)
t_i	increments in surface loads
$T_{sv} = GK\phi'$	St. Venant torque
t	thickness of the plate
$[T]$	transformation matrix
u_s, v_s	displacements of point S in the reference directions
\bar{u}_i, U_i	displacements in the initial and displaced configuration respectively (Fig. 2.5)
u_i	increment in displacement quantity
U	strain energy
U, V	global displacements
u^B, u^P	beam and plate displacements respectively
u_w^P	displacement of the web in x-direction (Fig. 4.2)
u_{ξ}, v_{η}	increments in displacements of the instantaneous shear center in the principal axes directions
\hat{u}, \hat{v}	displacements of the instantaneous shear center in the directions parallel to xy reference axes

$\Delta U_s, \Delta V_s$	increments in displacements of the original shear center in the global direction
V_x, V_y	shear stress resultants
v	volume of the element
v_t^p, v_b^p	displacement of the top and bottom flange in y-direction (Fig. 4.2)
$W_\omega = \int_A \sigma_z \bar{\omega}_n dA$	bimoment
W	potential of external loads
w_c	axial displacement (uniform) of C
ΔW_{cm}	increment in axial displacement of the middle node
\bar{x}, \bar{y}	x and y distances instantaneous shear center to original shear center
x_o, y_o	coordinates of the instantaneous centroid in the reference configuration (Fig. 5.3)

α	angle between the tangent at any point on the contour to y-axis (Fig. 2.1); and angle of inclination of principal axes to reference axes (Fig. 5.3)
$\beta = z/\ell$	dimensionless parameter (Fig. 2.6)
γ_{xz}, γ_{yz}	shear strains
$\Gamma, \Gamma + \Delta\Gamma$	initial and deformed configuration of the structure (Fig. 2.5)
δ	prefixed to other term denotes variations
∂	partial differentiation
ϵ	strain
ϵ_R	residual strain
$\epsilon_y, \epsilon_{st}$	yield and strain hardening strain respectively
ζ	dimensionless parameter; a quantity with this as a subscript indicates that the quantity is dependent on z
η	denotes tangential direction at point A (Fig. 2.1); and dimensionless parameter as defined in Chapter IV Equation 4-16
θ_x, θ_y	rotations about x and y axes respectively
λ	critical load or critical length parameter
ξ	dimensionless parameter as defined in Equation 4-16; and normal direction to the thin wall (Equation 2-1)
ρ	distance between a point on a cross section and the shear center (Fig. 2.1)
$\sigma_z, \sigma_{zy}, \sigma_{zx}$	normal and shear stresses respectively

$\sigma_{z\eta}$	tangential stress in the ' η ' direction
$\bar{\sigma}_{ij}$	Kirchhoff's stress tensor in configuration Γ
σ_{ij}	increment in stress tensor
σ_R	residual stress
σ_{cr}	critical stress
$\sigma_{ij}^B \quad \sigma_{ij}^P$	stresses due to beam and plate action respectively
σ_{rc}	residual stress in compression
Φ	angle of twist
ϕ	increment in twist
$\bar{\omega}_{SB}$	warping coordinate with B as origin of the contour and S as the pole
$\bar{\omega}_n$	normalized unit warping
κ	ratio of St. Venant torsional rigidity to warping rigidity
$\chi_\alpha \chi_\beta \chi_{\alpha\beta}$	curvatures of the plate middle surface in α and β local plate coordinate direction
ν	Poisson's ratio

CHAPTER I

INTRODUCTION

1.1 Introductory Remarks

Thin-walled beams occupy an important place in the field of modern structural engineering. Rolled, welded or rivetted metallic beams, columns, girders and elements of frames, are examples of thin-walled members. In addition, many spatial engineering structures, such as shear wall structures, have such proportions that they can be considered as thin-walled structures.

The use of cold-formed structural members is increasing, and hence the range of loading for which elastic analysis is applicable is also increasing. The stability of such structures has been the subject of many investigations and the study of stability analysis is an important aspect of design since it predicts an upperbound for the ultimate carrying capacity of the member. The general approach to such problems has been to formulate a set of equations for the specific problem under consideration. In some cases the design criteria is based on deflection limitations and hence this aspect of analysis should not be overlooked.

Thin-walled beam theory is based on the assumption that the cross section does not distort. However, in some cases, failure can be initiated by local buckling which involves distortion of the cross section. Hence it is necessary to design such members so that, at design load, adequate safety exists against failure by local buckling.

The problem becomes more complex when nonlinear material or geometry is considered. A three dimensional structure is often analyzed as a collection of two dimensional planar structures. While

this idealization has usually resulted in safe design, it does not necessarily represent the best model for the analysis of such structures. To the author's knowledge no general study of the inelastic behaviour of beam-columns is available. Today, many structures are designed by plastic design methods and each member must undergo considerable inelastic deformation in order for the whole frame to develop its full strength. These inelastic deformations may cause premature failure by various types of instability. Hence there is a need to study inelastic instability.

Although the general differential equations for thin-walled beams (68,74) are valid for complex geometry, loading and boundary conditions, the complexity of these equations is such that only a few problems have been solved using classical mathematics. More general approaches consist of approximating the differential equations using the finite difference technique, (26), or solving the equations by direct numerical integration (68). Even these methods offer only a partial improvement over classical methods of solution. On the other hand, the development of a general treatment by finite element method is encouraging and has resulted in a number of successful applications (7,8).

1.2 Purpose and Scope

The objectives of this investigation are:

- 1) to develop a general set of beam equations which are applicable to both elastic and inelastic analysis and adaptable to finite element analysis;
- 2) to develop general computational procedures for the finite element analysis of elastic and inelastic members, which are applicable to

stability problems; and,

3) to investigate the effect of distortion of the cross-section on the member buckling strength for some simple cases.

1.3 Outline of Contents

Beam equilibrium equations, in both total and incremental form, and without any assumptions relating stress resultants to deformations, are derived in two ways in Chapter 2. By specializing to elastic response the equations are shown to be equivalent to Vlasov's equations (74). A finite element model is then developed for the elastic case. Details of derivations of equations are contained in Appendix A. A comparison of nonlinear terms in the potential energy and virtual work formulations is carried out in Appendix B where the range of applicability of the derived equations is investigated.

In Chapter 3, solution techniques to solve small-deflection, beam-column, and bifurcation problems, using the elastic finite element equations of Chapter 2, are discussed. Numerical results for a variety of problems are compared with those obtained from classical solutions.

Chapter 4 introduces distortion of the cross-section and formulates the equilibrium equations, in general terms, in which local and member buckling effects are coupled. A finite element approximation to these equations is derived for the special case of elastic wide flange sections. Numerical results for a variety of local buckling problems in wide-flange sections are compared with available solutions in the literature. The coupling between local and member buckling is also investigated. Details of the derivation of the matrices required in this type of analysis are provided in Appendix C.

The extension of the formulation of the equation of Chapter 2 to the case of inelastic response, is carried out in Chapter 5. The finite element equations are formulated with respect to two different systems of local reference axes, and assembly of the 'tangent' stiffness and geometric stiffness matrices with respect to reference axes through the original centroid and shear center of the elastic section is discussed. Detailed derivations of the relevant section properties, stress resultants, submatrices and transformation matrices are contained in Appendices D and E.

Chapter 6 illustrates the application of the equations derived in Chapter 5, to the solution of inelastic small-deflection, beam-column and bifurcation problems. A short summary and discussion is contained in Chapter 7.

CHAPTER II

FORMULATION OF ELASTIC BEAM EQUATIONS

2.1 Introduction

This chapter treats the formulation of the governing equations for a thin-walled member of open cross-section by two approaches. A set of differential equations, identical with those of Vlasov (74), are derived from equilibrium considerations. It is then shown that the same set of equations may be derived from virtual work. A finite element formulation, for elastic members, is derived from the virtual work equations.

Original studies of the flexural buckling of compressed bars were made by Euler in the eighteenth century. Derivations of fundamental differential equations are associated with the names of Chwalla (9), Goodier (28), Kappus (9), Timoshenko (68), Vlasov (74), and others. Djanelidze (18) derived the governing equations for thin-walled sections by the energy method. The early studies of torsional and flexural buckling have been described by Bleich (13).

2.2 Governing Equations Derived From Equilibrium

A thin-walled open cross section is shown in Fig. 2.1. Let point 'C' be an arbitrary origin of coordinates and point 'S', whose coordinates are (e_x, e_y) , be an arbitrary reference point. Let the transverse load and support reactions pass through the 'S-axis', as shown in Fig. 2.2.

Define the following stress resultants

$$P = \int_A \sigma_z dA \quad (2-1a)$$

$$M_x = \int_A \sigma_z y dA \quad (2-1b)$$

$$M_y = \int_A \sigma_z x dA \quad (2-1c)$$

$$V_x = \int_A \sigma_{zx} dA \quad (2-1d)$$

$$V_y = \int_A \sigma_{zy} dA \quad (2-1e)$$

$$M_t = \int_A \{ \sigma_{zy} (x - e_x) - \sigma_{zx} (y - e_y) \} dA \quad (2-1f)$$

where σ_z , σ_{zx} , σ_{zy} are components of the stress tensor acting on the cross section, and A is the area of the section.

If the effect of displacements on the equilibrium equations is neglected the normal small deflection equilibrium equations result from a consideration of the equilibrium of an infinitesimal length of the beam (26), (Fig. 2.2), and are

$$M_x'' + p_y = 0 \quad (2-2a)$$

$$M_y'' + p_x = 0 \quad (2-2b)$$

$$M_t' + m_t = 0 \quad (2-2c)$$

where (') indicates differentiation with respect to z ; M_t is the torque about the S axis; and p_y , p_x and m_t are distributed loads and torques applied to the beam (Fig. 2.2). These equations represent the sum of the forces in the x and y directions and the moment about the S axis, respectively, for an infinitesimal length of beam. However, if the effect of displacements on the equilibrium equations is to be considered, Equations 2-2 are inadequate and it is necessary to include the effects of the change in orientation and location of the stresses acting on the cross-section in the summations.

Let u_s , v_s denote the displacements of the axis passing through S in the x and y directions, respectively; w_c denote the (uniform) axial displacement of point C (see Fig. 2.1); and ϕ denote the angle of twist.

It is now necessary to make some of the assumptions normally associated with the behaviour of thin-walled beams, (74), namely

- 1) Because of the bending and torsional flexibility of thin-walled open sections, the relative effect of shearing strain along the mid-surface of the plate is extremely small and can be neglected.
- 2) The shape of the projected cross-section is unaltered during deformation.

Consider now a longitudinal fibre of length Δz and area ΔA with its center at an arbitrary point A on the midsurface contour (Fig. 2.1). On the application of loads, the fibre displaces u_A , and v_A as shown in Fig. 2.3a. When it reaches an equilibrium configuration, it has developed a force of $\sigma_z \Delta A$ which acts along the deformed axis of the fibre. Let \bar{p}_x and \bar{p}_y denote the total change in transverse force per unit of length resulting from the projection of the normal and

shearing stresses due to the deformation. Assuming the section is thin so that shearing stresses act in the direction of the contour, these changes may be evaluated from Figs. 2.3b and 2.3c, which result in the rates of change shown in Fig. 2.3d. Summing over the cross-section yields

$$\bar{p}_y \Delta z = \int_A \left\{ \frac{\partial}{\partial z} \left(\sigma_z \frac{\partial v_A}{\partial z} \right) \Delta A - \int_A \frac{\partial}{\partial z} (\sigma_{z\eta} \phi) \Delta A \sin \alpha \right\} dz \quad (2-3a)$$

$$\bar{p}_x \Delta z = \int_A \left\{ \frac{\partial}{\partial z} \left(\sigma_z \frac{\partial u_A}{\partial z} \right) \Delta A - \int_A \frac{\partial}{\partial z} (\sigma_{z\eta} \phi) \Delta A \cos \alpha \right\} dz \quad (2-3b)$$

The change in torsional moment about S resulting from these deformations, may be evaluated from Figs. 2.3d and 2.4, as

$$\begin{aligned} \bar{m}_t \Delta z = & \left[\int_A \left\{ \frac{\partial}{\partial z} \left(\sigma_z \frac{\partial v_A}{\partial z} \right) - \frac{\partial}{\partial z} (\sigma_{z\eta} \phi) \sin \alpha \right\} (x - e_x) \Delta A \right. \\ & - \int_A \left\{ \frac{\partial}{\partial z} \left(\sigma_z \frac{\partial u_A}{\partial z} \right) - \frac{\partial}{\partial z} (\sigma_{z\eta} \phi) \cos \alpha \right\} (y - e_y) \Delta A \\ & \left. + \int_A \left\{ \frac{\partial}{\partial z} (\sigma_{zy} u_A) - \frac{\partial}{\partial z} (\sigma_{zx} v_A) \right\} \Delta A \right] \Delta z \end{aligned} \quad (2-3c)$$

Expressing the previously stated assumption for the direction of the shearing stress, as

$$\sigma_{zy} = \sigma_{z\eta} \cos \alpha \quad (2-4a)$$

$$\sigma_{zx} = -\sigma_{z\eta} \sin \alpha \quad (2-4b)$$

; expressing u_A and v_A by the kinematic relationships (Fig. 2.1)

$$v_A = v_s + (x - e_x)\phi \quad (2-5a)$$

$$u_A = u_s - (y - e_y)\phi \quad (2-5b)$$

; and carrying out the integration in Equations 2-3, yields

$$\bar{p}_x = (P u'_s)' + (P e_y \phi')' - (M_x \phi)'' \quad (2-6a)$$

$$\bar{p}_y = (P v'_s)' - (P e_x \phi')' + (M_y \phi)'' \quad (2-6b)$$

$$\begin{aligned} \bar{m}_t = & (M_y v'_s)' - (P e_x v'_s)' - (M_x u'_s)' + (P e_y u'_s)' \\ & + (M_\rho \phi')' - (V_x v_s)' + (V_y u_s)' \end{aligned} \quad (2-6c)$$

where it has been necessary to define the additional stress resultant

$$M_\rho = \int_A \sigma_z \{ (x - e_x)^2 + (y - e_y)^2 \} \Delta A \quad (2-7)$$

Augmenting Equations 2-2 by the effective changes in distributed forces expressed in Equations 2-6, yields the equilibrium equations including the effects of member displacements, as

$$M_x'' + (P v_s')' + (M_y \phi)'' - (P e_x \phi')' + p_y = 0 \quad (2-8a)$$

$$M_y'' + (P u_s')' - (M_x \phi)'' + (P e_y \phi')' + p_x = 0 \quad (2-8b)$$

$$\begin{aligned} M_t' + (M_y v_s')' - (P e_x v_s')' - (M_x u_s')' + (P e_y u_s')' \\ + (M_\rho \phi')' - (V_x v_s)' + (V_y u_s)' + m_t = 0 \end{aligned} \quad (2-8c)$$

It should be noted that Equations 2-8 are valid for arbitrary location of the reference points C and S and that it has been unnecessary to specify the distribution of σ_z and $\sigma_{z\eta}$.

2.3 Governing Equations Derived By Virtual Work

In this section incremental equilibrium equations and an incremental stiffness formulation are developed using the principle of virtual work. The principle of virtual work is selected since it is less restrictive than a potential energy formulation and the total and incremental equilibrium equations developed by this principle are valid for both elastic and inelastic members. Rectangular cartesian coordinates and the principle of virtual displacements are used throughout.

Referring to Fig. 2.5, let Γ represent the deformed equilibrium configuration (the initial configuration) of the structure under the surface loads \bar{T}_i , and $\Gamma + \Delta\Gamma$ represent the deformed equilibrium configuration under the loads T_i . Let $\bar{\sigma}_{ij}$, \bar{e}_{ij} , and \bar{u}_i be Kirchhoff's tensor, Green's strain tensor, and the displacements respectively in configuration Γ ; and S_{ij} , E_{ij} and U_i be Kirchhoff's stress tensor, Green's strain tensor and the displacements in configuration $\Gamma + \Delta\Gamma$.

Green's strain tensor in the equilibrium configurations Γ and $\Gamma + \Delta\Gamma$ are given by,

$$2 \bar{e}_{ij} = \bar{u}_{i,j} + \bar{u}_{j,i} + \bar{u}_{k,i} \bar{u}_{k,j} \quad (2-9a)$$

$$2 E_{ij} = U_{i,j} + U_{j,i} + U_{k,i} U_{k,j} \quad (2-9b)$$

Let

$$S_{ij} = \bar{\sigma}_{ij} + \sigma_{ij} \quad (2-10a)$$

$$E_{ij} = \bar{e}_{ij} + e_{ij} \quad (2-10b)$$

$$U_i = \bar{u}_i + u_i \quad (2-10c)$$

$$T_i = \bar{t}_i + t_i \quad (2-10d)$$

where σ_{ij} , e_{ij} , u_i , and t_i are increments in the corresponding quantities going from configuration Γ to $\Gamma + \Delta\Gamma$.

Applying the principle of virtual displacements in position $\Gamma + \Delta\Gamma$, and regarding the displacement increments u_i as variables, yields

$$\int_V S_{ij} \delta(E_{ij}) dV = \int_S T_i \delta U_i dS + \int_V F_i \delta U_i dV \quad (2-11)$$

Substituting for S_{ij} and E_{ij} Equation 2-11 becomes,

$$\begin{aligned}
\frac{1}{2} \int_V (\bar{\sigma}_{ij} + \sigma_{ij}) (\delta u_{i,j} + \delta u_{j,i} + u_{k,i} \delta u_{k,j} + u_{k,j} \delta u_{k,i} \\
+ \bar{u}_{k,i} \delta u_{k,j} + \bar{u}_{k,j} \delta u_{k,i}) dV = \int_S (t_i + \bar{t}_i) \delta u_i dS \\
+ \int_V F_i \delta u_i dV
\end{aligned} \tag{2-12}$$

The equilibrium equation in configuration Γ ; which may be obtained by letting $\sigma_{ij} = 0$, $t_i = 0$, and $u_i = 0$, is

$$\begin{aligned}
\frac{1}{2} \int_V \bar{\sigma}_{ij} (\delta u_{i,j} + \delta u_{j,i} + \bar{u}_{k,i} \delta u_{k,j} + \bar{u}_{k,j} \delta u_{k,i}) dV = \\
\int_S \bar{t}_i \delta u_i dS + \int_V F_i \delta u_i dV
\end{aligned} \tag{2-13}$$

The incremental equilibrium equation can be obtained, using Biot's (10) procedure, by finding the difference between the equilibrium equations for positions $\Gamma + \Delta\Gamma$ and Γ . Subtracting Equation 2-13 from Equation 2-12 the incremental equation for position $\Gamma + \Delta\Gamma$ is

$$\begin{aligned}
\frac{1}{2} \int_V \bar{\sigma}_{ij} \delta(u_{k,i} u_{k,j}) dV + \frac{1}{2} \int_V \sigma_{ij} \delta(u_{i,j} + u_{j,i} + u_{k,i} u_{k,j}) dV \\
+ \frac{1}{2} \int_V \sigma_{ij} \delta(\bar{u}_{k,i} u_{k,j} + \bar{u}_{k,j} u_{k,i}) dV = \int_S t_i \delta u_i dS
\end{aligned} \tag{2-14}$$

The first term in Equation 2-14 represents the work of the "initial stress" state during the virtual variations of increments in displacement gradients and is of the same order of magnitude as the second term. This gives rise to the "initial stress" or "geometric"

stiffness. The second term represents the work of the increments in the stress state during virtual variations of increments in strain. This gives rise to the normal "flexural stiffness". The third term arises because of the presence of the initial displacement gradient terms in the virtual variation of increments in strain. This gives rise to Marcal's (44) so-called "initial displacement" matrix (see Appendix B). The term on the right hand side represents the work done by the increments in the external loading on the virtual variation of displacement increments.

Equation 2-11 represents the final total equilibrium equations. In the following development Equation 2-11 will be written, for simplicity of notation, by replacing U_i with u_i , S_{ij} with σ_{ij} and T_i with t_i , Equation 2-11 then becomes

$$\begin{aligned} \frac{1}{2} \int_V \sigma_{ij} \delta(u_{i,j} + u_{j,i} + u_{k,i} u_{k,j}) dV &= \int_S t_i \delta u_i dS \\ &+ \int_V f_i \delta u_i dV \end{aligned} \quad (2-15)$$

However, the reader must now clearly distinguish between the symbology of Equation 2-15, which is in terms of total quantities, and Equation 2-14, which is in terms of incremental quantities. Equation 2-15 will form the basis of the remaining derivations in this section.

Using the symmetry of the stress tensor, Equation 2-15 can be written as

$$\int_V \sigma_{ij} \delta u_{i,j} dV + \frac{1}{2} \int_V \sigma_{ij} \delta(u_{k,i} u_{k,j}) dV = \int_S t_i \delta u_i dS \quad (2-16)$$

where body forces have been neglected.

This equation may be written symbolically as

$$\delta(I_1 + I_2 - I_3) = 0 \quad (2-17)$$

where

$$I_1 = \int_V \sigma_{ij} u_{i,j} dV \quad (2-18a)$$

$$I_2 = \frac{1}{2} \int_V \sigma_{ij} u_{k,i} u_{k,j} dV \quad (2-18b)$$

$$I_3 = \int_S t_i u_i dS \quad (2-18c)$$

For thin-walled beams, the stress tensor is of the form,

$$\sigma_{ij} = \begin{bmatrix} 0 & 0 & \sigma_{xz} \\ 0 & 0 & \sigma_{yz} \\ \sigma_{zx} & \sigma_{zy} & \sigma_z \end{bmatrix} \quad (2-19)$$

where σ_{zx} , σ_{zy} are related to $\sigma_{z\eta}$, by Equations 2-4 (see Fig. 2.1).

Substituting Equation 2-19 for σ_{ij} , and Equation 2-5 for u_i into Equation 2-17; and, applying the variation and integrating by parts; yields the Euler-Lagrange equilibrium equations and the natural and geometric boundary conditions. Details of this procedure are given in Appendix A.

The equilibrium equations are,

$$\frac{dP}{dz} + q_z = 0 \quad (2-20a)$$

$$(M_y)'' - (M_x \phi)'' + (P u_s')' + (P e_y \phi')' + q_x - m_y' = 0 \quad (2-20b)$$

$$(M_x)'' + (M_y \phi)'' + (P v_s')' - (P e_x \phi')' + q_y - m_x' = 0 \quad (2-20c)$$

$$W_\omega'' + M_x u_s'' - M_y v_s'' - (M_\rho \phi')' - (P e_y u_s')' + (P e_x v_s')' - m_t - T_{sv}' = 0 \quad (2-20d)$$

where q_z is the distributed axial load per unit of length; m_x and m_y are distributed couples per unit of length; W_ω is defined as the bimoment (see Appendix A); T_{sv} is defined as St. Venant's torque (see Appendix A); and the other stress resultants have been defined in Section 2-2.

It should be noted that the St. Venant torque, T_{sv} , does not arise entirely naturally from Equation 2-18a, but the virtual work from this effect has been added as described in Appendix A.

Equations 2-20 derived from the virtual work principle, are the same as Equations 2-8, derived from the equilibrium approach, except for minor details in notation. They apply to a thin-walled member regardless of the constitutive relationships and with respect to any pair of reference axes C and S. All the terms in which displacements appear are a result of second order geometric effects. Discarding these terms yields the small deflection beam equations, Equations 2-2.

2.4 Displacement Equations of Equilibrium

The solution of Equations 2-20 for the general statically

indeterminate case is a complex problem. Since stress resultants are themselves dependent upon the deformations, it is necessary to express them in terms of the dependent displacement variables before a solution for displacements can be attempted. If "large" displacements were included the expressions for the stress resultants would themselves include higher order terms. The introduction of these higher order terms adds to the complexity of the problem. Since, for the usual type of instability problem they have negligible effect on beam behaviour (see Appendix B), it is common practice to compute the stress resultants using only first order quantities.

Because a solution for displacements is required, it is always necessary to express at least the first stress resultants in each of Equations 2-20, and T_{sv} in Equation 2-20d, in terms of the displacement variables. The stress resultants in the remaining terms may be expressed either in terms of displacements or evaluated directly from statics. The selection of the technique to be used may depend on the type of problem under investigation but a more efficient numerical solution is obtained when these stress resultants are evaluated from statics, if this is possible.

The first order expressions for stress resultants in terms of displacements are derived in Appendix A and expressed by Equations A-26. These equations uncouple when we choose C as the centroid; S as the shear center; B as a sectorial centroid; and the x and y axes as principal axes of cross section (see Fig. 2.1). Under these conditions Equations A-26 become

$$P = E A w'_c \quad (2-21a)$$

$$M_x = -E I_x v_s'' \quad (2-21b)$$

$$M_y = -E I_y u_s'' \quad (2-21c)$$

$$W_\omega = E I_\omega \phi'' \quad (2-21d)$$

where I_x , I_y and I_ω are the principal moments of inertia, and the sectorial moment of inertia, respectively.

Equation 2-16, which is the variational equivalent of Equations 2-20, may then be written for elastic case, by substituting Equations 2-21 into Equation A-49, which yields the specialized equilibrium equation

$$\begin{aligned} \int_0^L \left[E A w_c' \delta w_c' + E I_x v_s'' \delta v_s'' + E I_y u_s'' \delta u_s'' + E I_\omega \phi'' \delta \phi'' + V_x \phi \delta v_s' \right. \\ \left. + V_x v_s' \delta \phi - V_y \phi \delta u_s' - V_y u_s' \delta \phi + P u_s' \delta u_s' + P v_s' \delta v_s' \right. \\ \left. + P e_y u_s' \delta \phi' + P e_y \phi' \delta u_s' - P e_x v_s' \delta \phi' - P e_x \phi' \delta v_s' \right. \\ \left. - M_x u_s' \delta \phi' + M_y v_s' \delta \phi' - M_x \phi' \delta u_s' + M_y \phi' \delta v_s' \right. \\ \left. + \{P I_p/A + M_x C_x + M_y C_y + W_\omega C_\omega + \left(\int_A \sigma_R \rho^2 dA \right) \} \phi' \delta \phi' + GK \phi' \delta \phi' \right. \\ \left. - (q_x \delta u_s + q_y \delta v_s + q_z \delta w_c + m_t \delta \phi + m_x \delta v_s' + m_y \delta u_s' + q_x d_y \delta \phi \right. \\ \left. - q_y d_x \delta \phi + q_x d_x \phi \delta \phi - q_y d_y \phi \delta \phi) \right] dz = 0 \quad (2-22) \end{aligned}$$

The coefficients C_x , C_y , C_ω and I_p are properties of the section, as

derived in Appendix A (Equation A-53), and d_x , d_y are the coordinates of the load axis from the S-axis.

It is emphasized that Equation 2-22 is valid only for linear elastic response where C, is the centroid, S is the shear centre and the axes are the principal axes of the cross section.

2.5 Comparison of Equations

A comparison of the variational Equation 2-22 with the specialized case derived by Bleich (13), reveals that he omitted the terms $(M_{xx} C_x) \phi''$ and $(M'_{xx} C_x) \phi'$. This omission has already been pointed out by Masur and Milbrandt (49). The same terms were omitted by Barsoum and Gallagher (7,8). Substituting Equation 2-21 into Equations 2-20 the equilibrium equations derived in this chapter agree with Timoshenko (68) and Vlasov's (74) equations, except that they have neglected the normal stress due to bimoments in the M_ρ term. Oden (54) omitted the change in the transverse forces and torsional moment resulting from the rotation and translation of shearing stresses (as shown in Fig. 2.3c, 2.3d and 2.4) in his derivation of these equations. If his equations are specialized to principal axes they therefore differ from Vlasov's and those derived in this chapter by the terms arising from these effects. It would be necessary to make numerical comparisons in order to arrive at conclusions regarding the significance of these terms omitted by other authors.

The conceptual difficulty of including all these factors in an equilibrium approach demonstrates the desirability of investigating the formulation from a variational point of view.

2.6 Review of Finite Element Beam Formulations

Turner (72), et al, showed that a 'new class' of stiffness

matrices had to be introduced into the equilibrium equations, when large deflections and stability were to be investigated. They presented the derivation for this stiffness matrix for an axially loaded member. The first published development of beam-column stiffness matrix was by Gallagher (78) and Padlog. Archer (2) also has discussed structural stability and gives an energy expression for the beam-column which is virtually a verbatim restatement of Gallagher. Arghyris (3) showed that, by using a large number of elements to represent a nonuniform column excellent convergence could be achieved for the buckling load, in spite of the fact that his geometric stiffness matrix was inconsistent. Martin (45) arrived at the initial stress stiffness matrices for axial force members and for beam-column problems. He expressed the bending displacement as a cubic polynomial and the axial displacement as a linear function.

Krajcinovic (40) developed a finite element formulation for a thin-walled member based on the use of hyperbolic functions to represent twist. These functions represent the exact displacement field for the stable formulation and yielded excellent results. His formulation cannot account for the effect of moment gradient on lateral buckling. Barsoum (7,8) and Gallagher's formulation is similar to Krajcinovic except that the effect of moment gradient can be accounted for and twist is expressed in terms of a cubic polynomial. They also investigated fifth order Hermitian polynomials and concluded that fifth order polynomials are superior to cubic polynomials in linear stability problems. They recommended the use of lower order displacement functions

for the incremental matrices. They also concluded that the desired accuracy can be achieved by choosing a larger number of elements when dealing with nonlinear problems. In addition, Powell (59) solved the problem of lateral buckling of I-section beams using the elastic and geometric stiffness.

The formulation developed in this dissertation uses cubic polynomials for the displacements u , v , and ϕ ; a linear function for

axial displacements in the case of elastic members with prismatic elements, and a second degree axial displacement function for elastic members with non-prismatic elements and for all inelastic problems. Stiffness matrices are derived for an element with a linear variation of geometric properties. Using this formulation, it is possible to carry out an approximate elastic analysis of tapered thin-walled beams of general cross section subjected to general loading and support conditions. The effect of residual stress is also included in the analysis. The resulting equations, for the elastic case, are similar to those derived by Barsoum and Gallagher (7,8) who used potential energy, rather than virtual work, for their formulation.

2.7 Finite Element Idealization

In the finite element approach the displacements are approximated by forming a linear combination of assumed shape functions, where the parameters are appropriate nodal displacements. Let $\{f_3\}$, $\{f_2\}$, and $\{f_1\}$ represent the cubic, quadratic and linear interpolating functions, respectively. Then we may write the displacements of the reference axes, in any element as

$$u_s = \langle f_3 \rangle \{ \underline{u} \} \quad (2-23a)$$

$$v_s = \langle f_3 \rangle \{ \underline{v} \} \quad (2-23b)$$

$$\phi = \langle f_3 \rangle \{ \underline{\phi} \} \quad (2-23c)$$

$$w_c = \langle f_1 \rangle \{ \underline{w}_c \} \quad (2-23d) \quad \begin{array}{l} \text{for elastic prismatic} \\ \text{elements} \end{array}$$

$$w_c = \langle f_2 \rangle \{ \underline{w}_c \} \quad (2-23e) \quad \begin{array}{l} \text{for elastic non-prismatic} \\ \text{and inelastic element.} \end{array}$$

where u_s, v_s, ϕ, w_c represent continuous displacements and $\{\underline{u}\}$, $\{\underline{v}\}$, $\{\underline{\phi}\}$ and $\{\underline{w}_c\}$ represent the corresponding nodal displacement vectors, as defined in Fig. 2.6. Substituting Equations 2-23 into Equations 2-22, we obtain for one element,

$$\begin{aligned}
& \int_0^l \left[\frac{EA}{\ell} \delta < \underline{w}_c > \{f'_2\} < f'_2 > \{\underline{w}_c\} + \frac{EI}{\ell^3} \delta < \underline{v} > \{f''_3\} < f''_3 > \{\underline{v}\} \right. \\
& + \frac{EI}{\ell^3} \delta < \underline{u} > \{f''_3\} < f''_3 > \{\underline{u}\} + \frac{EI}{\ell^3} \delta < \underline{\phi} > \{f''_3\} < f''_3 > \{\underline{\phi}\} \\
& + \frac{G\bar{k}}{\ell} \delta < \underline{\phi} > \{f'_3\} < f'_3 > \{\underline{\phi}\} + \frac{P}{\ell} \delta < \underline{u} > \{f'_3\} < f'_3 > \{\underline{u}\} \\
& + \frac{P}{\ell} \delta < \underline{v} > \{f'_3\} < f'_3 > \{\underline{v}\} + \frac{P}{\ell} \frac{I}{A} \delta < \underline{\phi} > \{f'_3\} < f'_3 > \{\underline{\phi}\} \\
& - \frac{M}{\ell} \delta < \underline{\phi} > \{f'_3\} < f'_3 > \{\underline{u}\} - \frac{M}{\ell} \delta < \underline{u} > \{f'_3\} < f'_3 > \{\underline{\phi}\} \\
& - V_y \delta < \underline{u} > \{f'_3\} < f'_3 > \{\underline{\phi}\} - V_y \delta < \underline{\phi} > \{f'_3\} < f'_3 > \{\underline{u}\} \\
& + \frac{M}{\ell} \delta < \underline{\phi} > \{f'_3\} < f'_3 > \{\underline{v}\} + \frac{M}{\ell} \delta < \underline{v} > \{f'_3\} < f'_3 > \{\underline{\phi}\} \\
& + V_x \delta < \underline{v} > \{f'_3\} < f'_3 > \{\underline{\phi}\} + V_x \delta < \underline{\phi} > \{f'_3\} < f'_3 > \{\underline{v}\} \\
& + \frac{P}{\ell} \frac{e}{\ell} \delta < \underline{\phi} > \{f'_3\} < f'_3 > \{\underline{u}\} + \frac{P}{\ell} \frac{e}{\ell} \delta < \underline{u} > \{f'_3\} < f'_3 > \{\underline{\phi}\} \\
& - \frac{P}{\ell} \frac{e}{\ell} \delta < \underline{\phi} > \{f'_3\} < f'_3 > \{\underline{v}\} - \frac{P}{\ell} \frac{e}{\ell} \delta < \underline{v} > \{f'_3\} < f'_3 > \{\underline{\phi}\} \\
& + \frac{(M_{x\zeta} C_{x\zeta} + M_{y\zeta} C_{y\zeta} + W_{\omega} C_{w\zeta})}{\ell} \delta < \underline{\phi} > \{f'_3\} < f'_3 > \{\underline{\phi}\} \left. \right] d\beta
\end{aligned}$$

$$\begin{aligned}
& - \delta \left(\sum_{i=1}^2 F_{xi} u_i + F_{yi} v_i + F_{zi} w_i + M_{xi} \theta_{xi} + M_{yi} \theta_{yi} + M_{zi} \theta_{zi} \right. \\
& \left. + (F_{xi} d_{xi} \phi_i^2 + F_{yi} d_{yi} \phi_i^2)/2 \right) = 0
\end{aligned} \tag{2-24}$$

where the subscript ζ indicates that the quantity is a variable with respect to the z coordinate.

Assuming all the geometric properties, the axial loads, and the moments vary linearly along the element, and integrating with respect to β yields, (see Appendix A, Equations A-54 and A-55)

$$[k_S] \{r_E\} + [k_G] \{r_E\} = \{R_E\} \tag{2-25}$$

where $\{r_E\}$ is defined in Fig. 2.6;

$[k_S]$ is the usual element stiffness matrix for the linear elastic problem and $[k_G]$ is called the "initial stress" or "geometric stiffness" matrix.

Equations 2-24 and 2-25 express the total equilibrium requirement implied in Equations 2-11 and 2-15. The matrix $[k_G]$ must be evaluated using the stress resultants in the final equilibrium position, which are directly dependent on the displacements, $\{r_E\}$.

The incremental equilibrium Equation 2-14 can be written in finite element form, neglecting the initial displacement matrix (see Appendix B), as

$$[k_S] \{\Delta r_E\} + [k_G] \{\Delta r_E\} = \{\Delta R_E\} \tag{2-26}$$

where $[k_S]$ and $[k_G]$ have exactly the same form as in Equation 2-25.

However a distinction occurs in that, for Equation 2-26 the geometric

stiffness is evaluated from the stress resultants at the beginning of the increment.

The expressions for $[k_S]$ and $[k_G]$ are derived for a typical element in Appendix A. They may be partitioned in the following form

$$[k_S] = \begin{bmatrix} k_{uu} & & & \\ & k_{vv} & & \\ & & k_{\phi\phi} & \\ & & & k_{ww} \end{bmatrix} \quad (2-27)$$

$$[k_G] = \begin{bmatrix} g_{uu} & \cdot & g_{u\phi} & \cdot \\ \cdot & g_{vv} & g_{v\phi} & \cdot \\ g_{\phi u} & g_{\phi v} & g_{\phi\phi} & \cdot \\ \cdot & \cdot & \cdot & \cdot \end{bmatrix} \quad (2-28)$$

where $[k_{uu}]$ ----- $[g_{\phi\phi}]$, are submatrices defined in Appendix A.

2.8 Assembly of Finite Element Equations

The element stiffness matrices of Section 2-7 have been evaluated with respect to nodal displacements referenced to a 'local' coordinate system, where u_s and v_s are shear center displacements in the directions of the principal axes; w_c is the uniform axial displacement of the centroid; and ϕ is the twist. In many cases it is convenient to select a different set of reference axis for the global system of nodal displacements.

Let the lateral loads be applied through an axis passing through an arbitrary point 'S' of the cross section (not the shear center), and the axial load be applied through C (not the centroid).

Let \bar{C} be the centroid of the section and \bar{S} the shear center and let the principal axes of the cross section be at an angle of α to the global axes, as shown in Fig. 2.7. The element displacements with respect to the local coordinate system can be related to those in the global coordinate system by the transformation

$$\{r_E\}_L = [T] \{r_E\}_G \quad (2-29)$$

where $[T]$ is given by

$$[T] = \begin{bmatrix} T_{11} & 0 \\ 0 & T_{22} \end{bmatrix} \quad (2-30)$$

; the submatrices are shown in Table 2-1;

$$\{r_E\}_L = \begin{Bmatrix} r_E^p \\ r_E^q \end{Bmatrix}_L \quad (2-31a)$$

where

$$\{r_E^p\}_L^T = \langle u^p, v^p, w^p, \phi_z^p, \left(\frac{du}{dz}\right)^p \ell, \left(\frac{dv}{dz}\right)^p \ell, \left(\frac{d\phi}{dz}\right)^p \ell \rangle_L \quad (2-31b)$$

and

$$\{r_E^q\}_G^T = \langle U^p, V^p, W^p, \phi_z^p, \theta_y^p, \theta_x^p, \left(\frac{d\phi}{dz}\right)^p \rangle_G \quad (2-31c)$$

; and p and q are nodal numbers.

Rewriting Equation 2-25 in this nomenclature yields

$$[k_S] \{r_E\}_L + [k_G] \{r_E\}_L = \{R_E\}_L \quad (2-32)$$

Substituting for $\{r_E\}_L$ in terms of $\{r_E\}_G$, and premultiplying by $[T]^T$ yields,

$$[T]^T [k_S] [T] \{r_E\}_G + [T]^T [k_G] [T] \{r_E\}_G = \{R_E\}_G \quad (2-33a)$$

or

$$[k_S]_G \{r_E\}_G + [k_G] \{r_E\}_G = \{R_E\}_G \quad (2-33b)$$

The formation of the complete stiffness matrix for the entire structure is obtained by direct addition for all the interface nodes (thus satisfying the equilibrium and compatibility requirements (35), and finally introducing the kinematic constraints. The stiffness matrix for the entire structure can be written as,

$$[K_S] \{r\} + [K_G] \{r\} = \{R\} \quad (2-34)$$

Where $[K_S]$ is the elastic flexural stiffness matrix; $[K_G]$ is the geometric or initial stress stiffness matrix; and $\{r\}$ is the assembled vector of global nodal displacements.

Equation 2-34 is the finite element form of the total equilibrium equations as expressed in Equation 2-15 and evaluated in Appendix A. The finite element form of the incremental equilibrium equations, Equation 2-14, with the simplifying assumptions of Appendix B, may be written as

$$[K_S] \{\Delta r\} + [K_G] \{\Delta r\} = \{\Delta R\} \quad (2-35)$$

Where $[K_S]$ and $[K_G]$ are identical to those of Equation 2-34 but $[K_G]$ is determined from initial stress prior to the load increment.

2.9 Summary

These equations up to and including those in Section 2.3, apply whether the member is elastic or inelastic. In the remainder of the chapter, the equations were specialized for the elastic case and a finite element formulation for this case was developed.

$$[T_{11}] =$$

$\cos \alpha$	$\sin \alpha$	$\bar{x} \sin \alpha - \bar{y} \cos \alpha$			
$-\sin \alpha$	$\cos \alpha$	$\bar{y} \sin \alpha + \bar{x} \cos \alpha$			
		1	$-x_0$	$-y_0$	
		1			
			$\ell \cos \alpha$	$\ell \sin \alpha$	$\ell(\bar{x} \sin \alpha - \bar{y} \cos \alpha)$
			$-\ell \sin \alpha$	$\ell \cos \alpha$	$\ell(\bar{y} \sin \alpha + \bar{x} \cos \alpha)$
					ℓ

TABLE 2-1 TRANSFORMATION MATRIX

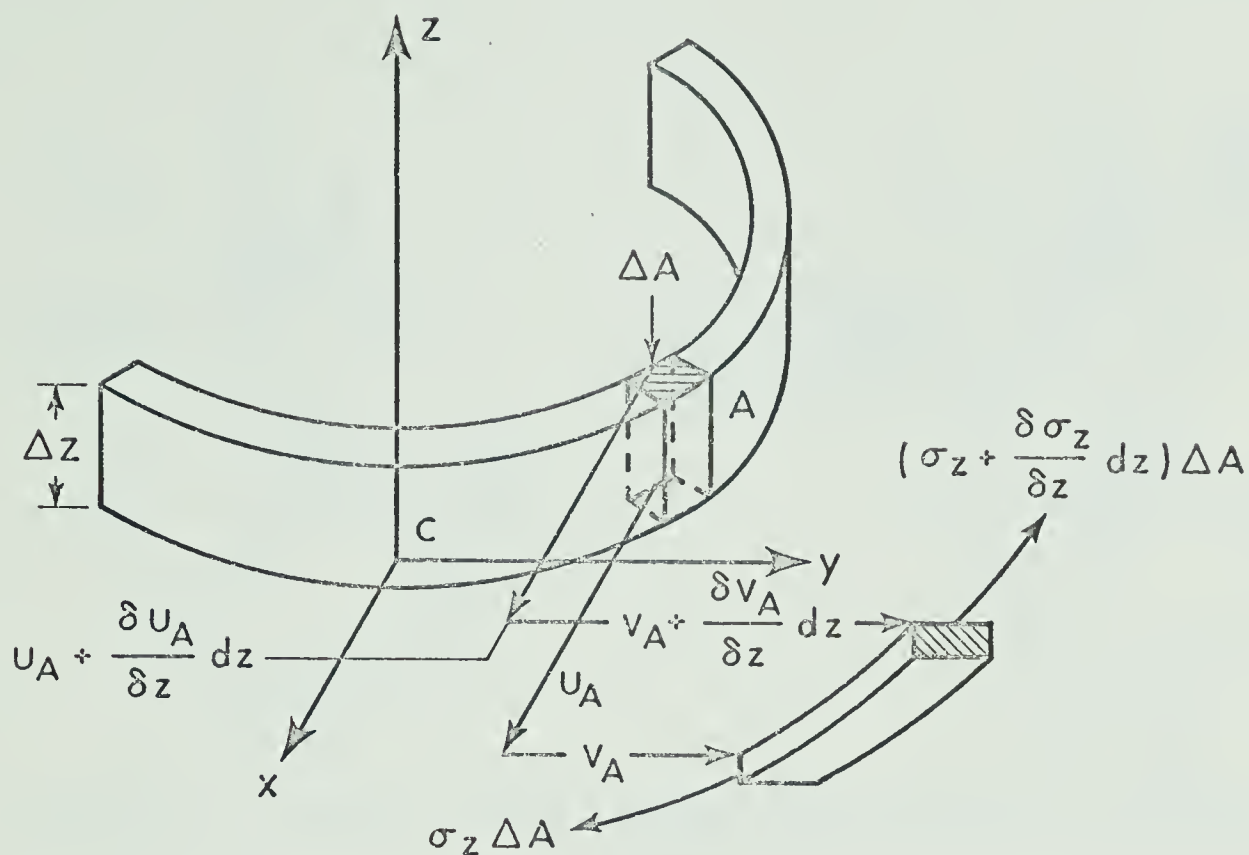


FIGURE 2.3a DISPLACEMENT OF A FIBRE DURING DEFORMATION

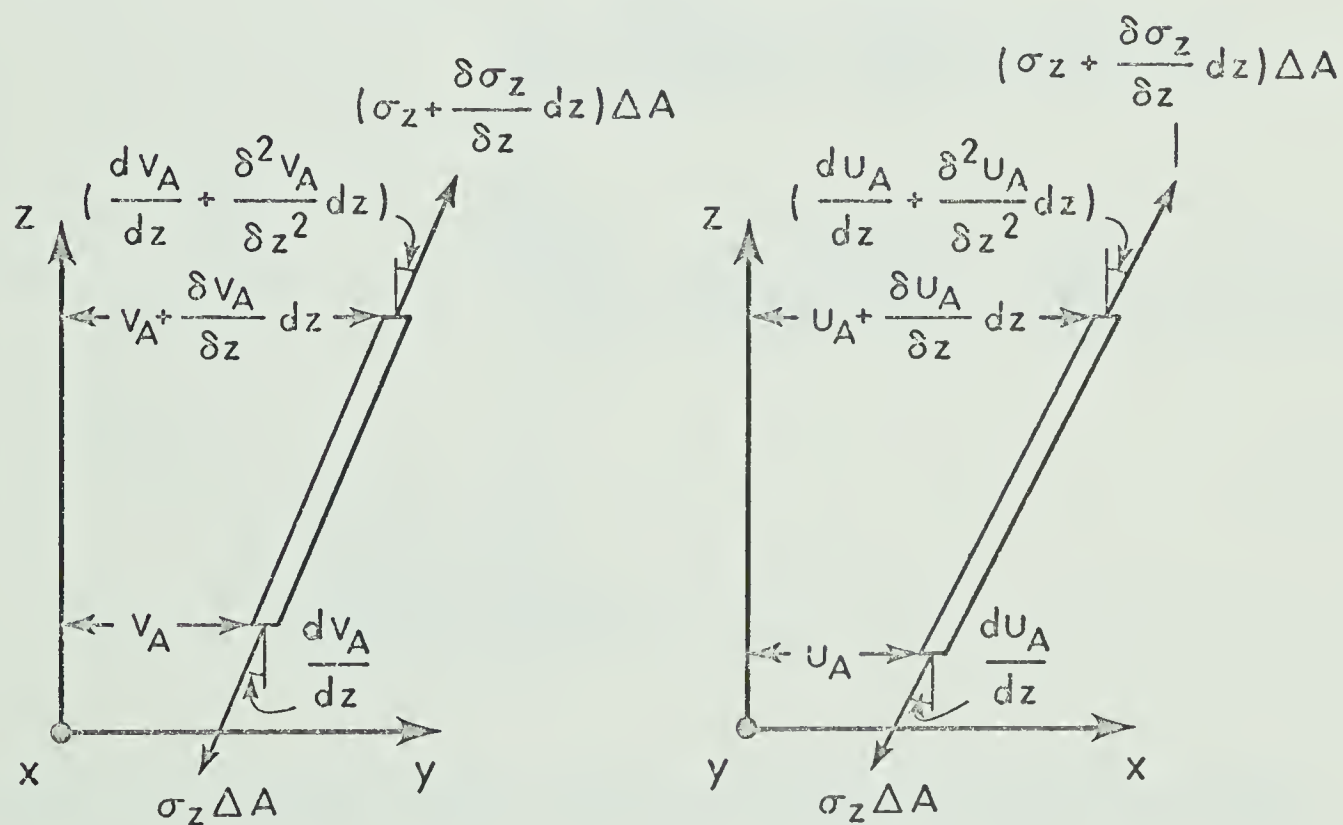


FIGURE 2.3b PROJECTIONS OF A DEFORMED BAR ON YZ & XZ PLANE

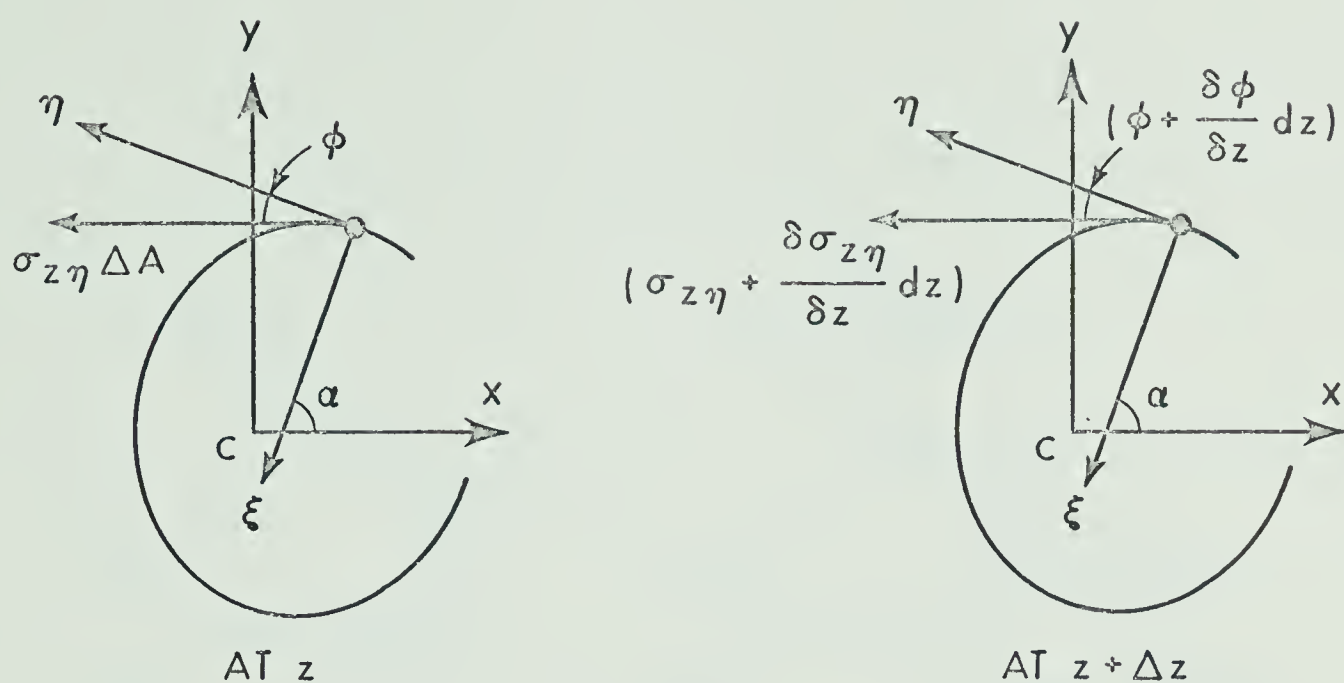


FIGURE 2.3c INTERNAL FORCES INDUCED DUE TO SHEARING DEFORMATION

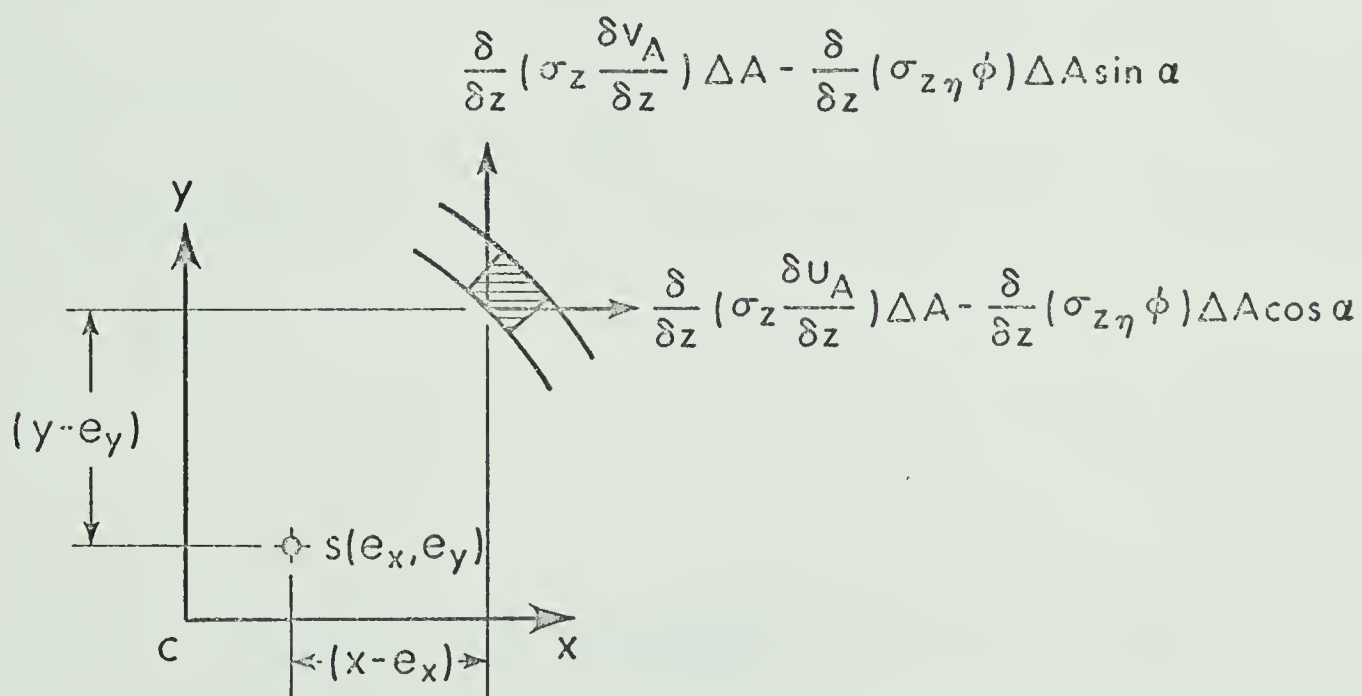


FIGURE 2.3d INPLANE FORCES INDUCED BY NORMAL AND SHEARING STRESSES

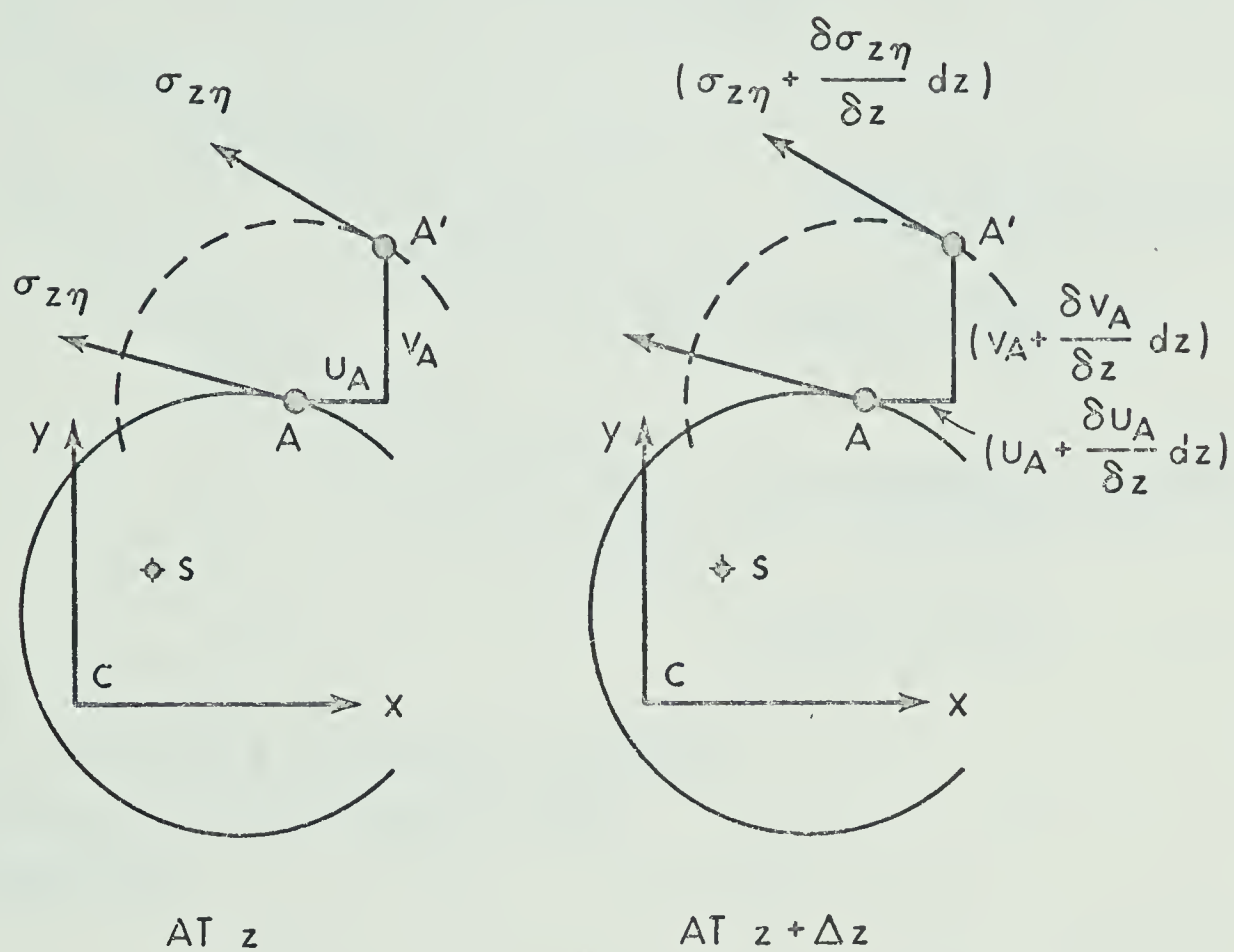


FIGURE 2.4 ADDITIONAL TORSIONAL MOMENT INDUCED DUE TO SHEAR STRESSES DURING DEFORMATION

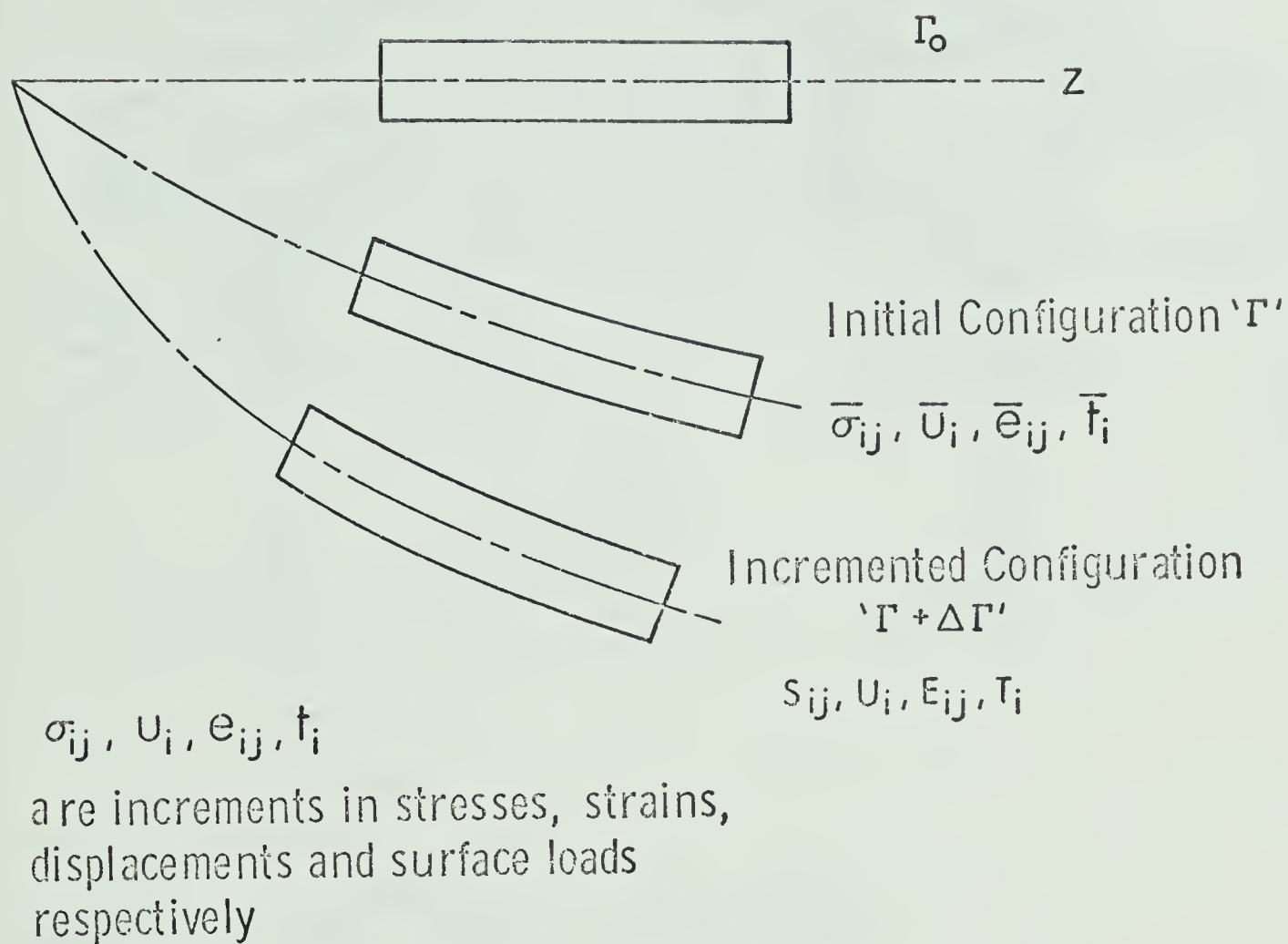
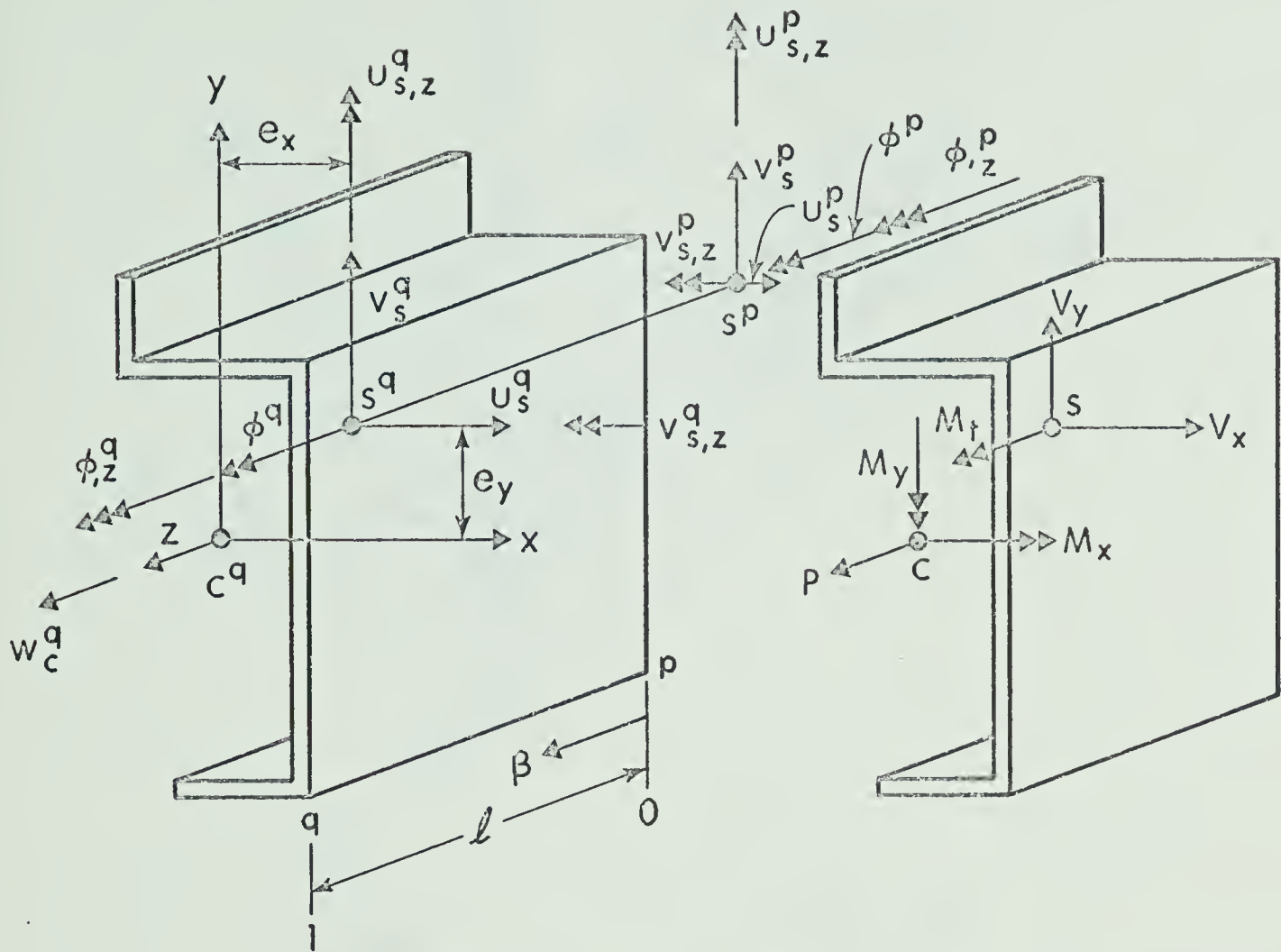


FIGURE 2.5 STRESS STRAIN AND DISPLACEMENT NOMENCLATURE IN INITIAL AND INCREMENTED CONFIGURATION



$$\{\underline{u}\}^T = \langle u_s^p, \ell u_{s,z}^p, u_s^q, \ell u_{s,z}^q \rangle$$

$$\{\underline{v}\}^T = \langle v_s^p, \ell v_{s,z}^p, v_s^q, \ell v_{s,z}^q \rangle$$

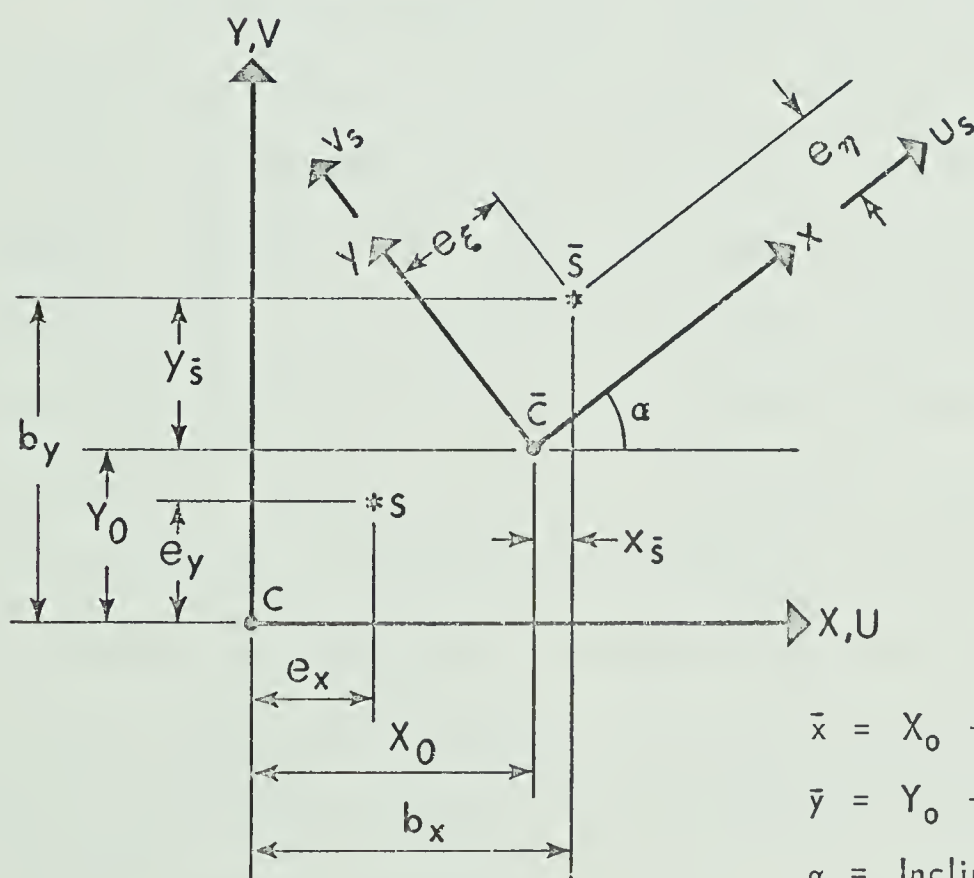
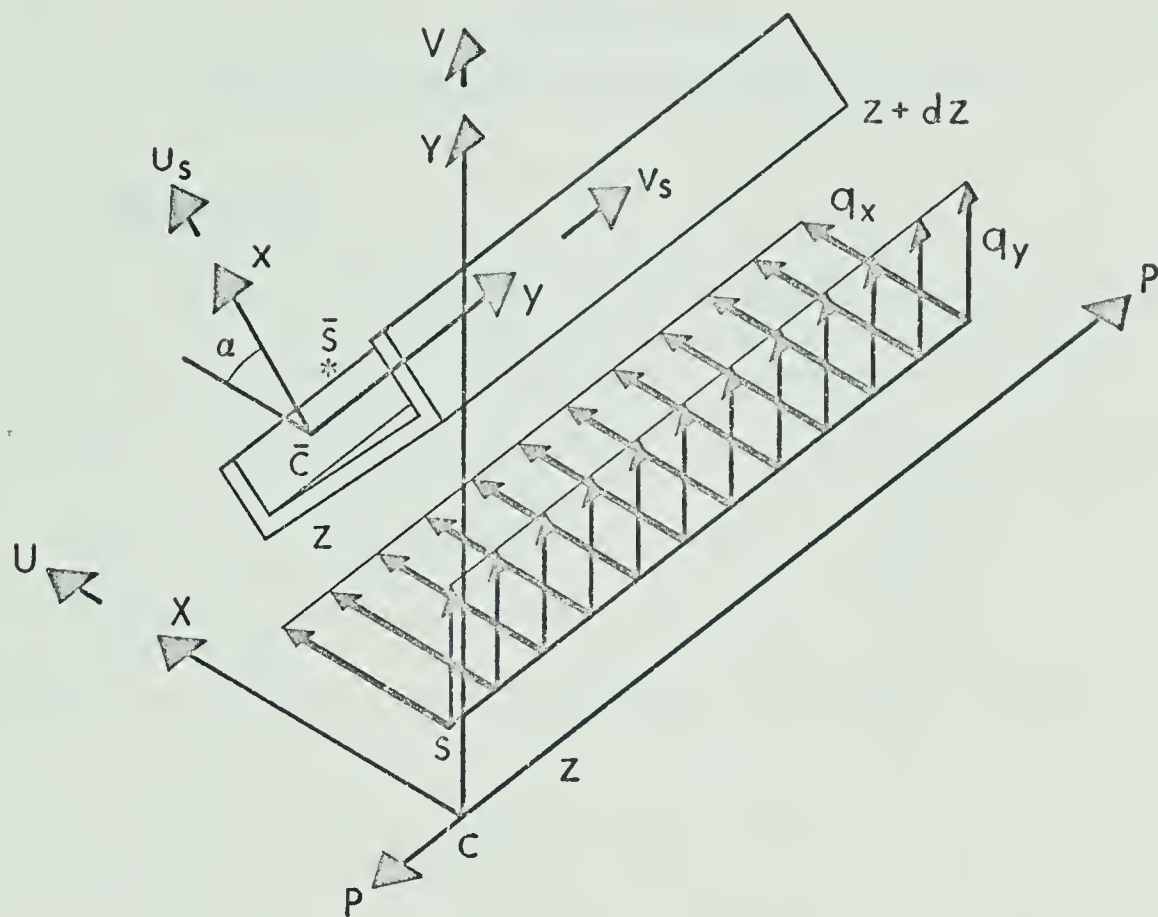
$$\{\underline{\phi}\}^T = \langle \phi^p, \ell \phi_z^p, \phi^q, \ell \phi_z^q \rangle$$

$$\{\underline{w}\}^T = \langle w_c^p, w_c^q \rangle \text{ For Elastic prismatic elements}$$

$$\{\underline{w}\}^T = \langle w_c^p, w_c^{(p+q)}, w_c^q \rangle \text{ For Elastic nonprismatic and inelastic elements}$$

$$\{r_E\}^T = \langle \{\underline{u}\}^T, \{\underline{v}\}^T, \{\underline{\phi}\}^T, \{\underline{w}\}^T \rangle$$

FIGURE 2.6 REFERENCE AXES, NODAL DISPLACEMENTS AND STRESS RESULTANTS



$$\bar{x} = X_0 + x_{\bar{s}} - e_x = b_x - e_x$$

$$\bar{y} = Y_0 + y_{\bar{s}} - e_y = b_y - e_y$$

α = Inclination of Principal axes to global axes

$$e_{\xi} = x_{\bar{s}} \cos \alpha + y_{\bar{s}} \sin \alpha$$

$$e_{\eta} = y_{\bar{s}} \cos \alpha - x_{\bar{s}} \sin \alpha$$

FIGURE 2.7 THIN-WALLED BEAM WITH RESPECT TO LOCAL AND GLOBAL ORIENTATION

CHAPTER III

SOLUTION OF ELASTIC BEAMS AND BEAM-COLUMNS

3.1 Introduction

In this chapter the elastic finite element formulation developed in Chapter II is applied to a number of different types of problems. The problems may be separated into three categories, namely; a) small deflection problems involving the solution of first order beam equations; b) buckling or bifurcation problems involving the eigenvalue solution of the incremental equilibrium equations; and c) beam-column type problems which include the effect of "prebuckling" deformations by satisfying the nonlinear total equilibrium equations. -

The study of beam-column response in the elastic range is motivated by a number of considerations. The elastic critical or 'buckling' load forms an upper bound on the carrying capacity of such a member. However if the design criteria is controlled by a deflection limitation then it is necessary to determine the loading condition at which this limitation is reached and useful to relate this load to the upper bound on carrying capacity. The range of loading for which an elastic analysis is applicable is limited by the proportional limit of the material and the actual carrying capacity is normally governed by inelastic beam-column response. It is useful, however, to study the elastic beam-column response as a prerequisite to solving the more realistic inelastic problem.

It might also be noted, that, with the current development of high strength materials, the range of loading for which elastic analysis is applicable is increasing. Since the buckling problem is based on a classical eigenvalue analysis, it ignores all deformations

prior to the attainment of the critical load and these, together with geometric misalignments, may make the eigenvalue estimate an unrealistically high upper bound. In this chapter, the finite element model derived in Chapter II is used to study both elastic beam-column behaviour and the classical eigenvalue or buckling analysis.

The method is also applied to beam-column problems with initial geometric imperfections. For this case Southwell (65) proposed an extrapolation technique by means of which experimental elastic critical loads can be predicted for concentrically loaded pin-ended columns, with sinusoidal imperfections. Gregory (29) and Ariaratnam (6) have extended the above method in the case of struts which fail by flexural torsional buckling. The elastic deformation of I-beams with sinusoidal initial crookedness or twist under the action of equal and opposite end moments has been carried out by Flint (20) and Massey (47) for simply supported beams, and by Horne (36) and Trahair (70)(71) for beam-columns. Recently Leicester (42) has shown the applicability of the Southwell plot to monosymmetrical beam-columns.

3.2 Solution of First Order Beam Equations

3.2.1 Introductory Remarks

The finite element model derived in Section 2.7 has been used to represent beam flexure by a number of investigators. Barsoum and Gallagher (7,8) and Powell et al (59) have included twist in their model using the same interpolation functions. However, neither of these studies investigated, in detail, the ability of the model to represent non-uniform torsional response.

The bimoment which arises in the derivation of the beam equation has been designated as W_{ω} . This bimoment is produced by restraint of warping deformations and the rate of change of bimoment produces a torque along the beam called the "warping torque", M_{ω} . A measure of magnitude for bimoment is given by the product of the distance between two parallel planes and the moment on one of them. A bimoment is assumed positive when the sense of one moment seen from the plane of the other moment is anticlockwise. A rigorous definition is given in Appendix A, Equation A-14. The distinctive feature of the bimoment is that when it is acting in an elastic body it produces internal stresses and strains which have conventional stress resultants of zero magnitude. When any beam is cut by an imaginary plane the bimoment acting on the section to one side of the plane is equal and opposite to that acting on the other side.

One type of problem that a model must be capable of analysing, to produce reliable results for thin-walled beams of open section, is the problem of nonuniform torsion, where the total torque is resisted by a combination of the warping torque, M_{ω} , and the St. Venant torque, M_t . The following examples test the capability of the model to represent stress conditions in beams subjected to nonuniform torsion.

3.2.2 Numerical Results for Nonuniform Torsion Problems

E-1 Nonuniform Torsion of a Prismatic Beam

In order to check the ability of the finite element model to represent nonuniform torsional behaviour, an 8WF31 cantilever beam of 50 inches length was analyzed with a 5 inch-kip torque applied at the free end. Eight elements were used and the finite element solution was

compared with the closed form solution (68). Fig. 3.1 shows the variation of the angle of twist ϕ , and its derivatives, along the length. In Fig. 3.2 the torsional moment of resistance due to St. Venant and warping are compared with the closed form solution (68). Since a cubic polynomial was used for twist, the variation of warping torsional moment of resistance is constant along the element whereas the variation of St. Venant resistance is quadratic. Fig. 3.3 shows a comparison of the twist curves along the length of the beam for different numbers of elements. The convergence characteristics of the solution are shown in Fig. 3.4.

E-2 Nonuniform Torsion of a Tapered I-Beam

Fig. 3.5 shows the comparison of the finite element analysis with Lee's (41) power series solution for nonuniform torsion of tapered beams. The finite element analysis agrees with the closed form solution (68) for a uniform beam, A, but this solution does not agree with Lee's results. For the tapered beams, B and C, Lee's analysis includes the torque about the longitudinal axis resulting from the projection of the inclined flange moments. This effectively reduces the torsional stiffness of the beam. Such an effect is not incorporated in the equilibrium equations of Chapter II and therefore cannot be represented by the finite element model. When the beam taper is considerable, as in these examples, the contribution of flange moment to the torsional moment is significant and hence there is a discrepancy between Lee's analysis and the results from the conventional beam equations.

3.3 Elastic Buckling Problems

3.3.1 Introductory Remarks

Many structures when loaded to a critical state will undergo a marked change in the character of deformation, which is not the result of material failure or alteration of mechanical properties. Such a change occurs because one mode of deformation becomes unstable and the structure seeks a stable configuration. The change in deformation which takes place when the structure passes from an unstable configuration to a stable configuration is generally known as buckling. The load at which this occurs is known as the critical or bifurcation load. The classical buckling problem ignores all deformations prior to the attainment of the buckling load and hence the eigenvalue analysis always forms an upper bound for the load.

3.3.2 Solution Scheme

A buckling problem is formulated by imposing a variation of displacements in the matrix equation 2-34 under constant load. The result is identical to the homogeneous form of Equation 2-35, i.e.: -

$$\left[[K_S] \{\Delta r\} + [K_G] \{\Delta r\} \right] = \{0\} \quad (3-1)$$

The above equation is satisfied, for a non-zero displacement vector, only if the stiffness matrix is singular, and the "buckling criterion" can be represented by the vanishing of the determinant of the stiffness matrix, i.e.: -

$$|[K_S] + [K_G]| = 0 \quad (3-2)$$

By assuming that throughout the loading range the stress state can be written in terms of some function whose intensity is governed by a single parameter, λ , the initial stress state takes the form

$$[K_G] = \lambda [\bar{K}_G] \quad (3-3)$$

where $[\bar{K}_G]$ represents the initial stress stiffness matrix computed for some nominal stress distribution. Introducing Equation 3-3 into Equation 3-1 yields

$$[K_S]\{\Delta r\} = -\lambda [\bar{K}_G]\{\Delta r\} \quad (3-4a)$$

or

$$\frac{1}{\lambda} \{\Delta r\} = -[K_S]^{-1} [\bar{K}_G]\{\Delta r\} \quad (3-4b)$$

The critical buckling load is now obtained by solving Equation 3-4b for the unknown eigenvalue λ . The eigenvalue solution for the following problems was determined using "NROOT" of the IBM-SSPackage (1). The buckling mode can be identified as the eigenvector corresponding to the lowest eigenvalue.

3.3.3 Numerical Examples

In order to verify the formulation a wide variety of problems have been solved and checked with closed form solutions. Table 3-1 shows the comparison of the results of a large number of critical loads computed by the finite element analysis with the corresponding available solutions. The table includes examples of Euler, lateral and lateral torsional buckling. Nomenclature is specified in Fig. 3.6. Some important additional examples are described below.

E-1 Torsional Buckling of a Symmetrical I-Beam

Table 3-2 shows a comparison of the results of Krajcinovic (40) and the present formulation. Krajcinovic used a hyperbolic function for the twist and claimed that the results from a cubic polynomial

would not be able to reflect the term κ (ratio of St. Venant torsional rigidity to warping rigidity) no matter how many elements were used. In the present formulation a four element approximation gives results closer to the exact solution.

E-2 Influence of Point of Load Application for Lateral Buckling of Beams

Fig. 3.7 shows the solution for lateral buckling of a beam with a single vertical concentrated central load applied at a distance d_y above or below the shear center. The section is that used by Powell (59), et. al., and is a 21" x 10" I beam with a uniform thickness of 1". The span is 300". The solution is compared to that of Timoshenko (68).

E-3 Elastic Buckling of Indeterminate Structures

Table 3-3 shows the comparison of finite element results with those of Horne and Ajmani (37) who developed a series solution to determine the critical loading on columns supported laterally by "side rails". The side rails, acting with the cladding and any bracing system, are assumed to provide a rigid lateral support at the points of attachment. They also provide an elastic torsional restraint. A 8WF 28 column, 69" in length and restrained laterally by side rails at a spacing of 23" and at an eccentricity of 3" from the centre line of the column, was analyzed when subjected to an axial load of P and a uniform moment of M about the major axis. At each rail position the torsional restraint was assumed to be 1040 in.K/Rad. As shown in Table 3-3, the load which causes lateral torsional buckling is 1972.19 kips, when the rotations are nonzero at lateral supports (case 8), and 6100 kips when the rotations are zero at lateral supports (case 17).

In the first case the column buckles in a lateral torsional buckling mode and in the second case the column buckles in an Euler mode. The mode shapes for these cases are shown in Fig. 3.8.

E-4 Euler Buckling of an Unsymmetrical Section

The unsymmetrical beam used by Vlasov (74) for unsymmetrical bending, shown in Fig. 3.9, was analyzed with an axial load applied at the centroid and with a span of 300". The eigenvalue corresponds to lateral torsional buckling. The finite element critical load is 1163 kips compared to a value of 1140 kips determined from the equations of Timoshenko (68).

E-5 Lateral Torsional Buckling of an Unsymmetrical Section Under Uniform Moment

End moments were applied about the X-axis for the beam of example E-4 and the critical moment to cause lateral torsional buckling about the minor axis was found to be 2.3706×10^4 inch-kips compared to a value of 2.367×10^4 inch-kips determined by the closed form solution (68).

E-6 Lateral-Torsional Buckling of an Unsymmetrical Section with Moment Gradient

A vertical load was applied at the mid-span of the beam of example E-4 and E-5 acting 2.42" above the shear centre as shown in Fig. 3.9. The critical load to cause lateral-torsional buckling was found to be equal to 263.27 kips. A classical solution of this problem involves the solution of three coupled ordinary differential equations and no closed form comparison is available.

E-7 Elastic Buckling of a Tapered Axially Loaded Member

A tapered WF column with the dimensions as shown in Fig. 3.10

was analyzed with the small end pinned and the larger end fixed. The finite element analysis estimates the buckling load 4.93 percent higher than that given by Culver (17), who has published a set of curves for this type of problem using Lee's (41) nonuniform torsion formulation.

E-8 Lateral Torsional Buckling of a Tapered Beam Under Moment Gradient

The beam described in E-7 was loaded with a moment at the larger end and the critical moment was found to be 1035 inch-kips which is 9.21 percent lower than the critical moment given by Culver (17). The discrepancy is attributed to the component of the flange bending moments in the z-direction, which were considered by Lee and Culver, and discussed in example E-2 of Section 3.2.2, and which are not taken into account in present analysis.

E-9 Interaction Surface for Critical Loading

Fig. 3.11 shows the influence buckling surface for an 8WF28 beam, 69" in length, when it is loaded by axial load and end moments.

3.4 Solution Methods for Beam-Column Problems

3.4.1 Introductory Remarks

The previous examples in this chapter have dealt with the small-deflection beam equations and elastic buckling or bifurcation problems. When pre-buckling deformations are considered it is necessary to solve a 'beam-column' type problem. This involves the solution of Equation 2-34 which, because of the dependence of $[K_G]$ on $\{r\}$, is nonlinear. There are a number of methods of solving this set of nonlinear equations. A 'Newton-Raphson' method was used to solve elastic beam-column problems and a 'Modified Newton-Raphson' was used to solve inelastic beam-column problems in this dissertation.

A description of these two methods, applied to elastic problems, is given in the remainder of this section. An equilibrium check is incorporated into both techniques.

3.4.2 Newton-Raphson Method

This method has been employed successfully by a number of investigators. For example, Walker and Hall (75) used it to study large deflections of beams, and Brebbia (14) and Connor used it to study the stability and geometrically non-linear behaviour of arbitrary shells. Initially, a small displacement solution of Equation 2-34 is obtained, for the first load increment, with $[K_G]$ set to zero. The element stress resultants are computed from the known displacements and the geometric stiffness matrix for the structure is evaluated. The total resisting force at any node is the sum of the resisting forces obtained from the flexural stiffness and the geometric stiffness. The difference between the resisting forces and the applied loads represents a set of unbalanced forces for the given configuration of the model. Knowing the set of unbalanced forces on the model, in this configuration, one can solve for the increments in the nodal displacements. The iteration is repeated till the configuration of the model maintains equilibrium with the applied loads. The following algorithm explains the procedure and is illustrated in Fig. 3.12a.

1. For any approximate $\{r\}_n$, compute $[K_G]_n$ and the unbalanced force vector,

$$\{\Delta R\}_{n+1} = \{R\} - [K_S]\{r\}_n - [K_G]_n \{r\}_n \quad (3-5)$$

2. Compute the increment in displacements to equilibrate the unbalanced forces,

$$\{\Delta r\}_n = \left[[K_S] + [K_G]_n \right]^{-1} \{\Delta R\}_n \quad (3-6)$$

3. Update the displacements

$$\{r\}_n = \{r\}_{n-1} + \{\Delta r\}_n \quad (3-7)$$

4. Repeat steps 1 to 3 until the unbalanced force vector is arbitrary small.
5. Apply a new load increment and repeat steps 1 to 4.

The principal disadvantage of this technique is that it is necessary to triangularize a new stiffness matrix for every iterate.

3.4.3 Iterative Initial Force Method (Modified Newton-Raphson Method)

This method retains the linear elastic matrix on the left hand side of the equation and keeps all the nonlinear terms on the right hand side. It is illustrated in Fig. 3.12b. For the n th iterate, Equation 2-34 can be written as,

$$[K_S]\{r\}_{n+1} = \{R\} - [K_G]\{r\}_n \quad (3-8)$$

and solved for the next estimate of nodal displacements

$$\{r\}_{n+1} = [K_S]^{-1} \{R\} - [K_S]^{-1} [K_G]\{r\}_n \quad (3-9)$$

The above procedure is repeated till the displacement for the $(n+1)^{th}$ iterate is the same as for the n^{th} iterate, at which time the unbalanced force vector is arbitrarily small. The matrix $[K_G]$ is updated only at the beginning of each load step.

To investigate the convergence of this method one may follow the procedure which Dupuis et al (79) used for direct iteration:

$$\{r\}_{n+1} = [K_S]^{-1}\{R\} - [K_S]^{-1}[K_G] \left\{ [K_S]^{-1}\{R\} - [K_S]^{-1}[K_G]\{r\}_{n-1} \right\} \quad (3-10)$$

continuing this back substitution yields

$$\begin{aligned} \{r\}_{n+1} = & ([I] - [G] + [G]^2 - [G]^3 \dots (-1)^n [G]^n) \times \\ & [K_S]^{-1}\{R\} + (-1)^{n+1} [G]^{n+1} \{r_o\} \end{aligned} \quad (3-11)$$

where

$$[G] = [K_S]^{-1} [K_G] \quad (3-12)$$

Assuming the displacements are initially zero the convergence depends on the expression

$$(-1)^n [G]^n [K_S]^{-1} \{R\} \quad \text{tending to zero}$$

If $\{\bar{u}_j\}$ are the eigenvectors of the matrix $[G]$, we may write

$$[K_S]^{-1} \{R\} = \sum_{j=1}^n c_j \{\bar{u}_j\} \quad (3-13)$$

Noting that $[K_S]$ and $[K_G]$ are symmetric matrices and $[K_S]$ is a positive definitive matrix, we have

$$\frac{1}{\lambda} \{\bar{u}\} = [G]\{\bar{u}\} \quad (3-14)$$

$$[G]^n \{\bar{u}\} = \frac{1}{\lambda^n} \{\bar{u}\} \quad (3-15)$$

$$\begin{aligned} [G]^n [K_S]^{-1} \{R\} &= [G]^n c_1 \{\bar{u}_1\} + [G]^n c_2 \{\bar{u}_2\} + \dots \\ &= c_1 \{\bar{u}_1\} / \lambda^n \end{aligned} \quad (3-16)$$

Since λ is greater than 1 when the current load is less than the buckling load, the method converges.

3.4.4 Solution Scheme for Beam-Columns with Geometric Misalignment

When the beam has an initial imperfection of $\{r_o\}$ Equation 2-34 can be written as

$$[K_S]\{r\} + [K_G]\{r\} = \{R\} - [K_G]\{r_o\} \quad (3-17)$$

The unbalanced load for the Newton-Raphson method

$$\{\Delta R\}_n = \{R\} - [K_S]\{r\}_n - [K_G]_n\{r\}_n - [K_G]_n\{r_o\} \quad (3-18)$$

and the corrections $\{\Delta r\}_{n+1}$ is given by the solution to

$$[[K_S] + [K_G]_n]\{\Delta r\}_{n+1} = \{\Delta R\}_n \quad (3-19)$$

where $\{r\}$ are the displacements from the initially imperfect configuration.

3.5 Elastic Beam-Column Response

3.5.1 Introductory Remarks

For beam-column type problems the load-deformation response was obtained by applying the load incrementally and iterating to find the equilibrium configuration for each loading condition as described in Section 3.4.2. A solution to this type of problem can be obtained for statically indeterminate, as well as statically determinate members, subjected to any combination of externally applied concentrated or distributed loads, moments, or torques, with or without elastic constraints.

3.5.2 Examples of Beam-Column with Initial Imperfection

E-1 Inplane response of a column (axial load)

Fig. 3.13 compares, with the solution of Timoshenko (68), the column response for an 8WF31 section of length 69" with an initial deflection of $0.01 \sin \frac{\pi z}{L}$, when subjected to an axial load. Deflection increases in a nonlinear manner and after $0.8P_{cr}$ the deflection increases rapidly.

E-2 In and out of plane response of a column

In Fig. 3.14 the load deflection response of a beam-column is shown, for initial deflections of $-0.01 \sin \pi z/L$ in u , v , and ϕ , when the member is subjected to axial load. When the load reaches the critical load corresponding to the Euler buckling load about the minor axis, the sign of the determinant changes. For loads above the critical value, the sign of the u -deflection changes. When the load reaches the torsional buckling load, the sign of the determinant changes again as well as the sign of the twist. The v -deflection continues to increase and becomes asymptotic to the line of the major axis Euler buckling load.

E-3 Out of plane response of a beam due to end moments

Fig. 3.15 shows the moment and out of plane response for an 8WF31 beam when there is an initial lateral deflection of $0.01 \sin \frac{\pi z}{L}$. Moment and deflection curves are drawn, neglecting the effect of moment about the minor axis on the equilibrium equation for torsional moment, and compared with the results obtained by Trahair (71). Curves are also drawn when this coupling effect is considered. Closed form and finite element solutions are compared for both cases.

E-4 Out of plane response of beam-column due to axial load and equal end moments

A 12WF50 with a sinusoidal imperfection is analyzed with the axial load applied at different eccentricities. The beam-column response curves are shown in Fig. 3.16 and compared with corresponding eigenvalue solutions.

3.6 Summary

In this chapter, some examples of solutions were presented for a) the first order beam equations, b) elastic buckling of both statically determinate and indeterminate structures, and c) the elastic analysis of beam-columns with imperfections.

No	Support Code		Loading		Intermediate	Computed Critical Load	Buckling Mode	% Error
	A	B	A	B				
1	H	R	$P_z = P$	$P_z = -P$		1,345 kips	EW	0.1258
2	H	R	$M_y = M$	$M_y = -M$		12,200" kips	LS	0.0656
3	H	R	$M_x = M$	$M_x = -M$		5,740" kips	LW	0.00931
4	H	R	$M_x = M$ $M_y = M$	$M_x = -M$ $M_y = -M$		5,180" kips	LW	0.00602
5	H	R	$P_z = P$	$P_z = -P$		1,345 kips	EW	0.126
6	H	R	$M_y = P$	$M_y = -P$		1,165 kips	LTB	0.0006
7	H	R	$P_z = P$	$P_z = M_x$		1,165 kips	LTB	0.0006
8	C	F	$M_x = P$ $M_y = P$	$M_x = -P$ $M_y = -P$	Buckling due to self weight	1,063 kips	EW	-0.00187
9*	H	R	$P_z = P$	$P_z = -P$		1,737.2 kips	TB	0
10	C	F	$F_y = P$	$F_y = P$		134.8 kips	LW	0
11	H	R			$F_y = P$ at all nodes $q\ell = 8P$	753.6 kips	LW	0.0222
12	H	R			$F_y(E) = P$	445 kips	LW	0.00225
13	C	F			$F_y = P$ at all nodes $q\ell = 8P$	133.5 kips	LW	-0.02554
14	HXW	HXW			$F_x = P$ at all nodes $q\ell = 6P$	$q = 73.13$ kips	LS	2.48

* Cruciform Section (for nomenclature see Fig. 3.6) Section adopted 8WF28 $\ell = 69"$

TABLE 3-1 COMPARISON OF FINITE ELEMENT ANALYSIS WITH TIMOSHENKO (68)

$\kappa \ell$	Exact Solution	Hyperbolic Krajinovic (40)	Cubic Polynomial			
			1 element	2	4	8
0	9.87	9.92	12.0	9.94385	9.87466	9.86993
1	13.87	14.01	16.0	13.9438	13.8747	13.8699
2	25.87	26.30	28.0	25.9438	25.8747	25.8699
3	45.87	46.99	48.0	45.9438	45.8747	45.8699
4	73.87	76.13	76.0	73.9438	73.8747	73.8699
5	109.87	113.65	112.0	109.944	109.875	109.87
10	409.87	423.20	412.0	409.944	409.875	409.87

TABLE 3.2 TORSIONAL BUCKLING OF SYMMETRICAL I-BEAM

TABLE 3-3 COMPARISON OF FINITE ELEMENT ANALYSIS WITH REPORTED RESULTS

Example No	Support Code		a_y	Loading		Spring Constant $K_\theta = 1040''K/rad$ at E	Computed Critical Load	Buckling Mode	% age Error	Ref.
	C	D		A	B					
1	F	F				$F_y = -P_y$ at E $F_y = q\ell_y = 8P$	570K	LW	5.86	66
2	F	F				"	952K	LW	5.38	66
3	F	F		$M_x = M_x$	$M_x = -M_x$	"	7227''K	LW	1.07	66
4	F	F		$P_z = P_z$	$P_z = -P_z$	$K_x = 59.5K/inch$	1680.3K	TB	0.059	68
5	F	F		$M_x = M_x$	$M_x = -M_x$	$K_\theta = 114''K/rad$ (uniform)	10,344''K	LW	1.61	66
6	u	u	-3	$M_x = M_x$	$M_x = -M_x$	$K_\theta = 1040''K/rad$ at A,B,C,D	9,688K	LW	0.092	37
7	u	u	-3	$P_z = P_z$ $M_x^z = 60P_x^z$	$P_z = -P_z$ $M_x^z = -60P_x^z$	"	151.687K	LTB	0	37
8	u	u	-3	$P_z = P_z$ $M_x^z = P_x^z$	$P_z = -P_z$ $M_x^z = -P_x^z$	"	1972.19K	LTB	0.621	37
9	u	u	-3	$P_z = P_z$ $M_x^z = P_x^z$	$M_x^z = M_x^z$	"	$1.834 \times 10^4''K$	LTB	2.57	37
10	u	u	-3	$P_z = P_z$ $M_x^z = P_x^z$	$P_z = -P_z$ $M_x^z = -P_x^z$	"	2169.34K	LTB	-	37
11	u	u	-3	$P_z = P_z$ $M_x^z = P_x^z$	$P_z = -P_z$ $M_x^z = -P_x^z$	"	2475.0K	TB	0.609	37
12	u	u	-3	$P_z = P_z$ $M_x^z = 50P_x^z$	$P_z = -P_z$ $M_x^z = -50P_x^z$	"	179.84K	LTB	0	37
13	u	u	0	$M_x = M_x$	$M_x = -M_x$	"	$4.6165 \times 10^4''K$	LW	0.358	37
14	u	u	0	$P_z = P_z$ $M_x^z = 20P_x^z$	$P_z = -P_z$ $M_x^z = -20P_x^z$	"	1940K	LTB	0.0	37
15	u θ	u θ	-3	$M_x = M_x$	$M_x = -M_x$	"	$3.28 \times 10^4''K$	LW		37

Table 3-3 (cont'd)

Example No	Support Code		a	Loading		Spring Constant	Computed Critical Load	Buckling Mode	% age Error	Ref.
	C	D		A	B					
16	u	u	0	$P_x = P$ $M_x^z = 60P$	$P_z = -P$ $M_x^z = -60P$	"	723K	LW	0	37
17	u θ	u θ	-3	$P_x = P$ $M_x^z = P$	$P_z = -P$ $M_x^z = -P$	"	6,100K	ES		37
18	u	u	0	$P_z = P$	$P_z = -P$	"	3,170K	TB	0.3154	37

SUPPORT CODE FOR A = H

FOR ALL THE PROBLEMS

SUPPORT CODE FOR B = R

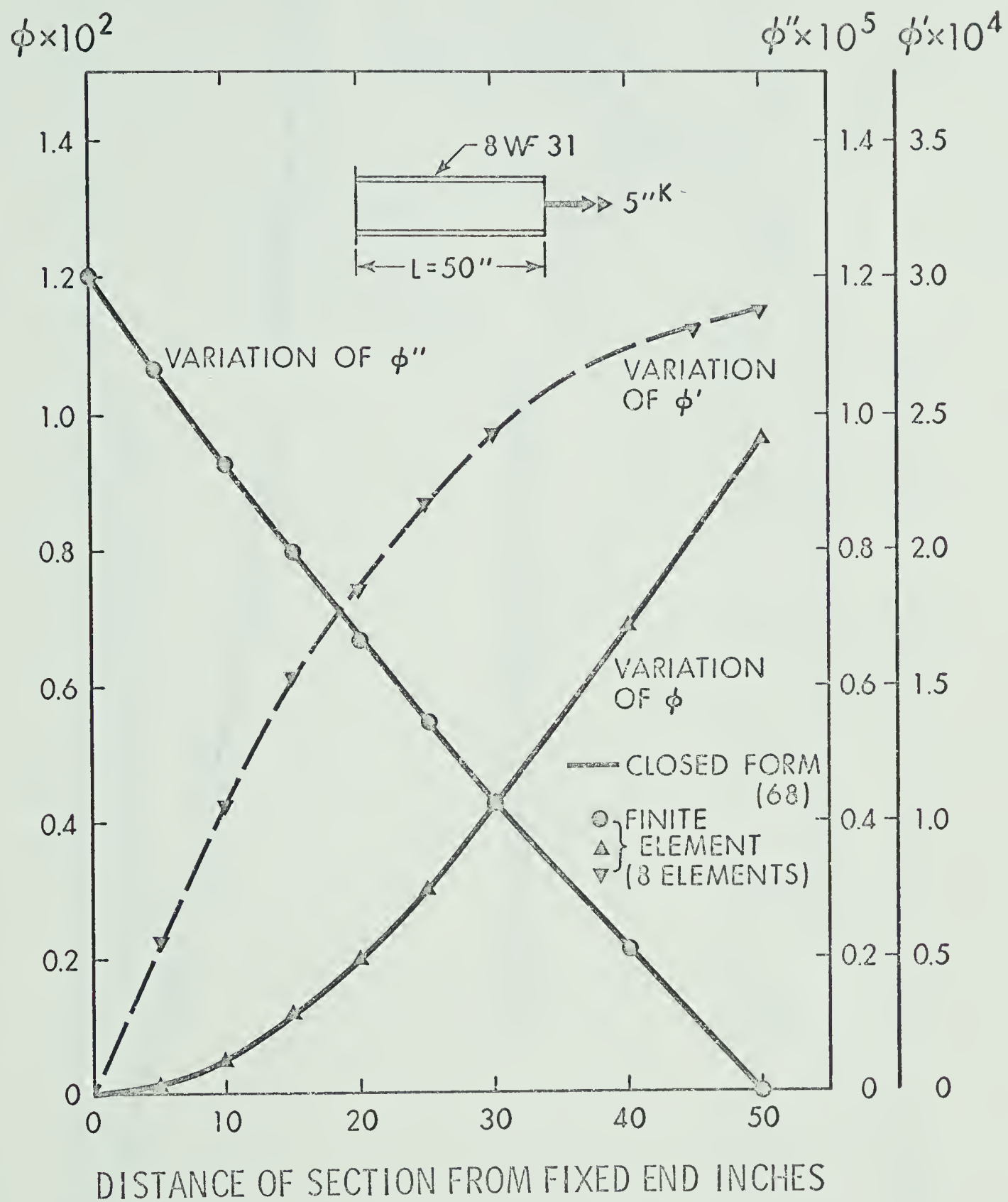


FIGURE 3.1 NON-UNIFORM TORSION OF WF BEAM

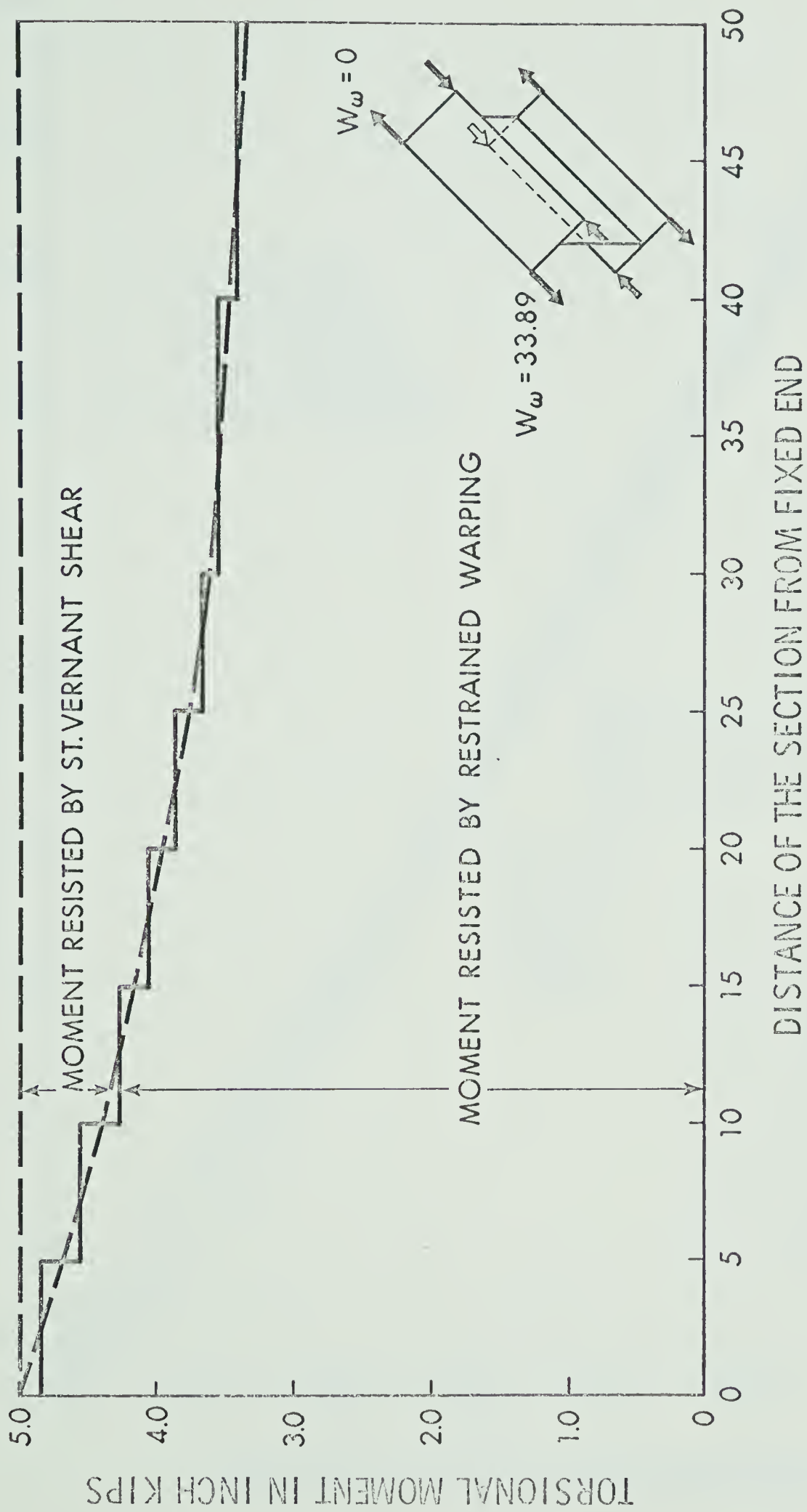


FIGURE 3.2 MOMENT OF RESISTANCE BY ST. VENANT AND WARPING SHEAR

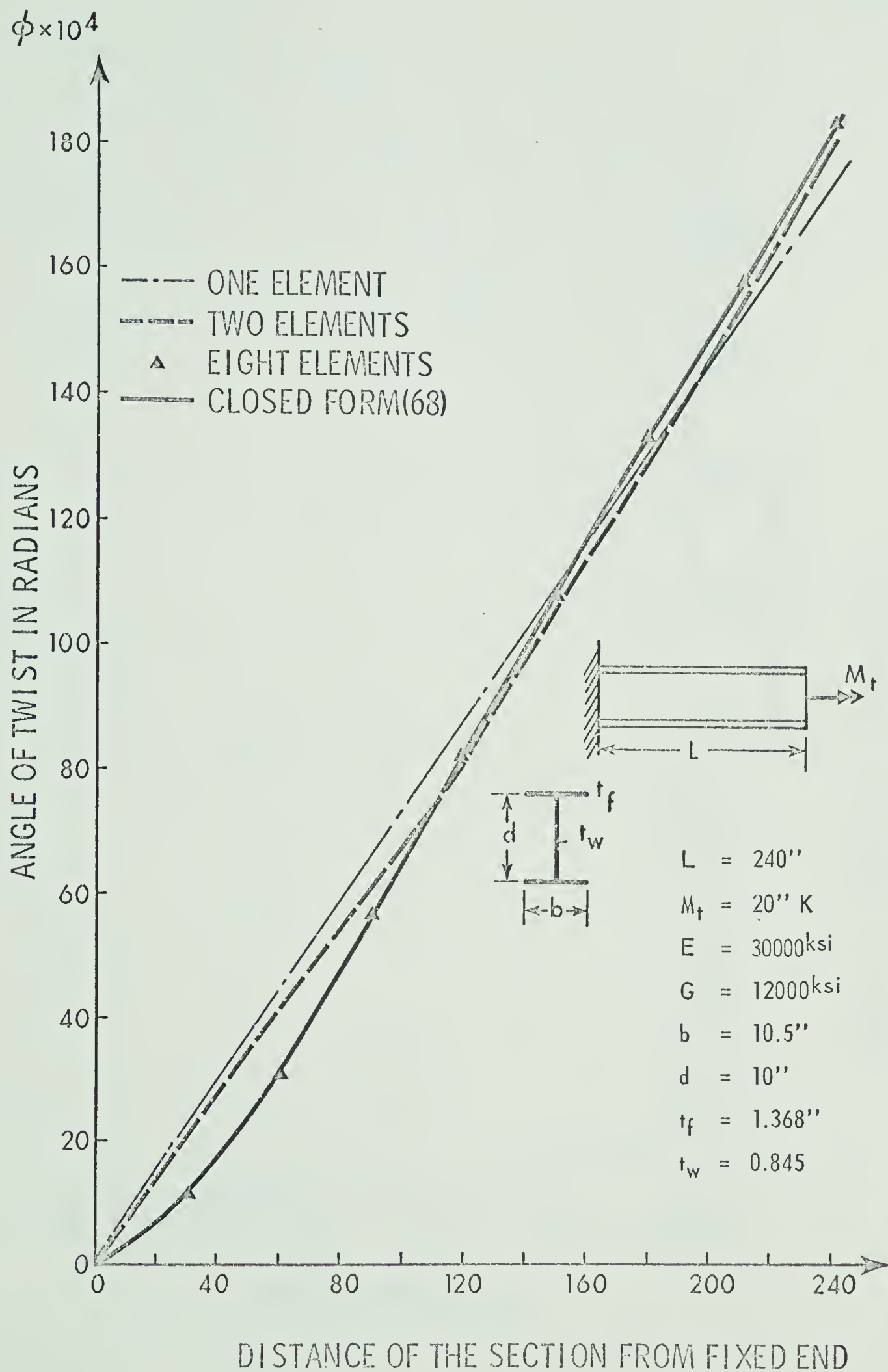


FIGURE 3.3 NON-UNIFORM TORSION - COMPARISON WITH DIFFERENT ELEMENTS

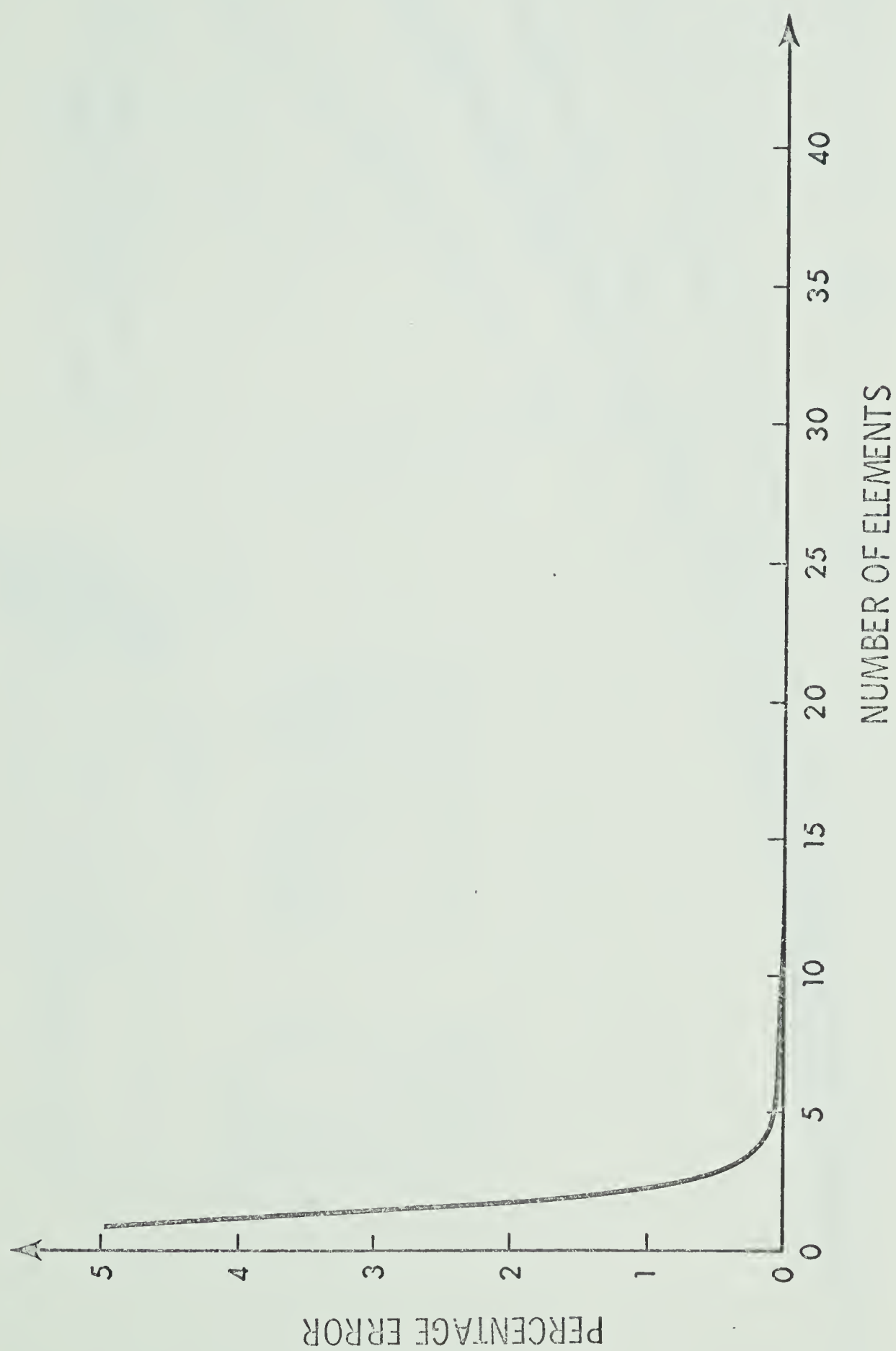


FIGURE 3.4 CONVERGENCE CHARACTERISTICS

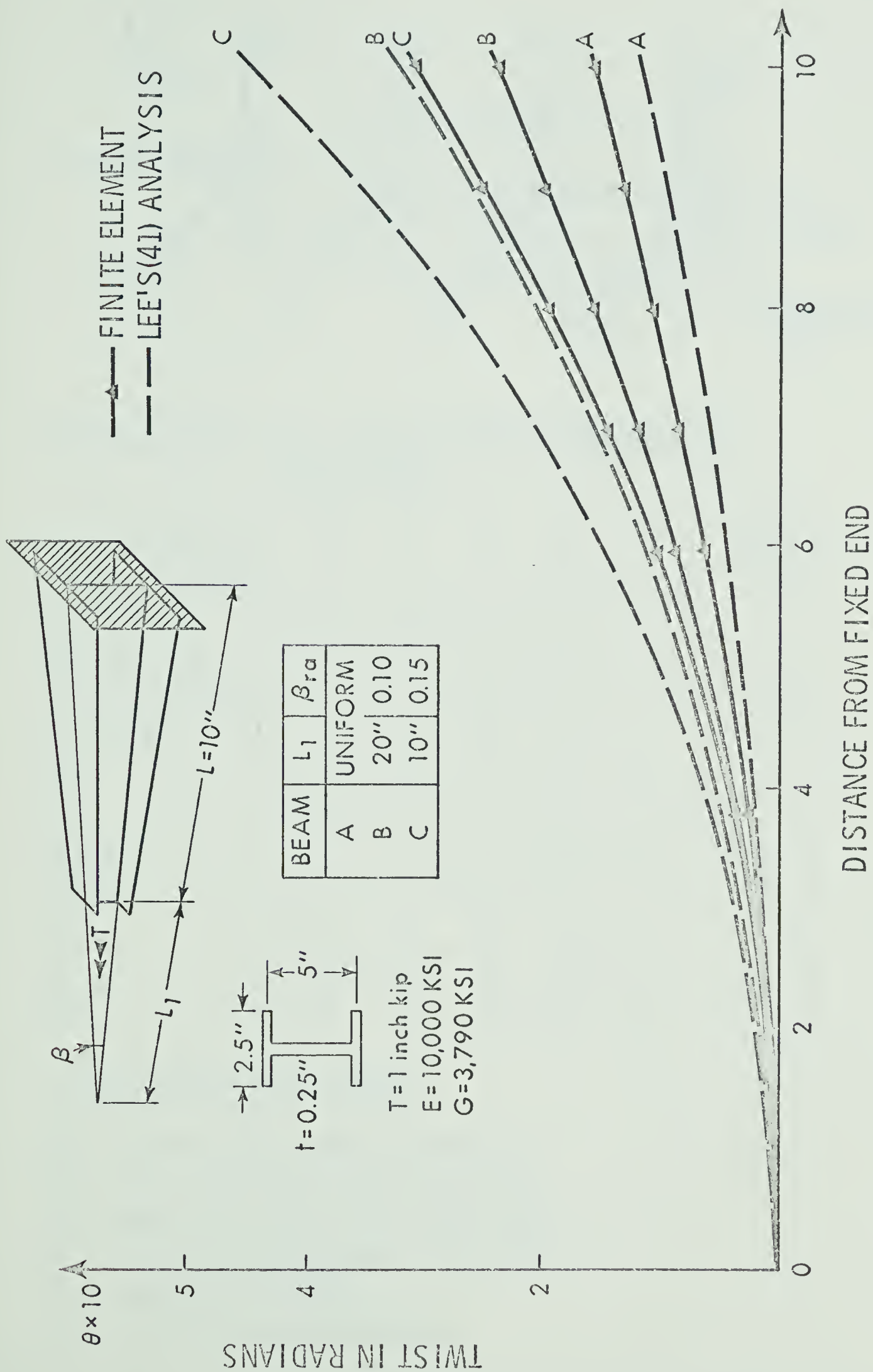
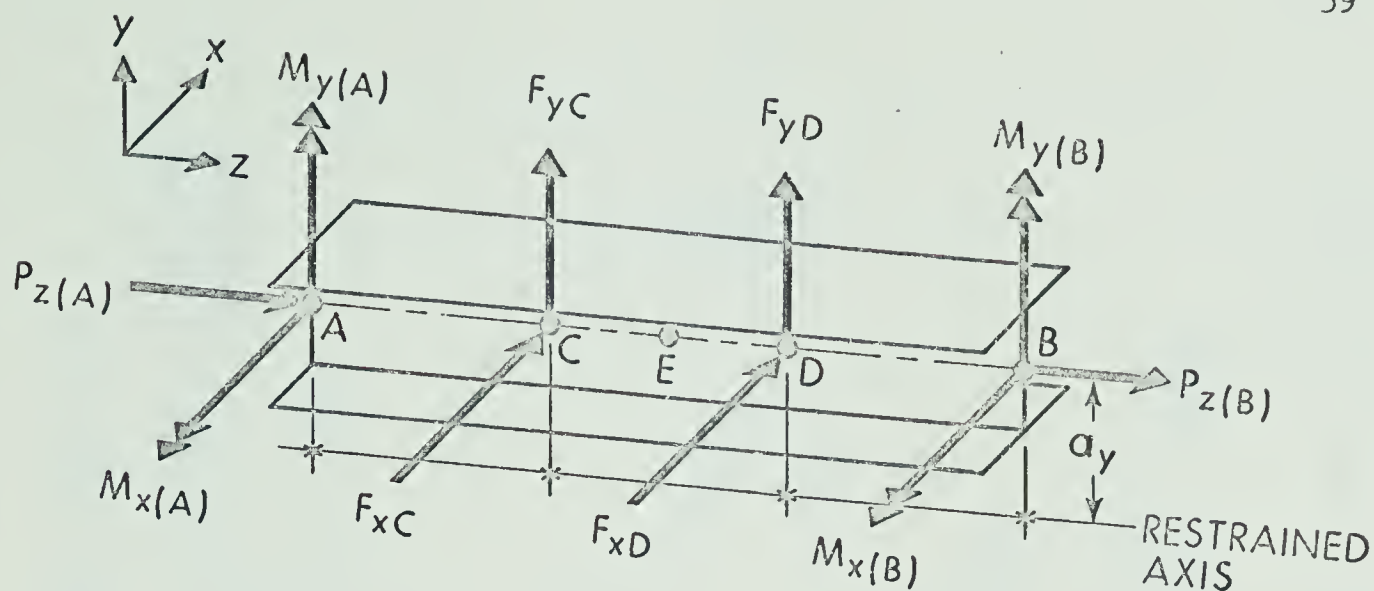


FIGURE 3.5 NON-UNIFORM TORSION OF TAPERED BEAMS



SUPPORT CODE WHEN MARKED DISPLACEMENTS ARE SUPPRESSED

Code \ Degree of freedom	u	v	w	θ_z	θ_y	θ_x	$\frac{d\theta_z}{dz}$
H(HINGE)	X	X	X	X			
R(ROLLER)	X	X		X			
C(CLAMPED)	X	X	X	X	X	X	X
F(FREE)							
HY	X	X	X	X	X		
HX	X	X	X	X		X	
HYW	X	X	X	X	X		X
HXW	X	X	X	X		X	X
U	X						
V		X					
U θ	X			X			

CODE FOR BUCKLING MODE

EW - Euler buckling about weak axis
 ES - Euler buckling about strong axis
 LW - Lateral buckling about weak axis
 LS - Lateral buckling about strong axis
 T - Torsional Buckling
 LTB Lateral torsional buckling

FIGURE 3.6 NOMENCLATURE FOR SUPPORT CONDITION AND BUCKLING MODE

- ▲ FINITE ELEMENT ANALYSIS
 - FROM LINEAR INTERPOLATION OF
VALUES IN P264, TIMOSHENKO(68)
- $cl^2/c_1 = 25.6$

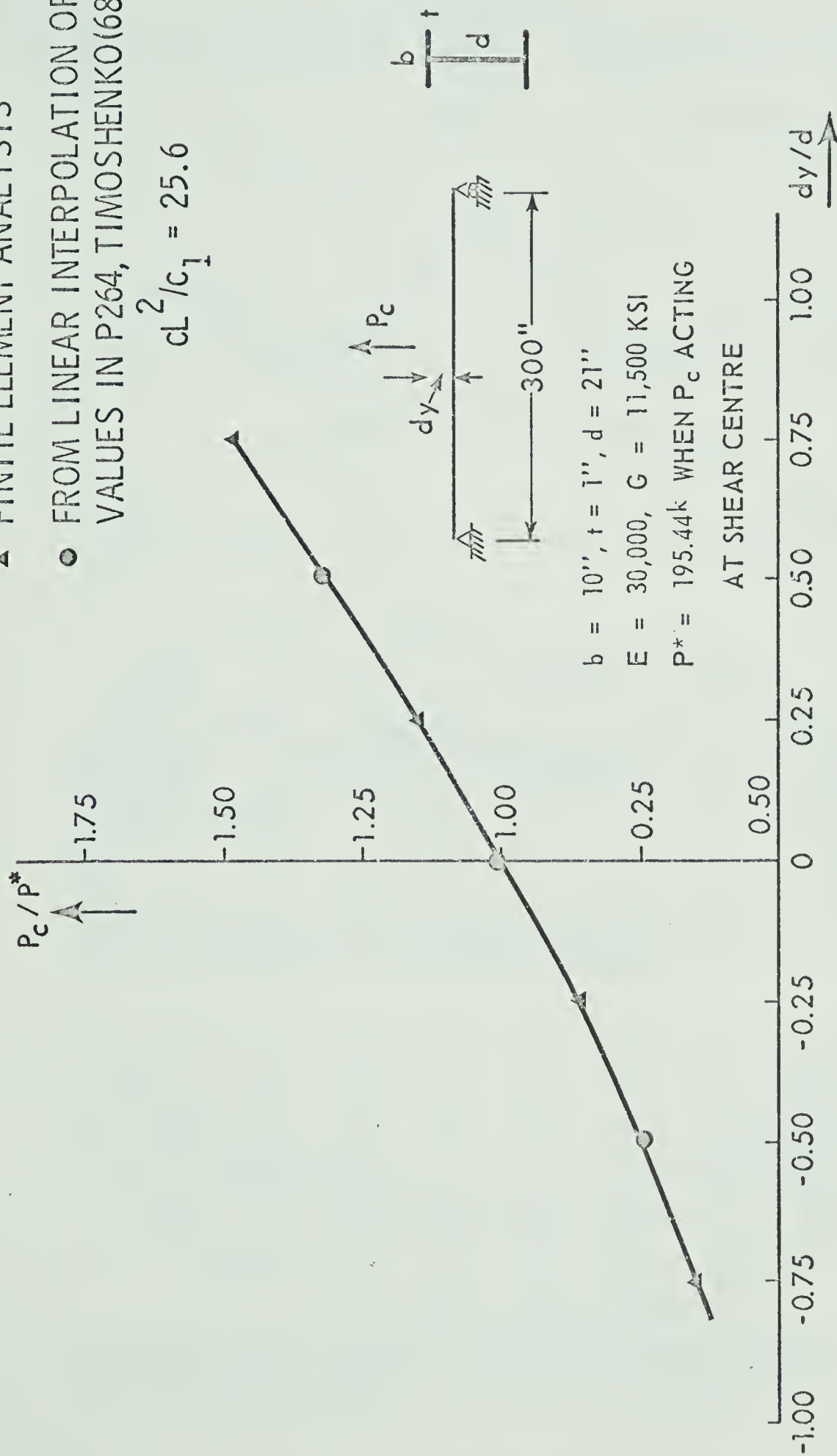
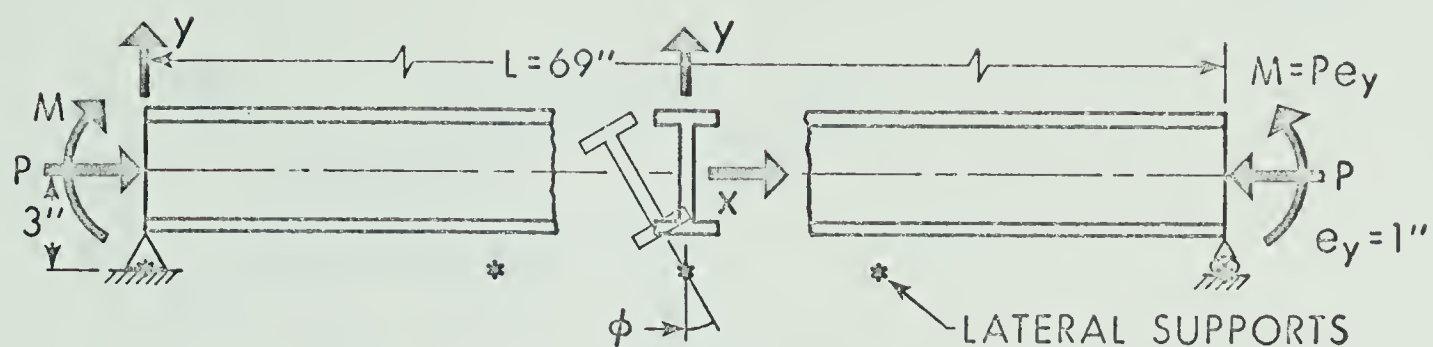
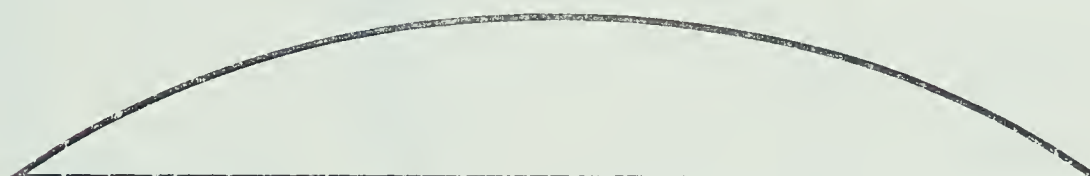
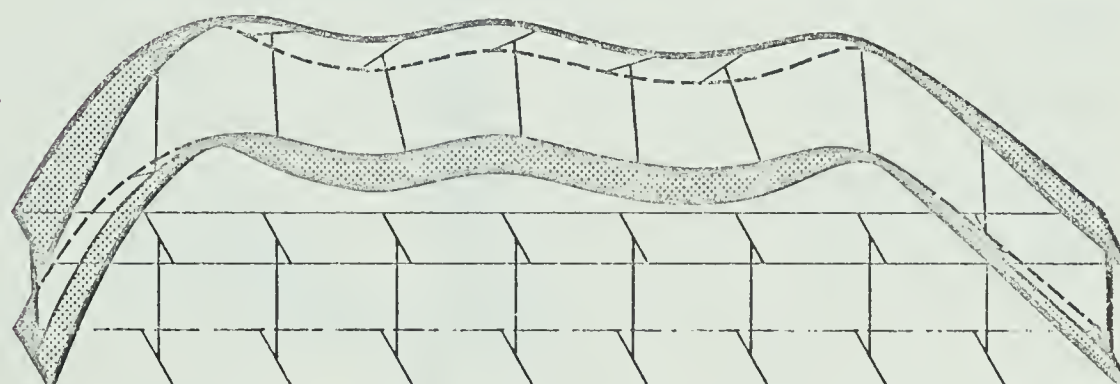


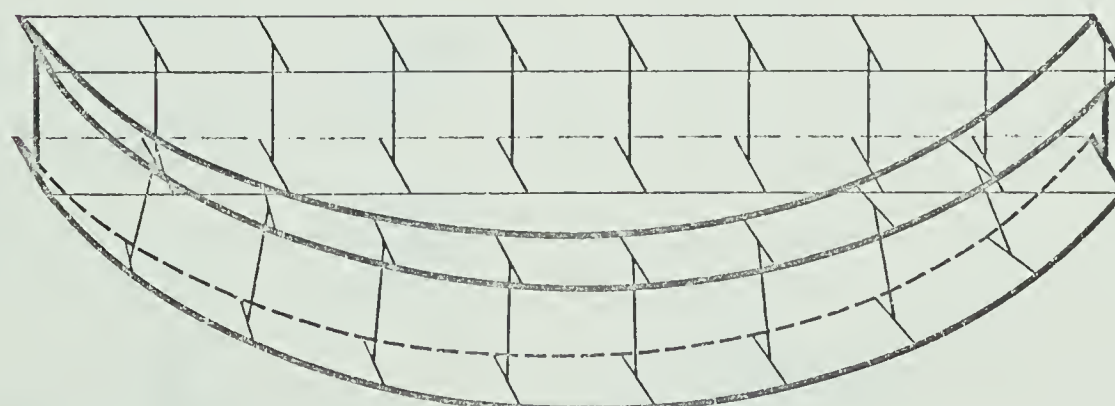
FIGURE 3.7 LATERAL BUCKLING OF A BEAM WHEN LOAD IS ACTING AT d FROM SHEAR-CENTRE y



U-DISPLACEMENT

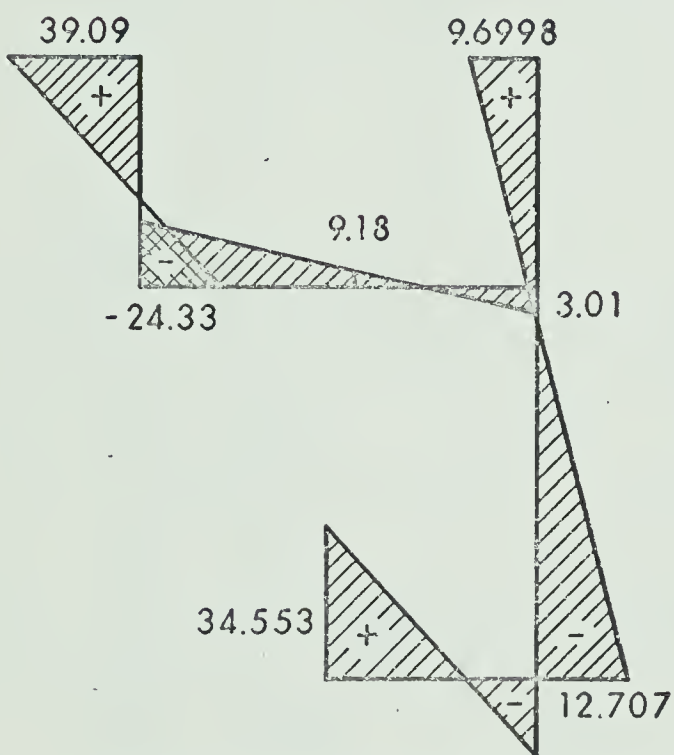
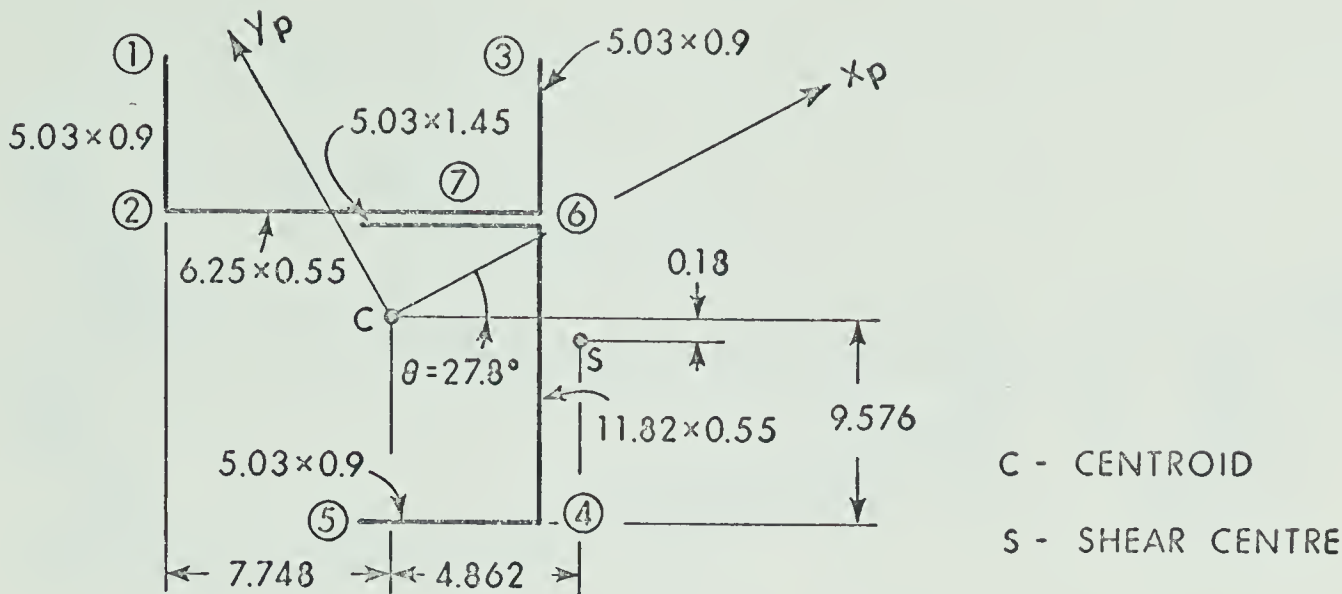
 ϕ -DISPLACEMENT

LATERAL TORSIONAL BUCKLING MODE WHEN ROTATIONS ARE NON-ZERO AT LATERAL SUPPORTS



EULER BUCKLING ABOUT THE MAJOR AXIS WHEN ROTATIONS ARE ZERO AT LATERAL SUPPORTS

FIGURE 3.8 COLUMNS SUPPORTED Laterally BY SIDE RAILS



$I_{xp} = 983.56 \text{ in}^4$
 $I_{yp} = 406.38 \text{ in}^4$
 $C_x = -3.736 \text{ in}$
 $C_y = -14.459 \text{ in.}$
 $I_p = 2119 \text{ in}^4$
 $I_\omega = 4824 \text{ in}^6$
 $C_w = 1.17908$

NORMALIZED WARPING COORDINATE

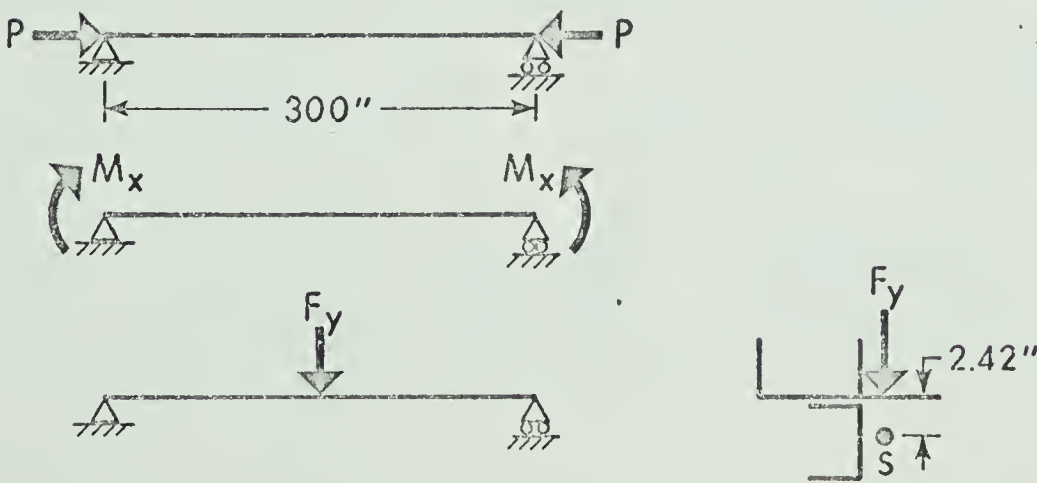
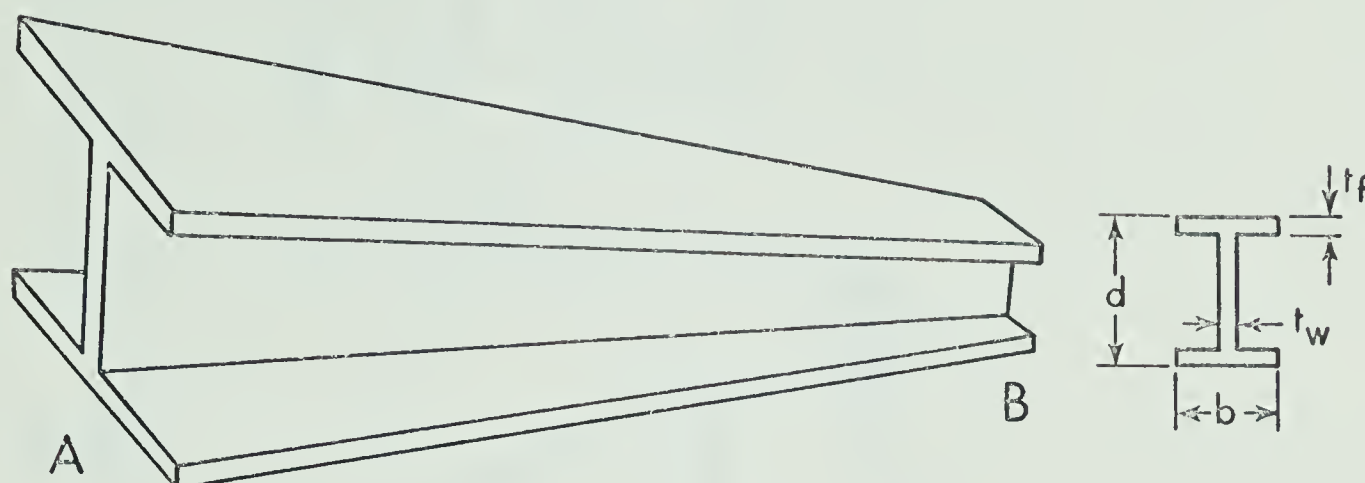


FIGURE 3.9 ELASTIC BUCKLING OF UNSYMMETRICAL SECTION



	A	B	$L = 198''$ $E = 30,000 \text{ ksi}$ $G = 11,500 \text{ ksi}$
d	20''	10''	
b	5''	2.5''	
t_f	0.3125''	0.3125''	
t_w	0.25''	0.25''	

Example	Support		Loading		Critical Load	% Error	Ref	B.M
	A	B	A	B				
E7	HYW	H		$P_z = -P$	37.87K	4.93	17	EW
E8	HYW	H	$M_x = -M$		1035.0''K	-9.21	17	LW

FIGURE 3.10 BUCKLING OF TAPERED BEAM-COLUMN

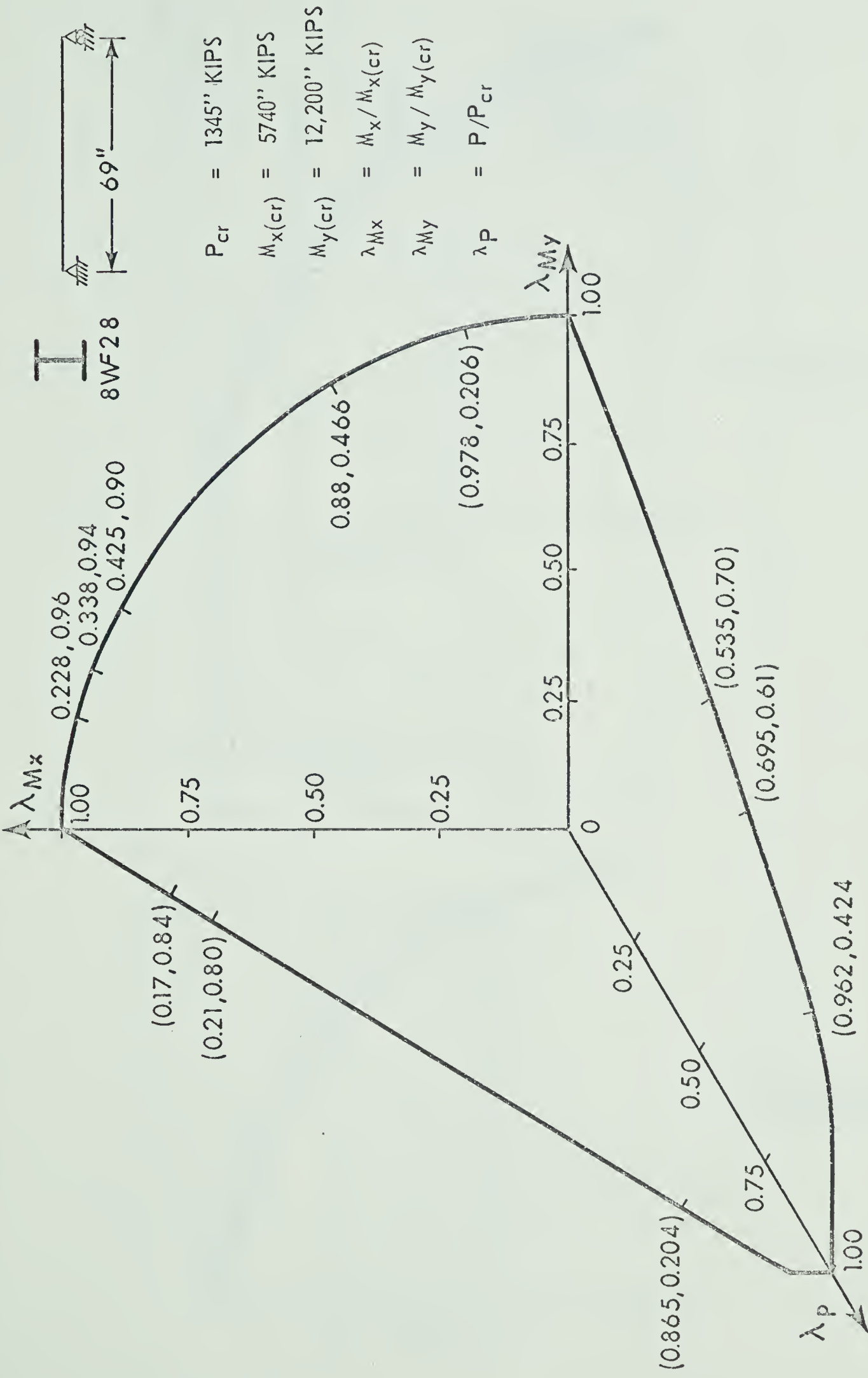


FIGURE 3.11 INFLUENCE BUCKLING SURFACE FOR WIDE FLANGE BEAM

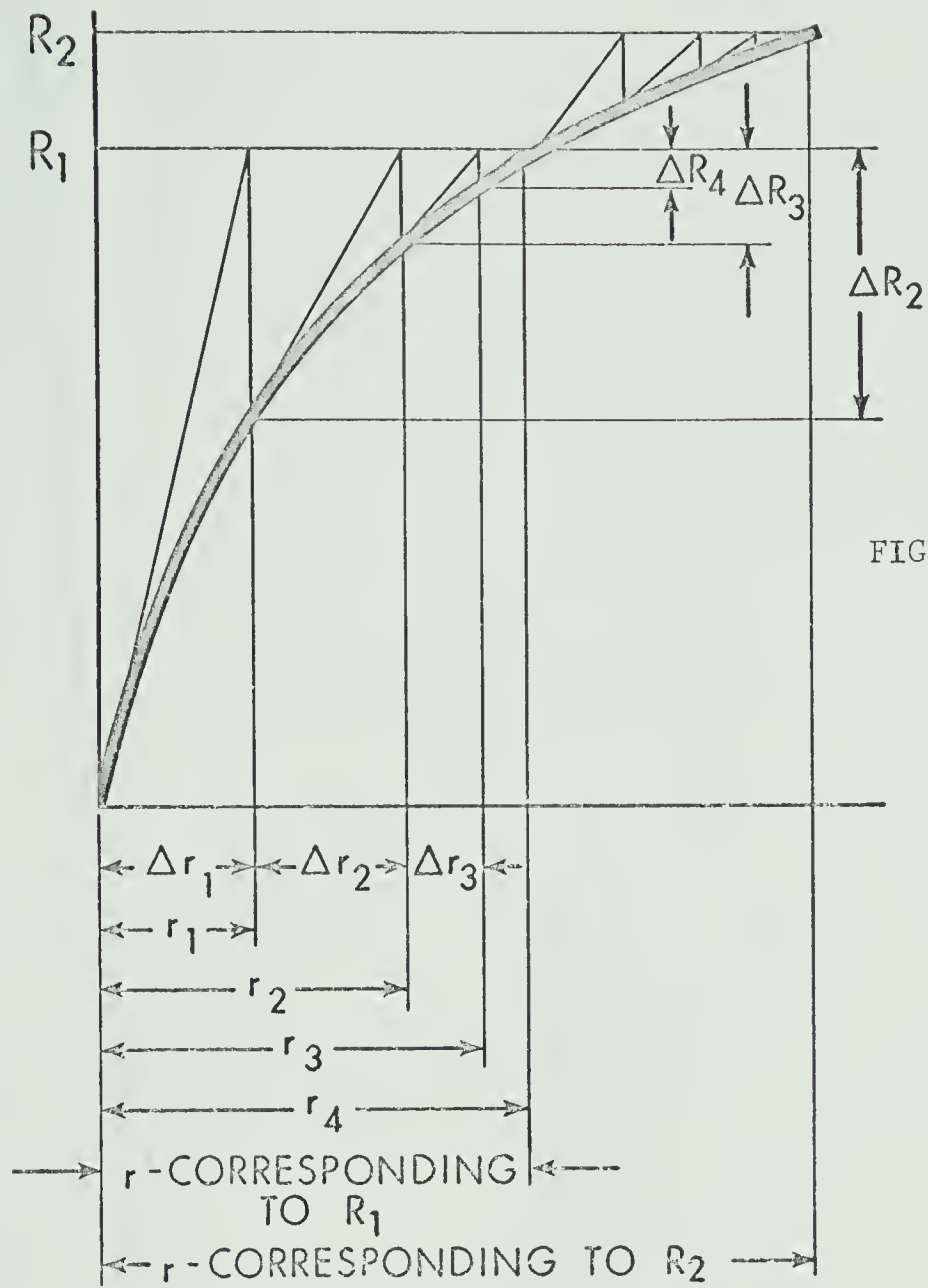


FIGURE 3.12a A NEWTON-RAPHSON METHOD

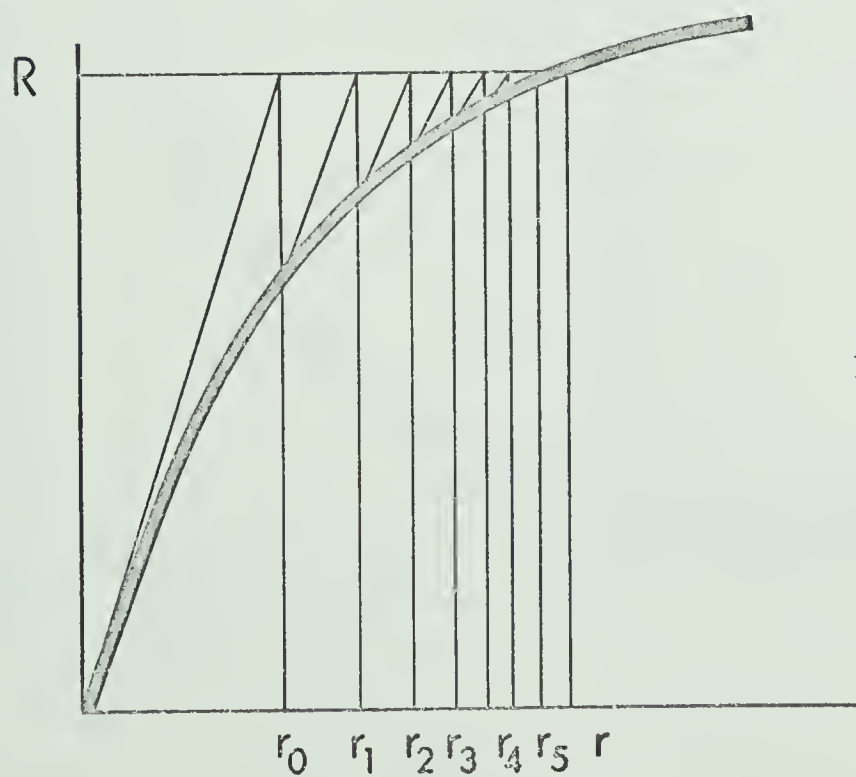


FIGURE 3.12b MODIFIED NEWTON-RAPHSON METHOD

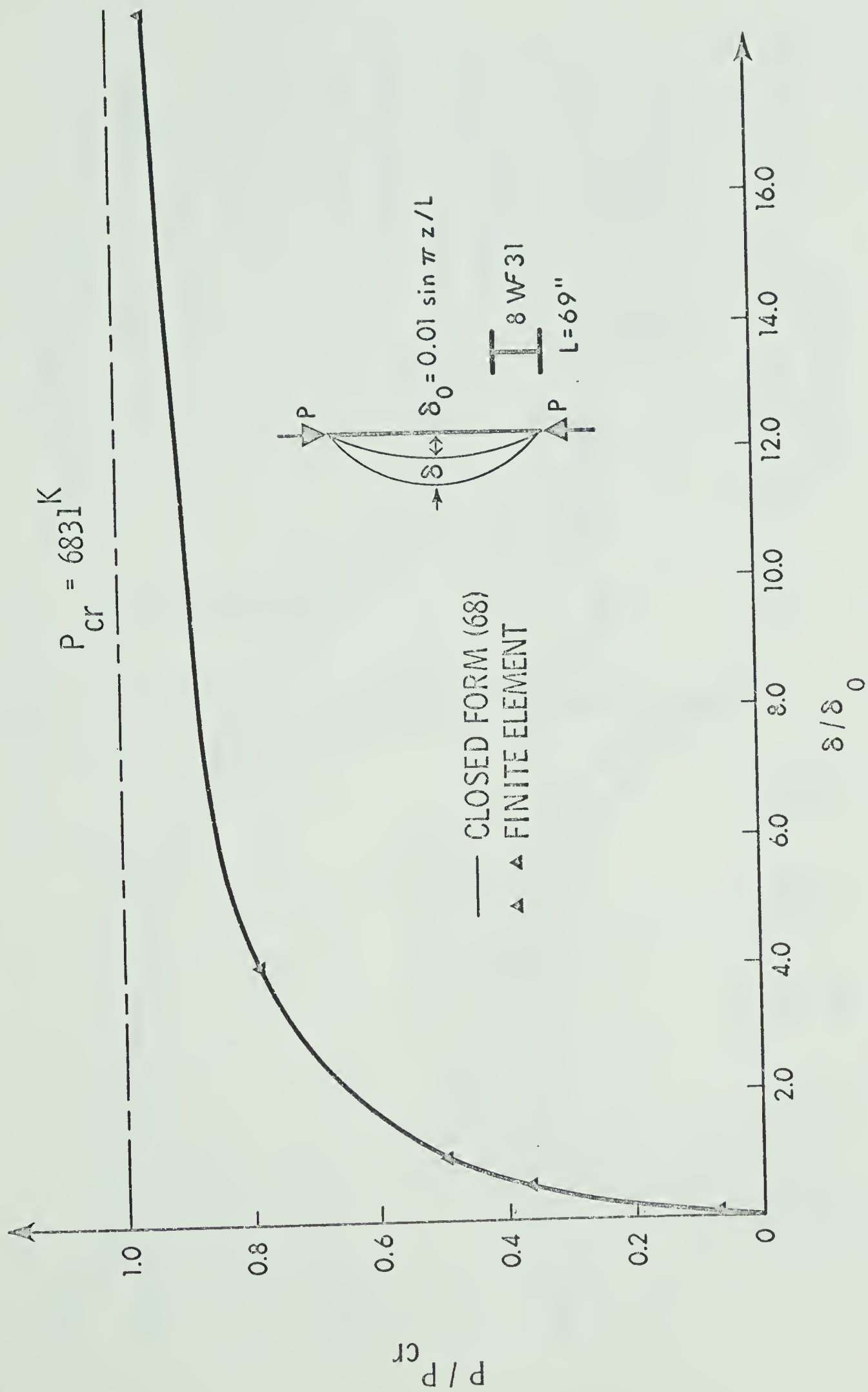


FIGURE 3.13 COLUMN WITH INITIAL IMPERFECTION

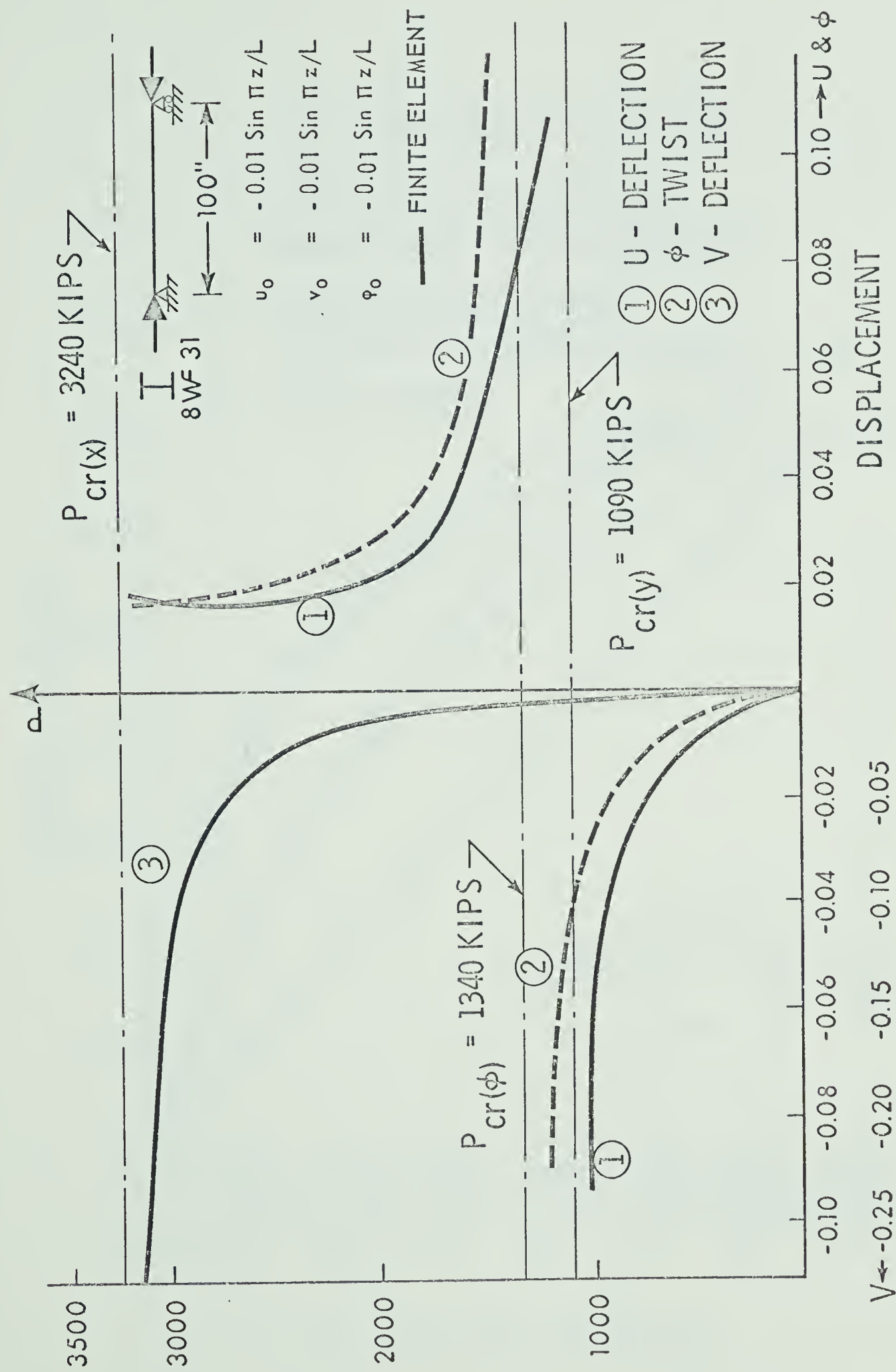


FIGURE 3.14 LOAD DEFLECTION RESPONSE OF AN INITIALLY IMPERFECT COLUMN

Critical Moment 4862.4 Inch Kips

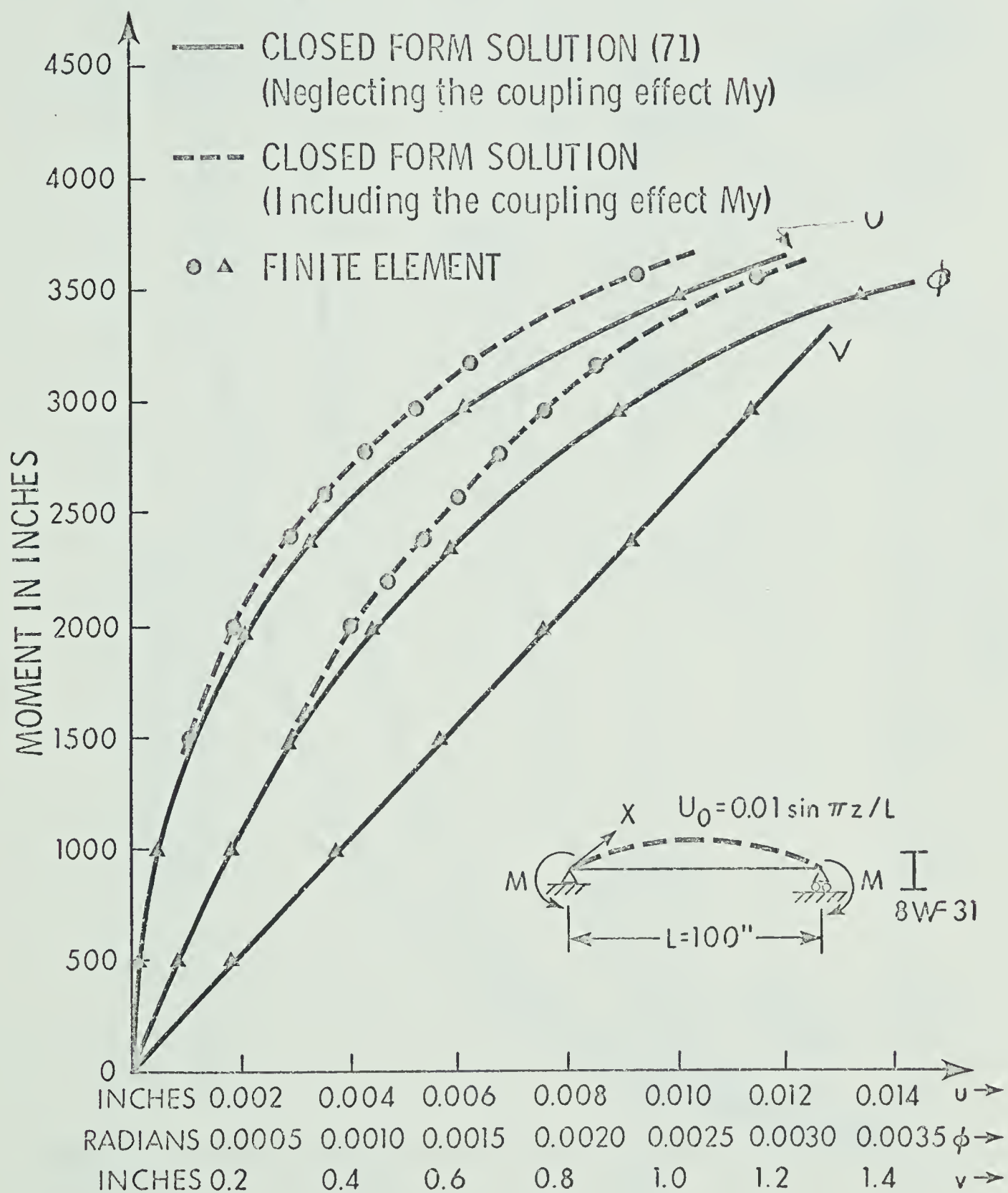


FIGURE 3.15 BEAM WITH INITIAL IMPERFECTION

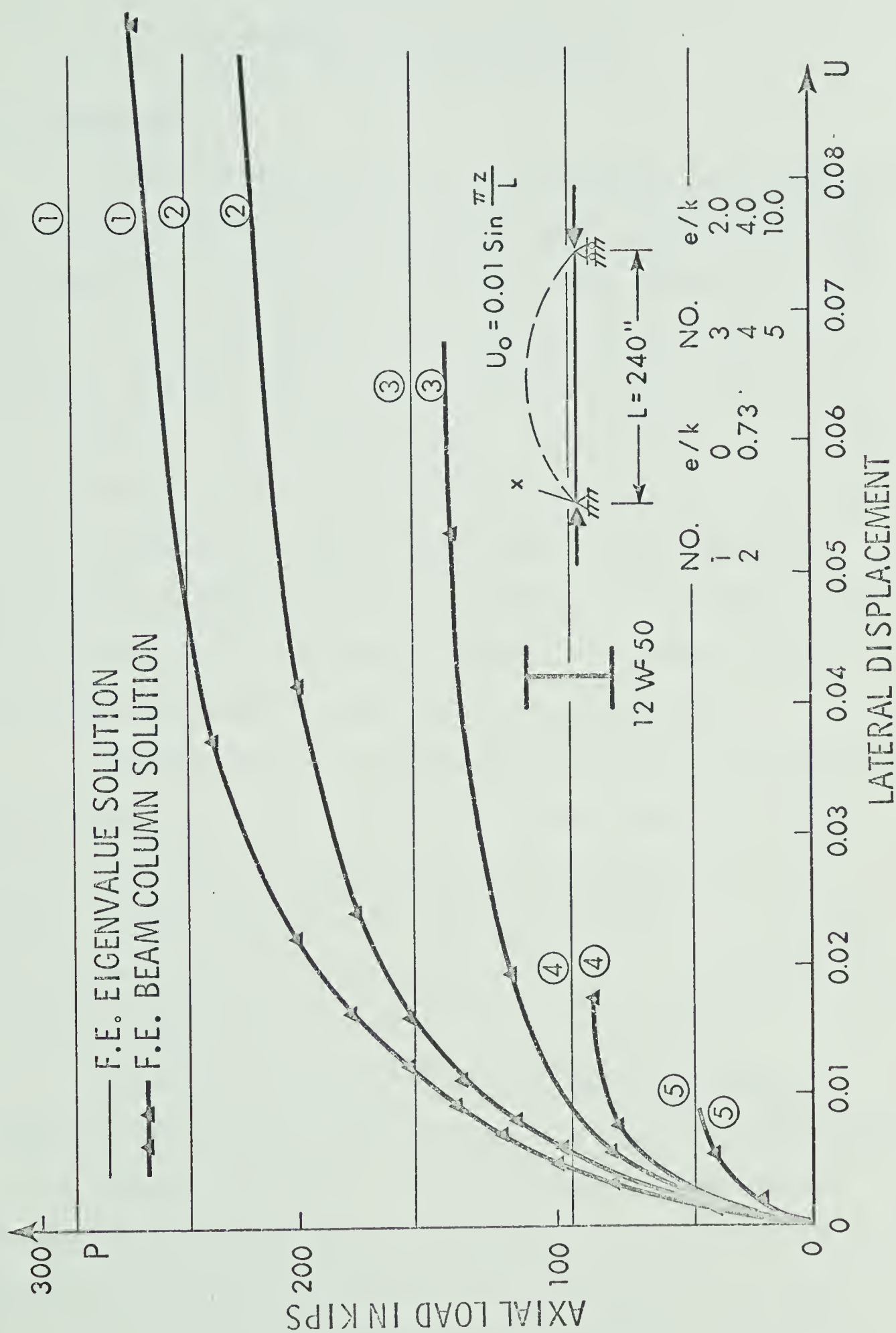


FIGURE 3.16 COLUMN WITH SINUSOIDAL IMPERFECTION

CHAPTER IV

LOCAL BUCKLING OF ELASTIC SECTIONS

4.1 Introduction

Thin-walled beams are made up of relatively thin plates, and under certain conditions, these plates may experience local buckling. Local buckling in combination with other buckling behaviour is often observed in failure of members. Local buckling of the various plate components, of which heavy structural sections consist, needs rarely to be considered, because these sections are proportioned so that they will not buckle locally at stresses below the yield point. However, with the introduction of high strength steels, sections which had previously been immune to local buckling prior to yield may no longer be so. In addition cold rolled steel shapes, and aluminum shapes often have proportions such that local buckling may occur.

Buckling theories of thin-walled members have been separately developed for member and local buckling. Member buckling is based on the assumption that the cross section does not distort while local buckling naturally involves a distortion of the section. In practice these phenomena may not be independent and hence it is reasonable to investigate conditions where both may occur simultaneously.

Bleich (13) studied the flexural torsional buckling of T-shaped stiffeners including the deformation of the web. Goldberg (27), et. al., presented a systematic buckling analysis, for members with arbitrary cross-sectional shape, considering the cross-sectional deformation, by starting with the usual plate and membrane equations, and arriving at eight first order simultaneous partial differential

equations. Their procedure consists of selecting a trial value of axial load and moment and evaluating the determinant of the final equations. The determinant will be zero if the trial values are chosen correctly. If not, a new set of trial values is chosen. Results of some specific examples were presented. For the shapes of sections which they studied, local buckling was critical for the lower slenderness ratios and occurred at a much lower stress than member buckling. Kollbrunner (39), et. al., treated the thin-walled beam using folded plate theory of structures. They arrived at the solution by solving a system of differential equations.

In this chapter, a general procedure for deriving virtual work equations is employed, which is suitable for determining the flexural and geometric stiffnesses, considering distortion of the cross-section. The matrices, however, are evaluated only for elastic prismatic symmetric wide flange sections.

4.2 Assumptions

In addition to the assumptions made in Chapter II the following assumptions are also made.

1. The original angle between the adjacent plates at their common edge is maintained during buckling.
2. Kirchhoff's hypothesis remains valid for each plate segment.

Assumption 2 of Section 2.2 is no longer applicable.

4.3 Equilibrium equations by virtual work including distortion of the section

4.3.1 General Equations

The virtual work form of the total equilibrium equations,

was expressed in Section 2.3, Equations 2-17 and 2-18, as

$$\delta(I_1 + I_2 - I_3) = 0 \quad (4-1)$$

where,

$$I_1 = \int_V \sigma_{ij} u_{i,j} dV \quad (4-2a)$$

$$I_2 = \frac{1}{2} \int_V \sigma_{ij} u_{k,i} u_{k,j} dV \quad (4-2b)$$

$$I_3 = \int_S t_i u_i dS \quad (4-2c)$$

The displacement at any point of the thin-walled beam cross-section may be considered as the sum of beam displacements and the individual plate deformations, i.e.

$$u_i = u_i^B + u_i^P \quad (4-3a)$$

Similarly the stresses σ_{ij} can be written as the sum of the stresses due to beam action σ_{ij}^B , and due to plate action, σ_{ij}^P .

$$\sigma_{ij} = \sigma_{ij}^B + \sigma_{ij}^P \quad (4-3b)$$

For the model adopted, the stress and displacements due to beam action are assumed to be uniform across the thickness whereas the stresses and displacements due to plate action are proportional to the distance from the middle surface of the plate in a manner consistent with Kirchhoff's hypothesis.

The derivation of the equilibrium equations, which couples the effects of cross-section distortion to the beam equations, may now

be carried out by evaluating the expressions in Equations 4.2. This is done below in Sections 4.3.2 to 4.3.4.

4.3.2 Evaluation of I_1

The integral I_1 of Equation 4-1 may be evaluated by substituting Equations 4-3a and 4-3b into Equation 4-2a.

$$I_1 = \int_V \sigma_{ij}^B u_{i,j}^B dV + \int_V \sigma_{ij}^P u_{i,j}^P dV \quad (4-4a)$$

$$= I_1^B + I_1^P \quad (4-4b)$$

where because of the linear variation of σ_{ij}^P and $u_{i,j}^P$

$$\int \sigma_{ij}^B u_{i,j}^P = \int \sigma_{ij}^P u_{i,j}^B = 0 \quad (4-4c)$$

Using the definition of stress resultants from Equations 2-1 these integrals may be written as

$$I_1^B = \int_0^{\ell} (Pw'_c - M_x v''_s - M_y u''_s + W_\omega \phi'' + T_{sv} \phi') dz \quad (4-5a)$$

$$I_1^P = - \sum_{i=1}^n \int_A (M_\alpha^P \chi_\alpha + M_\beta^P \chi_\beta + 2M_{\alpha\beta}^P \chi_{\alpha\beta})_i dA \quad (4-5b)$$

where A denotes the middle area of the plate; the summation is carried out for all plates; and χ_α , χ_β , $\chi_{\alpha\beta}$ denote the curvatures of the middle surface of the plate in the α and β local plate co-ordinate directions, shown in Fig. 4.1.

4.3.3 Evaluation of I_2

Integral I_2 of Equation 4-2b may be evaluated as follows,

neglecting the effect of σ_{ij}^P

$$I_2 = I_2^B + I_2^P + I_2^{BP} \quad (4-6)$$

where

$$I_2^B = \frac{1}{2} \int_V \sigma_{ij}^B u_{k,i}^B u_{k,j}^B dV \quad (4-7a)$$

$$I_2^P = \frac{1}{2} \int_V \sigma_{ij}^B u_{k,i}^P u_{k,j}^P dV \quad (4-7b)$$

$$I_2^{BP} = \int_V \sigma_{ij}^B u_{k,i}^B u_{k,j}^P dV \quad (4-7c)$$

and the symmetry of the stress tensor has been used in expression for I_2^{BP} .

Using the notation of Chapter II, Equation 4-7a becomes,

$$I_2^B = \frac{1}{2} \int_0^{\ell} (-2V_y \phi u_s' + 2V_x \phi v_s' + P(u_s'^2 + v_s'^2 + 2e_y u_s' \phi' - 2e_x v_s' \phi') + 2M_y v_s' \phi' - 2M_x u_s' \phi' + M_\rho \phi'^2) dz \quad (4-8)$$

Considering only the normal stresses in the z-direction; retaining only the out of plane plate displacement gradients (see Felippa (19)); and neglecting the effect of in-plane shears; Equation 4-7b may be written as

$$I_2^P = \sum_{i=1}^n \left[\frac{1}{2} \int_A \sigma_z^B \{ (u_{,z}^P)^2 + (v_{,z}^P)^2 \} dA \right]_i \quad (4-9)$$

Similarly Equation 4-7c becomes

$$I_2^{BP} = \sum_{i=1}^n \left[\int_V \sigma_z^B (u_{,z}^P u_{,z}^B + v_{,z}^P v_{,z}^B) dV \right]_i \quad (4-10)$$

4.3.4 Evaluation of I_3

If surface loads are regarded as line loads the integral I_3 remains as in Chapter II, and is expressed as Equation A-48 of Appendix A.

4.3.5 Expression for total virtual work

Substituting the expressions for I_1 , I_2 , I_3 into Equation 4-1 yields,

$$\delta \left[\int_0^\ell (P w'_c - M_x v''_s - M_y u''_s + W_\omega \phi'' + T_{sv} \phi') dz \right] \quad (4-11)$$

$$- \sum_{i=1}^n \int_A (M_\alpha^P \chi_\alpha + M_\beta^P \chi_\beta + 2M_{\alpha\beta}^P \chi_{\alpha\beta})_i dA$$

$$+ \frac{1}{2} \int_0^\ell \{ (-2V_y \phi u'_s + 2V_x \phi v'_s + p(u_s'^2 + v_s'^2 + 2e_y u'_s \phi' - 2e_x v'_s \phi'))$$

$$+ 2M_y v'_s \phi' - 2M_x u'_s \phi' + M_\rho \phi'^2 \} dz$$

$$+ \sum_{i=1}^n \left[\frac{1}{2} \int_A \sigma_z^B t \{ (u_{,z}^P)^2 + (v_{,z}^P)^2 \} dA + \int_V \sigma_z^B (u_{,z}^P u_{,z}^B + v_{,z}^P v_{,z}^B) dV \right]_i$$

$$- \int_S t_i u_i dS] = 0$$

Equation 4-11 applies to any thin-walled beam of open section, composed

of flat plate segments, for both elastic and inelastic response. The terms in Equation 4-11 arising from Equation 4-5a, I_1^B , give rise to the beam flexure tangent stiffness matrix, for inelastic response, and the conventional beam flexure stiffness matrix for elastic response. Those arising from Equation 4-5b give rise to the flexural stiffness matrix for plate bending. Equations 4-7a and 4-7b lead to the geometric stiffness matrix for the work done by the initial stress state on the out of plane beam and plate deformations, respectively, whereas Equation 4-7c represents the coupling effect between plate and beam stresses and deformations.

4.4 Specialization for Elastic WF Sections

For elastic response the conventional beam stress resultants appearing in Equation 4-11 are defined in Chapter II. The stress resultants, M_α^P , M_β^P , $M_{\alpha\beta}^P$ for the plate segments may be expressed as (see Fig. 4.1)

$$M_\alpha^P = -D (\chi_\alpha + \nu \chi_\beta) \quad (4-12a)$$

$$M_\beta^P = -D (\chi_\beta + \nu \chi_\alpha) \quad (4-12b)$$

$$M_{\alpha\beta}^P = -D (1 - \nu) \chi_{\alpha\beta} \quad (4-12c)$$

where ν is poisson's ration and $D = E t^3 / 12 (1 - \nu^2)$ (4-13)

Assuming a symmetric WF shape and designating the out of plane plate segment displacements by v_t^P , v_b^P and u_w^P as shown in Fig. 4.2; expressing the curvatures in Equation 4-11 in terms of the derivatives of these displacements; expressing the stress resultants, in the first set of braces in Equation 4-11, in terms of displacements; and,

approximating σ_z^B by the normal beam equation (the first three terms of Equation A-51); the component expressions of Equation 4-11 becomes

$$\delta(I_1^B) = \delta\left[\frac{1}{2} \int_0^{\ell} \{EA w_c'^2 + EI_x v_s''^2 + EI_y u_s''^2 + EI_w \phi''^2 + GK\phi'^2\} dz\right] \quad (4-14a)$$

$$\begin{aligned} \delta(I_1^P) = & \delta\left[\frac{D_t}{2} \int_A \{ (v_{t,zz}^P + v_{t,xx}^P)^2 - 2(1-\nu)(v_{t,xx}^P v_{t,zz}^P - \right. \\ & \left. (v_{t,xz}^P)^2) \} dz dx + \frac{D_b}{2} \int_A \{ (v_{b,zz}^P + v_{b,xx}^P)^2 - 2(1-\nu)(v_{b,xx}^P v_{b,zz}^P - \right. \\ & \left. (v_{b,xz}^P)^2) \} dx dz + \frac{D_w}{2} \int_A \{ (u_{w,yy}^P + u_{w,zz}^P)^2 - 2(1-\nu) \right. \\ & \left. (u_{w,yy}^P u_{w,zz}^P - (u_{w,yz}^P)^2) \} dy dz\right] \quad (4-14b) \end{aligned}$$

$$\begin{aligned} \delta(I_2^B) = & \delta\left[\frac{1}{2} \int_0^{\ell} \{-2V_y \phi u_s' + 2\phi V_x v_s' + P(u_s'^2 + v_s'^2 \right. \\ & \left. + \frac{I_p}{A} \phi'^2) + 2M_y v_s' \phi' - 2M_x \phi' u_s'\} dz\right] \quad (4-14c) \end{aligned}$$

$$\begin{aligned} \delta(I_2^P) = & \delta\left[\frac{1}{2} \int_V \left\{ \left(\frac{P}{A} + \frac{M_x d_w}{2I_x} + \frac{M_y X}{I_y} \right) (v_{t,z}^P)^2 \right. \right. \\ & \left. \left. + \left(\frac{P}{A} - \frac{M_x d_w}{2I_x} + \frac{M_y X}{I_y} \right) (v_{b,z}^P)^2 \right. \right. \\ & \left. \left. + \left(\frac{P}{A} + \frac{M_x Y}{I_x} \right) (u_{w,z}^P)^2 \right\} dV\right] \quad (4-14d) \end{aligned}$$

$$\begin{aligned}
\delta(I_2^{BP}) = & \delta \left[\int_V \left\{ \left(\frac{P}{A} + \frac{M_x d_w}{2I_x} + \frac{M_y X}{I_y} \right) v_{t,z}^p (v_{s,z} + x \phi_{,z}) \right. \right. \\
& + \left(\frac{P}{A} - \frac{M_x d_w}{2I_x} + \frac{M_y X}{I_y} \right) v_{b,z}^p (v_{s,z} + x \phi_{,z}) \\
& \left. \left. + \left(\frac{P}{A} + \frac{M_x Y}{I_x} \right) u_{w,z}^p (u_{s,z} - y \phi_{,z}) \right\} \right] dv \quad (4-14e)
\end{aligned}$$

Where the local coordinate system is shown in Fig. 4.2; u and v refer to X and Y coordinate directions; the subscripts b, t and w refer to 'bottom flange', 'top flange' and 'web' respectively; the superscript P indicates plate bending displacement; and, u_s , v_s , ϕ and w_c refer to beam bending displacements.

4.5 Finite Element Model

The plate segment displacements for a wide flange beam are assumed to be represented by the shape functions shown in Fig. 4.3. These functions imply that on any section perpendicular to the longitudinal axis the flange remains straight. With this model there are four degrees of freedom associated with cross section distortion at each node, in addition to the seven degrees of freedom associated with beam action at each node. The sketches in Fig. 4.3 show the deflected shape of the I-section due to unit values of the generalized displacement coordinates corresponding to each degree of freedom of the top flange while the others are kept zero. Shape functions for the bottom flange are similar to those for the top flange.

The plate displacements v_t^p can be written in terms of the nodal displacements as

$$v_t^p = \xi \begin{Bmatrix} (1 + 2\zeta^3 - 3\zeta^2) \\ (\zeta - 2\zeta^2 + \zeta^3) \\ (3\zeta^2 - 2\zeta^3) \\ (\zeta^3 - \zeta^2) \end{Bmatrix}^T \begin{Bmatrix} (v_t^p)_1 \\ \ell(v_{t,z}^p)_1 \\ (v_t^p)_2 \\ \ell(v_{t,z}^p)_2 \end{Bmatrix} \quad (4-15)$$

where ξ and ζ and η are the dimensionless parameters illustrated in Fig. 4.2, and expressed as

$$\xi = 2x/b_f; \quad \zeta = z/\ell; \quad \eta = 2y/d_w \quad (4-16)$$

and $(v_t^p)_1$, $\ell(v_{t,z}^p)_1$, $(v_t^p)_2$, $\ell(v_{t,z}^p)_2$ are the nodal values of the generalized coordinates as shown in Fig. 4.3.

Denoting the set of shape functions by, $\langle k_\zeta \rangle$ the displacements in the top and bottom flanges are expressed as

$$\begin{Bmatrix} v_t^p \\ v_b^p \end{Bmatrix} = \xi \begin{bmatrix} \langle k_\zeta \rangle & 0 \\ 0 & \langle k_\zeta \rangle \end{bmatrix} \begin{Bmatrix} \underline{v_t^p} \\ \underline{v_b^p} \end{Bmatrix} \quad (4-17)$$

Where $\underline{v_t^p}$ and $\underline{v_b^p}$ represent the vectors of generalized nodal coordinates.

Since the angle at the junction of the web and the flange remains unchanged

$$\theta_{t1}^w = \theta_{t1} = 2/b_f \{ (v_t^p)_{\xi=1} \} \quad (4-18)$$

Where θ_{t1}^w is the rotation at the top of the web, and θ_{t1} is the top flange rotation at node, 1. Using a similar notation at the bottom junction we may write these rotations along the element length as

$$\begin{Bmatrix} \theta_t d_w \\ \theta_b d_w \end{Bmatrix} = \frac{2d_w}{b_f} \begin{bmatrix} \langle k_\zeta \rangle & 0 \\ 0 & \langle k_\zeta \rangle \end{bmatrix} \begin{Bmatrix} \frac{v_t^p}{-t} \\ \frac{v_b^p}{-b} \end{Bmatrix} \quad (4-19)$$

Where anti-clockwise rotation is assumed as positive for the web, b_f is the flange width and d_w is the depth of the web.

Choosing the local coordinate system at the centre of the web, as shown in Fig. 4.2, the web displacements are expressed as

$$u_w^p = \frac{1}{8} \begin{Bmatrix} (1 + \eta) & (1 - \eta^2) \\ (\eta - 1) & (1 - \eta^2) \end{Bmatrix}^T \begin{Bmatrix} \theta_t d_w \\ \theta_b d_w \end{Bmatrix} \quad (4-20)$$

and using Equation 4-19, Equation 4-20 may be expressed in terms of the generalized coordinates, as

$$u_w^p = \frac{d_w}{4b_f} \begin{Bmatrix} (1 + \eta) & (1 - \eta^2) \\ (\eta - 1) & (1 - \eta^2) \end{Bmatrix}^T \begin{bmatrix} \langle k_\zeta \rangle & 0 \\ 0 & \langle k_\zeta \rangle \end{bmatrix} \begin{Bmatrix} \frac{v_t^p}{-t} \\ \frac{v_b^p}{-b} \end{Bmatrix} \quad (4-21)$$

Substituting the distributed displacements, in terms of nodal coordinates, into Equations 4-14 and integrating, we may write the element equilibrium relationship between the generalized forces and generalized displacements in the symbolic form

$$[[k_S] + [k_G]] \{r_E\} = \{R_E\} \quad (4-22)$$

where the matrices are derived in Appendix C and have the following structure.

$$[k_S] = \begin{bmatrix} k_{uu} & & & & \\ & k_{vv} & & & \\ & & k_{\phi\phi} & & \\ & & & k_{ww} & \\ & & & & k_{ll} \end{bmatrix} \quad (4-23a)$$

$$[k_G] = \begin{bmatrix} g_{uu} & \cdot & g_{u\phi} & \cdot & g_{ul} \\ & g_{vv} & g_{v\phi} & \cdot & g_{vl} \\ g_{\phi u} & g_{\phi v} & g_{\phi\phi} & \cdot & g_{\phi l} \\ \cdot & \cdot & \cdot & \cdot & \cdot \\ g_{lu} & g_{lv} & g_{l\phi} & \cdot & g_{ll} \end{bmatrix} \quad (4-23b)$$

and

$$\langle r_E \rangle = \langle \underline{u} \rangle \langle \underline{v} \rangle \langle \underline{\phi} \rangle \langle \underline{w} \rangle \langle \underline{l} \rangle \quad (4-23c)$$

The nodal vectors \underline{u} , \underline{v} , $\underline{\phi}$, and \underline{w} have been defined in Chapter II and nodal vector \underline{l} corresponds to the eight degrees of freedom associated with local buckling i.e.:

$$\{\ell\}^T = \langle v_{t1}^p, \ell(v_{t,z}^p)_1, v_{b1}^p, \ell(v_{b,z}^p)_1, v_{t2}^p, \ell(v_{t,z}^p)_2, v_{b2}^p,$$

$$\ell(v_{b,z}^p)_2 \rangle \quad (4-24)$$

Upon assembly, the equilibrium equations for the whole structure may be written as,

$$[[K_S] + [K_G]] \{r\} = \{R\} \quad (4-25)$$

The buckling problem arises from the variation of the homogeneous matrix equation in the form

$$[[K_S] + [K_G]] \{\Delta r\} = 0 \quad (4-26a)$$

or

$$([K_S] + \lambda[\bar{K}_G]) \{\Delta r\} = 0 \quad (4-26b)$$

Solving the above eigenvalue equation for the unknown value λ and multiplying it by the nominal stress distribution yields the critical stress.

4.6 Illustrative Solutions

E-1 Local Buckling of Plates

To test the plate buckling representation a number of problems were solved without coupling the local buckling to member buckling. In Table 4.1 the solutions for buckling of plates for various boundary conditions are compared with the closed form solutions. The nomenclature of Table 4.1 is indicated in Fig. 4.4. The buckling of a single plate can be simulated by setting the thickness of the other plates to zero. The model yields good results for flange plate buckling but is too stiff to yield accurate results for web plate buckling since only a linear variation curvature can be represented across the plate.

E-2 Uncoupled Local Buckling of Columns subjected to an Axial Load

Fig. 4.5 shows the results obtained when an axial load is applied to a symmetric wide-flange column of constant thickness and the critical local buckling load (uncoupled solution) is calculated for

various ratios of b_f/d_w . The minimum plate buckling coefficient, k_w , was computed from the critical stress, and the relationship of k_w to b_f/d_w is compared with Bulson's (15) theoretical curve in Fig. 4.5. It can be seen that the model closely represents the flange buckling of a wide flange beam, but, as is to be expected does not accurately reproduce web buckling behaviour because the assumed shape functions cannot represent the fundamental mode of this plate.

E-3 Interaction of Local and Member Buckling

Fig. 4.6 shows the buckling load for an axially loaded wide flange column for (a) uncoupled local buckling, (b) uncoupled Euler buckling, (c) interactive column and local buckling. The interaction curve gives values for the buckling coefficient only a few percent lower than the Euler column buckling curve. These results agree with those of Pfluger and Bulson (16). Curves are also shown for the case where the load is acting at an eccentricity of 5".

E-4 Interaction of Local and Lateral Buckling

Fig. 4.7 shows a comparison of the (uncoupled) elastic local buckling load and the (uncoupled) lateral buckling load, with the critical load including interactive effects, for a simply supported beam.

4.7 Summary

The formulation developed in this chapter can form the basis for elastic or inelastic buckling of a thin-walled beam with local and member buckling interaction. The model adopted in this chapter for elastic wide flange beams has eleven degrees of freedom at each node compared to eighteen degrees of freedom for the simplest finite element

plate representation, illustrated in Fig. 4.8.

The model developed in this chapter appears to yield good results for local flange buckling but should not be expected to represent web buckling. The results verify the validity of the classical approach to local buckling by showing that, for wide flange sections in the elastic range, the interactive effect is normally small, and local and member buckling are initiated as relatively detached phenomenon over most of the range of loading.

TABLE 4-1 SOLUTIONS FOR UNCOUPLED LOCAL BUCKLING (FIG. 4.4)

No	Problem Description	Support Conditions	ℓ	n	Dimensions of the Section				Computed Critical Load	% Error	Ref.
					b_f	t_f	d_w	t_w			
1	Local buckling of a single flange plate	Simply supported on edges A-A and B-B and C-C	16"	1 2 4 6 8	8"	0.125"	0	0	13.28K 12.935K 12.924K 12.924K 12.922K	2.94 0.271 0.186 0.186 0.174	21
2	Local buckling of a single flange plate	Clamped on edges A-A and B-B and supported on C-C	16"	8	8	0.125	0	0	17.89		not available
3	Local buckling of a single web plate	Simply supported on CD, CC, DD	16	2 4 6 8	-	0.125	4"	0.125	62.28K 59.00 56.64 56.50	17.50 11.30 6.86 6.60	21
4	"	"	"	8			"	0.25	451.78K	6.36	21
5	Axially loaded column	Simply supported on EE and FF	16	8	8	0.125	8	0.125	56.14K	1.51	15
6	Beam under uniform moment	Simply supported on EE and FF	16	8	8	0.125	8	0.125	221.0"K		not available
7	Combined axial load and moment $e = 1"$	Simply supported on EE and FF	16	8	8	0.125	8	0.125	49.087		not available

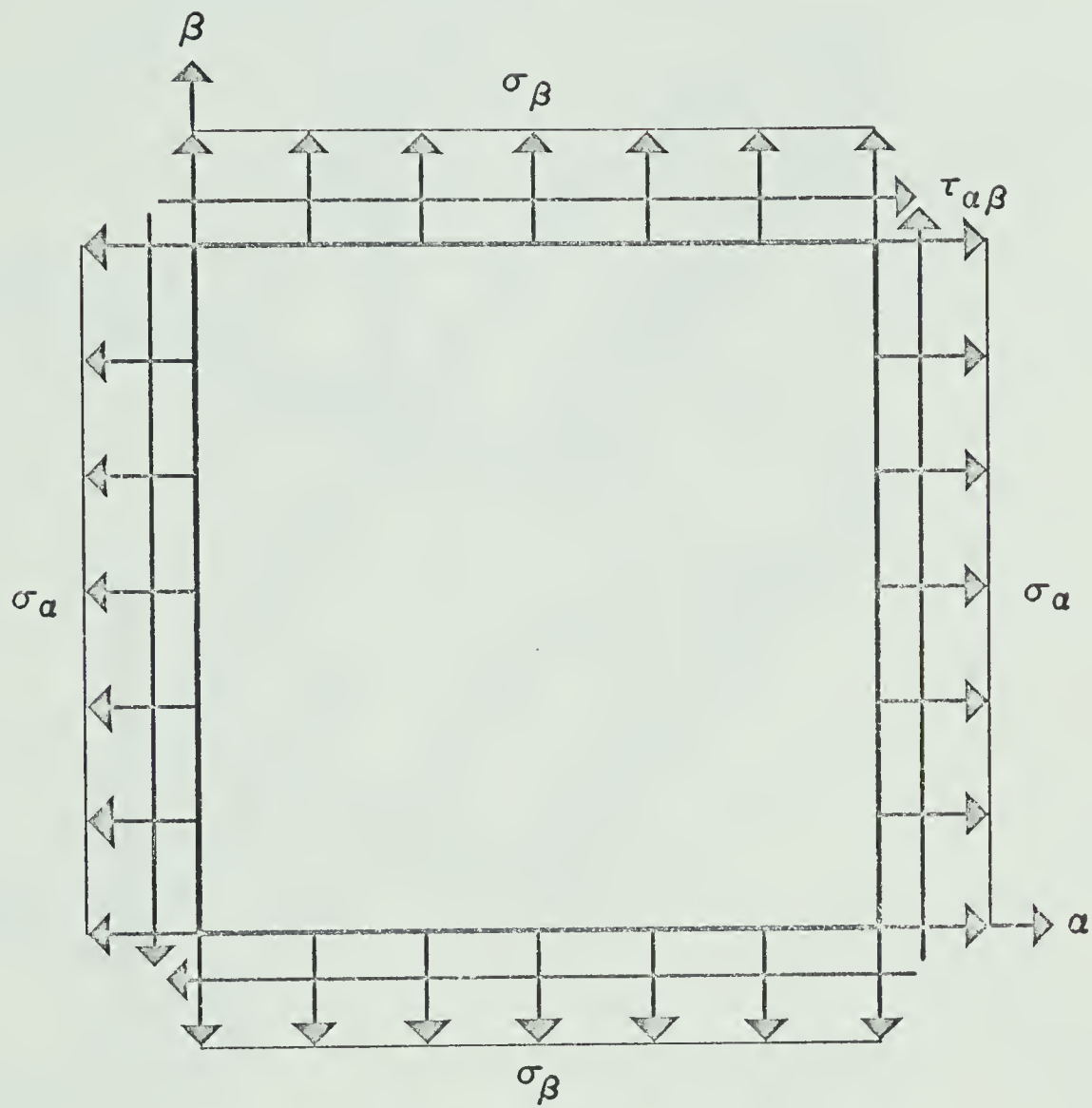


FIGURE 4.1 LOCAL PLATE CO-ORDINATE DIRECTIONS

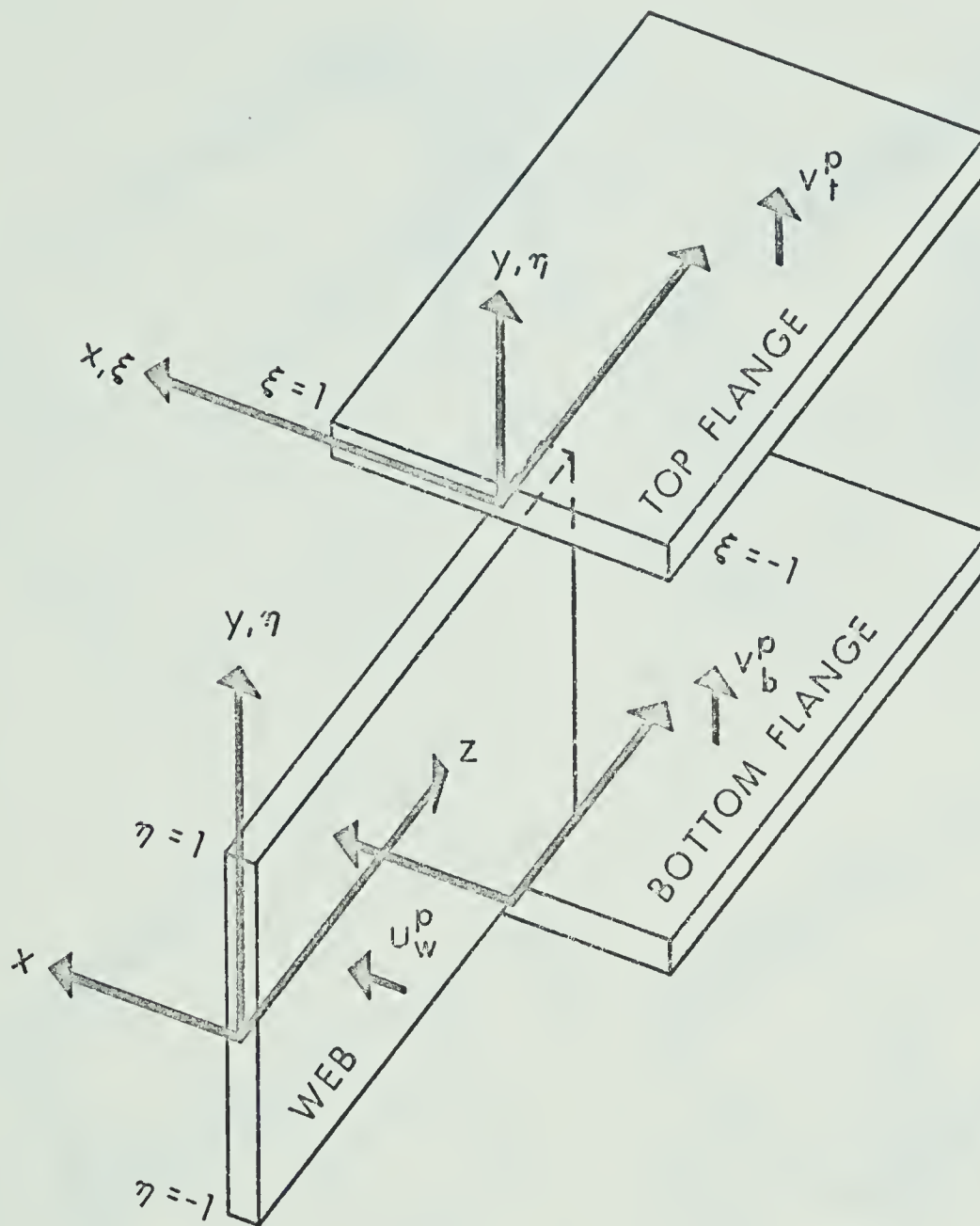


FIGURE 4.2 LOCAL COORDINATE SYSTEM FOR PLATE DEFORMATIONS

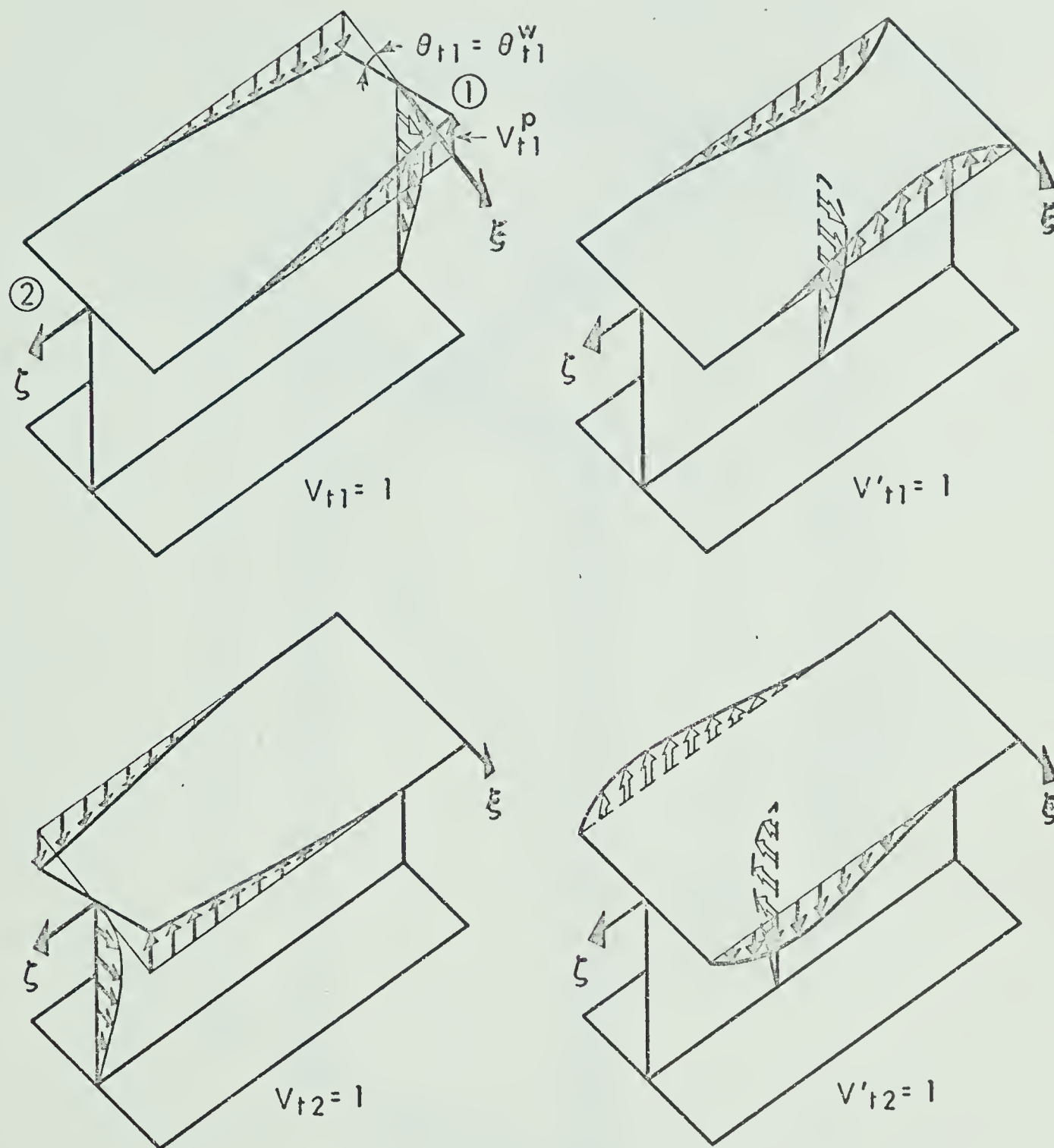
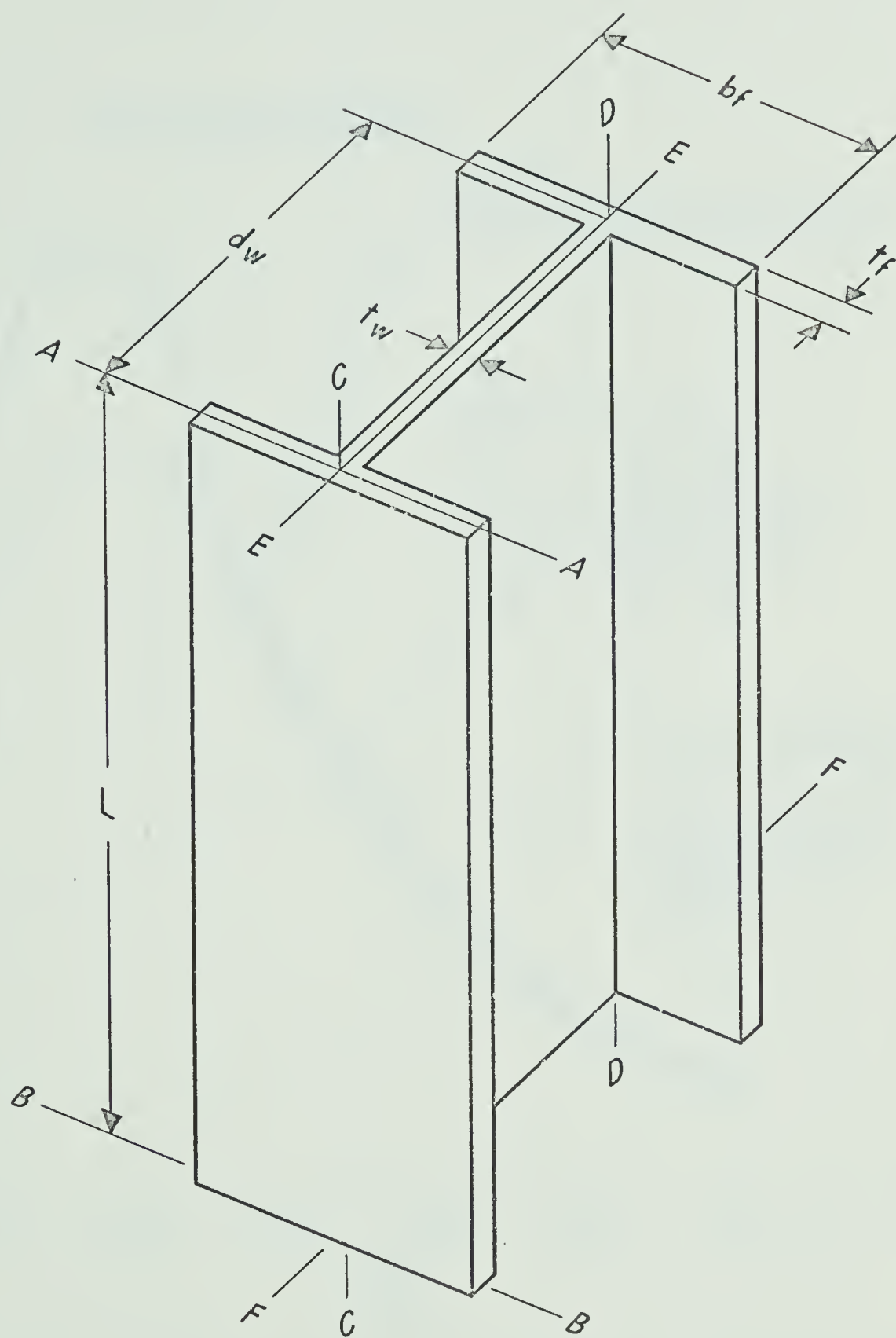


FIGURE 4.3 DEFLECTED SHAPE OF THE I-SECTION DUE TO UNIT VALUE OF THE GENERALIZED DISPLACEMENT



n - number of elements

FIGURE 4.4 GENERAL NOTATIONS

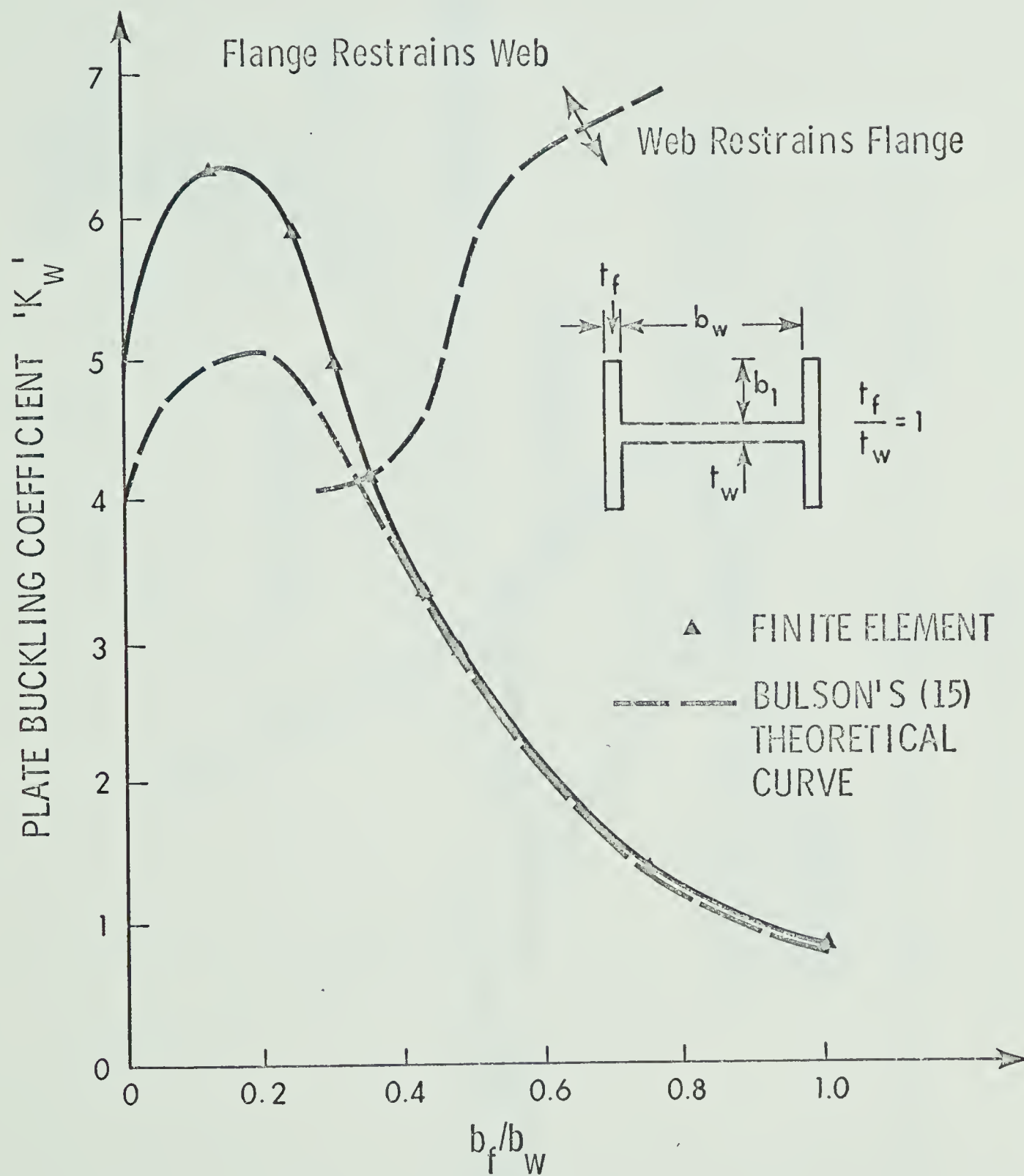


FIGURE 4.5 LOCAL BUCKLING OF COLUMNS SUBJECTED TO AXIAL LOAD

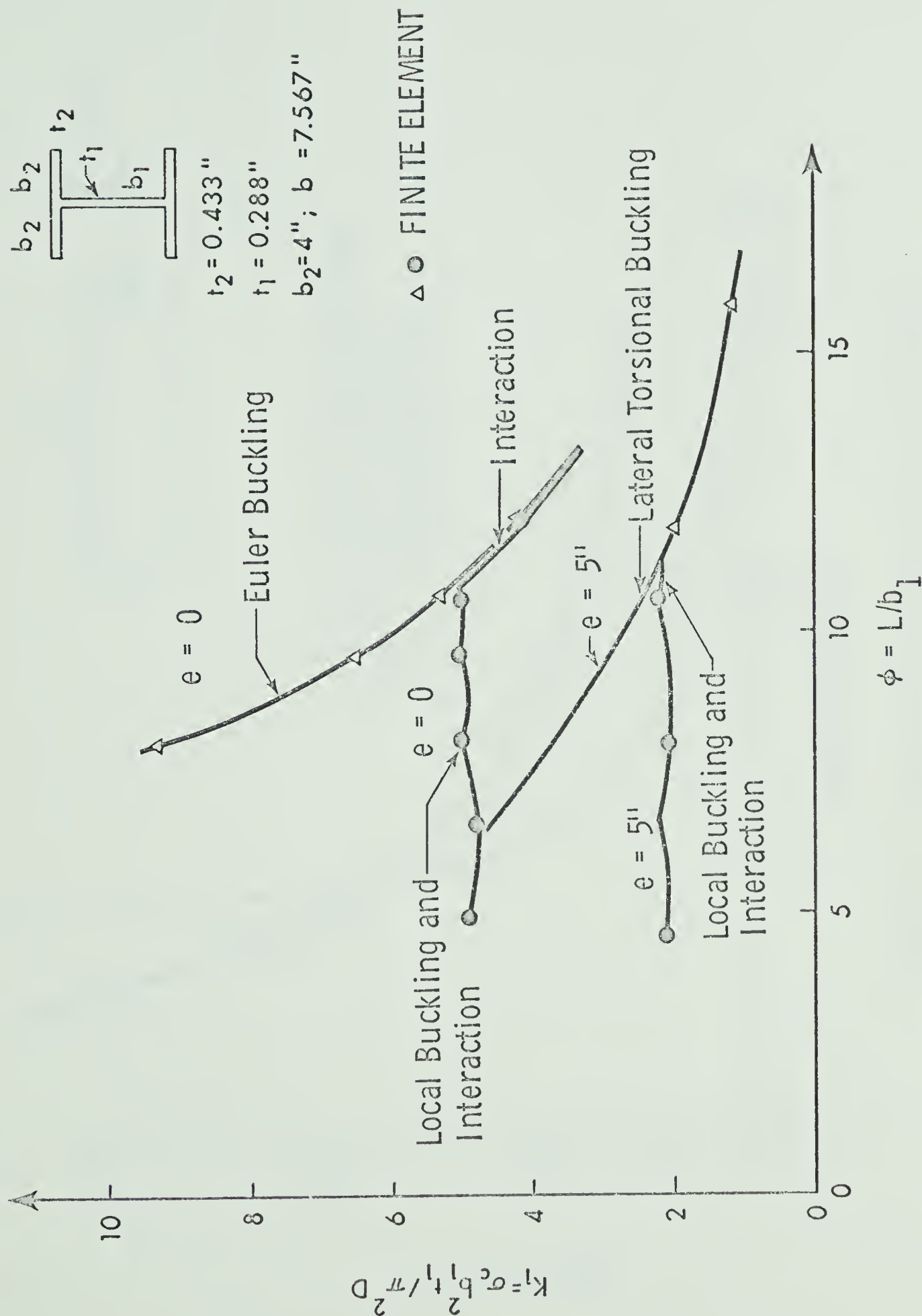


FIGURE 4.6 COLUMN/LOCAL BUCKLING INTERACTION

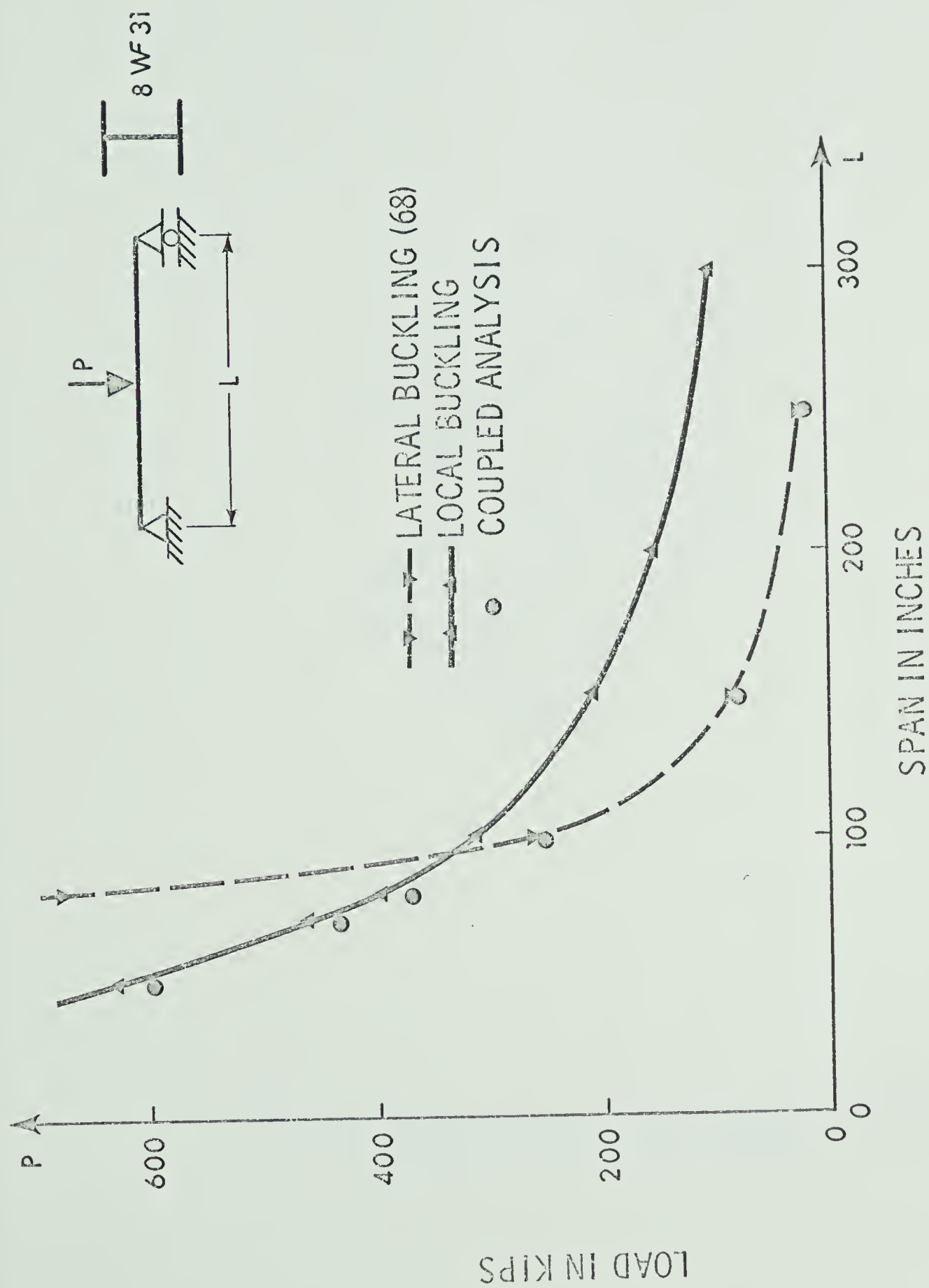


FIGURE 4.7 INTERACTION OF LATERAL AND LOCAL BUCKLING

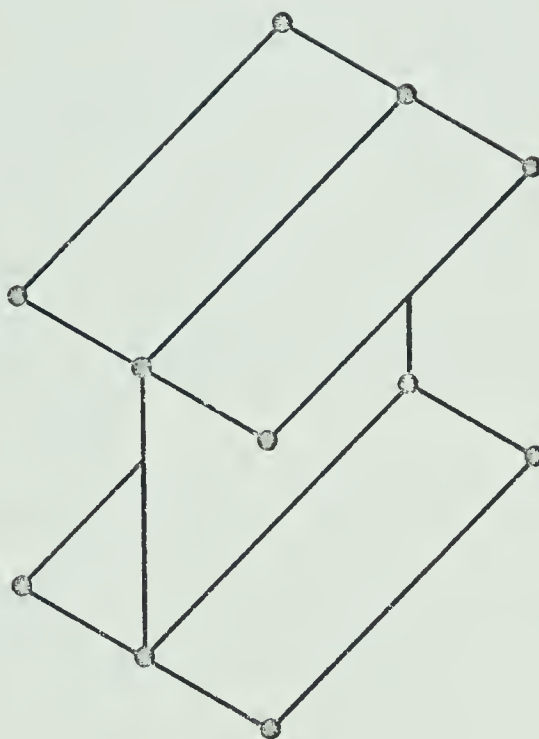


FIGURE 4.8 PLATE ELEMENTS WITH 18 DEGREES OF FREEDOM AT EACH NODE OF THE BEAM ELEMENT

CHAPTER V

FORMULATION FOR INELASTIC MEMBERS

5.1 Introduction

Nonlinear formulations relating kinematic and mechanical variables may fall into the three following categories: 1) nonlinear constitutive equations (material nonlinearity), 2) geometric nonlinearity, 3) combined material and geometric nonlinearity. The beam-column problems considered in Chapter III fall into the second category. This and the following chapter are devoted to beam-column problems falling into the third category. A comprehensive review of the application of finite element concepts to nonlinear problems in structural mechanics has been given by Oden (56).

Basically there are three types of finite element solution methods which can be adopted for nonlinear problems (30,34); 1) incremental methods without equilibrium checks; 2) incremental methods with equilibrium checks; 3) direct solution of the governing nonlinear equations. The first type of approach is computationally fast but has the disadvantage that equilibrium is not satisfied at each step and there is no direct indication of the errors involved in the solution. In the second type, incremental solutions due to a series of load steps are determined, equilibrium is checked, and corrections are made for each load step, if necessary. Unlike the first method this insures that the equilibrium equations are satisfied throughout the loading history. The beam-column solutions presented here have been carried out using this method. The third method has been successfully applied by Oden (55).

5.2 Formulation of Inelastic Incremental Equilibrium Equations

5.2.1 General Description of Solution Procedure

Details of the solution procedures for inelastic small deflection, beam-column and bifurcation problems are discussed in Chapter VI. However, since the formulation is, to some extent, dependent on the solution procedure adopted, a general description of this procedure for beam-column problems is given in this section.

The solution procedure for inelastic beam-columns employed in this study may be described as follows. In the formulation, strains, displacements and rotations are assumed to be 'small' and hence a second order small displacement theory is used. A linear incremental solution technique is adopted with equilibrium checks. This is similar to the method adopted by Murray (50) and Wilson (51,52), Sharifi (63), and Hofmeister and Greenbaum (34).

The incremental equilibrium Equation 2-35, was derived in Chapter II for elastic response. A similar equation is derived in this chapter and may be expressed as

$$[[K_S^T] + [K_G]] \{\Delta r\} = \{\Delta R\} \quad (5-1)$$

where $[K_S^T]$ is the tangent stiffness matrix for the increment of loading.

The Newton-Raphson method for inelastic response is explained in the following algorithm.

1) For any approximate $\{r\}_n$, the total strains may be determined from the kinematic relationships, Equation A-36. The stresses may then be computed directly from the stress-strain relationship, shown in Appendix D in Fig. D.1a.

2) Knowing the strains and stresses, the tangent stiffness matrix, the geometric stiffness matrix, and the unbalanced forces may be evaluated, as detailed in Appendix D. Equation 5-1 may be solved to determine the displacement increments to equilibrate the unbalanced forces, i.e.:

$$\{\Delta r\}_n = [[K_S^T]_n + [K_G]_n]^{-1} \{\Delta R\}_n \quad (5-2)$$

3) The displacements are updated

$$\{r\}_{n+1} = \{r\}_n + \{\Delta r\}_n \quad (5-3)$$

4) Steps 1 to 3 are repeated until the unbalanced force vector is arbitrarily small.

5) A new load increment is applied and steps 1 to 4 are repeated.

This procedure is identical to that of Section 3.4.2 except for the detailed evaluation of $[K_S^T]$ and $[K_G]$. However, a modified Newton-Raphson technique, holding the tangent stiffness constant for several iterations, was actually used for the numerical work.

The procedure of computing the error vector in nodal equilibrium is described as follows. The total forces at a node are the sum of a) the applied forces, b) the resisting forces due to stresses, which may be computed from statics for the stress resultants produced by any stress distribution, and c) the forces resulting from changes in geometry which may be evaluated as $[K_G]\{r\}$ for any set of stress resultants and displacements. The stress resultants are computed at the ends of each element by a numerical integration of stresses which have been previously determined from the element strains as detailed in

Appendix D. The difference between the applied loads and the sum of a) the resisting forces and b) the 'geometric' forces, represents the set of unbalanced forces, designated as $\{\Delta R\}$ in Equation 5-1, on the given configuration of the model.

5.2.2 Other Formulations

Other methods, such as the initial strain method (38), and the initial stress method (77), have been adopted for the analysis of elastic-plastic problems. In the initial strain method, fictitious loads are applied to the structure to produce elastic strains numerically equal to the plastic strains. Although this requires only one inversion of the stiffness matrix, an iterative solution for the fictitious forces must be carried out in order to control solution errors. The initial stress approach, developed by Zienkiewicz, et. al. (77), uses a slightly different incremental technique, treating discrepancies between elastic and elastic-plastic stress increments as unbalanced body forces and iterating until these forces disappear. The main advantage of these methods is that the assembled stiffness matrix remains unchanged.

5.2.3 Assumptions for Derivation of Tangent Stiffness

In deriving the tangent stiffness for a partially plastic beam section it is assumed that no strain reversal occurs. If one considers a section, which has already yielded, and an infinitesimal increment in bending moment is applied, the resistance to this moment is a measure of incremental bending stiffness. The yielded zones, will be increased somewhat, while some strain reversal may take place,

in the already yielded zones. These effects are neglected in this formulation and the additional moment is assumed to be resisted by all parts of the cross section with the stress increment determined from the tangent modulus relationship for the material at the current value of strain. The section properties relating increments in stress resultants to increments in displacements may then be computed by a transformed area concept. This concept may be utilized for thin-wall open beam sections since the stress is essentially uniaxial and the effect of shear stress on the principal stresses may be neglected.

5.2.4 Basis for Incremental Equilibrium Equations

Since the incremental equilibrium equations derived in Chapter II are virtual work equations, they may be used directly for the incremental formulation of inelastic problems. Equation 2-14 is

$$\begin{aligned} \frac{1}{2} \int_V \bar{\sigma}_{ij} \delta(u_{k,i} u_{k,j}) dV + \frac{1}{2} \int_V \sigma_{ij} \delta(u_{i,j} + u_{j,i} + u_{k,i} u_{k,j}) dV \\ + \frac{1}{2} \int_V \sigma_{ij} \delta(\bar{u}_{k,i} u_{k,j} + u_{k,i} \bar{u}_{k,j}) dV = \int_S t_i \delta u_i ds \end{aligned} \quad (5-4)$$

The physical interpretation of the terms in this equation was discussed in Section 2.3 and the initial displacement terms were shown in Appendix B to have negligible effect for this class of problem in the range of interest under consideration. They are therefore neglected in the following formulation.

An examination of the first term of Equation 5-4, from which the geometric stiffness arises, indicates that it is dependent only on the initial stress and the geometry of the deformation and therefore

is independent of the constitutive relationship. Hence the geometric stiffness terms derived in Chapter II remain unchanged and can be used directly in the solution of problems involving nonlinear material behaviour.

For inelastic material response, the location of the instantaneous centroid, shear centre and sectorial centroid, and the incremental principal axes are functions of the current strain distribution. For elastic response it was convenient to refer displacement increments to the original shear centre axis. However for inelastic response, the variation of increments in displacements, in Equation 5-4 may be referred to either

a) the original shear centre, centroid, sectorial centroid, and reference axes of the elastic section (reference points S, C and B, and coordinates $x-y$ of Fig. 5.2)

or

b) the instantaneous shear centre, instantaneous centroid and instantaneous sectorial centroid of the transformed section, in the instantaneous principal directions (reference points \bar{S} , \bar{C} and B' and coordinates $\xi-\eta$ of Fig. 5.2.)

The element equilibrium equations will be derived with respect to both of these reference systems. The formulation with respect to the original reference axes of the element (the $x-y$ coordinates of Fig. 5.2) will be referred to as 'Formulation 1'. The formulation with respect to the transformed section principal axes (the $\xi-\eta$ coordinates of Fig. 5.2) will be referred to as 'Formulation 2'. The transformation of displacements to the global coordinate system (reference points S^* and C^* , and coordinates X,Y) will be discussed in Section 5.4, and

becomes a part of the assembly process. It is shown in Appendix E that these two formulations are substantially the same.

5.2.5 Formulation of Incremental Equilibrium Equations - 'Formulation 1'

Neglecting the initial displacement matrix, and taking the variation with respect to the original reference system, Equation 5-4 may be written for one element as

$$\begin{aligned}
 \int_{\ell} \{ & \Delta P \delta w'_c - \Delta M_x \delta v''_s - \Delta M_y \delta u''_s + \Delta W_\omega \delta \phi'' + V_x \phi \delta v'_s \\
 & + V_x v'_s \delta \phi - V_y \phi \delta u'_s - V_y u'_s \delta \phi + P u'_s \delta u'_s + P v'_s \delta v'_s \\
 & + P e_y u'_s \delta \phi' + P e_y \phi' \delta u'_s - P e_x v'_s \delta \phi' - P e_x \phi' \delta v'_s \\
 & - M_x u'_s \delta \phi' + M_y v'_s \delta \phi' - M_x \phi' \delta u'_s + M_y \phi' \delta v'_s + M_\rho \phi' \delta \phi' \\
 & + T_{sv} \delta \phi' - (\Delta q_x \delta u_s + \Delta q_y \delta v_s + \Delta q_z \delta w_z + \Delta m_t \delta \phi + \Delta m_x \delta v'_s \\
 & + \Delta m_y \delta u'_s) \} dz = 0
 \end{aligned} \tag{5-5}$$

where $P, M_x, M_y, M_\rho, V_x, V_y$ are the total stress resultants existing prior to the load increment; and $\Delta P, \Delta M_x, \Delta M_y$ and ΔW_ω are increments in stress resultants, with respect to the x-y reference axes traveling along with the section, as shown in Fig. 5.2. The total stress resultants may be evaluated by direct integration of stresses as detailed in Appendix D.

If each element of area is 'transformed' such that the product of the current tangent modulus times the original element of area

is equal to the original modulus times the element of transformed area; the stress resultant increments, ΔP , ΔM_x , ΔM_y and ΔW_ω appearing in Equation 5-5 are given by Equation A-26, as

$$\Delta P = E A^T w'_c - E A^T y_o v''_s - E A^T x_o u''_s + E S^T_\omega \phi'' \quad (5-6a)$$

$$\Delta M_x = E A^T y_o w'_c - E I^T_x v''_s - E I^T_{xy} u''_s + E S^T_{\omega x} \phi'' \quad (5-6b)$$

$$\Delta M_y = E A^T x_o w'_c - E I^T_{xy} v''_s - E I^T_y u''_s + E S^T_{\omega y} \phi'' \quad (5-6c)$$

$$\Delta W_\omega = E S^T_\omega w'_c - E S^T_{\omega x} v''_s - E S^T_{\omega y} u''_s + E I^T_{\omega} \phi'' \quad (5-6d)$$

where A^T , I^T_x , I^T_{xy} , I^T_y , S^T_ω , $S^T_{\omega x}$, $S^T_{\omega y}$, I^T_ω represent the properties of the transformed section with respect to points C and S and the x-y reference axes. The distances x_o , y_o , of Equation 5-6, and e_x , e_y of Equation 5-5 refer to the location of \bar{C} and S, as shown in Fig. 5.3.

5.2.6 Formulation of Incremental Equilibrium Equations 'Formulation 2'

Taking the variation of displacement increments with respect to the instantaneous (transformed) principal axis reference system, Equation 5-4 may be written for one element as

$$\begin{aligned} \int_{\ell} \left[\Delta P \delta w'_\zeta - \Delta M_\xi \delta v''_\eta - \Delta M_\eta \delta u''_\xi + \Delta W_{\omega\zeta} \delta \phi'' + V_\xi v'_\eta \delta \phi + V_\xi \phi \delta v'_\eta \right. \\ \left. - V_\eta \phi \delta u'_\xi - V_\eta u'_\xi \delta \phi + P u'_\xi \delta u'_\xi + P v'_\eta \delta v'_\eta + P e_\eta u'_\xi \delta \phi' + P e_\eta \phi' \delta u'_\xi \right. \\ \left. - P e_\xi v'_\eta \delta \phi' - P e_\xi \phi' \delta v'_\eta - M_\xi u'_\xi \delta \phi' + M_\eta v'_\eta \delta \phi' - M_\xi \phi' \delta u'_\xi + M_\eta \phi' \delta v'_\eta \right. \\ \left. + M_{\rho\zeta} \phi' \delta \phi' + T_{sv} \delta \phi' - (\Delta q_\xi \delta u'_\xi + \Delta q_\eta \delta v'_\eta + \Delta q_\zeta \delta w'_\zeta + \Delta m_\zeta \delta \phi \right. \end{aligned}$$

$$\left. + \Delta m_{\xi} \delta v_{\eta}' + \Delta m_{\eta} \delta u_{\xi}' \right) dz = 0 \quad (5-7)$$

where ξ and η are the transformed section principal axes of Fig. 5.2; the displacement increments and coordinate relationships are shown in Fig. 5.3; and the stress resultant increments are shown in Fig. 5.4.

The stress resultant increments, ΔP , ΔM_{ξ} , ΔM_{η} , and $\Delta W_{\omega\zeta}$ appearing in Equation 5-7 may be written in the following uncoupled form (see Appendix A)

$$\Delta P = E A^T \frac{w'}{C} \quad (5-8a)$$

$$\Delta M_{\xi} = -E I_{\xi}^T v_{\eta}'' \quad (5-8b)$$

$$\Delta M_{\eta} = -E I_{\eta}^T u_{\xi}'' \quad (5-8c)$$

$$\Delta W_{\omega\zeta} = E I_{\omega\zeta}^T \phi'' \quad (5-8d)$$

where A^T is the transformed area; I_{ξ}^T and I_{η}^T , are the principal moments of inertia of the transformed section about the ξ - η axes; $I_{\omega\zeta}^T$ is the principal sectorial moment of inertia of the transformed section about \bar{S} ; M_{ξ} and M_{η} are the stress resultants about the principal axes; and $M_{\rho\zeta}$ is the stress resultant defined in Equation 2-7, about \bar{S} .

5.3 Finite Element Idealization

The finite element equations for one element may be obtained from Equations 5-5 and 5-6, or Equations 5-7 and 5-8, by substituting for the displacements in terms of shape functions and nodal parameters,

and carrying out the required integration. The total virtual work may be evaluated by summing the integrals over each element, and the reference axis in each element may be different providing the displacement variations are compatible at the junction of any two elements.

For sections with variable properties, a linear variation of axial displacement is incapable of representing a constant axial load. Therefore, an additional degree of freedom for axial displacement is introduced at the midpoint of an element to achieve a balance of axial forces at the nodes. Hence the quadratic displacement function of Equation 2-23e is used to represent the axial displacement.

To determine the element stiffness for 'Formulation 1', Equations 5-6 are substituted into Equation 5-5, and Equations 2-23a, b, c and e are then substituted for displacements. The element tangent stiffness matrix that arises in this substitution is derived in Appendix E. The geometric stiffness that arises is also discussed in Appendix E and differs from that in Equation 2-28 only in the $[g_{\phi\phi}]$ submatrix. The element equilibrium equations then become

$$[k_S^T] \{\Delta r_E\} + [k_G] \{\Delta r_E\} = \{\Delta R_E\} \quad (5-9)$$

where $\{\Delta r_E\}$ is defined in Fig. 2.6; $[k_S^T]$ is now a full matrix with submatrices denoted as

$$[k_S^T] = \begin{bmatrix} k_{uu}^T & & & \\ k_{vu}^T & , & k_{vv}^T & \text{sym.} \\ k_{\phi u}^T & , & k_{\phi v}^T & , & k_{\phi\phi}^T \\ k_{wu}^T & , & k_{wv}^T & , & k_{w\phi}^T & , & k_{ww}^T \end{bmatrix} \quad (5-10)$$

(Equation E-5 of Appendix E); and $[k_G]$ is of the same form as Equation 2-28, but $[g_{\phi\phi}]$ is given by Equation E-7a. In the derivation of Equations 5-9, and 5-10, a linear variation of stress resultants and section properties has been assumed.

To determine element stiffnesses for 'Formulation 2', Equations 2-23a, b, c and e are assumed to represent displacement increments referred to the \bar{S} and \bar{C} axes, in the ξ, η coordinate system. With this assumption, the evaluation of stiffness matrices based on Equations 5-7 and 5-8 may be carried out. This results in a set of element equilibrium equations of the same form as Equation 5-9. However, $[k_S^T]$ is now given by Equation E-10 and, as in the elastic case, is uncoupled. The form of $[k_G]$ is identical to that in "Formulation 1" but, because of the different reference axes, the stress resultants have different magnitudes. The displacement increment vector $\{\Delta r_E\}$ is shown in Fig. 5.5.

5.4 Transformation and Assembly

5.4.1 Reference Configurations

The element equilibrium Equation 5-9 has been derived for two different local coordinate systems. In general the location and

orientation of the local reference axes may vary from element to element. Prior to assembly it is therefore necessary to transform the nodal displacements and forces from the local coordinate system to a global coordinate system in order to maintain compatibility of deformations.

For inelastic analysis it is assumed that the global reference points C^* and S^* (Figs. 5.1 and 5.3), and the X-Y coordinate system, are the original elastic centroid, shear center, and centroidal reference axes, respectively. An arbitrary section after deformation is shown at P, in Fig. 5.1. This same section is shown at different stages of the deformation in Fig. 5.2. The original position is indicated as position I. Application of the load causes the section to be displaced to position II. The subsequent addition of a small load increment causes the section to be further displaced to position IV.

The movement from position II to position IV results from a simultaneous translation and rotation of the cross section. For convenience the movement caused by the increment of load will be considered to occur in two parts. The first part is the translational displacement from position II to III. The second part is the movement from position III to IV, caused by twist.

5.4.2 Displacement Transformation

"Formulation 1"

The nodal vector of Equation 5-9 for 'Formulation 1' is expressed in terms of displacement increments of points C and S of position II (Fig. 5.2) in the x and y coordinate directions which are the reference axes travelling with the cross section. These increments may

be related to the displacement increments of C^* and S^* , for a typical node by the transformation (Fig. 5.3).

$$\begin{Bmatrix} u_s \\ v_s \\ w_c \\ \phi \\ u'_s \\ v'_s \\ \phi' \end{Bmatrix} = \begin{bmatrix} \cos \phi & , & \sin \phi & & & & \\ -\sin \phi & , & \cos \phi & & & & \\ & & & 1 & & & \\ & & & & 1 & & \\ & & & & & \ell \cos \phi & , \ell \sin \phi \\ & & & & & -\ell \sin \phi & , \ell \cos \phi \\ & & & & & & \ell \end{bmatrix} \begin{Bmatrix} \Delta U_s \\ \Delta V_s \\ \Delta W_c \\ \Delta \phi \\ \Delta U'_s \\ \Delta V'_s \\ \Delta \phi' \end{Bmatrix} \quad (5-11)$$

For nodes p and q at the ends of an element, Equation 5-11 may be written symbolically as

$$\{\underline{u}_s^p\} = [T_p] \{\Delta \underline{U}^p\} \quad (5-12a)$$

$$\{\underline{u}_s^q\} = [T_q] \{\Delta \underline{U}^q\} \quad (5-12b)$$

where the transformation matrices of Equations 5-12 are defined by matrix of Equation 5-11, with ϕ taking the values of ϕ^p and ϕ^q in $[T_p]$ and $[T_q]$, respectively. Reordering the vector of element nodal displacements, it may be expressed in the local and global coordinate systems, as

$$\{\Delta r_E\}_L^T = \langle u_s^p, v_s^p, w_c^p, \phi^p, \ell u_{s,z}^p, \ell v_{s,z}^p, \ell \phi_{,z}^p, w_{cm}, \\ u_s^q, v_s^q, w_c^q, \phi^q, \ell u_{s,z}^q, \ell v_{s,z}^q, \ell \phi_{,z}^q \rangle \quad (5-13a)$$

and

$$\{\Delta r_E\}_G^T = \langle \Delta U_S^p, \Delta V_S^p, \Delta W_C^p, \Delta \phi^p, \Delta U_{S,z}^p, \Delta V_{S,z}^p, \Delta \phi_{,z}^p, \Delta W_{cm}, \\ \Delta U_S^q, \Delta V_S^q, \Delta W_C^q, \Delta \phi^q, \Delta U_{S,z}^q, \Delta V_{S,z}^q, \Delta \phi_{,z}^q \rangle \quad (5-13b)$$

which are related, through Equations 5-12, in the expression

$$\{\Delta r_E\}_L = \begin{Bmatrix} \underline{u}_S^p \\ \underline{w}_m \\ \underline{u}_S^q \end{Bmatrix} = \begin{bmatrix} T_p & & \\ & 1 & \\ & & T_q \end{bmatrix} \begin{Bmatrix} \Delta \underline{U}^p \\ \Delta \underline{W}_m \\ \Delta \underline{U}^q \end{Bmatrix} \quad (5-14a)$$

Symbolically we may write Equation 5-14a as

$$\{\Delta r_E\}_L = [T_1] \{\Delta r_E\}_G \quad (5-14b)$$

5.4.3 Displacement Transformation - "Formulation 2"

The nodal vector of Equation 5-9, for 'Formulation 2', is expressed in terms of the displacement increments of points \bar{C} and \bar{S} of position II of Fig. 5.2, in the ξ and η coordinate directions, (which represent the centroid and shear center of the displaced transformed section, and the principal axes of the displaced transformed section, respectively). Let α be the angle between the instantaneous ξ, η principal axes and the original x, y reference axes travelling with the section. The relationship between the displacement increments of C^* and S^* , defined in Section 5.4.2, and those in the vector $\{\Delta r_E\}$ of Equation 5-9, can now be derived as follows

From Fig. 5.2 and Fig. 5.3

$$u_{\xi} = \hat{u} \cos \alpha + \hat{v} \sin \alpha \quad (5-15a)$$

$$v_{\eta} = -\hat{u} \sin \alpha + \hat{v} \cos \alpha \quad (5-15b)$$

where u_{ξ} , v_{η} are the displacement increments of the instantaneous shear center along the principal axes directions, and \hat{u} , \hat{v} represent the displacement increments of the instantaneous shear center in the directions parallel to the x , y reference axes.

Expressing \hat{u} , \hat{v} in terms of u_s , v_s (the displacements of the original shear center in the direction of the reference axes) results in

$$\hat{v} = v_s + (b_x - e_x) \phi \quad (5-16a)$$

$$\hat{u} = u_s - (b_y - e_y) \phi \quad (5-16b)$$

Substituting Equation 5-16 into Equation 5-15 yields

$$\begin{aligned} u_{\xi} &= u_s \cos \alpha + v_s \sin \alpha + ((b_x - e_x) \sin \alpha - (b_y - e_y) \cos \alpha) \phi \\ v_{\eta} &= -u_s \sin \alpha + v_s \cos \alpha + ((b_y - e_y) \sin \alpha + (b_x - e_x) \cos \alpha) \phi \end{aligned} \quad (5-17)$$

where ϕ is the increment in Φ .

For the small displacement problem it can be assumed that

$$\phi = \phi_{\zeta} \quad (5-18)$$

Now u_s and v_s referenced to the configuration at position II should be transformed to the global system. If ΔU_s , ΔV_s are the increments of displacements of the original shear center, S^* , in the global system, then,

$$\Delta U_s \cos \phi + \Delta V_s \sin \phi = u_s \quad (5-19a)$$

$$-\Delta U_s \sin \phi + \Delta V_s \cos \phi = v_s \quad (5-19b)$$

Substituting Equations 5-19 into Equations 5-17 yields:

$$u_\xi = \Delta U_s \cos (\phi + \alpha) + \Delta V_s \sin (\phi + \alpha) + \{(b_x - e_x) \sin \alpha - (b_y - e_y) \cos \alpha\} \Delta \phi \quad (5-20a)$$

$$v_\eta = -\Delta U_s \sin (\phi + \alpha) + \Delta V_s \cos (\phi + \alpha) + \{(b_y - e_y) \sin \alpha + (b_x - e_x) \cos \alpha\} \Delta \phi \quad (5-20b)$$

Using the similar transformation for rotations

$$u'_\xi = \Delta U'_s \cos (\phi + \alpha) + \Delta V'_s \sin (\phi + \alpha) + \{(b_x - e_x) \sin \alpha - (b_y - e_y) \cos \alpha\} \Delta \phi' \quad (5-21a)$$

$$v'_\eta = -\Delta U'_s \sin (\phi + \alpha) + \Delta V'_s \cos (\phi + \alpha) + \{(b_y - e_y) \sin \alpha + (b_x - e_x) \cos \alpha\} \Delta \phi' \quad (5-21b)$$

The axial displacement of \bar{C} may be expressed in terms of the axial displacement of C as

$$\frac{w}{c} = \Delta w_C - y_o \theta_x - x_o \theta_y + \omega_{BB'} \phi'' \quad (5-22)$$

where $\omega_{BB'}$ is the unit relative warping of the transformed section sectorial centroid (B') and the sectorial centroid of the original section (B); and, θ_x , θ_y are the increments in rotations about reference axes x and y .

Neglecting ω_{BB} , we may write

$$\frac{w}{c} = \Delta w_C - (y_o \cos \phi + x_o \sin \phi) \Delta \theta_x - (x_o \cos \phi - y_o \sin \phi) \Delta \theta_y \quad (5-23)$$

or

$$\frac{w}{c} = \Delta w_C - (y_o \cos \phi + x_o \sin \phi) \Delta V'_s - (x_o \cos \phi - y_o \sin \phi) \Delta U'_s \quad (5-24)$$

Equations 5-20, 5-21 and 5-24 may be evaluated at the end nodes p and q of the element to establish the transformation of displacement increments. However it is also necessary to establish a transformation of the axial displacement for the mid-point node. This may be accomplished as follows.

Using the expression Equation 5-24 for the displacement of the middle node $\frac{w}{c}_m$, and designating the location with the subscript m, yields

$$\begin{aligned} \frac{w}{c}_m &= \Delta w_{cm} - (y_{om} \cos \phi_m + x_{om} \sin \phi_m) \Delta V'_{sm} \\ &\quad - (x_{om} \cos \phi_m - y_{om} \sin \phi_m) \Delta U'_{sm} \end{aligned} \quad (5-25)$$

For the assumed shape function Equation 5-25 reduces to

$$\begin{aligned} \frac{w}{c}_m &= \Delta w_{cm} + \frac{1}{\ell} (y_{om} \cos \phi_m + x_{om} \sin \phi_m) \left(\frac{3}{2} V^p \right. \\ &\quad \left. + \frac{1}{4} \Delta \theta_x^p \ell - \frac{3}{2} \Delta V^q + \frac{1}{4} \Delta \theta_x^q \ell \right) + \frac{1}{\ell} (x_{om} \cos \phi_m \\ &\quad - y_{om} \sin \phi_m) \left(\frac{3}{2} \Delta U^p + \frac{1}{4} \Delta \theta_y^p \ell - \frac{3}{2} \Delta U^q \right. \\ &\quad \left. + \frac{1}{4} \Delta \theta_y^q \ell \right) \end{aligned} \quad (5-26)$$

The increments of the displacements of the instantaneous coordinates may now be written in terms of those of C^* and S^* by the relation

$$\{\Delta r_E\}_L = [T_2] \{\Delta r_E\}_G \quad (5-27)$$

where $[T_2]$ is given in Table 5-1; $\{\Delta r_E\}_L$ is

$$\{r_E\}_L^T = \langle u_\xi^P, v_\eta^P, w_{\frac{P}{c}}, \phi^P, \ell u_{\xi,z}^P, \ell v_{\eta,z}^P, \ell \phi_{,z}^P, w_{\frac{P}{cm}}, \\ u_\xi^Q, v_\eta^Q, w_{\frac{Q}{c}}, \phi^Q, \ell u_{\xi,z}^Q, \ell v_{\eta,z}^Q, \ell \phi_{,z}^Q \rangle \quad (5-28a)$$

; and $\{\Delta r_E\}_G^T$ is given by Equation 5-13b.

5.4.4 Assembly

The element equilibrium relationship may now be expressed in terms of the original reference axis nodal displacements by using the appropriate displacement transformation from Section 5.4.2 or 5.4.3, and premultiplying by the consistent force transformation. Equation 5-9 then becomes

$$[k_S^T]_G \{\Delta r_E\}_G + [k_G]_G \{\Delta r_E\}_G = \{\Delta R_E\}_G \quad (5-29)$$

where

$$[k_S^T]_G = [T]^T [k_S^T] [T] \quad (5-30a)$$

$$[k_G]_G = [T]^T [k_G] [T] \quad (5-30b)$$

and

$$\{\Delta R_E\}_G = [T]^T \{\Delta R_E\}_L \quad (5-30c)$$

Assembly of the incremental equilibrium equations now proceeds by the direct stiffness method to yield

$$[K_S^T] \{\Delta r\} + [K_G] \{\Delta r\} = \{\Delta R\} \quad (5-31)$$

Equation 5-31 is now in the form of Equation 5-1 and forms the basis for the solution technique discussed in Section 5.2 and those employed in Chapter IV.

5.5 Tangent Stiffness Properties

The evaluation of the element tangent stiffness matrix $[k_S^T]$, which arises in Equation 5-9, as described in Section 5.3, is carried out in Appendix E. Appendix E presupposes that the values of A^T , I_ξ^T , I_η^T , I_ω^T , e_ξ , e_η , x_o , y_o and the angle α are known at each end of the element. For any given set of total displacements $\{r\}$, the strains may be determined at any point on the cross section from the kinematic relationship, Equation A-36. The transformed section properties may then be computed as detailed in Appendix D. This provides all the information required for the evaluation of $[k_S^T]$.

5.6 Stress Resultants

5.6.1 Stress Resultants for $[k_G]$

The evaluation of $[K_G]$, which arises in Equation 5-9 as described in Section 5.3, requires that the total stress resultants be known. The terms which arise in Section 5.3 are identical to the terms depending on the stress resultants in Equation 2-24, for the elastic case, except that, for 'Formulation 1' the stress resultants and displacement increments are referred to the C, S, x-y reference system,

while, for 'Formulation 2' they are referred to the \bar{C} , \bar{S} , ξ - η reference system. All coefficient matrices remain the same as those of section A-6, except that the expression for $[g_{\phi\phi}]$ arising from the evaluation of M_ρ is now expressed directly in terms of this stress resultant.

For any set of nodal displacements the strain is determined from Equation A-36. The stresses are determined in each region of the plate segment from the stress-strain relationship. The axial load and bending moment stress resultants are calculated with respect to the reference axis passing through the centroid, C , of the beam cross section by simple statics as described in Appendix D.3. The stress resultant W_ω is also computed by simple statics about S .

For Formulation 1, these stress resultants are now used directly in the evaluation of $[k_G]$ as detailed in Appendix E. The shear stress resultants required for the evaluation are obtained from the equations

$$V_x = \frac{dM_y}{dz} \quad (5-32a)$$

$$V_y = \frac{dM_x}{dz} \quad (5-32b)$$

For Formulation 2, the required stress resultants are obtained from the above evaluations as (Fig. 5.6)

$$M_\xi = (M_x - P y_o) \cos \alpha - (M_y - P x_o) \sin \alpha \quad (5-33a)$$

$$M_\eta = (M_y - P x_o) \cos \alpha + (M_x - P y_o) \sin \alpha \quad (5-33b)$$

$$V_\xi = \frac{dM_\eta}{dz} \quad (5-33c)$$

$$V_{\eta} = \frac{dM_{\xi}}{dz} \quad (5-33d)$$

5.6.2 Stress Resultants for Evaluating Unbalanced Forces

The resisting stress resultants M_x, M_y computed in Section 5.6.1 are with respect to the local reference axes moving with the cross section. In order to compute the unbalanced residual force vector in the global system, the stress resultants, $\langle M_x, M_y, M_T \rangle$, with respect to the local system may be transformed to the global system using the following transformation matrix

	x	y	z
X	$\cos \phi$	$\sin \phi$	$-\frac{dU}{dz}$
Y	$-\sin \phi$	$\cos \phi$	$\frac{dV}{dz}$
Z	$\frac{dU}{dz}$	$-\frac{dV}{dz}$	1

(5-34)

Since the torsional moment is relatively small, and this work is primarily concerned with prebuckling deformations, the contributions of the torsional moment to the moments about the X and Y axes (i.e. $-\frac{dU}{dz} M_T$ and $\frac{dV}{dz} M_T$) have been neglected in the computations.

The contribution of the element to the unbalanced load vector of Equation 5-31 may now be evaluated by adding the approximate nodal stress resultants as determined above, into the applied load vector $\{\Delta R\}$.

5.7 Summary

In this chapter the finite incremental equilibrium equations,

for inelastic beam-columns, have been formulated with respect to two reference systems. It should be noted that the incremental stiffness matrix developed in Formulation 2 is not exact, since the rotation of the principal axes throughout the element length is not taken into account. Using the formulations developed in this chapter, inelastic beam-column and bifurcation problems are solved in Chapter VI.

TABLE 5-1 TRANSFORMATION MATRIX

	ΔU_s^P	ΔV_s^P	ΔW_c^P	$\Delta \phi^P$	$\Delta U_{s,z}^P$	$\Delta V_{s,z}^P$	$\Delta \phi_{,z}^P$	ΔW_{cm}
u_{ξ}^P	$\cos(\phi^P + \alpha^P)$	$\sin(\phi^P + \alpha^P)$		$\frac{\bar{x}^P \sin \alpha^P - \bar{y}^P \cos \alpha^P}{\bar{y}^P \sin \alpha^P}$				
v_{η}^P	$-\sin(\phi^P + \alpha^P)$	$\cos(\phi^P + \alpha^P)$		$\frac{\bar{x}^P \cos \alpha^P + \bar{y}^P \sin \alpha^P}{\bar{y}^P \sin \alpha^P}$				
w_c^P			1		$y_o^P \sin \phi^P$ $-x_o^P \cos \phi^P$	$-y_o^P \cos \phi^P$ $-x_o^P \sin \phi^P$		
ϕ^P				1				
$\ell u_{\xi,z}^P$					$\ell \cos(\phi^P + \alpha^P)$	$\ell \sin(\phi^P + \alpha^P)$	$(\bar{x}^P \sin \alpha^P - \bar{y}^P \cos \alpha^P) \ell$	
$\ell v_{\eta,z}^P$					$-\ell \sin(\phi^P + \alpha^P)$	$\ell \cos(\phi^P + \alpha^P)$	$(\bar{x}^P \cos \alpha^P + \bar{y}^P \sin \alpha^P) \ell$	
$\ell \phi_{,z}^P$							ℓ	
w_{cm}	$\frac{3}{2} \frac{\tilde{x}}{\ell}$	$\frac{3}{2} \frac{\tilde{y}}{\ell}$			$\frac{1}{4} \tilde{x}$	$\frac{1}{4} \tilde{y}$		1

Table 5-1 (cont'd)

	$-\frac{3}{2} \frac{\tilde{x}}{\ell}$	$-\frac{3}{2} \frac{\tilde{y}}{\ell}$		$\frac{1}{4} \tilde{x}$	$\frac{1}{4} \tilde{y}$	w_{cm}
	$\cos(\phi^q + \alpha^q)$	$\sin(\phi^q + \alpha^q)$	$\frac{\tilde{x}^q \sin \alpha^q - \tilde{y}^q \cos \alpha^q}{\tilde{x}^q \cos \alpha^q + \tilde{y}^q \sin \alpha^q}$			u_{ξ}^q
	$-\sin(\phi^q + \alpha^q)$	$\cos(\phi^q + \alpha^q)$				v_{η}^q
			1	$y_O^q \sin \phi^q$ $-x_O^q \cos \phi^q$	$-y_O^q \cos \phi^q$ $-x_O^q \sin \phi^q$	w_C^q
			1			ϕ^q
				$\ell \cos(\phi^q + \alpha^q)$	$\ell \sin(\phi^q + \alpha^q)$	$\ell u_{\xi,z}^q$
				$-\ell \sin(\phi^q + \alpha^q)$	$\ell \cos(\phi^q + \alpha^q)$	$\ell v_{\eta,z}^q$
						$\ell \phi_{,z}^q$
ΔW_{cm}	ΔU_S^q	ΔV_S^q	ΔW_C^q	$\Delta \phi^q$	$\Delta V_{S,z}^q$	$\Delta \phi_{,z}^q$

where $\bar{x} = (b_x - e_x)$; $\bar{y} = (b_y - e_y)$
 $\tilde{x} = x_{om} \cos \phi_m - y_{om} \sin \phi_m$
 $\tilde{y} = y_{om} \cos \phi_m + x_{om} \sin \phi_m$

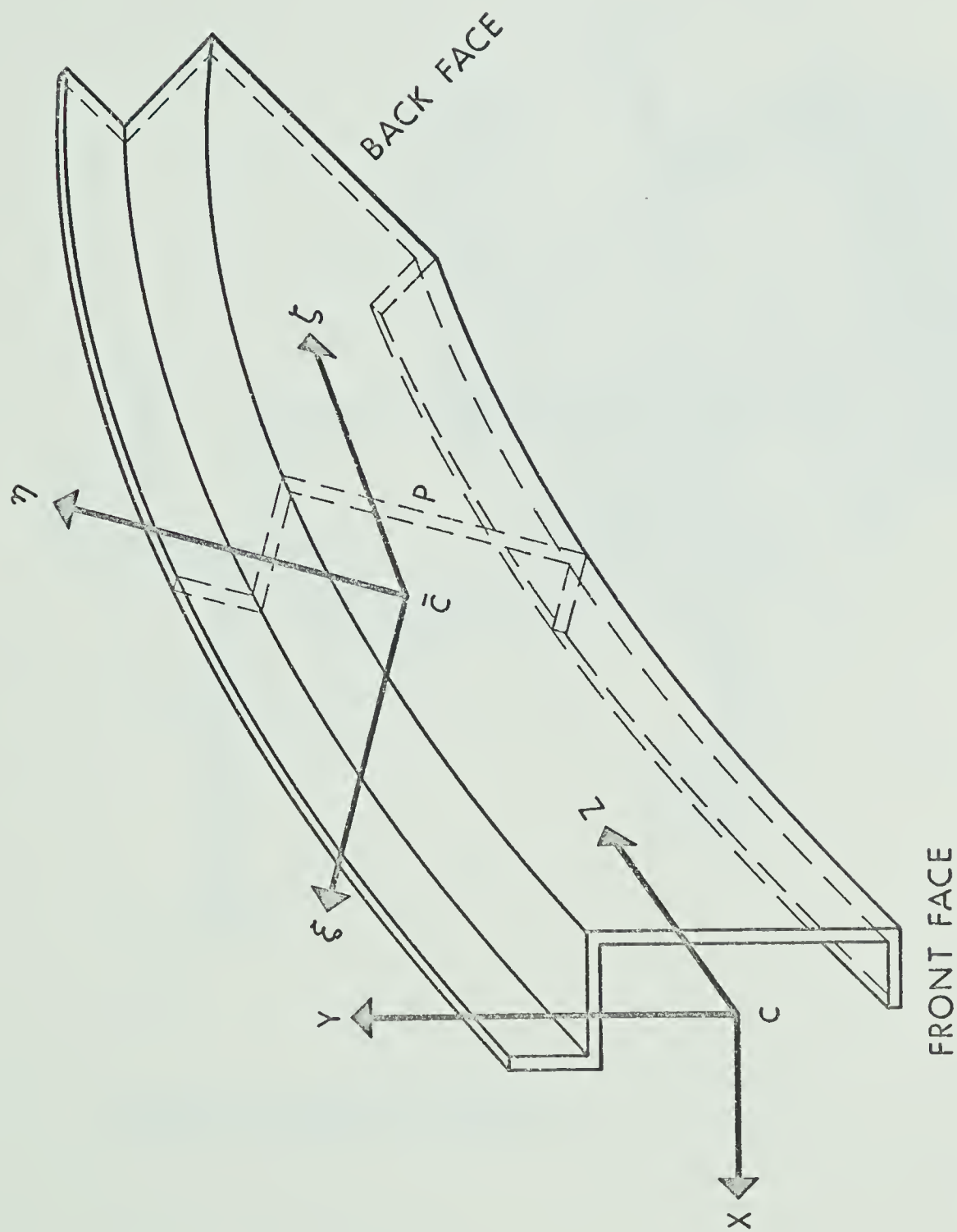


FIGURE 5.1 ISOLATED BEAM-COLUMN



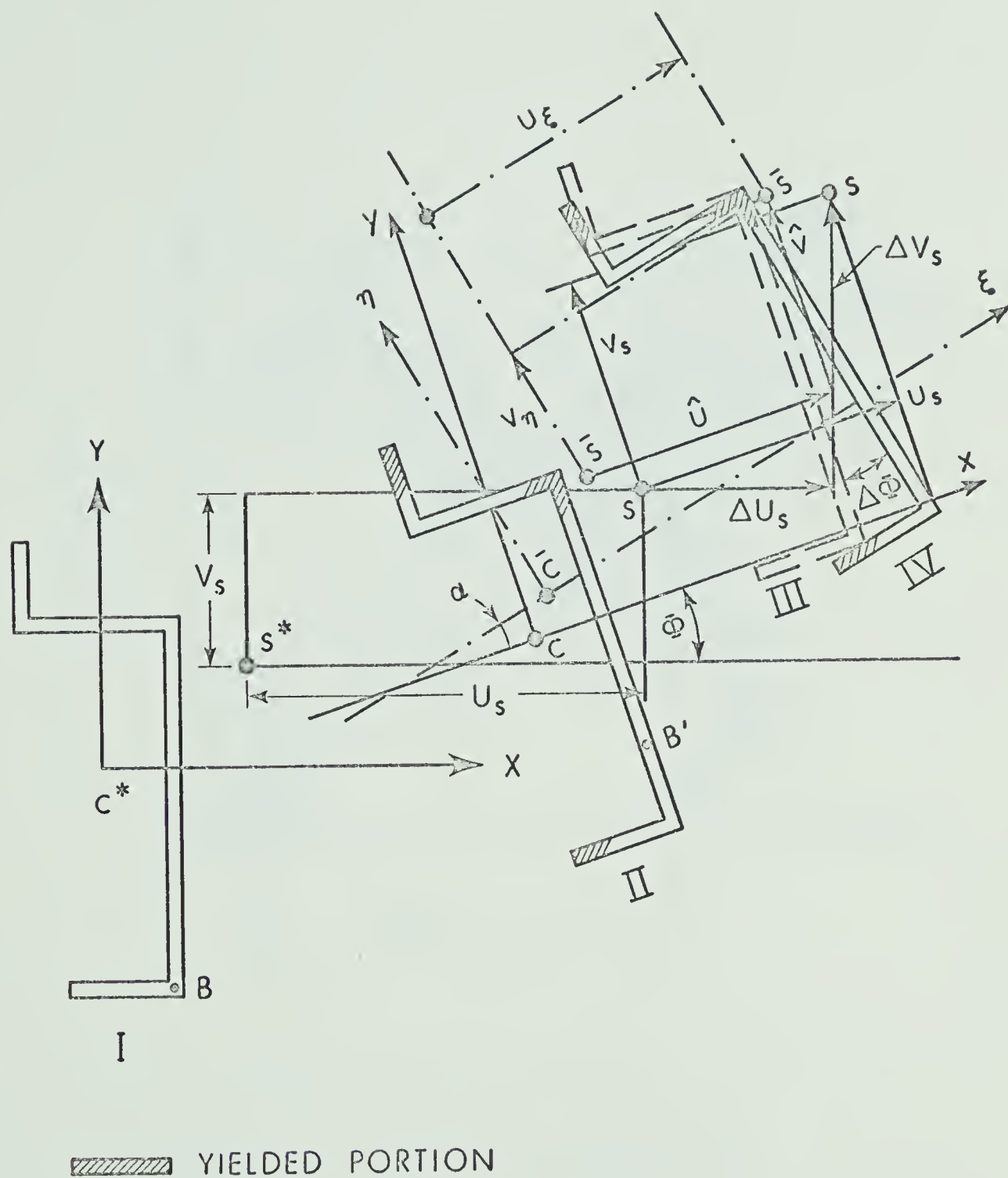


FIGURE 5.2 CROSS SECTION OF THE COLUMN IN DISPLACED POSITION

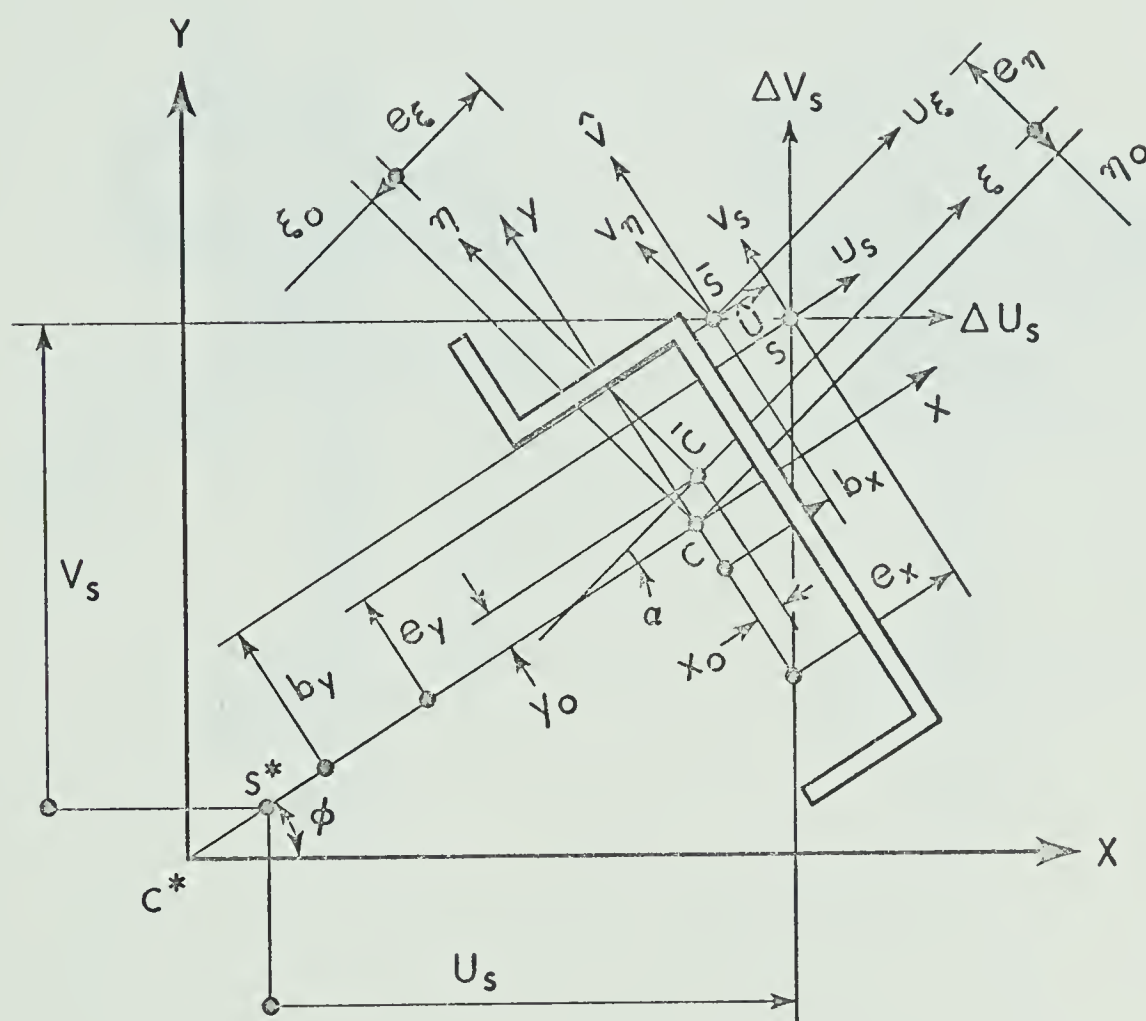
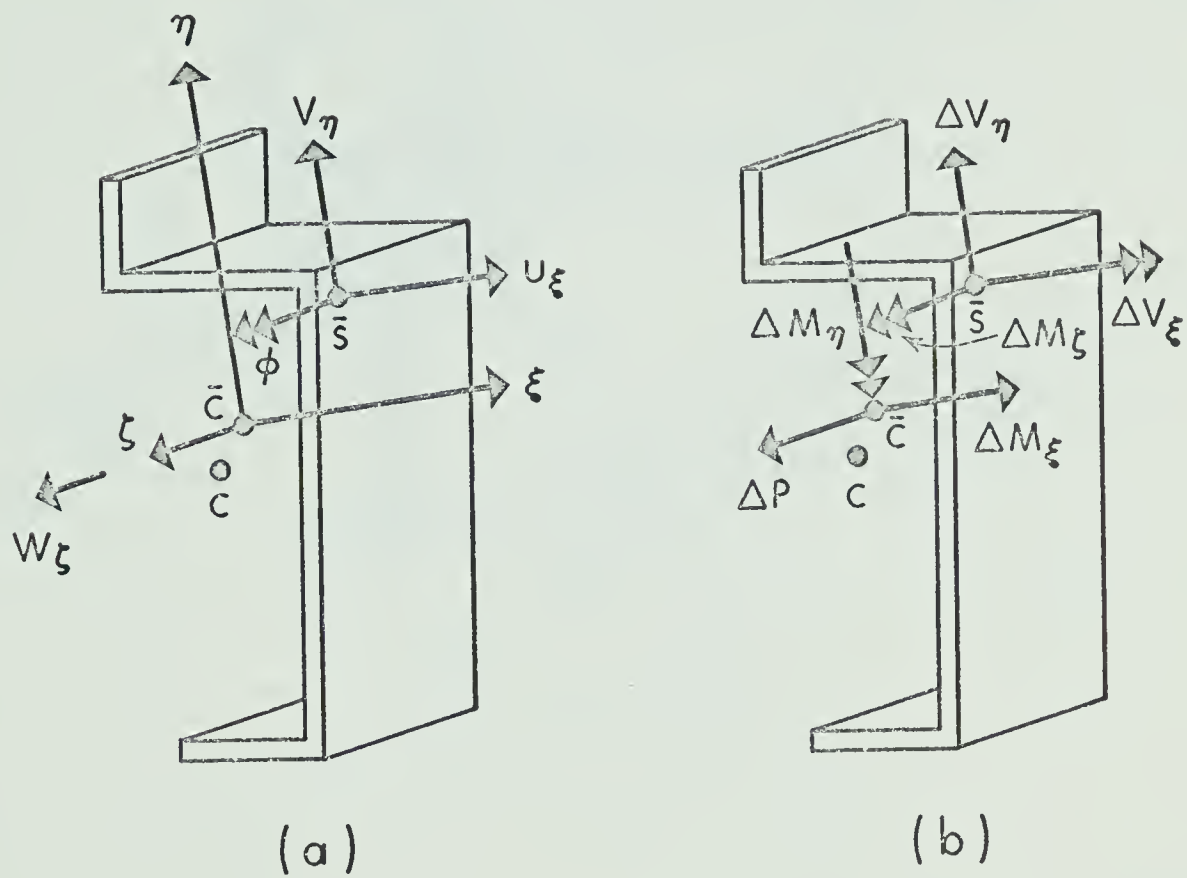
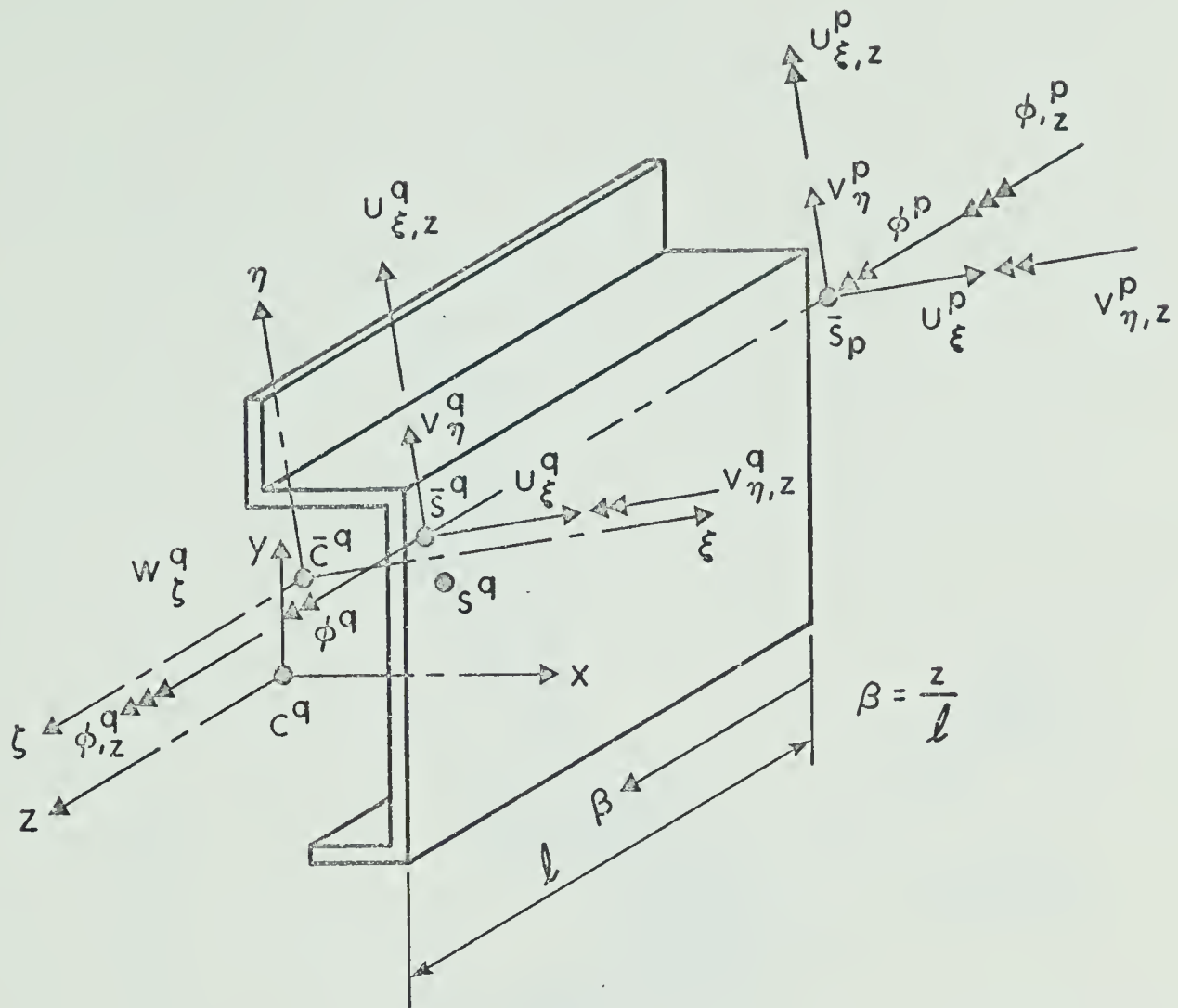


FIGURE 5.3 COORDINATE TRANSFORMATION







$$\{\underline{u}\}^T = \langle u_{\xi}^p, l u_{\xi,z}^p, u_{\xi}^q, l u_{\xi,z}^q \rangle$$

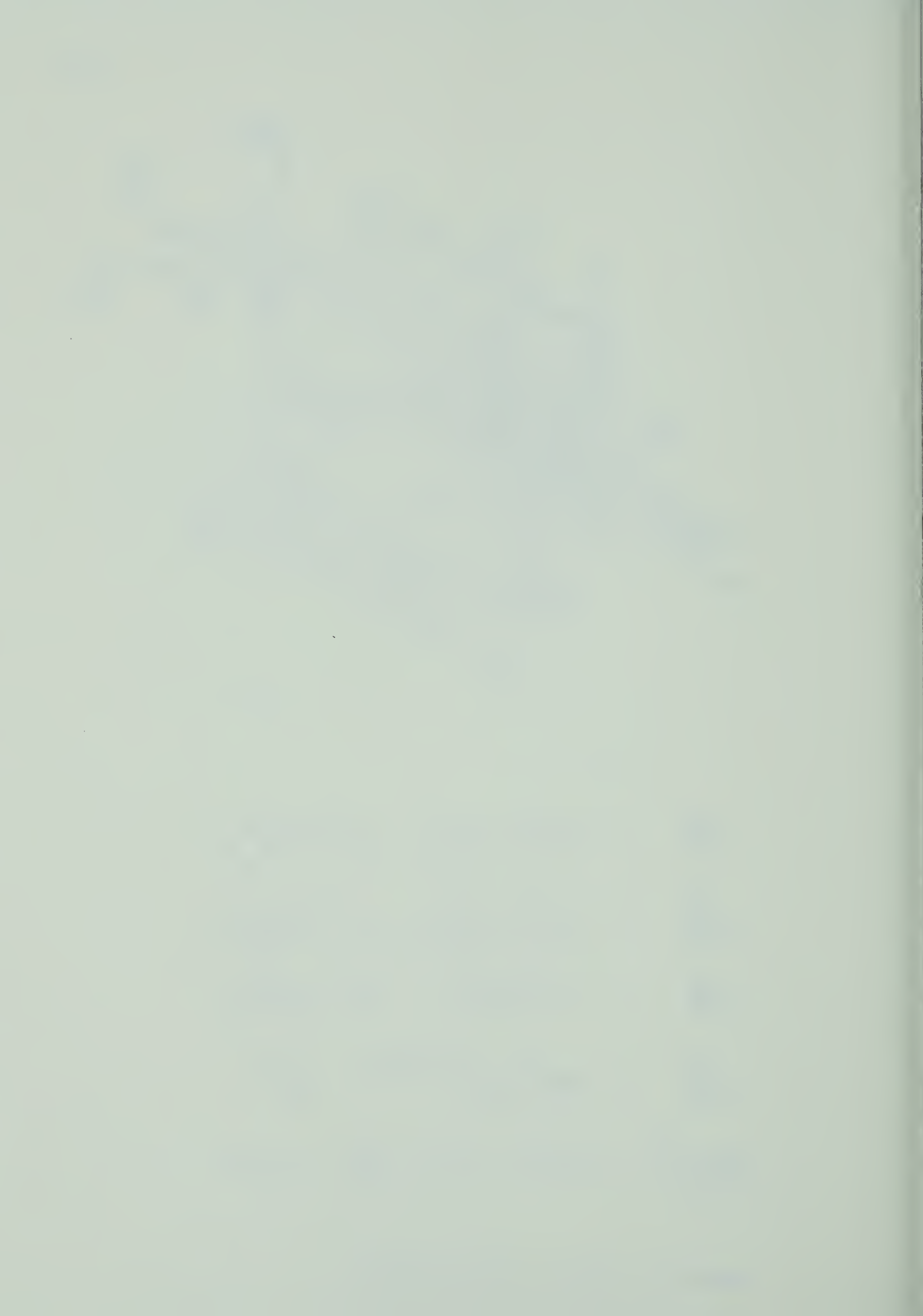
$$\{\underline{v}\}^T = \langle v_{\eta}^p, l v_{\eta,z}^p, v_{\eta}^q, l v_{\eta,z}^q \rangle$$

$$\{\underline{\phi}\}^T = \langle \phi^p, l \phi_{,z}^p, \phi^q, l \phi_{,z}^q \rangle$$

$$\{\underline{w}\}^T = \langle w_{\zeta}^p, w_{\zeta}^{(p+q)/2}, w_{\zeta}^q \rangle$$

$$\{\Delta r_E\}^T = \langle \langle \underline{u} \rangle, \langle \underline{v} \rangle, \langle \underline{\phi} \rangle, \langle \underline{w} \rangle \rangle$$

FIGURE 5.5 ELEMENT, NODAL PARAMETERS



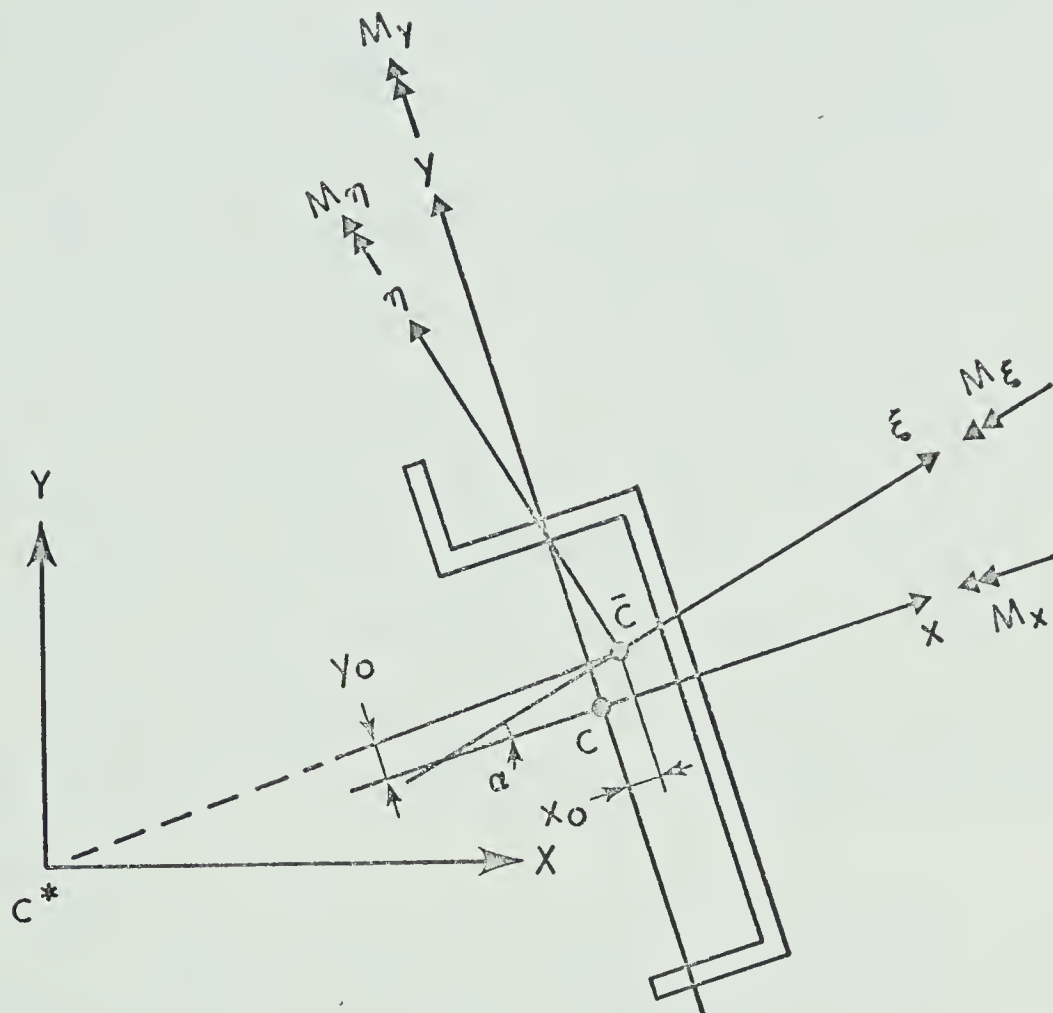


FIGURE 5.6 TRANSFORMATION FOR STRESS RESULTANTS

CHAPTER VI

SOLUTION FOR INELASTIC MEMBERS

6.1 Introduction

To date no general study of the inelastic behaviour of beam-columns bent out of plane is available, but a number of solutions for special cases have been obtained. The ultimate load carrying capacity of H-columns under biaxial loading has been studied by Birnstiel (11,12,32). Their procedure requires successive trials and corrections and is based on an indirect incremental load analysis in which strain history is considered. Recently Smith (64) considered the biaxially loaded column in terms of the equations of three dimensional elasticity taking into account the nonlinear effects of the end tractions. Inelastic lateral-torsional buckling problems have been investigated by Galambos (24,25), Fukumoto (22,23) and others (47). However, a comprehensive theoretical solution is not yet available for general loading conditions.

In this chapter inelastic beam-column problems and inelastic buckling problems are solved using the formulations developed in Chapter V. Inelastic beam-column problems are solved by Formulation 2 (discussed in Section 5.2.6) using an iterative incremental technique, and inelastic buckling problems are solved as an eigenvalue solution for critical length by both Formulations 1 and 2.

6.2 In-plane Behaviour of Inelastic Beams

The term 'in-plane' behaviour is used to describe behaviour in which the deflection of the shear centre is in a principal direction of the cross section. In order to verify the model, and the solution

technique, the in-plane behaviour of simple beam-columns has been studied. The bending moment acting at any section of a beam-column is composed of the primary moment M_o (i.e. the static moment computed from original geometry), and the secondary moment (i.e. moments resulting from a change in the equilibrium equations due to the deflection of the member). For in-plane problems the secondary moment is expressed as Pv where v is the deflection in the principal direction. Assuming a portion of the member becomes plastic, the deflection v increases and the secondary moment becomes a proportionately larger component of the resisting moment. Eventually the beam-column is unable to support an increase of primary moment and thereafter the value of primary moment decreases as the deflection increases. For this type of problem, lateral and local buckling are assumed to be prevented, and the strains and displacements are assumed to be small.

The incremental finite element equation of Chapter V expressed as Equation 5-1 and Equation 5-31, may now be applied to beam-column problems by using the procedure outlined in Section 5.2.1.

For any iterate Equation 5-1 can be written as

$$[[K_S^T]_n + [K_G]_n] \{\Delta r_n\} = \{E\}_n \quad (6-1)$$

where $\{E\}_n$ is the vector of unbalanced residual nodal forces for the current configuration. This vector is evaluated, as described in Section 5.2.1, as

$$\{E\}_n = \{R\} - \{F\}_n - [K_G]_n \{r\}_n \quad (6-2)$$

where $\{R\}$ is the vector of total applied loads; $\{F\}_n$ is the vector of

resisting forces resulting from the stress resultants in the current configuration, computed as described in Section 5.6.2; and $[K_G]_n \{r\}_n$ represents the vector of forces resulting from the change in geometry from the original configuration, as discussed in Section 5.2.1.

In the case of in-plane beam-column response, with constant axial load, $[K_G]$ is constant. When $\{R\}$ is applied to the structure, the response is $\{r\}_1 = \{\Delta r\}_1$ for the first iterate, which can be computed from equation

$$[[K_S^T]_1 + [K_G]]\{\Delta r\}_1 = \{E\}_1 = \{R\}_1 \quad (6-3)$$

After the first and succeeding iterates, nodal point displacements are updated by adding the incremental displacements to the previous displacements. Strains and stresses are then computed from the total displacements.

In general the incremental equation is given by Equation 6-1 and iteration is repeated until the structure is in equilibrium with the applied forces. In the solution scheme $[K_S^T]$ is kept unchanged for some iterations, as discussed in Section 5.2.1, until the rate of convergence begins to deteriorate, at which time the matrix is updated with properties based upon the current displacements. This is a modified Newton-Raphson procedure. Since the nature of the problem is very sensitive to the applied forces and the type of stress-strain curve, an under-relaxation factor was used on the residual force vector. The procedure may diverge if the matrix is not updated often enough. This was also observed by Haisler (30) and Stricklin.

As has already been stated in Section 5.3 a linear variation of axial displacements is incapable of establishing equilibrium of

axial forces with variable section properties.

To achieve a balance of axial load at the end nodes of the elements, an additional degree of freedom at the mid-point of an element was introduced. Equilibrium is obtained as follows. Consider an element k whose resisting axial forces at node p and q are denoted by P_p^k and P_q^k and an adjacent element $(k+1)$, whose axial forces are P_p^{k+1} and P_q^{k+1} . The unbalanced force at the $(k+1)^{th}$ node is $P_p^{k+1} - P_q^k$. For inelastic problems, $P_p^k \neq P_q^k$ for a linear variation of curvature and a constant axial strain. Hence the unbalanced force $P_q^k - P_p^k$ on the element k was equilibrated by a force at the midpoint of the element k . Iteration was carried out until this unbalanced axial force at the center node was reduced to an arbitrarily small quantity and the axial loads at each end node were balanced. It was possible to achieve this condition because of the linear variation of axial strain. The axial stiffness with this additional degree of freedom is derived in Appendix A.

6.3 Solutions of Typical In-plane Inelastic Problems

E-1 Inelastic Bending of Simple Beam-Column of Rectangular Cross Section

An inelastic bending analysis was carried out for a cantilever beam of rectangular cross section, with dimensions and loading as shown in Fig. 6.1. The stress-strain curve of Fig. D.1a was used in the numerical solution of all problems with the values of E , E_s shown in Table 6-3a. The element idealization is also shown in the figure. For a constant axial load and a specified displacement at the free end, the reaction Q at the free end, where the transverse displacement is specified, determines one half the loading corresponding to the

displacement of a simply supported beam-column with a concentrated load at the center. The load vs end deflection curves are shown in Fig. 6.1 for the cases of $P/P_y = 0$; $P/P_y = 0.152$; $P/P_y = 0.632$. Moment curvature relationships are also shown and compared with theoretical values in Fig. 6.2. The results are compared with second order elastic and second order rigid plastic solutions in Fig. 6.1.

E-2 Inelastic Bending of a Simple WF Beam-Column

As in example E-1, one half of a simply supported beam-column with a concentrated load at the center was simulated by the cantilever shown in Fig. 6.3. Displacement was again specified at the free end. The figure shows the load vs deflection plot for both strain hardening and elastic-ideally plastic cases, and compares the results with the second order rigid plastic solution.

E-3 Beam-Column: Moment at one end

The behaviour of a beam-column, shown in Fig. 6.4, is represented by relating the applied moment, M_o , to the end rotation, θ_o . The beam was subjected to an axial load of $0.49 P_y$, which was kept constant. An end moment M_o was applied about the major axis of the member at one end. The solution was obtained by specifying the displacement θ_o and iterating with this as a displacement boundary condition. Instability is demonstrated by the decrease in moment capacity beyond the maximum value. The figure shows the comparison of experimental and computed end rotation curves. The discrepancy between theoretical and experimental results is consistent with that of Kauren (73) and Galambos who reported a computed maximum value for M_o/M_p of 0.55 compared with the experimental value of 0.60.

E-4 Beam-Column with equal End Moments

The section analyzed was an 8WF31 with residual stress distribution as shown in Fig. 6.5. P was kept constant at $0.7P_y$. Hence the column is inelastic from the beginning of loading. Half the beam is considered because of symmetry. End A was free to move vertically and loading was applied by imposing an end rotation. Very small increments in rotation were specified at this end and iteration was carried out to find the equilibrium configuration. The end moment - rotation curve is shown in Fig. 6.5 and compared with the curve given in the Lehigh University design aids (57). (The Lehigh University design aid is based on $\sigma_y = 36\text{ksi}$, $\sigma_{rc} = 0.3 \sigma_y$, and no strain hardening.) Convergence of this problem was slow and hence the solution scheme was not carried out beyond the peak.

6.4 Solution of General Beam-Column Problems

In the examples of Section 6.3, all displacements except those in the y - z plane were suppressed. Some examples of the more general beam-column problem, in which out-of-plane displacements also occur, are presented in this section.

E-1 Twist of An Inelastic Beam-Column

In order to test the behaviour of the model when inelastic torsional response occurs, a cantilever WF beam, as shown in Fig. 6.6, was subjected to applied axial loads of 40k at each node and a torque, M_T , applied at the free end. The analysis of this problem was principally carried out to test the convergence of the bimoment in the inelastic range. No theoretical solution is available for comparison,



but convergence of unbalanced forces was achieved.

E-2 Inelastic H-Columns under Biaxial Bending

A 14WF43 section with a doubly eccentric axial load, applied at eccentricities of $e_x = 0.5"$ and $e_y = 5"$, and $L/r_y = 117$, was analysed and compared with the results obtained by Harstead (32) and Birnstiel, et. al., (11). Their procedure is given in Table 6-1. This problem involves coupling of axial deformations, bending deformations about two axes, and nonuniform torsional deformation in the inelastic range of Beam-column response. The load was incremented until the displacements no longer converged. Fig. 6.7 shows the load and midpoint displacement relationships. Unlike the case of the problems discussed in Section 6.3, boundary displacement increments cannot be adopted for loading, since the adjustment of the end displacements in the proper ratios is difficult. The procedure of incrementing the forces yielded results until a maximum load was attained, but numerical difficulties did not permit an evaluation in the unloading region. The results agree well with Birnstiel's analysis.

E-3 Inelastic Lateral Response with Initial Imperfections

An 8WF31 beam-column with the residual stress distribution shown in Fig. 6.8 was analyzed while subjected to a constant axial load of 120 kips ($P/P_y = 0.4$) and with an initial lateral displacement of $u = 0.01 \sin \pi z/L$. A beam-column solution was carried out until, with an end moment of 440 inch-kips, the residual force resultants no longer converged. Moment vs in-plane and out-of-plane response is shown in Fig. 6.8. For the same problem the eigenvalue solution yields a critical length of 100" for end moments of 480 inch-kips, and this is shown as an upper bound in the figure.

6.5 Inelastic Buckling

6.5.1 Formulation of Problem

Inelastic buckling (or bifurcation) analyses can be carried out if it is assumed that, as for the beam-column problems, a reasonable estimate of the load carrying capacity may be obtained by employing Shanley's (62) tangent modulus concepts. The basic assumption is that no strain reversal occurs, and therefore the effective incremental stiffness at any section may be determined from the instantaneous tangent modulus values at all parts of the cross section. Since the stress in the member is essentially uniaxial, the effective strain, for the determination of tangent moduli, is considered to be the longitudinal strain. The incremental section properties may then be computed by a transformed area concept, as discussed in Section 5.2.3 and 5.5.

In addition to the above, the following assumptions are made for bifurcation problems:

1. The members are initially straight and prismatic.
2. The projection of the cross section on a plane normal to the centroidal axis does not distort.
3. Displacements of a point may be obtained by superimposing warping displacements on plane section displacements, each of which are consistent with simple beam theory (54,68,74).
4. The residual stress distribution satisfies statics.
5. Variation of the longitudinal stress across the plate thickness may be neglected.
6. The effect of prebuckling displacements on the equilibrium equations may be neglected.
7. Boundary conditions are such that the structure remains statically



determinate.

8. The stress-strain curve is trilinear (Fig. D.1a).

It should be noted that it is due to assumptions 1) and 6) that the more realistic but numerically more difficult, beam-column problem is converted to a bifurcation problem. The remaining assumptions are the same as those used for beam-columns, except for (7).

A bifurcation loading condition has been attained if it is possible to determine nontrivial solutions to Equation 5-31, for $\{\Delta R\} = 0$. The condition required to satisfy this requirement is that the determinant of the coefficient matrix is equal to zero, i.e.

$$\det \{[K_S^T] + [K_G]\} = 0 \quad (6-4)$$

If $[K_S^T]$ were independent of load and $[K_G]$ were linearly dependent on load the critical loading could be obtained from a standard eigenvalue analysis. However, for an arbitrary cross section, subjected to arbitrary loads the matrix $[K_S^T]$ is highly sensitive to the loading condition after inelastic response has been initiated.

The critical loading may now be determined in a number of ways. Fukumoto (22,23) has evaluated the determinant and extrapolated or interpolated this value to determine the loading for which Equation 6-4 is satisfied. Harris and Pifko (31) have used an iterative approach on the load and found the load level for which the eigenvalue was one. The procedure used in this dissertation is to iterate for an eigenvalue to determine the critical length rather than the critical load.

6.5.2 Inelastic Buckling by Direct Method

For any arbitrary statically determinate loading, equilibrium is established, including the effects of inelastic material response but neglecting the effect of displacements on the equilibrium equations, by an iterative procedure detailed in Table 6.2. Knowing the strain throughout the member the tangent stiffness matrix $[K_S^T]$ can be established as outlined in Section 5.5 and detailed in Appendix E. The prebuckling stress resultants can also be established by simple integration as detailed in Appendix D3. This permits the evaluation of $[K_G]$ as detailed in Appendix E.

An examination of the stiffness matrices in Appendix E shows that Equation 6-4 may be written as

$$[[K_1] + [K_2] + [K_3]] \{\Delta r\} + [K_G] \{\Delta r\} = \{\Delta R\} \quad (6-5)$$

where K_1 , K_2 and K_3 contain terms dependent on the inverse of L , L^2 and L^3 respectively. Noting that $[K_G]$ is proportional to the inverse of L , defining the critical length L_c as $L_c = \lambda L$, and factoring λ ; the condition for the existence of nontrivial solutions of Equation 6-5 with $\{\Delta R\} = 0$ may be written as

$$\frac{1}{\lambda^2} [[K_3] + \lambda[K_2] + \lambda^2[K_1]] \{\Delta r\} = - [K_G] \Delta r \quad (6-6)$$

This equation may be abbreviated as

$$\frac{1}{\lambda_{i+1}^2} [[K (\lambda_i)]] \Delta r = - [K_G] \Delta r \quad (6-7)$$

For any general problem under any general loading, assuming a value for λ_i , an eigenvalue solution will yield λ_{i+1} . Equation 6-7 may be iterated until $\lambda_{i+1} = \lambda_i$ at which time the critical length has been

determined. When the equations corresponding to δu , δv and $\delta \phi$ $[K_S^T]$ matrix are uncoupled from that of δw , these uncoupled equations do not depend on λ . Hence the first iterate of Equation 6-7 gives the exact solution for critical length. When the tangent properties are assumed to be the same all along the length, then also the first iterate will lead to an exact solution for critical length. Only such problems are considered in this dissertation since no solutions with the more general coupling are available for comparison.

It should be noted that the procedure described for the solution of Equation 6-7 is only valid if $[K_G]$ is proportional to the inverse of L and therefore the stress resultants must remain constant at each node as the member length is scaled. A simultaneous scaling of the transverse loading is required to satisfy this condition. Since stress resultants are not proportional to loading for statically indeterminate inelastic structures the method is applicable only to statically determinate structures.

6.5.3 Inelastic Buckling by a Beam-column Approach

In order to account for prebuckling deformation, a beam-column equilibrium configuration can be established for any trial loading, by the procedure discussed in Section 6.2. Knowing the deflections, the total moment at any section may be computed and the tangent flexural stiffness and geometric stiffnesses may be evaluated as discussed in Section 6.5.2. Solving the eigenvalue problem, a critical length can be determined from one iterate of Equation 6-7. If this critical length is the same as the actual length of the column the trial loading is the critical one. If the critical length is

greater (less) than the actual length, the true loading level is less (greater) than the critical state. In this case the load may be incremented (decremented) and the resulting eigenvalue problem is solved by successive trials until $\lambda = 1$. This procedure is time consuming and expensive and hence has not been generally adopted in the present investigation. However, the procedure was used for example E-2 of Section 6.4 and the results are shown in Fig. 6.19 where they are compared with those from the methods of Section 6.5.2.

6.6 Solution of Inelastic Buckling Problems

E-1 Flexural and Lateral Torsional Buckling of Double Angle Strut

Double angle struts are used in building structures as compression members in trusses. They are usually subjected to axial load and the secondary bending moment arising from the connections is neglected. The details of the section analyzed and the residual strain distribution are shown in Fig. 6.9a and Table 6-3b. The St-Venant torsional stiffness, GK_T , was kept at the elastic value in order to compare with the results obtained by Nuttall(53). Nuttall's solution was obtained by imposing a uniform axial strain, evaluating transformed section properties numerically and solving the normal stability equations for critical length. For this particular problem the yy axis buckling strength virtually coincided with the lateral torsional buckling strength, since $(1 - e_y^2/r_o^2)$ is approximately one throughout the loading range. Fig. 6.9b shows the plot of σ/σ_y values against the slenderness ratio, L/r_x , for lateral torsional buckling and xx axis buckling. The influence of the residual stress and the significance of the inelastic response is apparent. The results obtained from the finite element analysis agree with the results of Nuttall.

E-2 Flexural and Lateral Torsional Buckling of Hat-shaped Sections

Hat shaped sections are often used as chord members of open web steel joists. The dimensions of the section analyzed, the normalized warping coordinates and the residual stress distribution are shown in Fig. 6.10a, b and c, respectively. Critical buckling occurs about the minor axis as shown in Fig. 6.11. Critical lengths for lateral torsional buckling are also computed and compared with the results obtained by Heaton (33).

E-3 Inelastic Lateral Buckling of a Doubly Symmetric Section

The inelastic beam buckling curve for an 8WF31 section subjected to equal end moments is shown in Fig. 6.12. This curve consists of three parts. The first and last part of the curve represent classical elastic buckling with $E=E$ and $E=E_s$ respectively. The intermediate portion of the curve represents buckling in the inelastic range and is applicable when some parts of the cross section have yielded while other parts are elastic. The strain hardening and elastic curves are hyperbolas which do not intersect. The curve for inelastic buckling provides a transition between these two idealizations. The St. Venant constant was assumed to vary linearly with the transformed area. A solution of the problem was obtained by Galambos (25). The importance of the residual stress distribution is again demonstrated and the comparison is reasonably good.

E-4 Inelastic Lateral Buckling of Mono-Symmetrical Sections

The double angle section of E-1 was analysed for inelastic lateral buckling. The inelastic buckling curve is shown in Fig. 6.13. Only a theoretical elastic buckling solution is available for comparison.

E-5 Inelastic Lateral Torsional Buckling of an Unsymmetrical Section (example 1)

In the case of mono or doubly symmetric sections the response of the beam-column is in-plane until the buckling occurs. But in the case of unsymmetrical sections the beam will deflect laterally and twist from the start of the application of the load. The eigenvalue solution of the problem will give an upper bound for the load since prebuckling deformations are neglected. Fig. 6.14 shows the inelastic lateral torsional buckling of an angle section (67) subjected to end moments. The experimental point of Thomas and Leigh is shown on the plot. The discrepancy is probably due to the fact that prebuckling deformations have been neglected.

E-6 Inelastic Lateral-Torsional Buckling of an Unsymmetrical Section (example 2)

Results for a similar type of problem to example E-5 are shown in Fig. 6.15, for the inelastic lateral torsional buckling of an unsymmetrical section when one channel is placed over the other. An elastic solution to this problem was obtained (in E-4 of Section 3.3.3). No comparative solution is available.

E-7 Inelastic Lateral Torsional Buckling of Beam-Columns (Axial Load-Equal Eccentricity)

Fig. 6.16 shows a comparison of the finite element analysis for inelastic torsional buckling of an 8WF31 beam-column, under an axial load with constant eccentricity, with that of Galambos (24). Since the secondary moment due to prebuckling deformation is neglected the inelastic properties are assumed to be the same at all sections. Hence properties for only one section need be calculated. The results of the finite element analysis agree well with those of Galambos.

E-8 Inelastic Lateral Torsional Buckling of Beam-Column with Moment Gradient

Fig. 6.17 compares the critical end moment required to produce lateral torsional buckling of an 8WF31, subjected to constant axial load, to that obtained by Fukumoto (22,23). In contrast to the preceding comparative solutions, Fukumoto's solution included the effect of in-plane prebuckling displacements in arriving at an equilibrium configuration. The critical load is then determined as that for which the determinant vanishes. In the finite element analysis an eight elements idealization is used and the results are compared with Fukumoto's analysis. The effect of prebuckling displacements is apparently small.

E-9 Inelastic Lateral Buckling of a Wide Flange Beam Subjected to a Central Load

In Fig. 6.18 the critical moment vs slenderness ratio curve is shown for an 18WF50 beam subjected to a central load. A large reduction in the buckling strength results when the presence of residual stress initiates inelastic behaviour. The curves are compared with Massey's, et. al., (48) recommended curve obtained from a theoretical analysis. Massey used $M_{FP}/M_y = 1.05$ to 1.06 and $M_p/M_y = 1.14$ to 1.15 , which are applicable to most wide flange sections, where M_{FP} is the bending moment at which the flanges are fully yielded. In Massey's analysis, residual stress distribution is not taken into account. In the present analysis, the computed points assume the loads act through the shear centre. When the load is considered to act at the top or bottom flange the problem must be solved by a trial and error solution for the critical length.

E-10 Inelastic Lateral Torsional Buckling with Biaxial Bending

An inelastic buckling analysis was carried out for the beam-column problem of example E-2 of Section 6.4. Fig. 6.19 shows a plot of critical loads for biaxial bending of the section determined from an eigenvalue analysis and neglecting prebuckling deformations. The curves are drawn for two cases: a) without residual stress b) with residual stress. In addition to the eigenvalue analysis of Section 6.5.2, the method of Section 6.5.3 was also applied. For a column length of 221" ($L/r_x = 37.6$) and a load of 125 kips the critical length obtained was 283 inches, showing that the load level was below the ultimate load. At $P = 134$ kips the critical length was found to be 226 inches indicating that 134 kips was very near to the ultimate load. However, the critical load based upon the eigenvalue analysis and neglecting prebuckling deformation (i.e. the method of Section 6.5.2), is 27% greater than beam-column result obtained by either the method of Section 6.5.3 or 6.4. In such situations the effect of prebuckling displacement cannot be ignored.

6.7 Summary and Conclusions

In this chapter the inelastic equations derived in Chapter V have been applied to a variety of problems. Inelastic beam-column problems were solved by a modified Newton-Raphson technique. Although this technique was shown to yield good results for in-plane problems and yields results for a more general biaxial bending beam-column problem, which corresponds to the only known available solution of this problem, the technique is difficult to apply. Problems solved in this way require considerable computing time and it is necessary to

input information controlling the load step size and under-relaxation parameters, in addition to a criterion for updating the coefficient matrices.

The solution of inelastic stability problems neglecting pre-buckling deformation, was shown to yield results which compare well with existing solutions in the literature, for a wide variety of applications. The determination of maximum load carrying capacity, including the effects of prebuckling deformations by the method of Section 6.5.3, yields the same results as the beam-column solution of Section 6.5.4, and at the same time yields an upper bound to the carrying capacity at any stage of the analysis.

TABLE 6-1

Birnstiel's Procedure for Solution of H-Columns Under Biaxial Bending

1. Assume trial values of curvatures corresponding to M_x , M_y , W_ω and axial strain
2. Numerically integrate the curvatures to determine the displaced position of the column
3. Calculate the values of internal bending moment and axial load at each station. Because the values of axial force differ (in the inelastic range) select the value at mid point as the control value of P
4. On the basis of the displaced position and P compute the external bending moment at each station
5. Compare external moments with internal moment. If they do not agree adjust curvatures corresponding to M_x and M_y
6. Repeat steps 2 to 5 until convergence is attained in step 5
7. Determine external torque at each station
8. Compute internal torque at each section
9. Compare external torque to internal torque. If they do not agree adjust $d^2\phi/dz^2$ and integrate numerically to determine ϕ
10. Repeat 7 to 9 until convergence is attained in step 9
11. Repeat 6 and 10 until convergence is attained in 5 and 9
12. Repeat steps 1 to 11 until the desired displacement or ultimate carrying capacity is attained

TABLE 6-2

ALGORITHM FOR DETERMINING INELASTIC CRITICAL LENGTHS

Step 1. Determine Static Stress Resultants

- (a) Subdivide the member into elements of equal length.
- (b) Compute the elastic section properties A , I_x , I_y , I_{xy} , K_T , I_ω and \hat{I}_x and \hat{I}_y , where

$$\hat{I}_x = I_x(1 - I_{xy}^2/I_x I_y) \quad (6-8a)$$

$$\hat{I}_y = I_y(1 - I_{xy}^2/I_x I_y) \quad (6-8b)$$

with C and S located at the centroid and shear centre of the section, (Fig. 2.1).

- (c) Solve for displacements, with $[K_G] = 0$ and $[K_S]$ determined from elastic properties.
- (d) Compute stress resultants \hat{P} , \hat{M}_x , \hat{M}_y and \hat{W}_ω at each node for this small deflection solution.

Note: The stress resultants determined in this way are those which equilibrate the external forces.

Step 2. Determine Strains (Iteratively) Which Produce Static Stress Resultants

- (a) Compute strains from the initial approximate displacements, as

$$\epsilon = w'_c - y v''_s - x u''_s + \bar{\omega} \phi'' + \epsilon_R \quad (6-9)$$

- (b) Calculate stress resultants, P , M_x , M_y and W_ω , (see Appendix D) for the given strain distribution.

Table 6-2 (cont'd)

(c) Compute the unbalance in stress resultants, as

$$\bar{P} = \hat{P} - P \quad (6-10a)$$

$$\bar{M}_x = \hat{M}_x - M_x \quad (6-10b)$$

$$\bar{M}_y = \hat{M}_y - M_y \quad (6-10c)$$

$$\bar{W}_\omega = \hat{W}_\omega - W_\omega \quad (6-10d)$$

(d) Compute equivalent unbalanced stress resultants, P^* ,

M_x^* , M_y^* and W_ω^* about C and S, where

$$P^* = \bar{P} \quad (6-11a)$$

$$W_\omega^* = \bar{W}_\omega \quad (6-11b)$$

$$M_x^* = \bar{M}_x - \bar{M}_y I_{xy}/I_y \quad (6-11c)$$

$$M_y^* = \bar{M}_y - \bar{M}_x I_{xy}/I_x$$

(e) Estimate strain increments from the equation

$$\Delta\epsilon_i = \frac{P^*}{A} + \frac{M_x^*}{\hat{I}_x} y + \frac{M_y^*}{\hat{I}_y} x + \frac{W_\omega^*}{\hat{I}_\omega} \bar{\omega} \quad (6-12)$$

and a new approximate strain, as

$$\epsilon_{i+1} = \epsilon_i + \Delta\epsilon_i \quad (6-13)$$

(f) Iterate on steps (2-b) to (2-e) until the unbalanced stress resultants are negligible.

Table 6-2 (cont'd)

Note: A set of strains have now been determined which will provide stress resultants to equilibrate the external forces, assuming the prebuckling displacements have negligible effect on the equilibrium equations.

Step 3. Computation of Tangent and Geometric Stiffness Matrices

- (a) The tangent stiffness matrix, $[K_s^T]$, of Equation 6-4 may now be evaluated as outlined in Section 5.3.1 and detailed in Appendices D and E.
- (b) The geometric stiffness matrix, $[K_G]$, of Equation 6-4 may now be evaluated as outlined in Chapter 5 detailed in Appendices D and E.

Step 4. Solution for Critical Length

- (a) Equation 6-7 is solved for λ , to determine the critical length $L_C = \lambda L$, as described in the solution procedure.



TABLE 6-3a PARTICULARS OF BEAM-COLUMN PROBLEMS

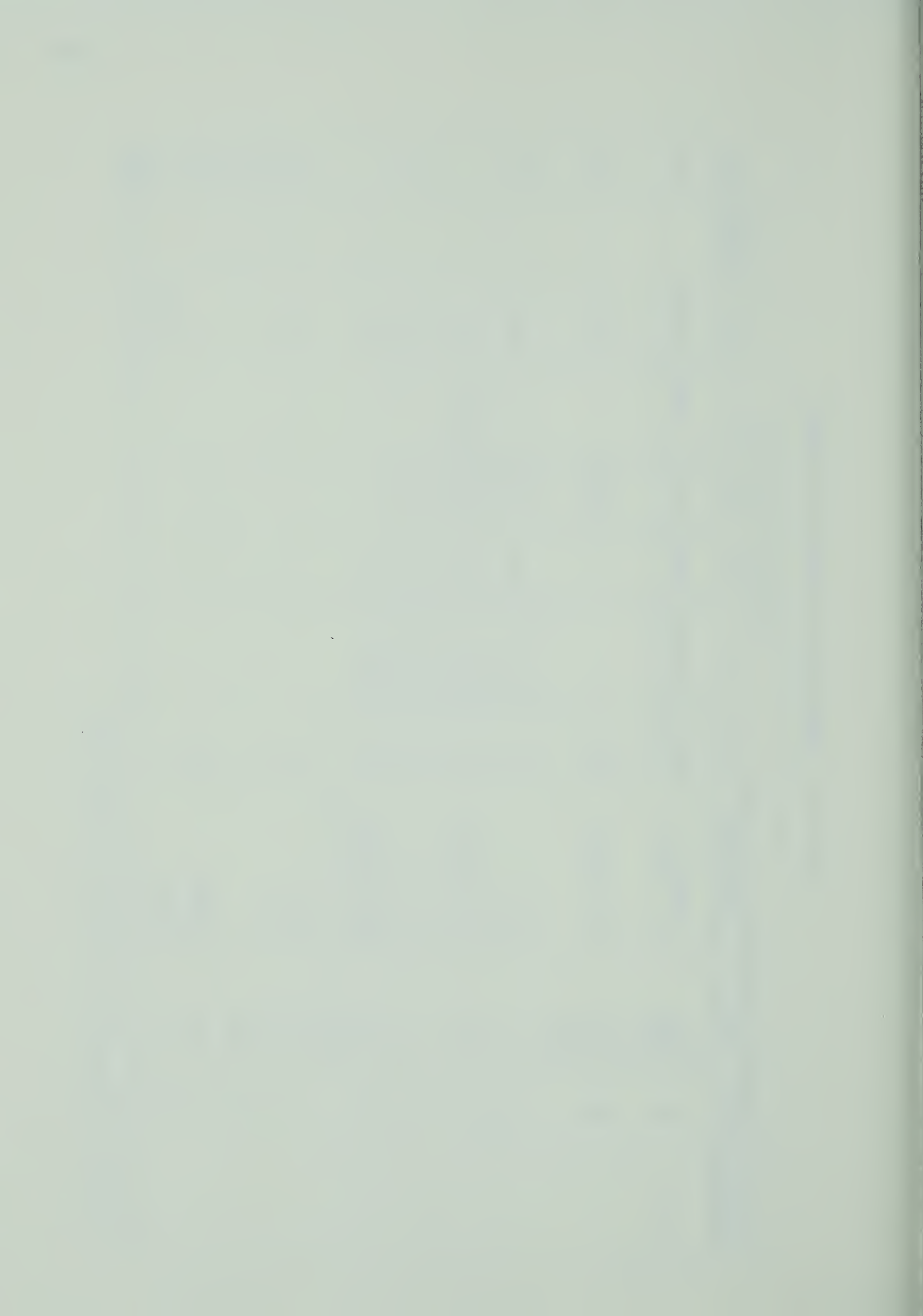
Reference Section	Example No	Reference Fig.	Cross Sectional Dimension	Material Properties						Loading Case ⁺	Ref.
				σ_y	E	E _s	ϵ_{st}	G	σ_{rc}		
6.3	E1	6.1	1"x12"rectangle	33ksi	30,000ksi	900ksi	0.012		no	G	
"	E2	6.3	8WF31	36	"	"	"		no	"	
"	E3	6.4	"	"	"	"	"		9 ksi	E	73
"	E4	6.5	"	"	"	"	"		"	D	57
6.4	E1	6.6	"	"	"	"	"	11500ksi	"	H	
"	E2	6.7	14WF43	"	"	"	"	"	no	I	11
"	E3	6.8	8WF31	33	"	"	"	"	9.9ksi	D	

+ For the nomenclature for loading see Table 6.3c

TABLE 6-3b PARTICULARS OF BUCKLING PROBLEMS

Reference Section	Example No	Reference Fig.	Cross Sectional Dimension	Material Properties						Loading Case ⁺	Ref.
				σ_y	E	E _s	ϵ_{st}	G	σ_{rc}		
6.6	E1	6.9a and 6.9b	2-7"x4x $\frac{3}{8}$ LS	44ksi	29,600ksi	600ksi	0.012	11,500ksi	13ksi	A	53
"	E2	6.10 and 6.11	Hat section	55	"	"	0.015	"	7.5	A	33
"	E3	6.12	8WF31	33	30,000	900	0.012	"	9.9	B	25
"	E4	6.13	2-7"x4"x $\frac{3}{8}$ LS	44	29,600	600	0.012	11,500	13	B	
"	E5	6.14	2x2.5x.25L	47	30,000	900	0.012	"	no	C	67
"	E6	6.15 and 3.9	one channel over the other	36	30,000	900	"	"	no	C	
"	E7	6.16	8WF31	33	"	"	"	"	9.9	D	24
"	E8	6.17	"	"	"	"	"	"	"	E	22
"	E9	6.18	18WF50	36	"	"	"	"	6	F	48
"	E10	6.19	14WF43	"	"	"	"	"	11.88	I	11 32

+ For the nomenclature for loading see Table 6-3c





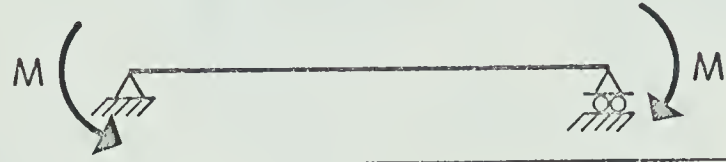



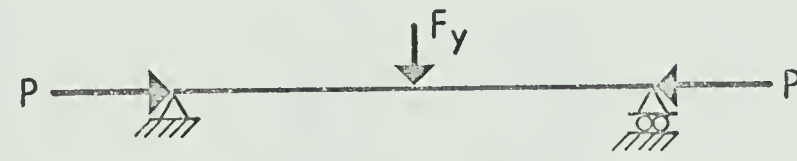
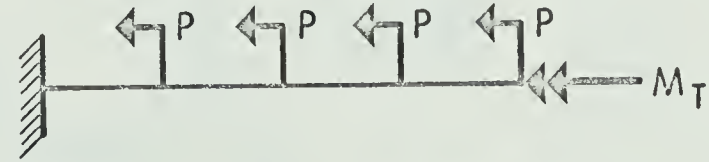

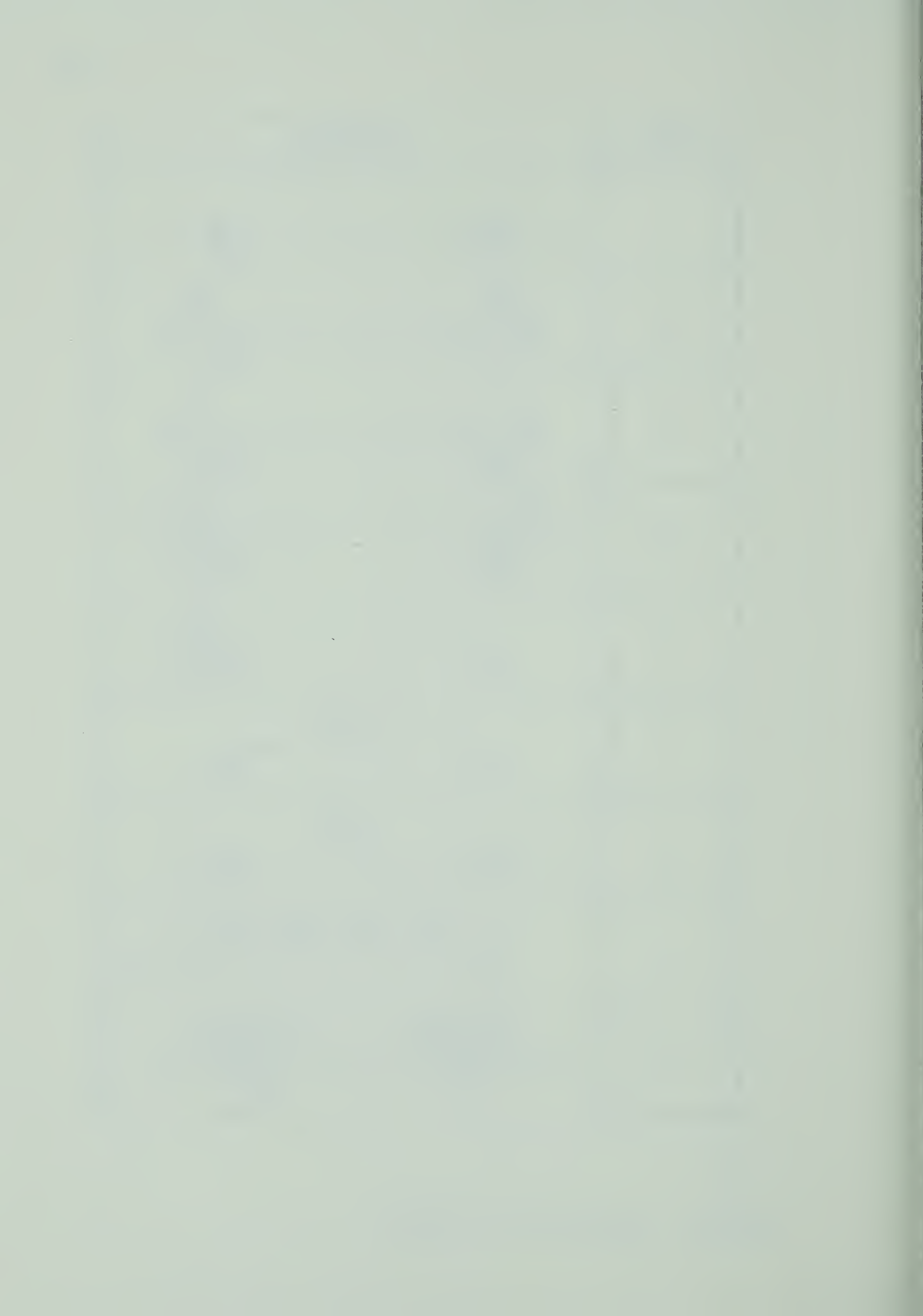
CASES	LOADING
A	
B	
C	
D	
E	
F	
G	
H	
I	

TABLE 6.3c NOMENCLATURE FOR LOADING



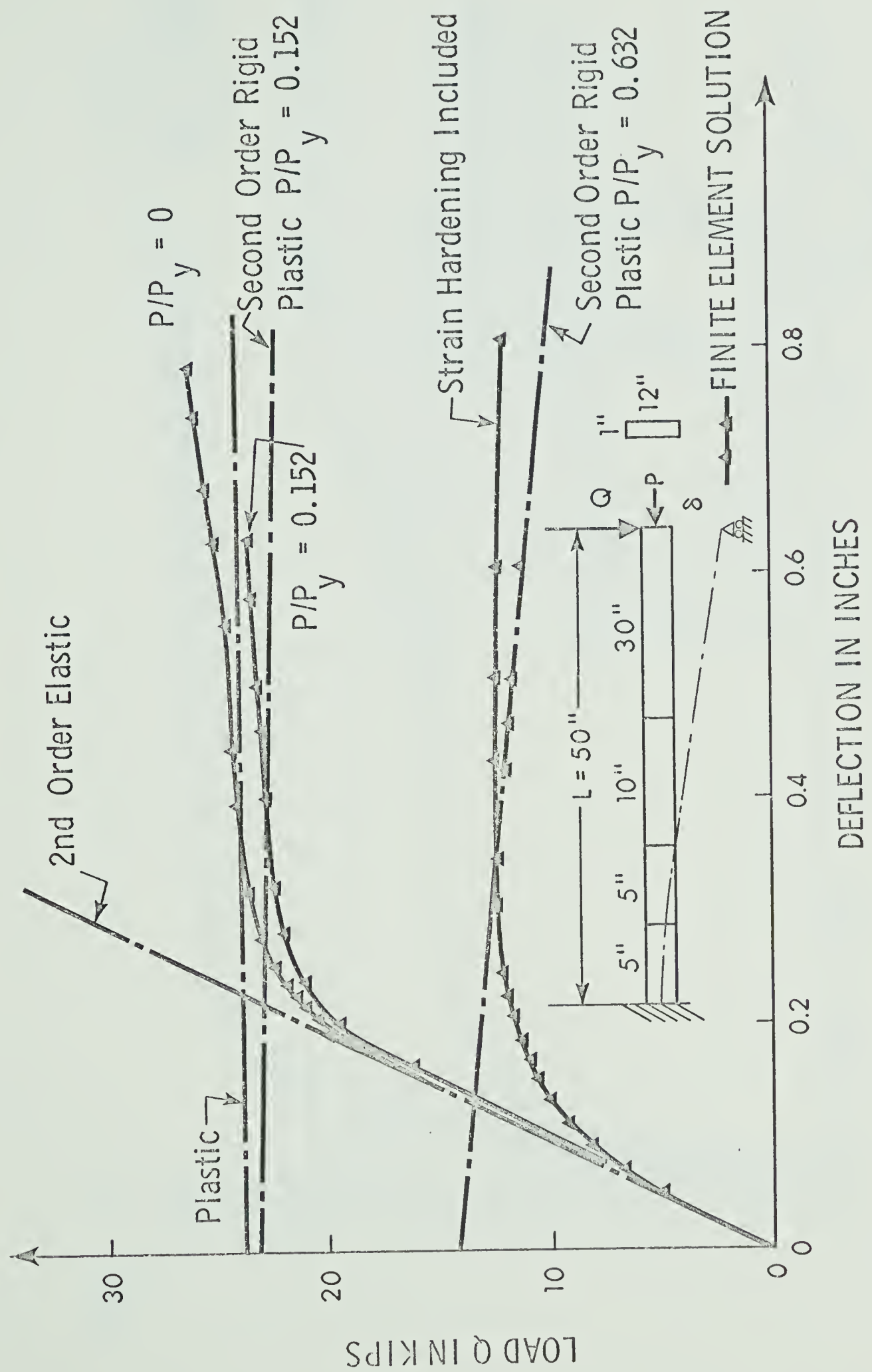


FIGURE 6.1 LOAD VS END DEFLECTION PLOT

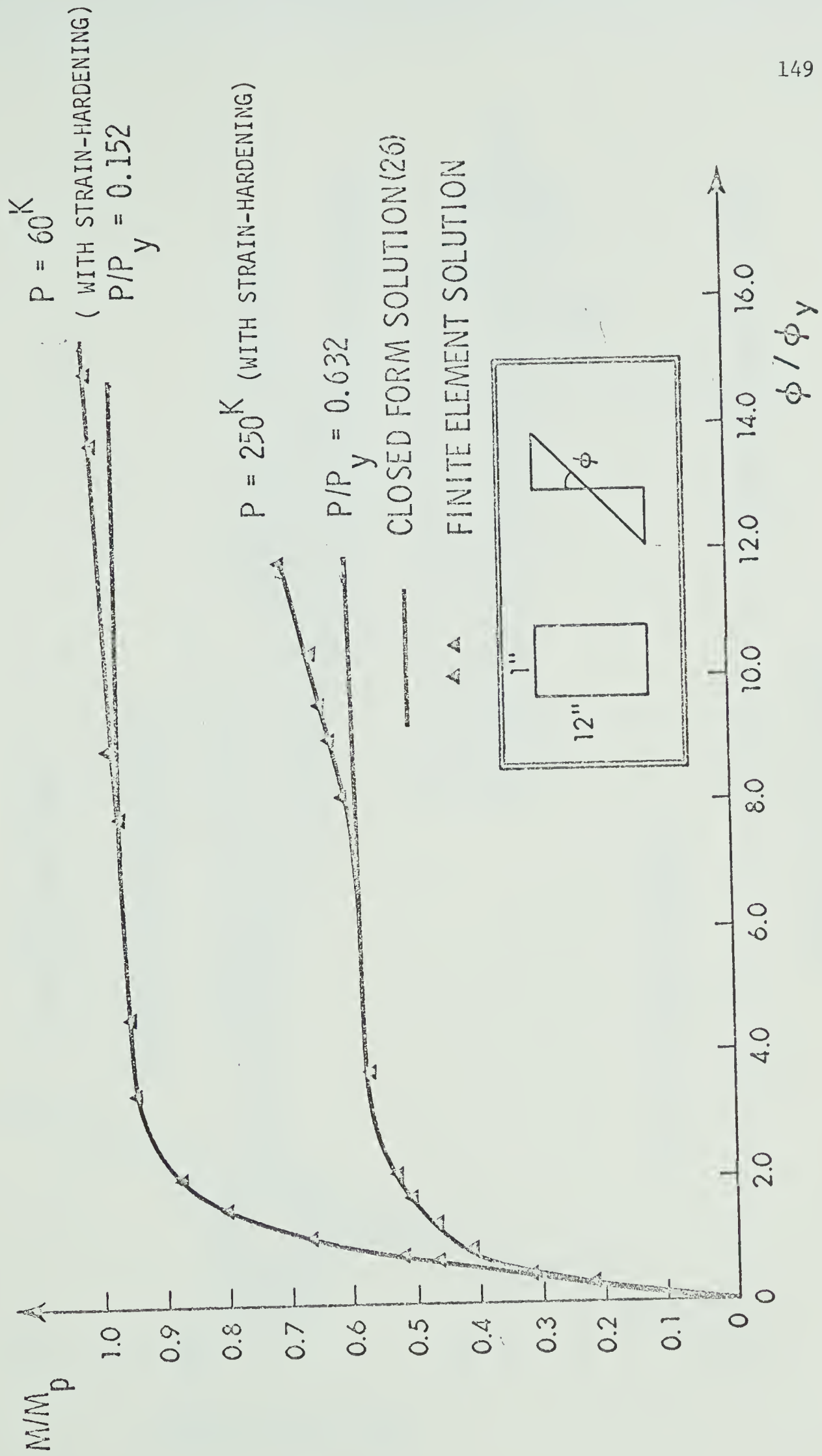


FIGURE 6.2 MOMENT VS. CURVATURE RELATIONSHIP

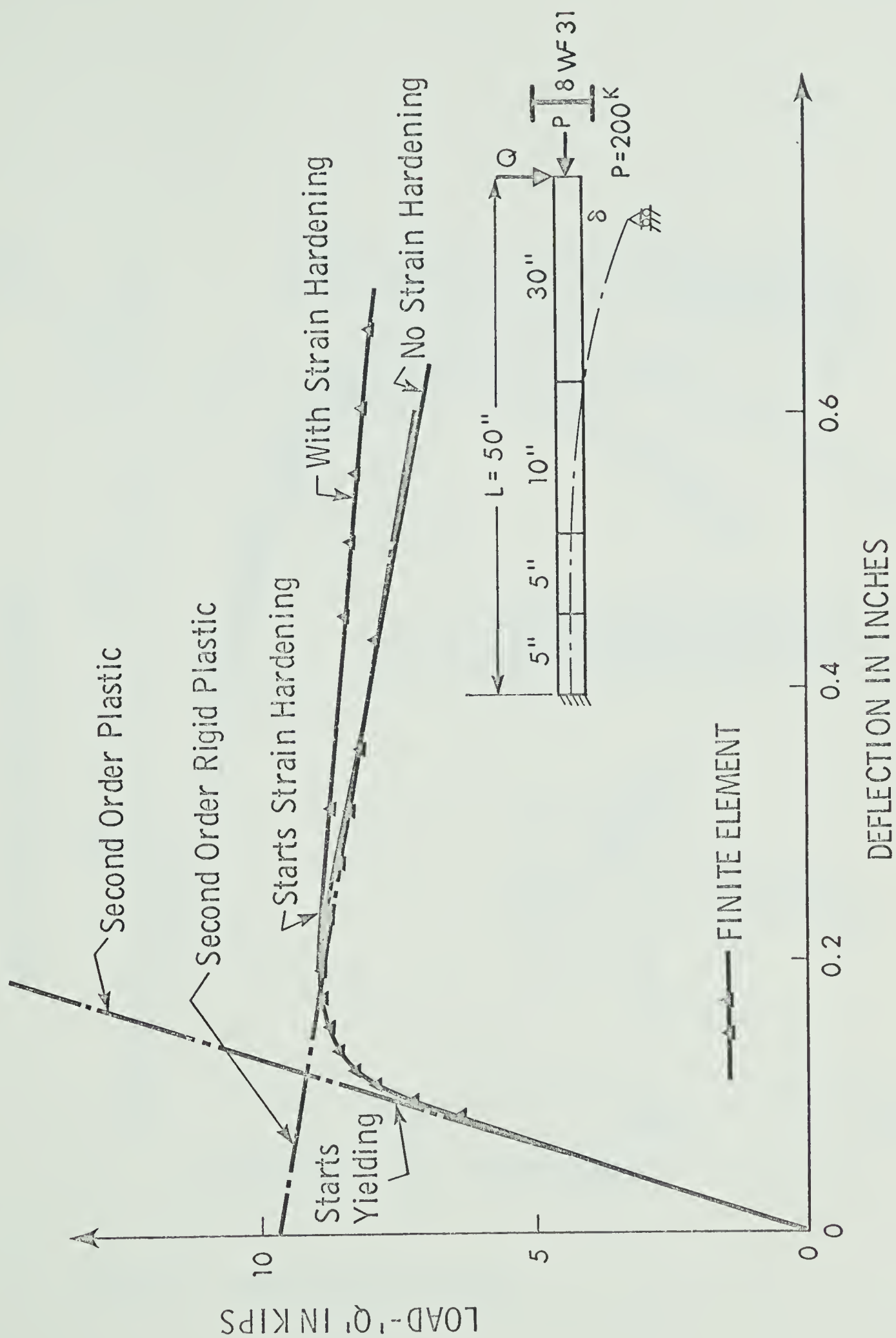


FIGURE 6.3 LOAD VS END DEFLECTION PLOT FOR WF BEAM-COLUMN

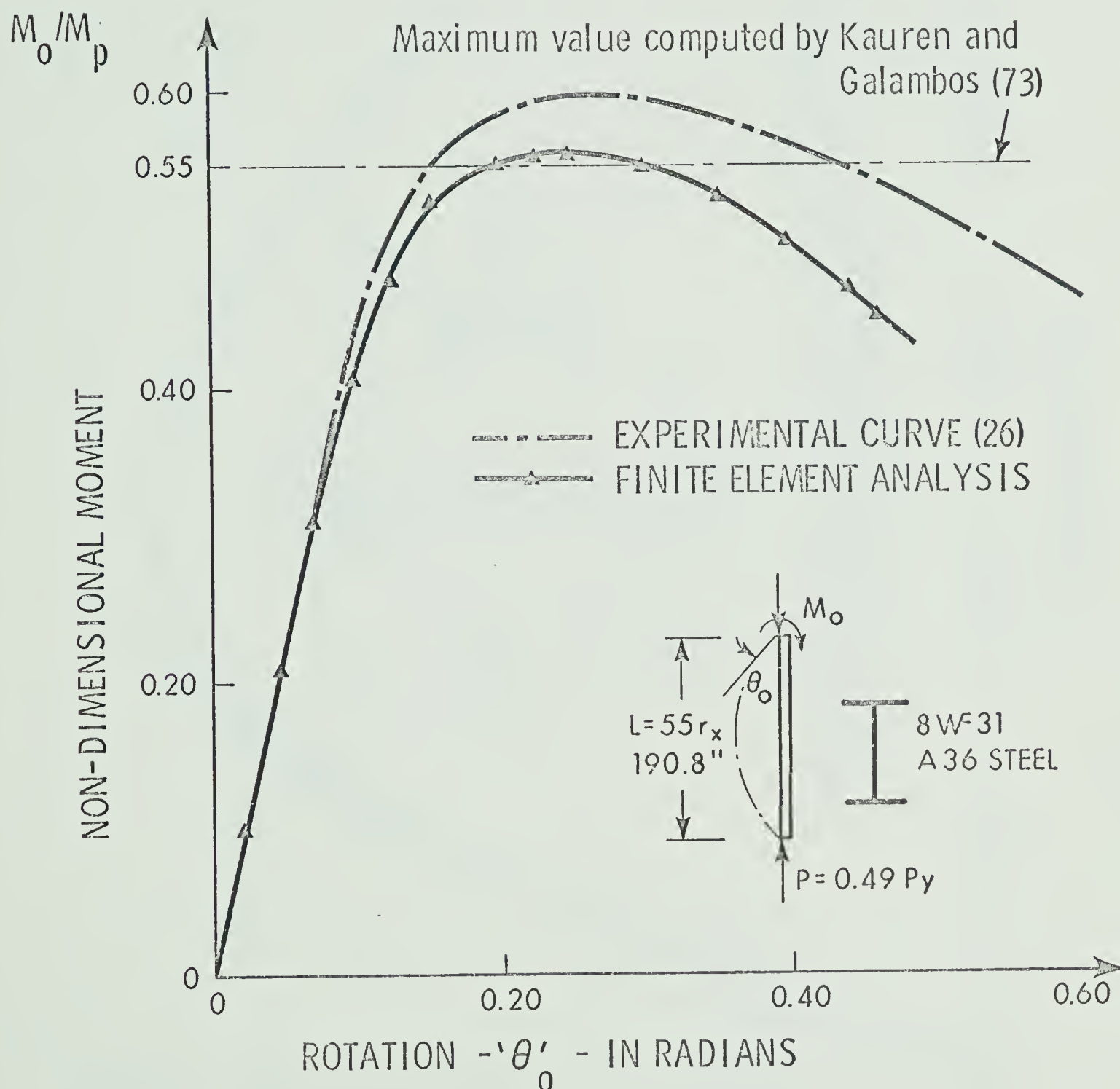


FIGURE 6.4 MOMENT VS END ROTATION

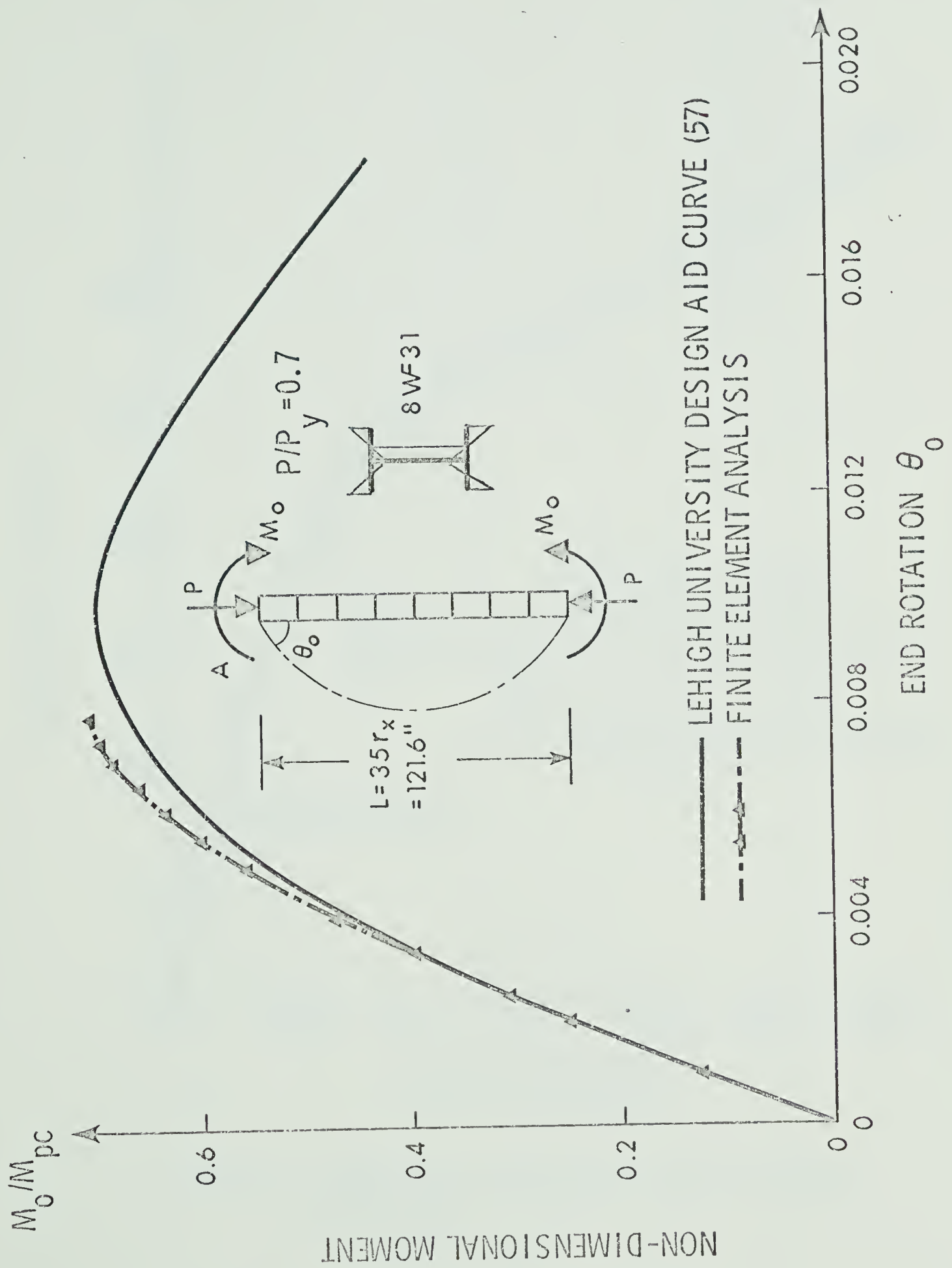


FIGURE 6.5 MOMENT VS END ROTATION

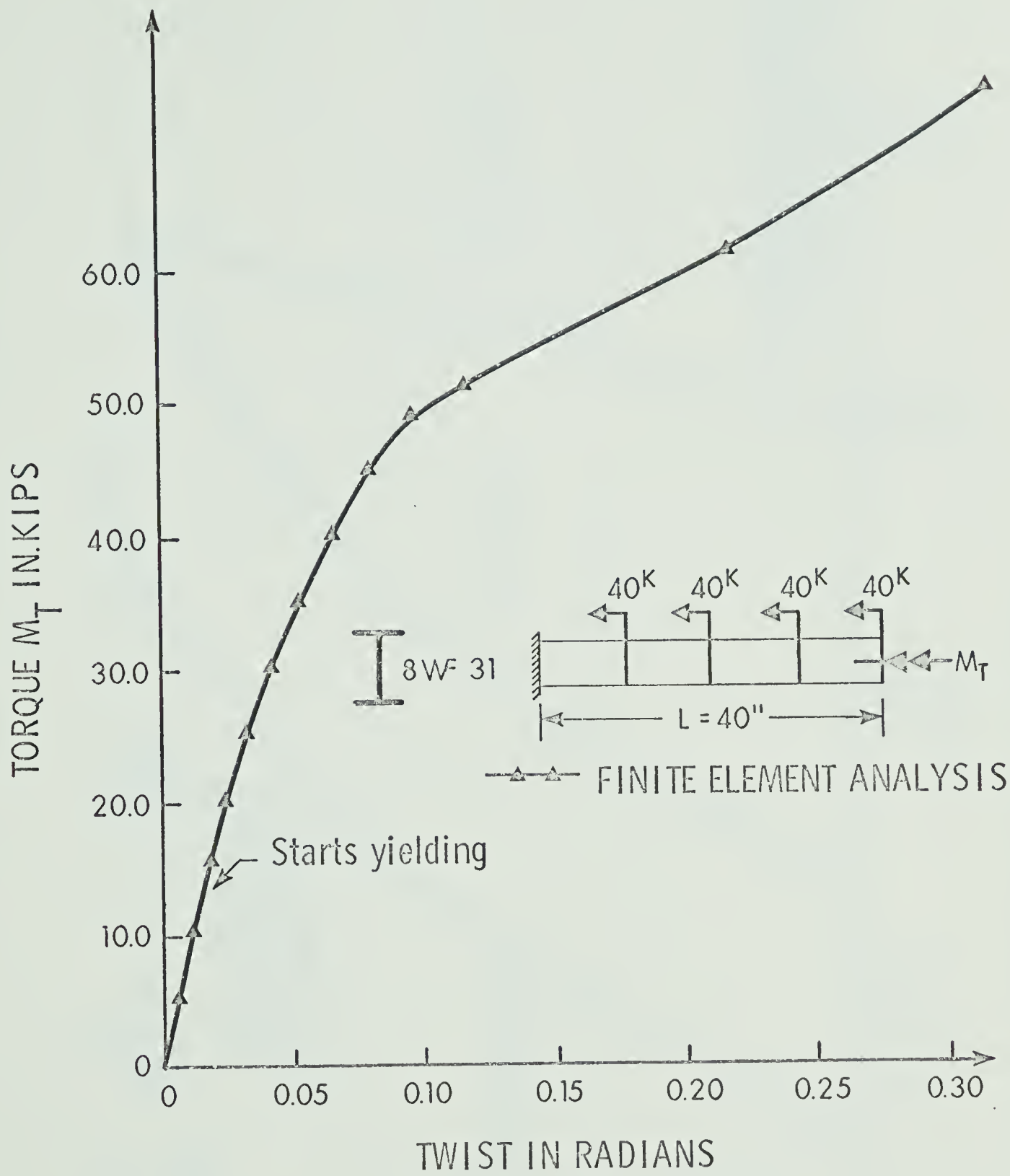


FIGURE 6.6 TORQUE TWIST RELATIONSHIP FOR AN INELASTIC BEAM-COLUMN

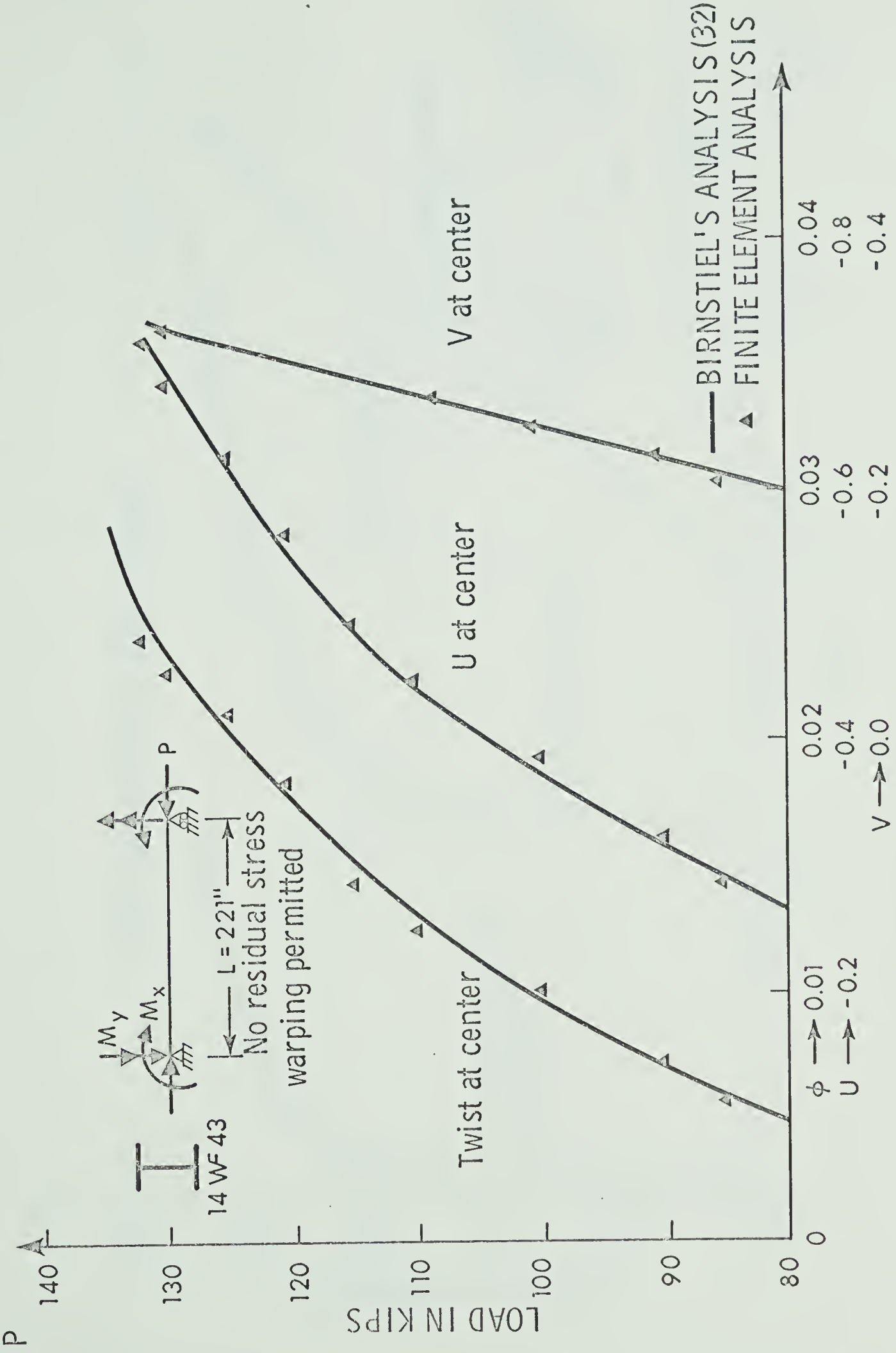


FIGURE 6.7 LOAD VS MID-SPAN DISPLACEMENTS



FIGURE 6.8 MOMENT VS IN AND OUT OF PLANCE RESPONSE

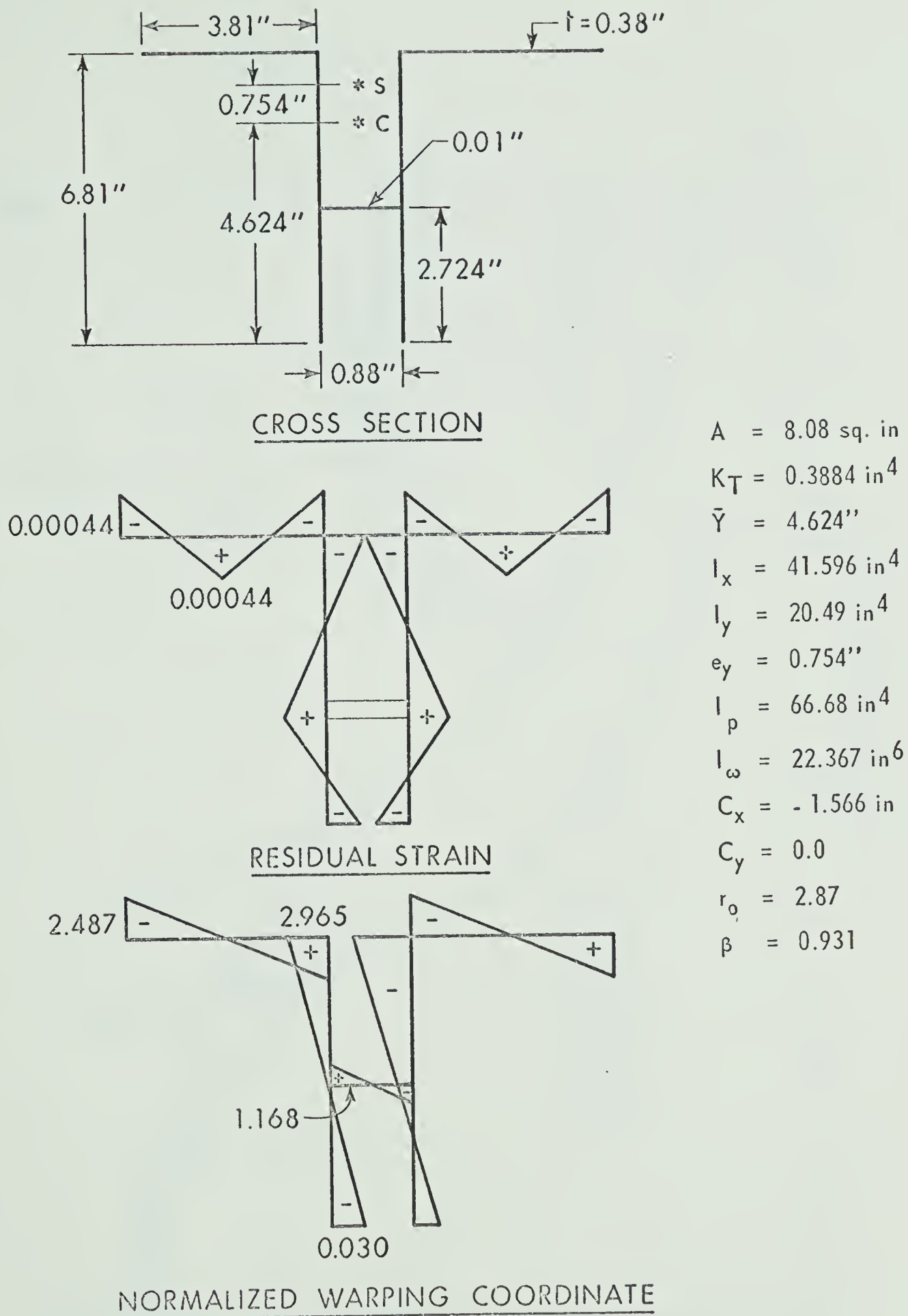


FIGURE 6.9a CROSS SECTION PROPERTIES OF A DOUBLE ANGLE SECTION

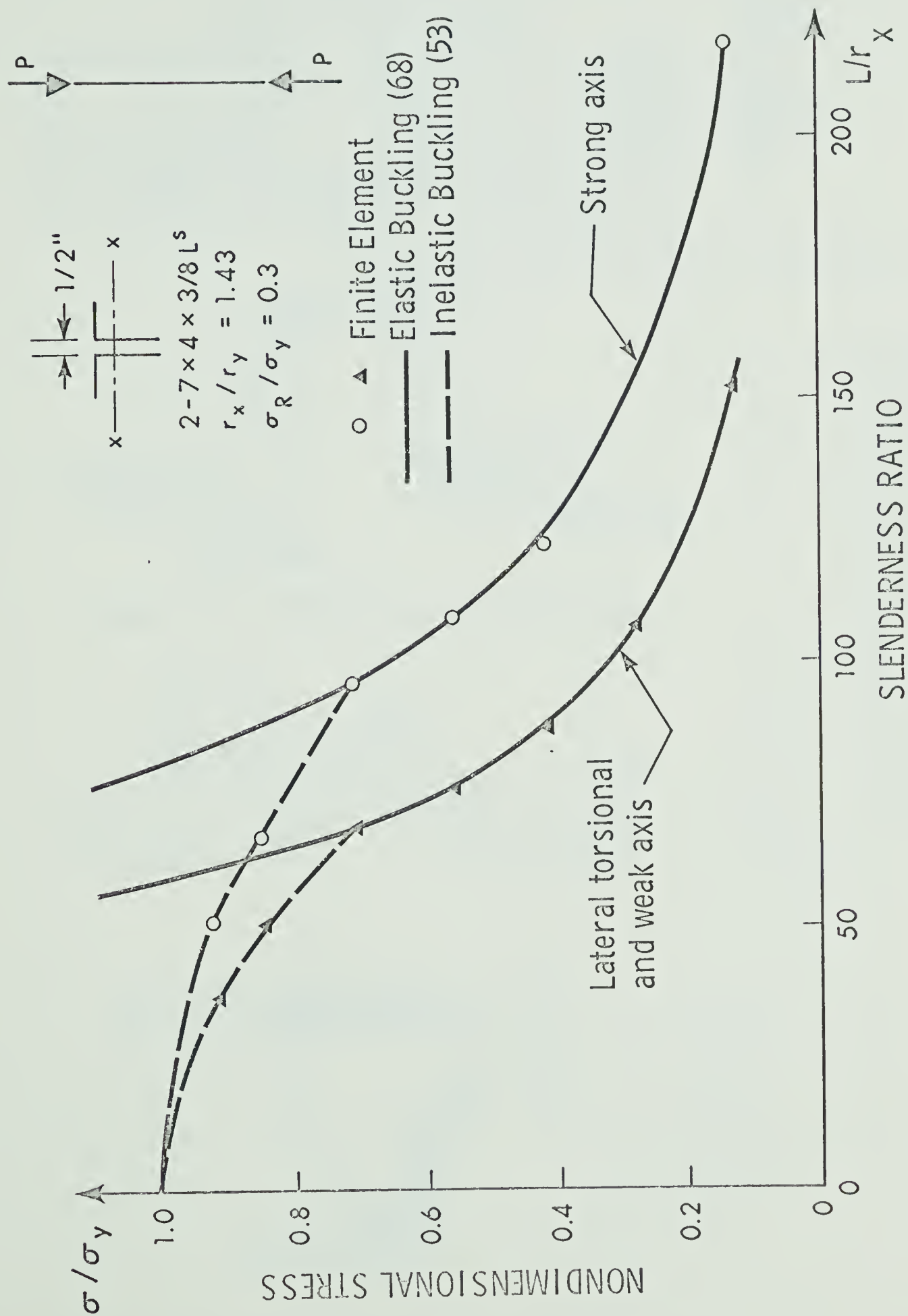


FIGURE 6.9b INELASTIC BUCKLING OF DOUBLE ANGLE STRUT

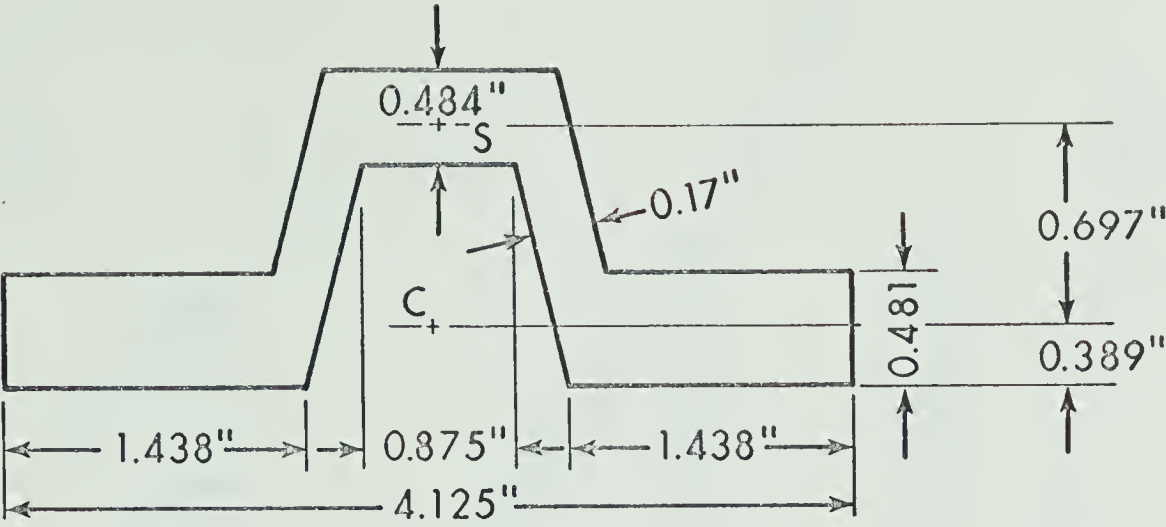


FIGURE 6.10a HAT SECTION (L of 33)

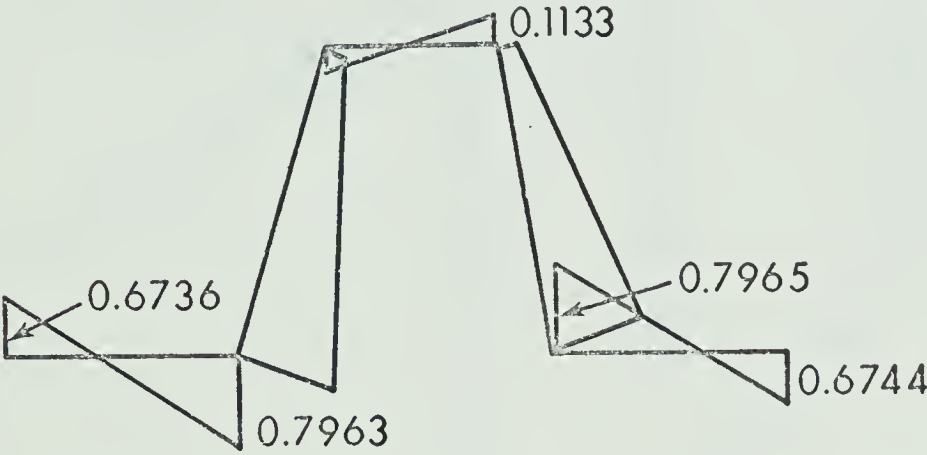
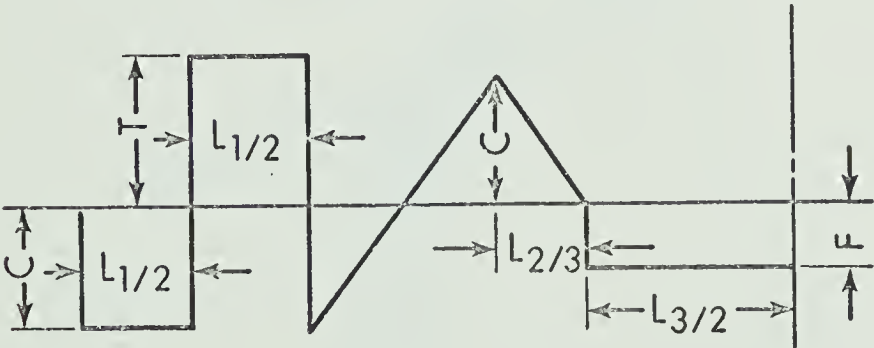


FIGURE 6.10b NORMALIZED WARPING COORDINATE



$A = 2.31953 \text{ in}^2$

$K_T = 0.1510 \text{ in}^4$

$\bar{Y} = 0.389''$

$I_x = 0.69714 \text{ in}^4$

$I_y = 2.9285 \text{ in}^4$

$e_y = 0.697''$

$I_p = 4.575 \text{ in}^4$

$I_\omega = 0.36323 \text{ in}^6$

$C_x = -2.3016''$

$C_y = 0$

$C = 7.5 \text{ KSI}$

$T = 7.6 \text{ KSI}$

$F = 1.1 \text{ KSI}$

$\sigma_y = 55 \text{ KSI}$

FIGURE 6.10c RESIDUAL STRESS DISTRIBUTION

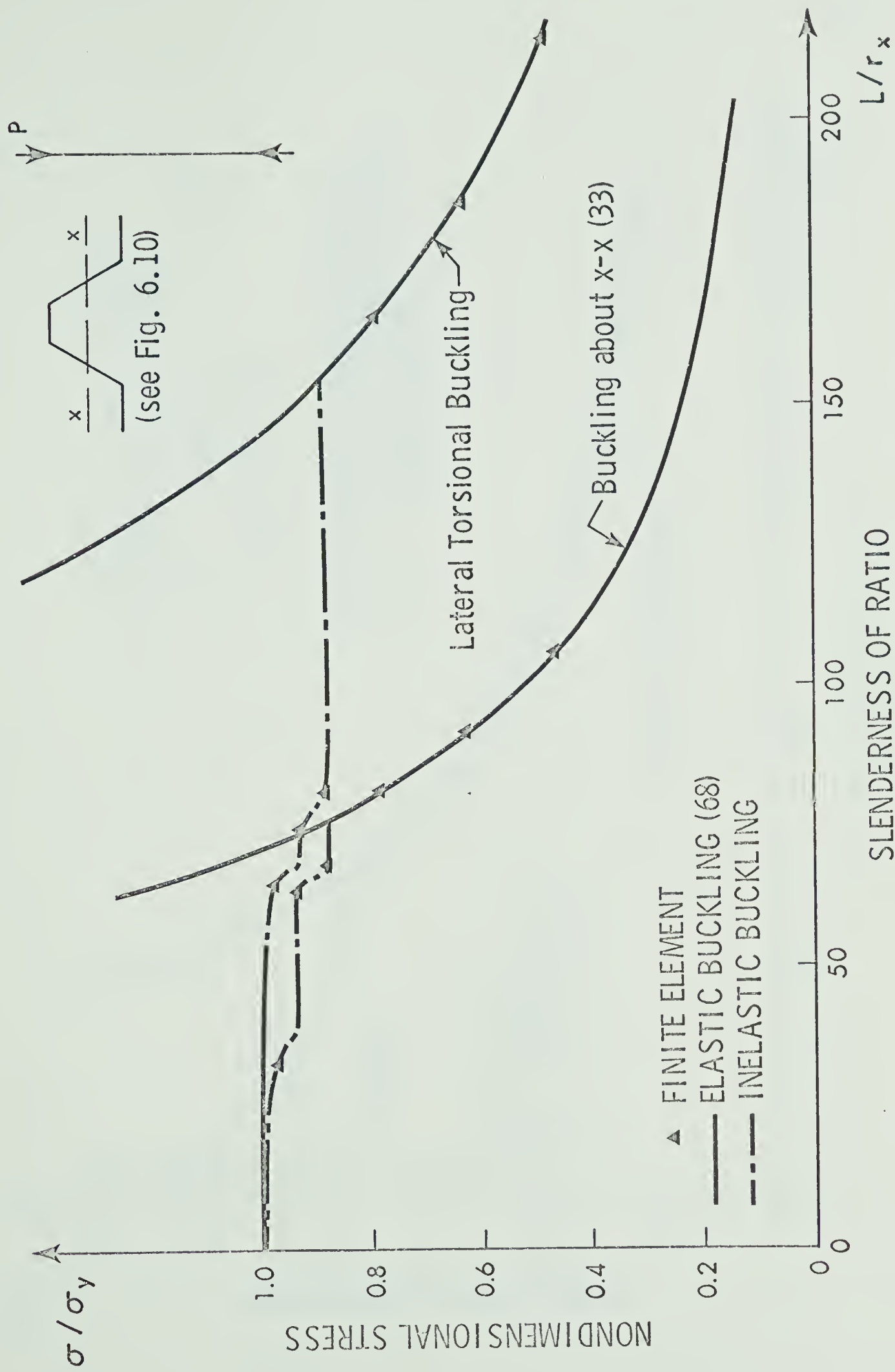


FIGURE 6.11 INELASTIC BUCKLING OF A COLUMN (HAT SECTION)

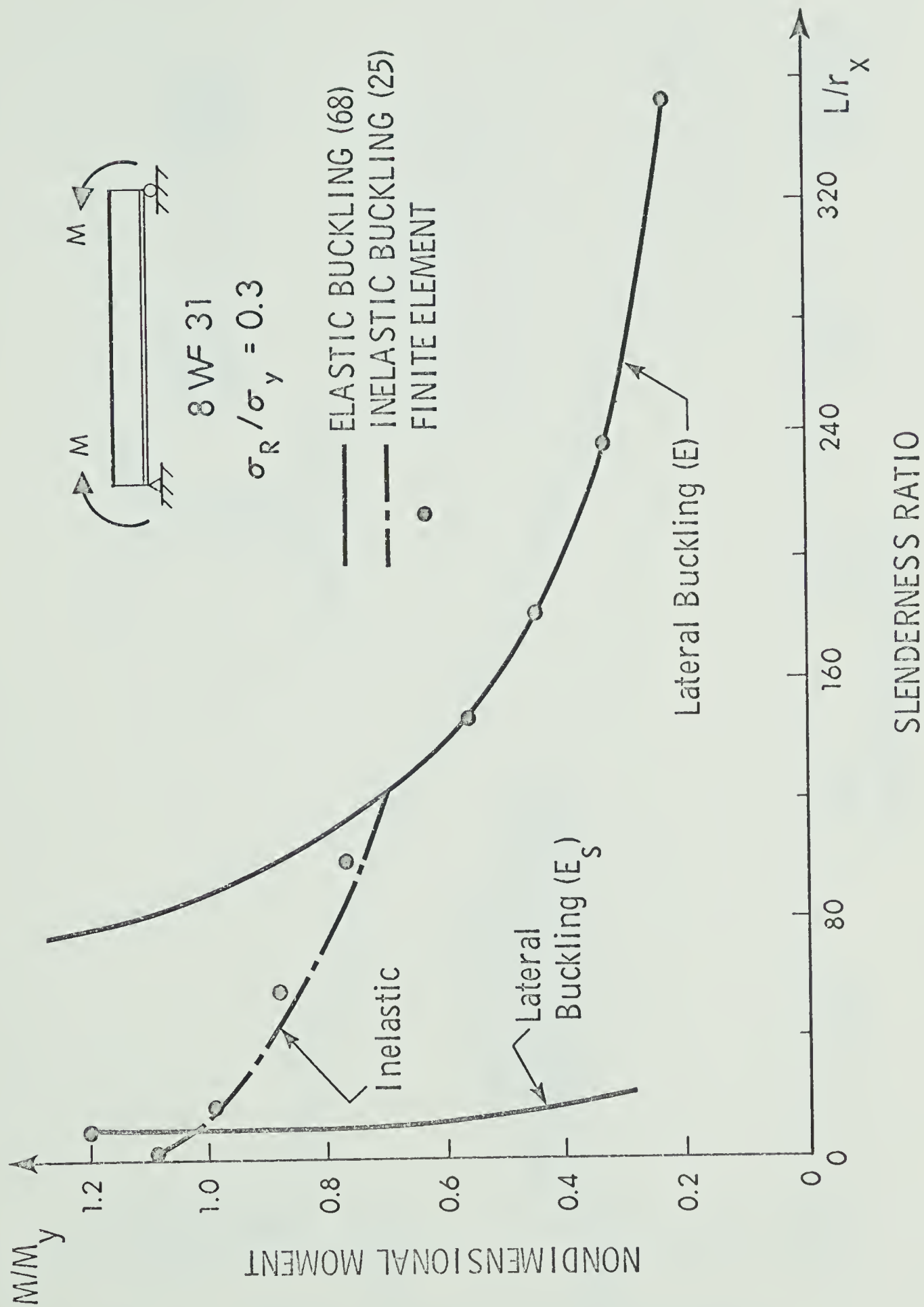


FIGURE 6.12 INELASTIC LATERAL BUCKLING OF A WIDE FLANGE BEAM (UNIFORM MOMENT)

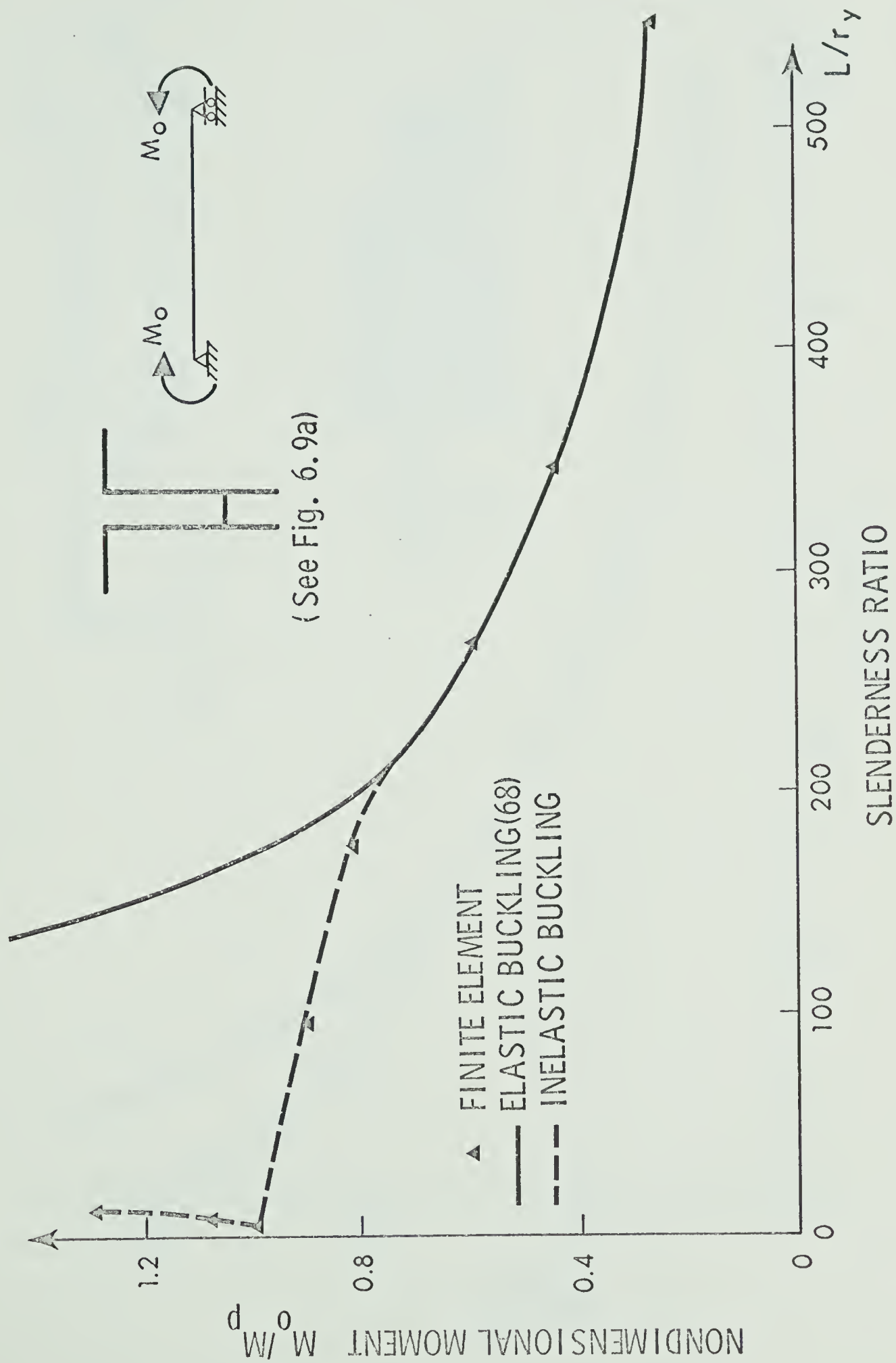


FIGURE 6.13 INELASTIC LATERAL BUCKLING OF A BEAM (DOUBLE ANGLE SECTION - UNIFORM MOMENT)

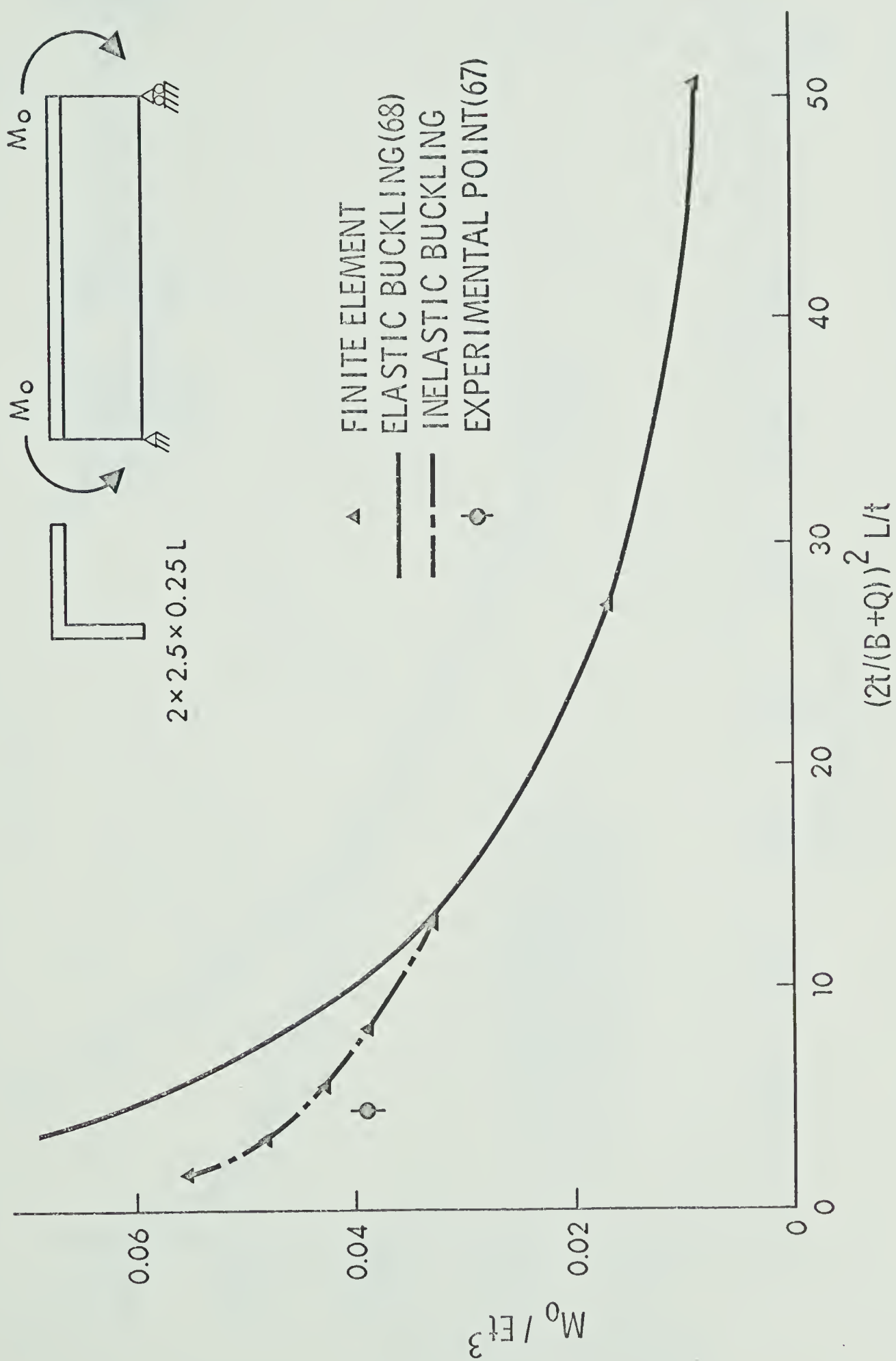


FIGURE 6.14 INELASTIC LATERAL TORSIONAL BUCKLING OF A BEAM (ANGLE SECTION-UNIFORM MOMENT)

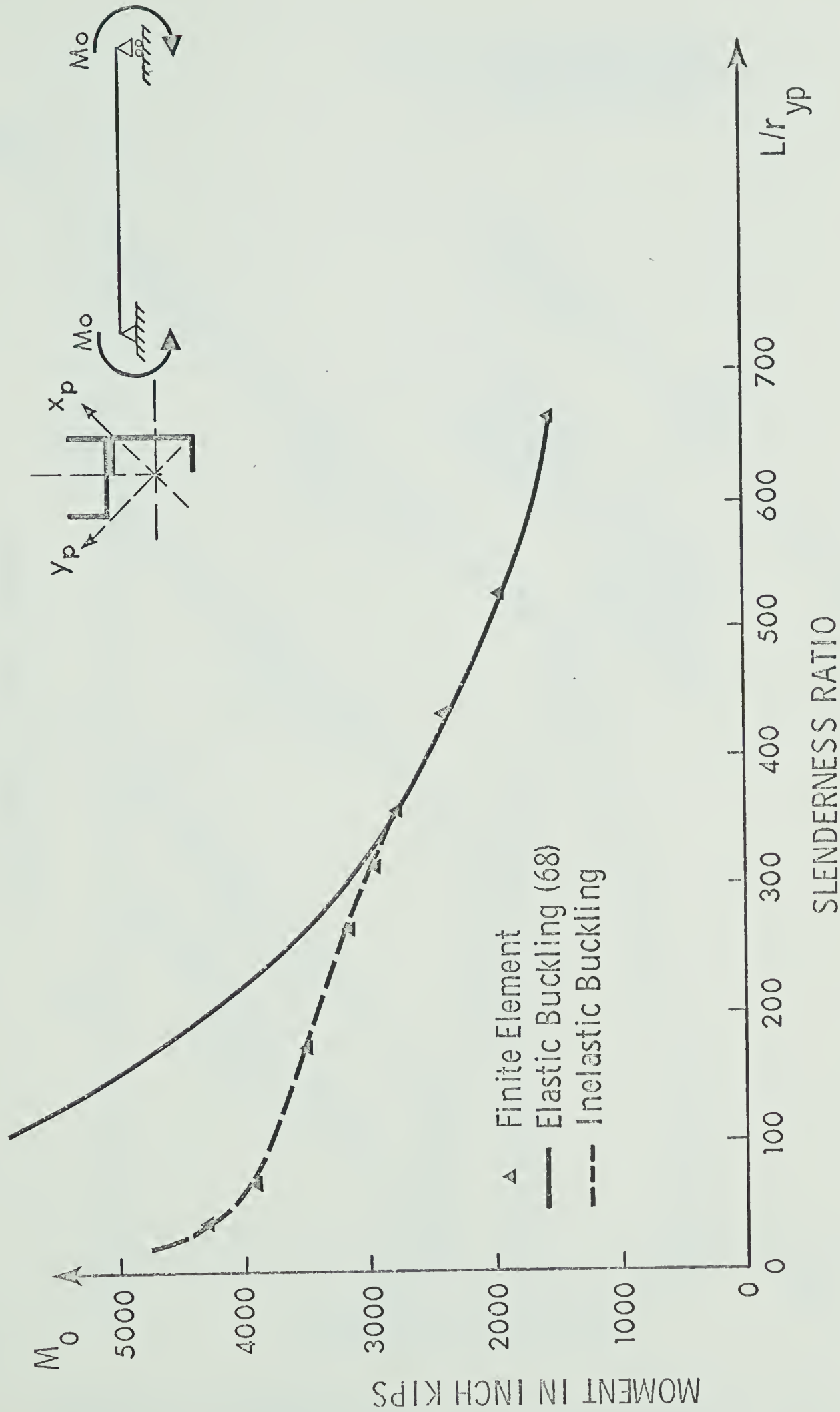


FIGURE 6.15 INELASTIC LATERAL - TORSIONAL BUCKLING OF A BEAM OF UNSYMMETRICAL SECTION (UNIFORM MOMENT)

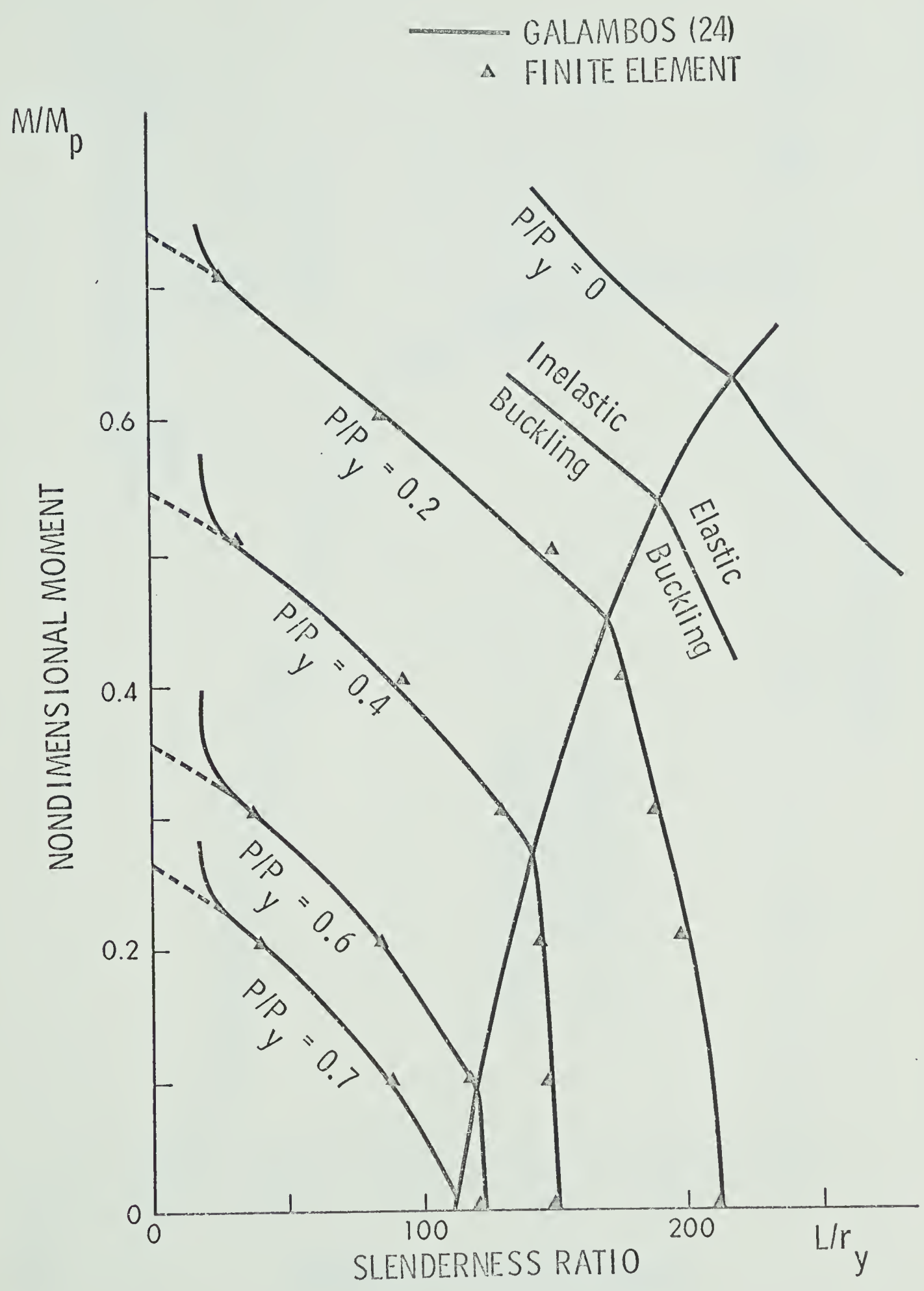


FIGURE 6.16 INELASTIC LATERAL TORSIONAL BUCKLING OF A WIDE FLANGE BEAM-COLUMN

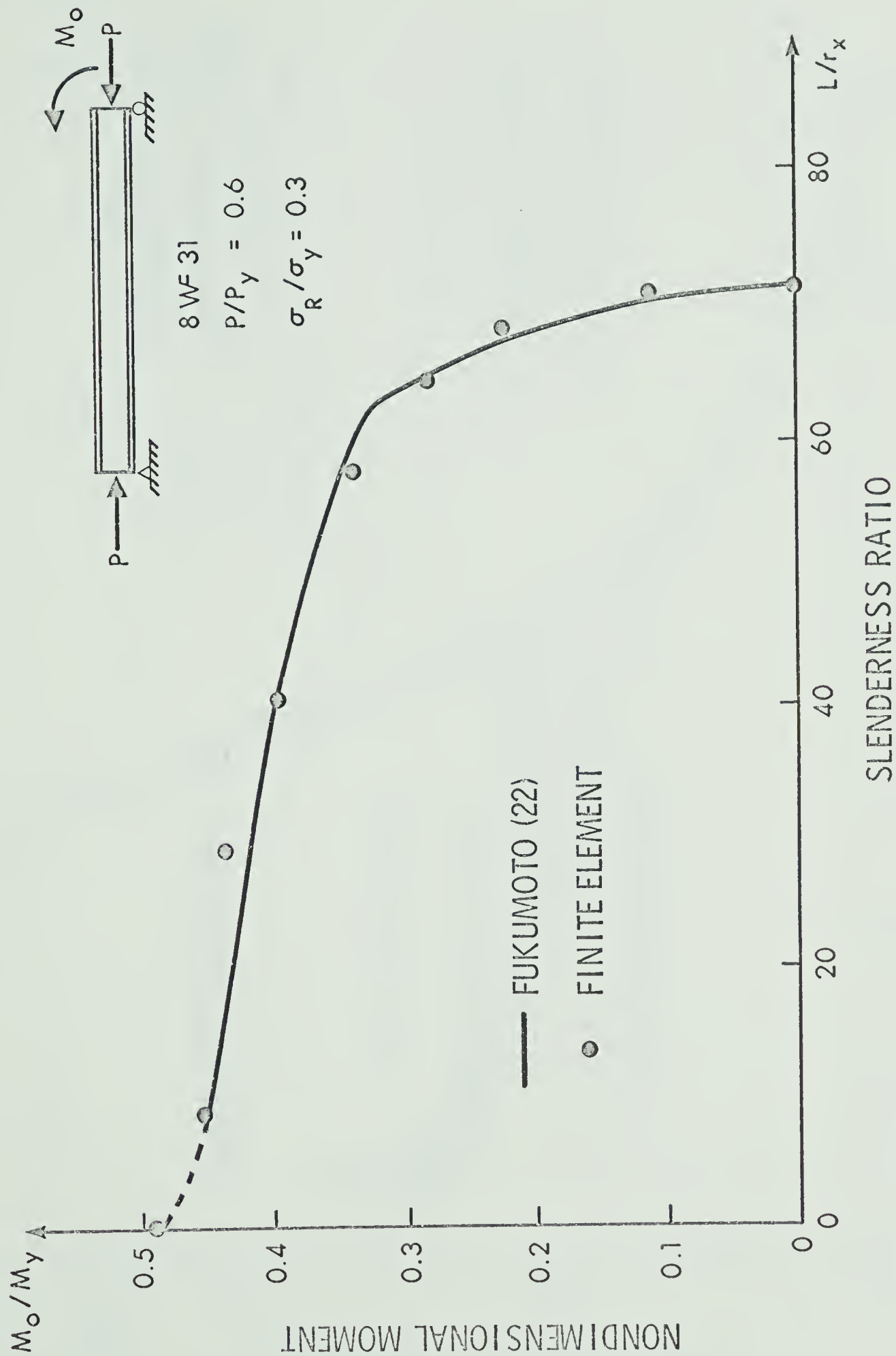


FIGURE 6.17 INELASTIC LATERAL TORSIONAL BUCKLING OF A BEAM-COLUMN WITH MOMENT GRADIENT

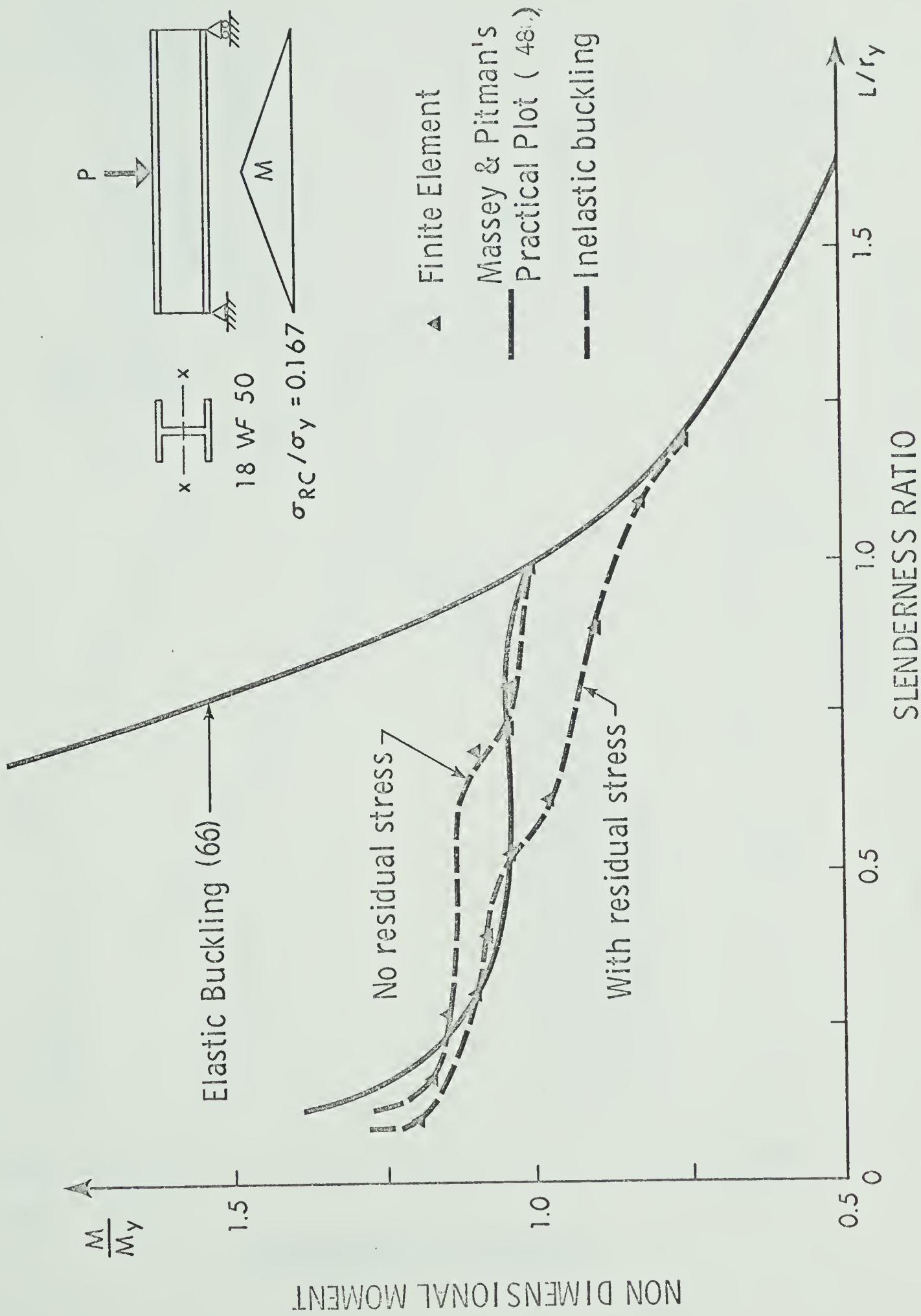


FIGURE 6.18 INELASTIC LATERAL BUCKLING OF WIDE-FLANGE BEAM (CENTRAL LOAD)

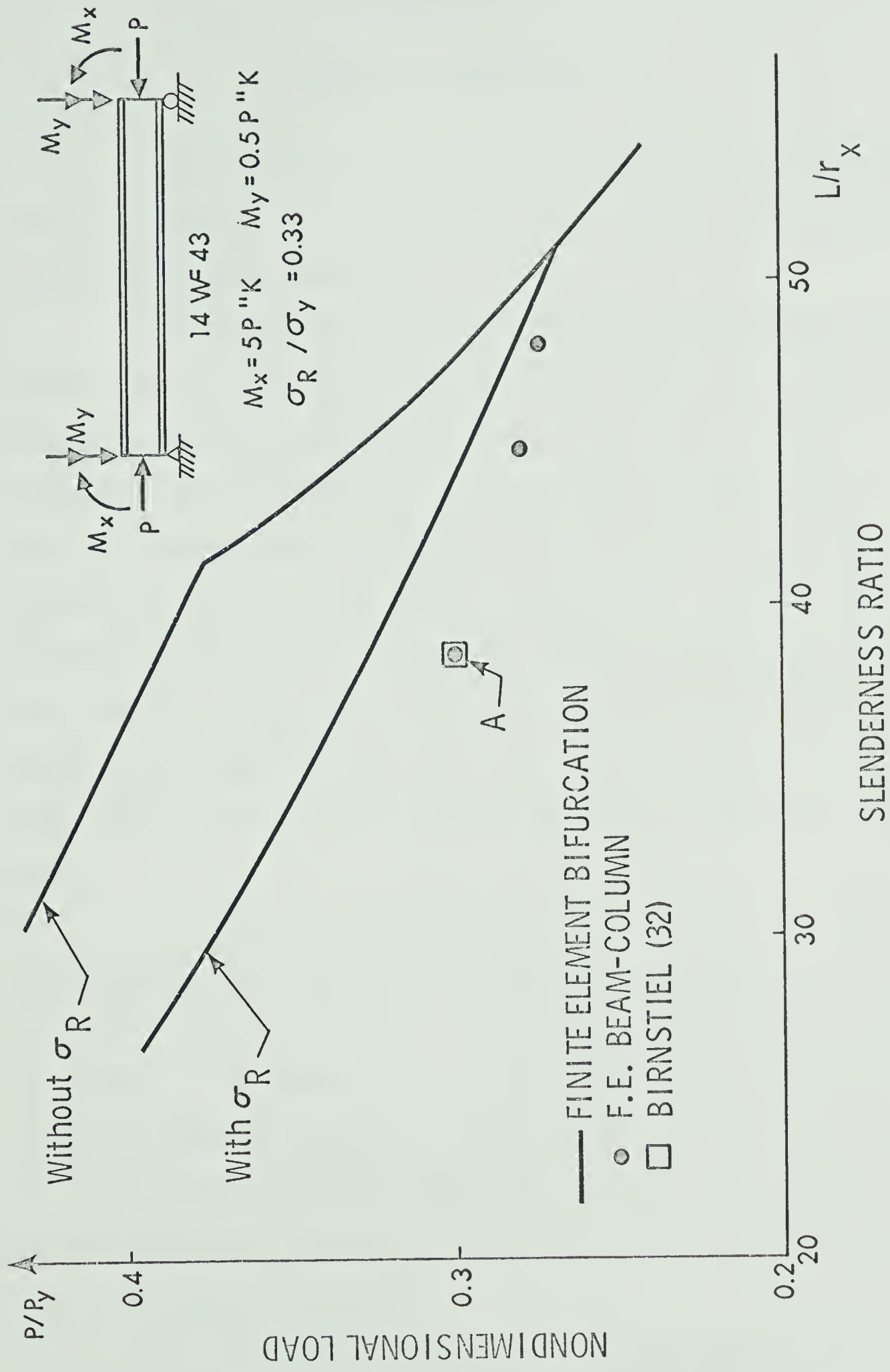


FIGURE 6.19 INELASTIC BUCKLING OF BIAXIAL BENDING WITH AXIAL LOAD

CHAPTER VII

SUMMARY AND CONCLUSIONS

A general approach to the elastic and inelastic analysis of thin-walled members of arbitrary open cross section has been presented using finite element analysis.

Both incremental and total equilibrium equations have been derived, using the principle of virtual work, which are applicable to elastic and inelastic analysis. For the elastic case, a special application of the formulation is the numerical determination of critical loading, and the associated mode shapes which may be determined from an eigenvalue solution. The eigenvalue analysis essentially neglects the prebuckling deformations. However, initial imperfections have been introduced into the model, and by using an incremental iterative procedure, the nonlinear load-deflection response, rather than critical load, has been obtained and numerical comparisons were made.

The displacement functions utilized in the beam and beam-column analyses were augmented for symmetrical wide-flange sections by representing local buckling patterns with the shape functions shown in Chapter IV. By coupling the local and member buckling, numerical results verified the validity of the classical approach showing that for these sections, the interactive effect is small, and local and member buckling are initiated as relatively detached phenomenon over most of the range of loading.

Two formulations have been developed for the inelastic problems. The inelastic beam-column problems were solved by an

iterative incremental technique based on an equilibrium balance of applied loads and resisting forces in the current configuration of the structure. These problems were found to be very sensitive to the type of stress strain curve and applied forces in the inelastic range and hence an under relaxation factor was used on the residual force vector. The convergence of these problems was slow when the load was near the peak load. In spite of the use of a modified Newton-Raphson's procedure the solution was found to be most expensive from the standpoint of computer expenditure.

Inelastic buckling problems were solved using standard eigenvalue solutions to evaluate the critical length. This procedure is applicable to thin-walled prismatic members, with arbitrary shaped open cross section, for any statically determinate loading condition, with a trilinear stress-strain curve and including the effects of residual stress. The analysis is capable of predicting lateral, torsional and lateral-torsional buckling modes, and yields reasonable results for large classes of problems. The formulations which were developed, were found to yield the same results. It is shown in Appendix B that for the class of problems investigated in this dissertation it is unnecessary to include the higher order terms in the initial stress and stress-strain increments unless investigating the post-buckling behaviour, since the maximum load carrying capacity will normally be obtained before these higher order terms have any significant effect.

Even though only single member problems are solved in this work, the same formulation may be applied to solve for instability of planar frames composed of arbitrary open thin-walled

sections. However, more efficient numerical techniques must be developed before geometric and material non-linearities of the types considered in this dissertation can be practically incorporated into the design process.

LIST OF REFERENCES

1. Anon., "System/360 Scientific Subroutine Package (360-cm-03x) Version," Programs Manual, IBM Applications Program Manual, H20-0205-3, 1968.
2. Archer, J.S., "Consistent Matrix Formulations For Structural Analysis Using Finite-Element Techniques," American Institute of Aeronautics and Astronautics Journal, Vol. 3, No. 10, pp 1910-1918, October, 1965.
3. Argyris, J.H., "Recent Advances in Matrix Methods of Structural Analysis," Progress in Aeronautical Sciences, Pergamon Press, 1964.
4. Argyris, J.H. and Kelsey, S., "Energy Theorems and Structural Analysis," Butterworths Publication, 1960.
5. Argyris, J.H., Kelsey, S., and Kamel, "Matrix Methods of Structural Analysis; a precis of Recent Developments," Chapter in "Matrix Methods of Structural Analysis," Fraeijs de Veubeke, Editor, Pergamon Press, Oxford, 1964.
6. Ariaratnam, S.T., "The Southwell Method for Predicting Critical Loads of Elastic Structures," Quarterly Journal of Mechanics and Applied Mathematics, Vol. 14, 1961, pp 137-153.
7. Barsoum, R.S., "A Finite Element Formulation for the General Stability Analysis of Thin-Walled Members," thesis presented to the Cornell University, September, 1970, in partial fulfillment of the requirement for the degree of Doctor of Philosophy.
8. Barsoum, R.S., and Gallagher, R.H., "Finite Element Analysis of Torsional and Torsional-Flexural Stability Problems," International Journal for Numerical Methods in Engineering, Vol. 2, No. 1, 1970.
9. Barta, T.A., "On the Torsional-Flexural Buckling of Thin-Walled Elastic Bars with Monosymmetric Open Cross-Section," "Thin-Walled Structures," edited by Chilver, A.H., John Wiley and Sons, Inc., 1967.
10. Biot, M.A., "Mechanics of Incremental Deformations," John Wiley and Sons, 1965.
11. Birnstiel, C., and Michalos, J., "Ultimate Load of H-Columns Under Biaxial Bending," Journal of the Structural Division, ASCE, Vol. 89, No. ST2, Proc. Paper 3503, April, 1963, pp 161-197.
12. Birnstiel, C., "Experiments on H-Columns Under Biaxial Bending," Journal of the Structural Division, ASCE, Vol. 94, No. ST10, Proc. Paper 6186, October, 1968, pp 2429-2449.
13. Bleich, F., "Buckling Strength of Metal Structures," McGraw-Hill, New York, 1952.

14. Brebbia, C., and Connor, J., "Geometrically Non-Linear Finite Element Analysis," Journal of the Engineering Mechanics Division ASCE, Vol. 95, No. EM2, Proc. Paper 6516, April, 1969, pp 463-483.
15. Bulson, P.S., "The Local Instability of Structural Sections with Flange Reinforcements," Symposium on Thin-Walled Structures Their Design and Their Use in Buildings held at University College Swansea, Edited by Rockey, K.C., and Hill, H.V., Crosby Lockwood & Son Ltd., 1968.
16. Bulson, P.S., "Local Stability and Strength of Structural Sections," "Thin-Walled Structures" edited by Chilver, A.H., John Wiley and Sons, 1967, pp 153-207.
17. Culver, C.G., and Preg, Jr. S.M., "Elastic Stability of Tapered Beam-Columns," Journal of the Structural Division, ASCE, Vol. 94, No. ST2, Proc. Paper 5796, February, 1968, pp 455-470.
18. Djanelidze, G.J., "Variational Formulation of Vlasov's Theory of Thin-Walled Rods," Prikladnaia Matematika I Mekhanika., Vol. 7 No. 6, 1943, pp 455-462 (in Russian).
19. Felippa, C.A., "Refined Finite Element Analysis of Linear and Non-Linear Two-Dimensional Structures," report to the National Science Foundation under Grant GK-75, Department of Civil Engineering, University of California, Berkely, October, 1966.
20. Flint, A.R., "The Stability and Strength of Slender Beams," Engineering, Vol. 170, December, 1950, pp 545-549.
21. Flugge, W., "Handbook of Engineering Mechanics," McGraw-Hill Book Company, 1962.
22. Fukumoto, Y., "Inelastic Lateral-Torsional Buckling of Beam-Columns," thesis presented to the Lehigh University at Bethlehem, Pa., 1963, in partial fulfillment of the requirement for the degree of Doctor of Philosophy.
23. Fukumoto, Y., and Galambos, T.V., "Inelastic Lateral-Torsional Buckling of Beam-Columns," Journal of the Structural Division, ASCE, Vol. 92, No. ST2, Proc. Paper 4770, April, 1966, pp 41-61.
24. Galambos, T.V., "Inelastic Lateral Torsional Buckling of Wide-Flange Columns," thesis presented to the Lehigh University at Bethlehem, Pa., 1959, in partial fulfillment of the requirement for the degree of Doctor of Philosophy.
25. Galambos, T.V., "Inelastic Lateral Buckling of Beams," Journal of the Structural Division, ASCE, Vol. 89, No. ST5, Proc. Paper 3683, October, 1963, pp 217-242.
26. Galambos, T.V., "Structural Members and Frames," Prentice-Hall Inc., Englewood Cliffs, N.J., 1968.

27. Goldberg, J.E., and Bogdenoff, J.L., and Glanz, W.D., "Lateral and Torsional Buckling of Thin-Walled Beams," International Association of Bridge and Structural Engineering, Pub, Vol. 24, 1964, pp 92.
28. Goodier, J.N., "Torsional and Flexural Buckling of Bars of Thin-Walled Open Sections Under Compressive and Bending Loads," Journal of Applied Mechanics, Vol. 9, No. 3, September, 1942, pp A-103 - A-107.
29. Gregory, M., "The Application of the Southwell Plot on Strains to Problems of Elastic Instability of Frames Structures Where Buckling of Members in Torsion or Flexure Occurs," Australian Journal of Applied Science, Vol. 11, No. 1, March, 1960, pp 49-64.
30. Haisler, W.E., Stricklin, J.A. and Stebbins, F.J., "Development and Evaluation of Solution Procedures for Geometrically Non-Linear Structural Analysis by the Direct Stiffness Method," Paper presented at the AIAA/ASME 12th Structures, Structural Dynamics, Materials Conference, Anaheim, California, April 19-21, 1971.
31. Harris, H.G., and Pifko, A.B., "Elastic-Plastic Buckling of Stiffened Rectangular Plates," Proceedings of the Symposium on Application of Finite Element Methods in Civil Engineering, Nashville, Tennessee, November, 1969.
32. Harstead, G.A., and Birnstiel, C., and Leu, K.C., "Inelastic H-Columns under Biaxial Bending," Journal of the Structural Division, ASCE, Vol. 94, No. ST10, Proc. Paper 6173, October, 1968, pp 2371-2398.
33. Heaton, D.A., and Adams, P.F., "Buckling Strength of Hot-Rolled Hat Shaped Sections," Structural Engineering Report No. 26, Department of Civil Engineering, University of Alberta, July, 1970.
34. Hofmeister, L.D., Greenbaum, G.A., and Evensen, D.A., "Large Strain Elasto-Plastic Finite Element Analysis," American Institute of Aeronautics and Astronautics Journal, Vol. 9, No. 7, July, 1971, pp 1248-1254.
35. Holand, I., and Bell, K. (Editors), "Finite Element Methods in Stress Analysis," TAPIR (Technical University of Norway Press) Trondheim, 1969.
36. Horne, M.R., "The Stanchion Problem in Frame Structures Designed According to the Ultimate Carrying Capacity," Proceedings of Institution of Civil Engineers, London, Part III, Vol. 5, No. 1, April, 1956, pp 105-160.
37. Horne, M.R., and Ajmani, M.L., "Stability of Columns Supported Laterally by Side Rails," International Journal of Mechanical Sciences, Vol. 11, February, 1969, pp 159-174.

38. Khojasteh-Bhakt, M., "Analysis of Elastic-Plastic Shells of Revolution Under Axi-Symmetric Loading by Finite-Element Method," Report to National Aeronautics and Space Administration Under Grant NSG274-S2, Department of Civil Engineering, University of California, Berkely, April, 1967.
39. Kollbrunner, F., and Hajdin, N., "Displacement Method in the Theory of Thin-Walled Members and a New Calculation-Model for the Thin-Walled Bars with Deformable Contours," International Association of Bridge and Structural Engineering Publication, Vol. 28-II, 1968, pp 87-100 (in German).
40. Krajcinovic, Dusan, "A Consistent Discrete Elements Technique for Thin-Walled Assemblages," International Journal of Solids and Structures, Vol. 5, No. 7, July, 1969, pp 639-661.
41. Lee, L.H.N., "Non Uniform Torsion of Tapered Beams," Journal of the Franklin Institute, July, 1956, pp 37-44.
42. Leicester, R.H., "Southwell Plot for Beam-Columns," Journal of the Engineering Mechanics Division, ASCE, Vol. 96, No. EM6, Proc. Paper 7750, December, 1970, pp 945-965.
43. Mallet, R.H., and Marcal, P.V., "Finite Element Analysis of Nonlinear Structures," Journal of the Structural Division, ASCE, Vol. 94, No. ST9, Proc. Paper 6115, September, 1968, pp 2081-2105.
44. Marcal, P.V., "Finite Element Analysis of Combined Problems of Non-Linear Material and Geometric Behaviour," Task Order NR-064-512, Brown University Technical Report, No. 1, March, 1969.
45. Martin, H.C., "On the Derivation of Stiffness Matrices for the Analysis of Large Deflection and Stability Problems," Matrix Methods in Structural Mechanics, Proceedings of the Conference held at Wright-Patterson Air Force Base, Ohio, AFFDL-TR-66-80, November, 1966.
46. Martin, H.C., "Finite Element Formulations of Geometrically Nonlinear Problems," Proceedings of U.S.-Japan Seminar on Matrix; Methods of Structural Analysis and Design, Tokyo, Japan, September, 1969.
47. Massey, P.C., "Elastic and Inelastic Lateral Instability of Beams," The Engineer, Vol. 216, October, 1963, pp 672-674.
48. Massey, P.C., and Pitman, F.S., "Inelastic Lateral Stability Under a Moment Gradient," Journal of the Engineering Mechanics Division, ASCE, Vol. 92, No. EM2, Proc. Paper 4779, April, 1966, pp 101-111.
49. Masur, E.F., and Milbrandt, K.P., "Collapse Strength of Redundant Beams After Lateral Buckling," Journal of Applied Mechanics, ASME, Vol. 24, No. 2, pp 283-288, June, 1957.

50. Murray, D.W., "Large Deflection Analysis of Plates," report to National Science Foundation NSF Grant GK-75, Department of Civil Engineering, University of California, Berkely, September, 1967.
51. Murray, D.W., and Wilson, E.L., "An Approximate Nonlinear Analysis of Thin Plates," Proceedings of the Second Conference on the Matrix Methods in Structural Mechanics, Ohio, 15-17 October, 1968, pp 1207-1230.
52. Murray, D.W., and Wilson, E.L., "Large Deflection Plate Analysis By Finite Elements," Journal of the Engineering Mechanics Division, ASCE, Vol. 95, No. EM1, February, 1969, pp 143-165.
53. Nuttall, N.J., and Adams, P.F., "Flexural and Lateral-Torsional Buckling Strength of Double Angle Struts," Structural Engineering Report No. 26, Department of Civil Engineering, University of Alberta, Fall, 1970.
54. Oden, J.T., "Mechanics of Elastic Structures," McGraw-Hill Book Company, 1967.
55. Oden, J.T., "Numerical Formulation of Nonlinear Elasticity Problems," Journal of the Structural Division, ASCE, Vol. 93, No. ST3, Proc. Paper 5290, June, 1967, pp 235-255.
56. Oden, J.T., "Finite Element Applications in Nonlinear Structural Analysis," Proceedings of the Symposium on "Application of Finite Element Methods in Civil Engineering," ASCE, Nashville, November, 1969, pp 419-456.
57. Parikh, B.P., Daniels, J.H., and Lu, L.W., "Plastic Design of Multi-Story Frames---Design Aids Booklet," Fritz Engineering Laboratory Report No. 273.24, Lehigh University, Summer, 1965.
58. Powell, G.H., "Theory of Nonlinear Elastic Structures," Journal of the Structural Division, ASCE, Vol. 95, No. ST12, Proc. Paper 6943, December, 1969, pp 2687-2701.
59. Powell, G.H., and Klingner, R., "Elastic Lateral Buckling of Steel Beams," Journal of the Structural Division, ASCE, Vol. 96, No. ST9, Proc. Paper 7555, September, 1970, pp 1919-1932.
60. Przemieniecki, J. S., "Theory of Matrix Structural Analysis, McGraw-Hill, New York, 1968.
61. Rajasekaran, S., and Murray, D.W., "Inelastic Buckling of Thin-Walled Members," paper accepted for presentation in First Speciality Conference on Cold-Formed Steel Structures, University of Missouri-Rolla, August 19-20, 1971.
62. Shanley, F.R., "Inelastic Column Theory," Journal of Aeronautical Sciences, Vol. 14, No. 5, May, 1947.

63. Sharifi, P., and Popov, E.P., "Nonlinear Buckling Analysis of Sandwich Arches," Proceedings Third Canadian Congress of Applied Mechanics," Calgary, May 17-21, 1971.
64. Smith, J.C., "Ultimate Load Analysis of Columns Subjected to Bending About Two Axes," thesis presented to the Purdue University, in 1966, in partial fulfillment of the requirements for the degree of Doctor of Philosophy.
65. Southwell, R.V., "On the Analysis of Experimental Observations in Problems of Elastic Stability," Proceedings of Royal Society, Vol. 135A, 1932, pp 601.
66. Taylor, A.C., and Ojalvo, M., "Torsional Restraint of Lateral Buckling," Journal of the Structural Division, ASCE, Vol. 92, No. ST2, Proc. Paper 4776, April, 1966, pp 115-129.
67. Thomas, B.F., and Leigh, J.M., "The Behaviour of Laterally Unsupported Angles," Melbourne Research Laboratories, Clayton, Victoria, December, 1970.
68. Timoshenko, S.P., and Gere, J.M., "Theory of Elastic Stability," McGraw-Hill Book Company, Inc., New York, 1961.
69. Timoshenko, S., and Goodier, J.N., "Theory of Elasticity," McGraw-Hill Book Company, Inc., Second Edition, 1951.
70. Trahair, N.S., "The Ultimate Load Carrying Capacity of Slender Stanchions Bent About the Major Axis," Proceedings of Institution of Civil Engineers, London, England, Vol. 19, August, 1961, pp 479-502.
71. Trahair, N.S., "Deformations of Geometrically Imperfect Beams," Journal of Structural Division, ASCE, Vol. 95, No. ST7, Proc. Paper 6682, July, 1969, pp 1475-1496.
72. Turner, M.J., Dill, E.H., Martin, H.C., and Melosh, R.J., "Large Deflections of Structures Subjected to Heating and External Loads," Journal of the Aerospace Sciences, Vol. 27, February, 1960, pp 97-106.
73. VanKaren, R.C., and Galambos, T.V., "Beam-Column Experiments," Journal of the Structural Division, ASCE, Vol. 90, No. ST2, Proc. Paper 3876, April, 1964, pp 223-256.
74. Vlasov, V.Z., "Thin-Walled Elastic Beams," 2nd Edition, Israel Program for Scientific Translations, Jerusalem, 1961, (Translated from Russian).
75. Walker, A.C., and Hall, D.G., "Analysis of the Large Deflection of Beams Using Rayleigh Ritz Finite Element Method," Aeronautical Quarterly, Vol. 19, November, 1968, pp 355-367.

76. Zienkiewicz, O.C., and Cheng, Y.K., "The Finite Element Method, in Structural and Continuum Mechanics, McGraw-Hill, London, 1967.
77. Zienkiewicz, O.C., Valliappan, S., and King, I.P., "Elastic-Plastic Solution of Engineering Problems - Initial Stress - Finite Element Approach," International Journal of Numerical Methods in Engineering, Vol. 1, 1969, pp 75-100.
78. Gallagher, R.H., and Padlog, J., "Discrete Element Approach to Structural Instability Analysis", American Institute of Aeronautics and Astronautics Journal, Vol. 1, No. 6, June, 1963, pp 1437-1439.
79. Dupuis, G.A., Pfaffinger, D.D., and Marcal, P.V., "Effective Use of the Incremental Stiffness Matrices in Nonlinear Geometric Analysis", Task Order NR-064-512, Brown University Technical Report, No. 5, September, 1970.

APPENDIX A

DETAILS OF ELASTIC FORMULATION

APPENDIX A

DETAILS OF ELASTIC FORMULATION

A-1 Expressions For Torque and Bimoment

The twisting stress resultant, or torque, about the arbitrary point S of Fig. 2.1, was defined in Section 2.1 as

$$M_t = \int_A \{ \sigma_{zy} (x - e_x) - \sigma_{zx} (y - e_y) \} dA \quad (2-1f)$$

Let ρ be the distance from S to A, and let r_n and r be the projections of ρ on the tangent at A and the perpendicular to the tangent at A, respectively, as shown in Fig. 2.1. Then r and r_n may be written as

$$r = (y - e_y) \sin \alpha + (x - e_x) \cos \alpha \quad (A-1a)$$

$$r_n = (y - e_y) \cos \alpha - (x - e_x) \sin \alpha \quad (A-1b)$$

where α is the angle between the y axis and the tangent at A.

Substituting the expressions for components of shearing stress, from Equations 2-4, into Equation 2-1f, and simplifying with Equation A-1a, we may write

$$M_t = \int_A \sigma_{z\eta} (r - \xi) dA \quad (A-2)$$

where ξ is the coordinate orthogonal to η . The approximation is required since Equations 2-4 are not exact.

If $\sigma_{z\eta}$ is assumed to vary linearly through the thickness we may write

$$\sigma_{z\eta} = \sigma_{z\eta}^A - 2 \frac{\sigma_{z\eta}^*}{t} \xi \quad (A-3)$$

where $\sigma_{z\eta}^*$ is the deviation of the stress at $\xi = t/2$ from that at A, as shown in Fig. A.1. Substituting Equation A-3 into Equation A-2, and treating A as an arbitrary point, yields

$$M_t = \int_E^F \sigma_{z\eta}^A r t ds + 2 \int_A \frac{\sigma_{z\eta}^*}{t} \xi^2 dA \quad (A-4)$$

where s is a coordinate along the midsurface contour (Fig. 2.1).

Equation A-4 may be written symbolically as

$$M_t = M_\omega + T_{sv}/2 \quad (A-5)$$

where M_ω is known as the warping torque and T_{sv} is known as the St. Venant torque. A study of torsion of general cross-section (69) shows that the torque resisted by shear stresses perpendicular to the contour is also $T_{sv}/2$ so that we may write the total torque as

$$M_t = M_\omega + T_{sv} \quad (A-6)$$

If it is understood in the following that $\sigma_{z\eta}$ is the shear stress along the midsurface contour, M_ω may be evaluated as follows. By definition

$$M_\omega = \int_E^F \sigma_{z\eta} t r ds \quad (A-7)$$

Integrating by parts, with B as the origin of the coordinate s , yields

$$M_\omega = \left[\int_B^A r ds \sigma_{z\eta} t \right]_E^F - \int_E^F \frac{\partial}{\partial s} (\sigma_{z\eta} t) \left(\int_B^A r ds \right) ds \quad (A-8)$$

Recognizing that $\sigma_{z\eta}$ must be zero at E and F, and using the equilibrium

relationship

$$\frac{\partial}{\partial s} (\sigma_{z\eta} t) + \frac{\partial (\sigma_z t)}{\partial z} = 0 \quad , \quad (\text{A-9})$$

Equation A-8 may be written as

$$M_\omega = - \frac{d}{dz} \left\{ \int_E^F \sigma_z \bar{\omega}_{SB} dA \right\} \quad (\text{A-10})$$

where we define

$$\bar{\omega}_{SB} = - \int_B^A r ds \quad (\text{A-11})$$

This may also be written as

$$\bar{\omega}_{SB} = - \left\{ \int_E^A r ds - \int_E^B r ds \right\} = -(\omega - \omega_B) \quad (\text{A-12})$$

where

$$\omega_A \equiv \int_E^A r ds = \omega \quad (\text{A-13})$$

is the sectorial coordinate of point A with respect to the origin E and the pole S.

The bimoment stress resultant, W_ω is defined as the quantity being differentiated in Equation A-10, i.e.

$$W_\omega = \int_E^F \sigma_z \bar{\omega}_{SB} dA \quad (\text{A-14})$$

Equation A-6 may now be written as

$$M_t = - W'_\omega + T_{sv} \quad (\text{A-15})$$

A-2 Derivation of Stress Resultants in Terms of Displacements

To convert the equilibrium Equations 2-2, 2-8 or 2-20 to displacement equations of equilibrium, it is necessary to express the stress resultants, P , M_x , M_y and M_t , in terms of displacements. This may be accomplished by deriving an expression for strain, as follows.

The in-plane displacements at any point A on the midsurface contour are illustrated in Fig. 2.1, and may be expressed in terms of the displacements at the arbitrary reference point S, as

$$v_A = v_s + (x - e_x) \phi \quad (2-5a)$$

$$u_A = u_s - (y - e_y) \phi \quad (2-5b)$$

If η_A is the displacement at A in the (positive) tangential direction then

$$\eta_A = v_A \cos \alpha - u_A \sin \alpha \quad (A-16)$$

Substituting Equations 2-5 into Equation A-16, and simplifying with Equation A-1a, yields

$$\eta_A = v_s \cos \alpha - u_s \sin \alpha + r\phi \quad (A-17)$$

Using assumption 1, of Section 2.2, we may now write

$$\frac{\partial \eta}{\partial z} + \frac{\partial w}{\partial s} = 0 \quad (A-18)$$

Substituting Equation A-17 into Equation A-18, and using the relations (see Fig. 2.1)

$$\sin \alpha = - \frac{dx}{ds} \quad (A-19a)$$

$$\cos \alpha = \frac{dy}{ds} \quad (A-19b)$$

results in

$$\frac{\partial w}{\partial s} = -v'_s \frac{dy}{ds} - u'_s \frac{dx}{ds} - r\phi' \quad (A-20)$$

Integrating, from B to an arbitrary point A, yields

$$w|_B^A = -v'_s (y - y_B) - u'_s (x - x_B) + \phi' (\bar{\omega}_{SB}) \quad (A-21)$$

where $\bar{\omega}_{SB}$ has been defined in Equations A-11 and A-12. Equation A-21 may also be written as

$$w_A = w_c - y v'_s - x u'_s + \bar{\omega}_{SB} \phi' \quad (A-22)$$

where

$$w_c = w_B + y_B v'_s + x_B u'_s \quad (A-23)$$

The longitudinal strain may now be obtained from the kinematic relationship in Equation A-22 by differentiating with respect to z . For an elastic material the resulting stress is

$$\sigma_z = E w'_c - E y v''_s - E x u''_s + E \bar{\omega}_{SB} \phi'' \quad (A-24)$$

The primary stress resultants, required in Equations 2-20, may now be evaluated, for an elastic response, by substituting Equation A-24 into the definitions of Equations 2-1a, 2-1b, 2-1c and A-14. This results in

$$\begin{Bmatrix} P \\ M_y \\ M_x \\ W_\omega \end{Bmatrix} = \begin{bmatrix} \int dA & \int \bar{x} dA & \int \bar{y} dA & \int \bar{\omega}_{SB} dA \\ \int \bar{x} dA & \int \bar{x}^2 dA & \int \bar{x}\bar{y} dA & \int \bar{\omega}_{SB} \bar{x} dA \\ \int \bar{y} dA & \int \bar{x}\bar{y} dA & \int \bar{y}^2 dA & \int \bar{\omega}_{SB} \bar{y} dA \\ \int \bar{\omega}_{SB} dA & \int \bar{\omega}_{SB} \bar{x} dA & \int \bar{\omega}_{SB} \bar{y} dA & \int \bar{\omega}_{SB}^2 dA \end{bmatrix} \begin{Bmatrix} Ew'_c \\ -Eu''_s \\ -Ev''_s \\ E\phi'' \end{Bmatrix} \quad (A-25)$$

Each integral in the matrix defines a property of the cross-section which is designated by the notation below.

$$\begin{Bmatrix} P \\ M_y \\ M_x \\ W_\omega \end{Bmatrix} = \begin{bmatrix} A & A \bar{x} & A \bar{y} & S_\omega \\ A \bar{x} & I_y & I_{xy} & S_{\omega y} \\ A \bar{y} & I_{yx} & I_x & S_{\omega x} \\ S_\omega & S_{\omega y} & S_{\omega x} & I_\omega \end{bmatrix} \begin{Bmatrix} Ew'_c \\ -Eu''_s \\ -E v''_s \\ E\phi'' \end{Bmatrix} \quad (A-26)$$

The expressions for the stress resultants contained in Equation A-26 may now be substituted directly into the equilibrium Equations 2-20, although it leads to considerable simplification if the off-diagonal terms are made to vanish by properly selecting the reference points.

Selecting C as the centroid, and the axes as principal axes, results, by definition, in

$$A \bar{x} = A \bar{y} = I_{xy} = 0$$

The sectorial linear static moments, $S_{\omega x}$ and $S_{\omega y}$ vanish if the point S is located at the shear center. To establish the location of this point, the distance r in Fig. 2.1 may be expressed as

$$\mathbf{r} = \mathbf{r}_O - e_x \cos \alpha - e_y \sin \alpha \quad (\text{A-27})$$

Using the definition A-11 and the relations A-19 we may then write

$$\bar{\omega}_{SB} = - \int_B^A \mathbf{r}_O \, dS + e_x (y - y_B) - e_y (x - x_B) \quad (\text{A-28})$$

Substituting into the definitions of Equation A-26 and assuming the centroidal location of C and principal orientation of the axes, the requirements that $S_{\omega x}$ and $S_{\omega y}$ vanish are

$$\begin{aligned} S_{\omega y} &= \int \bar{\omega}_{SB} \, x \, dA = \int \bar{\omega}_{CB} \, x \, dA - e_y I_y = - \int \omega_{CE} \, x \, dA \\ &\quad - e_y I_y = 0 \end{aligned} \quad (\text{A-29a})$$

$$\begin{aligned} S_{\omega x} &= \int \bar{\omega}_{SB} \, y \, dA = \int \bar{\omega}_{CB} \, y \, dA + e_x I_x = - \int \omega_{CE} \, y \, dA \\ &\quad + e_x I_x = 0 \end{aligned} \quad (\text{A-29b})$$

Solving for the location of the shear center yields

$$e_y = - \frac{S_{\omega y c}}{I_y} \quad (\text{A-30a})$$

$$e_x = \frac{S_{\omega x c}}{I_x} \quad (\text{A-30b})$$

Where $S_{\omega xc}$ and $S_{\omega yc}$ are identified with the corresponding integrals in Equations A-29.

The sectorial static moment, S_ω , will vanish if the point B is selected at a sectorial centroid. To locate such a point we use the definition from Equations A-26 and Equation A-12 to write

$$S_{\omega} = \int_E^F \bar{\omega}_{SB} dA = - \int_E^F \omega dA + \int_E^F \omega_B dA = 0 \quad (A-31)$$

Solving, the point B must be located such that

$$\omega_B = \frac{1}{A} \int_E^F \omega dA \quad (A-32)$$

In accordance with the accepted nomenclature, when S is the shear center and B is a sectorial centroid, $\bar{\omega}_{SB}$ is designated as $\bar{\omega}_n$, the normalized unit warping.

Since all the off-diagonal terms in Equation A-25 and A-26 have now been made to vanish, the displacement derivatives are easily expressed in terms of stress resultants and Equation A-24 may be written as

$$\sigma_z = \frac{P}{A} + \frac{M_y}{I_y} x + \frac{M_x}{I_x} y + \frac{W_{\omega}}{I_{\omega}} \bar{\omega}_n \quad (A-33)$$

For thin-walled elastic sections the stress resultant T_{sv} may be written as (68)

$$T_{sv} = G K \phi' \quad (A-34)$$

where

$$K = \sum b t^3 / 3 \quad (A-35)$$

A-3 Residual Stress and Strain

If residual strain exists in the section the total strain may be written, using Equation A-22, as

$$\epsilon_z = w'_c - y v''_s - x u''_s + \bar{\omega}_{SB} \phi'' + \epsilon_R \quad (A-36)$$

where ϵ_R is the residual strain. The stress, for elastic response is then

$$\sigma_z = E w'_c - E y v''_s - E x u''_s + E \bar{\omega}_{SB} \phi'' + \sigma_R \quad (A-37)$$

The residual stress distribution must satisfy the following equilibrium requirements

$$\int_A \sigma_R dA = \int_A \sigma_R y dA = \int_A \sigma_R x dA = 0 \quad (A-38)$$

and

$$-W''_{\omega R} + T'_{svR} + (M'_{\rho\phi})' = 0 \quad (A-39)$$

where

$$W_{\omega R} = \int_A \sigma_R \bar{\omega}_n dA \quad (A-40)$$

and T_{svR} is the residual St. Venant Torque.

A-4 Virtual Work Derivation of Equilibrium Equations

The virtual work equilibrium equations for members of thin-walled open cross-sections may be derived from Equation 2-16; on substitution of the relevant form of displacements, from Equations 2-5 and A-22; using the appropriate assumptions for the stress field, expressed by Equations 2-19 and 2-4; integrating over the area of the section; and making use of the definitions of stress resultants.

Equation 2-16 has been written symbolically as Equation 2-17

$$\delta (I_1 + I_2 - I_3) = 0 \quad (2-17)$$

where I_1 , I_2 , and I_3 are defined in Equations 2-18. The operation of taking the variation is carried out separately for each of the integrals as follows.

Expanding I_1 for the nonzero stress components yields

$$I_1 = \int_V \{ \sigma_{zx} (w_{,x} + u_{,z}) + \sigma_{zy} (w_{,y} + v_{,z}) + \sigma_z w_{,z} \} dv \quad (A-41)$$

substituting for the displacements from Equations 2-5 and A-22, yields

$$\begin{aligned} I_1 = & \int_V \left[\sigma_{zx} \{ u'_s - \phi' (y - e_y) - u'_s + \phi' \frac{\partial \bar{\omega}_{SB}}{\partial x} \} \right. \\ & + \sigma_{zy} \{ v'_s + \phi' (x - e_x) - v'_s + \phi' \frac{\partial \bar{\omega}_{SB}}{\partial y} \} \\ & \left. + \sigma_z \{ w'_c - y v''_s - x u''_s + \bar{\omega}_{SB} \phi'' \} \right] dv \end{aligned} \quad (A-42)$$

Using Equations 2-4 this may be written as

$$\begin{aligned} I_1 = & \int_0^{\ell} \int_A \left[\sigma_{z\eta} \phi' \{ (y - e_y) \sin \alpha + (x - e_x) \cos \alpha \} \right. \\ & + \sigma_{z\eta} \phi' \left\{ \frac{\partial \bar{\omega}_{SB}}{\partial x} \frac{dx}{ds} + \frac{\partial \bar{\omega}_{SB}}{\partial y} \frac{dy}{ds} \right\} \\ & \left. + \sigma_z (w'_c - y v''_s - x u''_s + \bar{\omega}_{SB} \phi'') \right] dA dz \end{aligned} \quad (A-43)$$

The terms in $\sigma_{z\eta}$ add out by virtue of Equations A-1a and A-11. Integrating the remaining σ_z terms and using the definitions of the stress resultants, yields

$$I_1 = \int_0^{\ell} [P w'_c - M_x v''_s - M_y u''_s + W_{\omega} \phi''] dz \quad (A-44)$$

Expanding I_2 for the nonzero stress components yields

$$\begin{aligned} I_2 = & \int_v \{ \sigma_{zx} (u_{,x} u_{,z} + v_{,x} v_{,z}) + \sigma_{zy} (u_{,y} u_{,z} + v_{,y} v_{,z}) \} dv \\ & + \frac{1}{2} \int_v \sigma_z (u_{,z}^2 + v_{,z}^2) dv \\ & + \frac{1}{2} \int_v \{ 2 \sigma_{zx} w_{,x} w_{,z} + 2 \sigma_{zy} w_{,y} w_{,z} + \sigma_z w_{,z}^2 \} dv \end{aligned} \quad (A-45)$$

The last integral in this equation contains product terms in w displacement gradients and is considered of higher order.

Substituting the displacement assumptions into the first two integrals of Equation A-45 yields

$$\begin{aligned} I_2 = & \int_0^{\ell} \int_A \{ \sigma_{zx} \phi (v'_s + \phi' (x - e_x)) - \sigma_{zy} \phi (u'_s - \phi' (y - e_y)) \} dA dz \\ & + \int_0^{\ell} \int_A [\sigma_z \{ u'_s - (y - e_y) \phi' \}^2 + \sigma_z \{ v'_s + (x - e_x) \phi' \}^2] dA dz \\ = & \int_0^{\ell} (V_x \phi v'_s - V_y \phi u'_s + T_{rn} \phi \phi') dz \\ & + \int_0^{\ell} [\frac{P}{2} (u_s'^2 + v_s'^2 + 2 e_y u'_s \phi' - 2 e_x v'_s \phi') \\ & + \frac{1}{2} (2 M_y v'_s \phi' - 2 M_x u'_s \phi') + \frac{M_{\rho} \phi'^2}{2}] dz \end{aligned} \quad (A-46)$$

where the stress resultant T_{rn} is defined as

$$T_{rn} = \int_A \sigma_{zn} r_n dA \quad (A-47)$$

This stress resultant has not been included in any set of beam equations to the author's knowledge. It is presumed small and omitted from the final equations.

The integral I_3 is evaluated by assuming q_x , q_y , and m_t act along the S axis and m_x , m_y , and q_z act along the C axis. Then

$$I_3 = \int_L (q_x u_s + q_y v_s + q_z w_c + m_t \phi + m_x v'_s + m_y u'_s) dz \quad (A-48)$$

Adding Equations A-44, A-46 and A-48; dropping the T_{rn} term; and augmenting the equation by the virtual work due to St. Venant torsion; Equation 2-17 becomes

$$\begin{aligned} & \int_L \{ P \delta w'_c - M_x \delta v''_s - M_y \delta u''_s + W_\omega \delta \phi'' + V_x \phi \delta v'_s \\ & + V_x v'_s \delta \phi - V_y \phi \delta u'_s - V_y u'_s \delta \phi + P u'_s \delta u'_s + P v'_s \delta v'_s \\ & + P e_y u'_s \delta \phi' + P e_y \phi' \delta u'_s - P e_x v'_s \delta \phi' - P e_x \phi' \delta v'_s \\ & - M_x u'_s \delta \phi' + M_y v'_s \delta \phi' - M_x \phi' \delta u'_s + M_y \phi' \delta v'_s + M_\rho \phi' \delta \phi' \\ & + T_{sv} \delta \phi' - (q_x \delta u_s + q_y \delta v_s + q_z \delta w_c + m_t \delta \phi + m_x \delta v'_s \\ & + m_y \delta u'_s) dz = 0 \end{aligned} \quad (A-49)$$

These are the equilibrium equations referred to any arbitrary origin of coordinates C and reference axis S (see Fig. 2.1) and make no assumption as to the distribution of σ_z and $\sigma_{z\eta}$ other than those required for St. Venant torsion. They are therefore suitable to use as a basis for a finite element idealization.

Integrating by parts yields the Euler-Lagrange equilibrium Equations 2-20 and the natural and geometric boundary conditions shown in Table A-1. The force quantities associated with the natural boundary conditions give the generalized forces corresponding to the displacement coordinates.

A-5 Evaluation of M_ρ for Elastic Response

The stress resultant, M_ρ , defined as

$$M_\rho = \int_A \sigma_z \{ (x - e_x)^2 + (y - e_y)^2 \} dA \quad (2-7)$$

$$= \int_A \sigma_z \rho^2 dA \quad (A-50)$$

arises in the equilibrium derivation (Section 2.2) and the virtual work derivation (Section A-4) of the governing equations. For elastic response σ_z is expressed by Equation A-37. If x and y are principal centroidal coordinates and S is the shear center Equation A-37 may be written as (see Equation A-33)

$$\sigma_z = \frac{P}{A} + \frac{M_y}{I_y} x + \frac{M_x}{I_x} y + \frac{W_\omega}{I_\omega} \bar{\omega}_n + \sigma_R \quad (A-51)$$

Substituting Equation A-51 into Equation 2-7 yields

$$\begin{aligned}
M_\rho &= \int_A \left\{ \frac{P}{A} + \frac{M_y}{I_y} x + \frac{M_x}{I_x} y + \frac{W_\omega}{I_\omega} \bar{\omega}_n + \sigma_R \right\} \rho^2 dA \\
&= \frac{P}{A} I_P + M_x C_x + M_y C_y + W_\omega C_\omega + \int_A \sigma_R \rho^2 dA
\end{aligned} \tag{A-52}$$

where

$$C_x = H_x / I_x - 2 e_y \tag{A-53a}$$

$$C_y = H_y / I_y - 2 e_x \tag{A-53b}$$

$$C_\omega = H_\omega / I_\omega \tag{A-53c}$$

$$H_x = \int_A y(x^2 + y^2) dA \tag{A-53d}$$

$$H_y = \int_A x(x^2 + y^2) dA \tag{A-53e}$$

$$H_\omega = \int_A \bar{\omega}_n (x^2 + y^2) dA \tag{A-53f}$$

$$I_P = I_x + I_y + A(e_x^2 + e_y^2) \tag{A-53g}$$

Equation A-52 is valid only when C is the centroid, S is the shear center and the axes are principal axes of the Section. Expressions for the numerical evaluation of all the necessary section properties, for any arbitrary thin-walled section, are given in Appendix D.

A-6 Evaluation of Element Flexural Stiffness Matrix $[k_s]$ and Geometric Stiffness Matrix $[k_G]$

It was assumed in Section 2.7 that continuous displacements

are given in terms of nodal displacements by Equations 2-23. The interpolating functions may be expressed as

$$\begin{aligned} \langle f_3 \rangle &= \langle (1 - 3\beta^2 + 2\beta^3), (\beta - 2\beta^2 + \beta^3), (3\beta^2 - 2\beta^3), \\ &\quad (\beta^3 - \beta^2) \rangle \end{aligned} \quad (A-54a)$$

$$\langle f_1 \rangle = \langle (1 - \beta), \beta \rangle \quad (A-54b)$$

$$\langle f_2 \rangle = \langle (2\beta - 1)(\beta - 1), -4\beta(\beta - 1), \beta(2\beta - 1) \rangle \quad (A-54c)$$

where the nondimensional coordinate, β and the nodal vectors $\{\underline{u}\}$, $\{\underline{v}\}$, $\{\underline{\phi}\}$ and $\{\underline{w}\}$ are defined in Fig. 2.6.

To obtain Equation 2-25 from Equation 2-24 it is necessary to carry out the integration in Equation 2-24, assuming A , I_x , I_y , I_ω , P , M_x , M_y , e_x , e_y all vary linearly in the form

$$A_\zeta = A_p + (A_q - A_p)\beta \quad (A-55)$$

where p and q are adjacent nodal numbers, the integrated matrices may all be written in terms of coefficient matrices of the form

$$[k_{st}^{mnj}] = \int_0^1 \beta^j \{f_m^s\} \langle f_n^t \rangle d\beta \quad (A-56)$$

where m, n = the degree of the interpolation vector (see Equations A-54); s and t indicate the order of differentiation of the respective vectors; and j is the exponent of β . The numerical values of these matrices for specific values of s, t, m, n and j are given in Table A-2.

The matrices arising from Equation 2-24, which are designated symbolically in Equations 2-27 and 2-28, then become

$$\frac{\ell^3}{E} [k_{uu}] = I_{yp} [k_{22}^{330}] + (I_{yq} - I_{yp}) [k_{22}^{331}] \quad (A-57a)$$

$$\frac{\ell^3}{E} [k_{vv}] = I_{xp} [k_{22}^{330}] + (I_{xq} - I_{xp}) [k_{22}^{331}] \quad (A-57b)$$

$$\begin{aligned} \frac{\ell^3}{E} [k_{\phi\phi}] &= I_{\omega p} [k_{22}^{330}] + (I_{\omega q} - I_{\omega p}) [k_{22}^{331}] + G\bar{K}_p \\ &\quad [k_{11}^{330}] + G(\bar{K}_q - \bar{K}_p) [k_{11}^{331}] \end{aligned} \quad (A-57c)$$

$$\frac{\ell}{E} [k_{ww}] = A_p [k_{11}^{220}] + (A_q - A_p) [k_{11}^{221}] \quad (A-57d)$$

$$\ell[g_{uu}] = \ell[g_{vv}] = P_p [k_{11}^{330}] + (P_q - P_p) [k_{11}^{331}] \quad (A-57e)$$

$$\begin{aligned} \ell[g_{u\phi}] &= \ell[g_{\phi u}]^T = -v_y \ell([k_{10}^{330}] + [k_{11}^{331}]) \\ &\quad - M_{xp} [k_{11}^{330}] + P_p e_{yp} [k_{11}^{330}] + (P_q e_{yp} \\ &\quad - 2 P_p e_{yp} + P_p e_{yq}) [k_{11}^{331}] + (P_q - P_p) \\ &\quad (e_{yq} - e_{yp}) [k_{11}^{332}] \end{aligned} \quad (A-57f)$$

$$\ell[g_{v\phi}] = \ell[g_{\phi v}]^T = v_x \ell([k_{10}^{330}] + [k_{11}^{331}]) + M_{yp}$$

$$\begin{aligned} & [k_{11}^{330}] - P_p e_{xp} [k_{11}^{330}] - (P_q e_{xp} - 2 P_p e_{xp} \\ & + P_p e_{xq}) [k_{11}^{331}] - (P_q - P_p)(e_{xq} - e_{xp})[k_{11}^{332}] \quad (A-57g) \end{aligned}$$

$$\ell[g_{\phi\phi}] = \left(\frac{P}{A_p} \frac{I}{pp} + M_{xp} C_{xp} + M_{yp} C_{yp} + W_{\omega p} C_{\omega p} \right)$$

$$\begin{aligned} & [k_{11}^{330}] + \left\{ \left(\frac{P}{A_p} \frac{I}{pp} + M_{xp} C_{xp} + M_{yp} C_{yp} \right. \right. \\ & + W_{\omega q} C_{\omega p} - 2 \left(\frac{P}{A_p} \frac{I}{pp} + M_{xp} C_{xp} + M_{yp} C_{yp} \right. \\ & + W_{\omega p} C_{\omega p} \left. \right) + \left(\frac{P}{A_q} \frac{I}{pq} + M_{xp} C_{xq} + M_{yp} C_{yq} \right. \\ & + W_{\omega p} C_{\omega q} \left. \right) \left. \right\} [k_{11}^{331}] + \left\{ (P_q - P_p) \right. \\ & \left(\frac{I}{A_q} \frac{pq}{pq} - \frac{I}{A_p} \frac{pp}{pp} \right) + (M_{xq} - M_{xp})(C_{xq} - C_{xp}) \\ & + (M_{yq} - M_{yp})(C_{yq} - C_{yp}) + (W_{\omega q} - W_{\omega p}) \\ & \left. (C_{\omega q} - C_{\omega p}) \right\} [k_{11}^{332}] \quad (A-57h) \end{aligned}$$

In Equation A-57c

$$\overline{K}_p = (K_p + M_{\rho R p} / G) \quad (A-58a)$$

where

$$M_{\rho R} = \int_A \sigma_R \rho^2 dA \quad (A-58b)$$

and K is St. Venant's constant.

If the thin-walled beam is supported on an elastic medium suitable spring constants may be added into the flexural stiffness matrix.

Natural Boundary Conditions	Geometric Boundary Conditions
at $z = 0$ or $z = \ell$	at $z = 0$ or $z = \ell$
$P = 0$	$\delta w_c = 0$
$(M'_x + V_x \phi + P v'_s - P e_x \phi' + M_y \phi') = 0$	$\delta v_s = 0$
$M_x = 0$	$\delta v'_s = 0$
$(M'_y - V_y \phi + P u'_s + P e_y \phi' - M_x \phi') = 0$	$\delta u_s = 0$
$M_y = 0$	$\delta u'_s = 0$
$(-W'_\omega + P e_y u'_s - P e_x v'_s - M_x u'_s$ $+ M_y v'_s + M_\rho \phi' + T_{sv}) = 0$	$\delta \phi = 0$
$W_\omega = 0$	$\delta \phi' = 0$

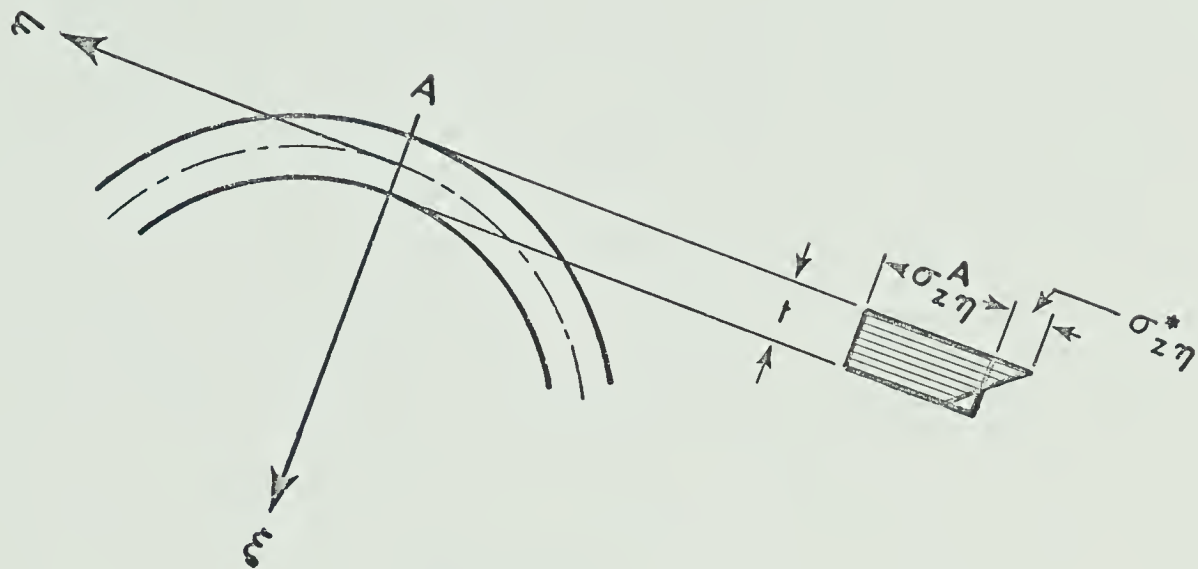
TABLE A-1

BOUNDARY CONDITIONS

$30[k_{11}^{330}] = \begin{bmatrix} 36 & 3 & -36 & 3 \\ 3 & 4 & -3 & -1 \\ -36 & -3 & 36 & -3 \\ 3 & -1 & -3 & 4 \end{bmatrix}$	$[k_{22}^{330}] = \begin{bmatrix} 12 & 6 & -12 & 6 \\ 6 & 4 & -6 & 2 \\ -12 & -6 & 12 & -6 \\ 6 & 2 & -6 & 4 \end{bmatrix}$
$30[k_{11}^{331}] = \begin{bmatrix} 18 & 3 & -18 & 0 \\ 3 & 1 & -3 & -0.5 \\ -18 & -3 & 18 & 0 \\ 0 & -0.5 & 0 & 3 \end{bmatrix}$	$[k_{22}^{331}] = \begin{bmatrix} 6 & 2 & -6 & 4 \\ 2 & 1 & -2 & 1 \\ -6 & -2 & 6 & -4 \\ 4 & 1 & -4 & 3 \end{bmatrix}$
$30[k_{10}^{330}] = \begin{bmatrix} -15 & -3 & -15 & 3 \\ 3 & 0 & -3 & .5 \\ 15 & 3 & 15 & -3 \\ -3 & -.5 & 3 & 0 \end{bmatrix}$	$210[k_{11}^{332}] = \begin{bmatrix} 72 & 15 & -72 & -6 \\ 15 & 4 & -15 & -3 \\ -72 & -15 & 72 & 6 \\ -6 & -3 & 6 & 18 \end{bmatrix}$
$[k_{12}^{230}] = \begin{bmatrix} 4 & 3 & -4 & 1 \\ -8 & -4 & 8 & -4 \\ 4 & 1 & -4 & 3 \end{bmatrix}$	$[k_{12}^{231}] = \begin{bmatrix} 1 & 2/3 & -1 & 1/3 \\ -4 & -4/3 & 4 & -8/3 \\ 3 & 2/3 & -3 & 7/3 \end{bmatrix}$
$3[k_{11}^{220}] = \begin{bmatrix} 7 & -8 & 1 \\ -8 & 16 & -8 \\ 1 & -8 & 7 \end{bmatrix}$	$6[k_{11}^{221}] = \begin{bmatrix} 3 & -4 & 1 \\ -4 & 16 & -12 \\ 1 & -12 & 11 \end{bmatrix}$

TABLE A-2

COEFFICIENT MATRICES



$\sigma_{z\eta}^A$ Warping Shear

$\sigma_{z\eta}^*$ St. Venant Shear

FIGURE A1 SHEAR STRESSES IN A THIN-WALLED BEAM

APPENDIX B

COMPARISON OF ELASTIC FORMULATIONS

APPENDIX B

COMPARISON OF ELASTIC FORMULATIONS

B-1 Introduction

The governing equations of this dissertation were derived from the principle of virtual work. It has been shown in Chapter II and Appendix A that the total equilibrium equations, Equations 2-20, are essentially the same as those of Vlassov (74). However, the incremental equilibrium equations, derived from virtual work following the procedure of Biot (10) and developed by Felippa (19), Murray (50), Hofmeister et al (34), and others, differ, from the potential energy derivation, in the higher order terms.

The most consistent derivation of nonlinear terms in finite element formulations is based upon the potential energy approach and due to Mallet and Marcal (43). The objectives of this appendix are

- a) to compare the present method of formulation with that of Mallet and Marcal;
- b) to indicate the modifications required in the virtual work formulation to make it correspond to the incremental formulation of Mallet and Marcal;
- c) to demonstrate by numerical comparison that, for members of thin-walled open sections, the formulation adopted in this dissertation yields reliable results in the range of interest. The beam-column formulation of Mallet and Marcal is used for this comparison.

B-2 Formulation of Beam-Column Equations

B-2-1 Virtual Work Formulation

The incremental equilibrium equation described in Chapter II, is given by Equation 2-14 which may be written in the following notation

$$\int_V \bar{\sigma}_{ij} \delta(e_{ij}^1) dv + \int_V \sigma_{ij} \delta(e_{ij}) dv = \int_S t_i \delta u_i ds \quad (B-1)$$

where

$$e_{ij} = e_{ij}^0 + e_{ij}^1 + e_{ij}^2 \quad (B-2)$$

and e_{ij}^0 , e_{ij}^2 , e_{ij}^1 contain linear terms in displacement increments and product terms of initial and incremental displacements, respectively, i.e.:

$$e_{ij}^0 = \frac{1}{2}(u_{i,j} + u_{j,i}) \quad (B-3a)$$

$$e_{ij}^1 = \frac{1}{2} u_{k,i} u_{k,j} \quad (B-3b)$$

$$e_{ij}^2 = \frac{1}{2}(\bar{u}_{k,i} u_{k,j} + \bar{u}_{k,j} u_{k,i}) \quad (B-3c)$$

In Table B-1 linear incremental formulations are compared for the in-plane beam-column problem

- a) when only first order terms are included in $\bar{\sigma}_{ij}$ and e_{ij}
- b) when the higher order terms are included in $\bar{\sigma}_{ij}$ and e_{ij}

B-2-2 Mallet and Marcal's Formulation

The strain energy for the beam element is written as

$$U = \frac{1}{2} \int_V E(w_{,z} - y v_{,zz} + v_{,z}^2/2)^2 dv \quad (B-4a)$$

$$= \int_{\ell} \langle d \rangle \left[\frac{EA}{2} [\hat{k}_S] + \frac{EA}{6} [\hat{n}_1] + \frac{EA}{12} [\hat{n}_2] \right] \{d\} dz \quad (B-4b)$$

where

$$[\hat{k}_S] = \begin{bmatrix} 1 & 0 & 0 \\ 0 & 0 & 0 \\ 0 & 0 & I/A \end{bmatrix} \quad (B-4c)$$

$$[\hat{n}_1] = \begin{bmatrix} 0 & v_{,z} & 0 \\ v_{,z} & w_{,z} & 0 \\ 0 & 0 & 0 \end{bmatrix} \quad (B-4d)$$

$$[\hat{n}_2] = \begin{bmatrix} 0 & 0 & 0 \\ 0 & 3/2(v_{,z}^2) & 0 \\ 0 & 0 & 0 \end{bmatrix} \quad (B-4e)$$

and

$$\langle d \rangle = \langle w_{,z}, v_{,z}, v_{,zz} \rangle \quad (B-4f)$$

For equilibrium

$$\delta U + \delta W = 0 \quad (B-5a)$$

Hence equilibrium equation is

$$\int_{\ell} \langle \delta d \rangle \left[EA[\hat{k}_S] + \frac{EA}{2} [\hat{n}_1] + \frac{EA}{3} [\hat{n}_2] \right] \{d\} dz + \delta W = 0 \quad (B-5b)$$

Retaining only linear terms in the increments in displacements, the incremental equilibrium equation may be written as

$$\int_{\ell} \delta \Delta d \left[EA[\hat{k}_S] + EA[\hat{n}_1] + EA[\hat{n}_2] \right] \frac{1}{d} \{\Delta d\} dz + \{\delta \Delta W\} = 0 \quad (B-6)$$

Equation B-6 is the same as the incremental equilibrium equation developed by using the virtual work formulation for case b (Table B-1).

Expressing $[d]$ in terms of the generalized coordinates $\{\beta\}$ through a linear transformation of the form

$$\{d\} = [D] \{\beta\} \quad (B-7)$$

the potential energy is

$$U = \langle \beta \rangle \left[\frac{1}{2} [\bar{k}_S] + \frac{1}{6} [\bar{n}_1] + \frac{1}{12} [\bar{n}_2] \right] \{\beta\} \quad (B-8a)$$

The equilibrium equation is

$$\left[[\bar{k}_S] + \frac{1}{2} [\bar{n}_1] + \frac{1}{3} [\bar{n}_2] \right] \{\beta\} + \{Q\} = 0 \quad (B-8b)$$

where $\{Q\}$ is the vector of generalized forces associated with the $\{\beta\}$ displacement coordinates.

The incremental equilibrium equation is

$$\left[[\bar{k}_S] + [\bar{n}_1] + [\bar{n}_2] \right]_{\beta} \{\Delta\beta\} + \{\Delta Q\} = 0 \quad (B-8c)$$

where

$$[\bar{k}_S] = \int_0^{\ell} EA [D]^T [\hat{k}_S] [D] dz \quad (B-9a)$$

$$[\bar{n}_1] = \int_0^{\ell} EA [D]^T [\hat{n}_1] [D] dz \quad (B-9b)$$

$$[\bar{n}_2] = \int_0^{\ell} EA [D]^T [\hat{n}_2] [D] dz \quad (B-9c)$$

B-2-3 Comparison of Formulations

The derivations in Chapter II and Appendix A show that by

ignoring the initial displacement matrix, and using only first order terms in $\bar{\sigma}_{ij}$, σ_{ij} and e_{ij} (as in Table B-1, case a) the virtual work formulation is consistent with the formulation of the classical beam equations normally applied to stability problems. These equations may be regarded as examples of the lowest level of nonlinear equations in the hierarchy of nonlinear formulations discussed by Mallet and Marcal. In this work the term "virtual work equations" refers to sets of equations derived by assumptions consistent with those for case a, of Table B-1. The term "potential energy equations" refers to sets of equations derived in a manner consistent with the derivation of Mallet and Marcal, or case b, Table B-1.

B-3 Nonlinear Analysis of Beam-Columns

In Section B-2 a comparison was made of the nonlinear terms arising in the virtual work and potential energy formulations. The question arises as to the range of reliability of the virtual work formulation. Some indication of this is achieved by comparing the numerical result for a typical in-plane beam-column problem. Such a comparison is carried out in the following.

B-3-1 Mallet and Marcal's Linear Incremental Formulation

Using the nomenclature of Mallet and Marcal, the linear incremental potential energy formulation is written as

$$[[K_S] + [N_1] + [N_2]]_r \{\Delta r\} = \{\Delta R\} \quad (B-10)$$

where element matrices are given by

$$[k_S] = [T]^T [\bar{k}_S] [T] \quad (B-11a)$$

$$[n_1] = [T]^T [\bar{n}_1] [T] \quad (B-11b)$$

$$[n_2] = [T]^T [\bar{n}_2] [T] \quad (B-11c)$$

and $[\bar{k}_S]$, $[\bar{n}_1]$, $[\bar{n}_2]$ and $[T]$ are specified in Figs. B.1, B.2, B.3, and B.4 respectively. The vector of generalized coordinates, $\{\beta\}$, specifies the centroidal displacements through the relations

$$w = \beta_1 + \beta_2 z \quad (B-12a)$$

and

$$v = \beta_3 + \beta_4 z + \beta_5 z^2 + \beta_6 z^3 \quad (B-12b)$$

The generalized coordinates are related to the nodal displacements, $\{r\}$ through the transformation

$$\{\beta\} = [T] \{r\} \quad (B-13)$$

where

$$\{r\}^T = \langle v_p, \theta_{xp}, w_p, v_q, \theta_{xq}, w_q \rangle \quad (B-14)$$

The total equilibrium equation may be written as

$$[[K_S] + \frac{1}{2} [N_1] + \frac{1}{3} [N_2]] \{r\} = \{R\} \quad (B-15)$$

The solution to this set of equations was obtained by a Newton-Raphson procedure where iteration was carried out until the unbalanced nodal forces, $\{E\}$, evaluated as

$$\{E\} = \{R\} - [[K_S] + \frac{1}{2} [N_1] + \frac{1}{3} [N_2]] \{r\} \quad (B-16)$$

were negligible. A flow chart of this procedure is shown in Fig. B.5.

B-3-2 Incremental Virtual Work Formulation

The incremental virtual work equations may be written as

$$[[K_S] + [K_G]] \{\Delta r\} = \{\Delta R\} \quad (B-17)$$

The element geometric stiffness matrix, $[\bar{k}_G]$ for the generalized coordinates is obtained by summing $[\bar{n}_1]$ and $[\bar{n}_2]$ of the previous formulation, with β_4 , β_5 , and β_6 equal to zero and $\beta_2 = P/AE$. This is equivalent to discarding the matrix $[\bar{n}_2]$ and retaining only the 3x3 main diagonal submatrix in the definition of $[\bar{n}_1]$.

The total equilibrium equation is written as

$$[[K_S] + [K_G]] \{r\} = \{R\} \quad (B-18)$$

The solution to this set of equations was also obtained by a Newton-Raphson procedure where iteration was carried out until the unbalanced nodal forces, $\{E\}$ evaluated as

$$\{E\} = \{R\} - [[K_S] + [K_G]] \{r\} \quad (B-19)$$

were negligible.

B-4 Numerical Results

The beam-column shown in Fig. B.6 was subjected to an increasing axial load and a constant transverse load of 5 kips applied at the central point, A. The contribution of the matrices $[K_S]$ and $[K_G]$ to the equilibrium of point A is shown in Fig. B.6. The stiffness of the structure approaches zero as P/P_{cr} approaches 1.

The same beam-column was analyzed by the method of Mallet and Marcal. The contribution of the matrices to the equilibrium of the transverse force at A are shown in Table B-2. The results are also plotted in Fig. B.7.

A comparison of the load deflection plots by the two methods is shown in Fig. B.8. While it is apparent that the second order incremental stiffness matrix $[N_2]$ or a suitable equivalent must be included to analyze post-buckling behaviour, it is also apparent that the pre-buckling behaviour may be closely approximated by omitting these terms. In addition, inelastic material response may be expected to occur prior to any significant stiffening effect from the difference in the large displacement terms between the matrices $[N_1]$ and $[N_2]$. It is therefore concluded that the inclusion of inelastic material response is more significant for this class of problem than the inclusion of higher order geometric effects.

B-5 Summary and Conclusion

It has been shown that the virtual work formulation can be made to correspond to the linear incremental potential energy formulation by including the higher order terms in the expression for initial stress, and stress and strain increments.

It is seen from numerical results that it is unnecessary to include the higher order terms unless investigating the post-buckling behaviour. Because of the influence of inelastic material response the maximum load carrying capacity will normally be attained before these higher order terms have any significant effect.

It has also been shown that the virtual work formulation employed is consistent with the classical differential equation

formulation of the problem.

TABLE B-1 LINEAR INCREMENTAL FORMULATION

	a) First order terms in $\bar{\sigma}_{ij}$, e_{ij} (neglecting initial displacement in e_{ij})	b) Second order terms in $\bar{\sigma}_{ij}$, and initial displacement terms in σ_{ij} , e_{ij}
e_{ij}^0	$w_{,z} - y v_{,zz}$	$w_{,z} - y v_{,zz}$
e_{ij}^1	$v_{,z}^2 / 2$	$v_{,z}^2 / 2$
e_{ij}^2	neglected	$\bar{v}_{,z} v_{,z}$
$e_{ij} = e_{ij}^0 + e_{ij}^1 + e_{ij}^2$	$\epsilon_z = w_{,z} - y v_{,zz}$	$w_{,z} - y v_{,zz} + \bar{v}_{,z} v_{,z}$
σ_{ij}	Product terms in incremental displacements neglected	
σ_{ij}	$\sigma_z = E(w_{,z} - y v_{,zz})$	$E(w_{,z} - y v_{,zz} + \bar{v}_{,z} v_{,z})$
	$\bar{\sigma}_z = E(\bar{w}_{,z} - y \bar{v}_{,zz})$	$E(\bar{w}_{,z} - y \bar{v}_{,zz} + \bar{v}_{,z}^2 / 2)$
$\int_v \bar{\sigma}_{ij} \delta(e_{ij}^1) dv$	$= EA \int_l \begin{Bmatrix} \delta w_{,z} \\ \delta v_{,z} \\ \delta v_{,zz} \end{Bmatrix}^T \begin{bmatrix} 0 & 0 & 0 \\ 0 & \bar{w}_{,z} & 0 \\ 0 & 0 & 0 \end{bmatrix} \begin{Bmatrix} w_{,z} \\ v_{,z} \\ v_{,zz} \end{Bmatrix} dz$	$= EA \int_l \begin{Bmatrix} \delta w_{,z} \\ \delta v_{,z} \\ \delta v_{,zz} \end{Bmatrix}^T \begin{bmatrix} 0 & 0 & 0 \\ 0 & (\bar{w}_{,z} + \frac{\bar{v}_{,z}^2}{2}) & 0 \\ 0 & 0 & 0 \end{bmatrix} \begin{Bmatrix} w_{,z} \\ v_{,z} \\ v_{,zz} \end{Bmatrix} dz$

Table B-1 (cont'd)

	Case (a)	Case (b)
$\int_V \sigma_{ij} \delta(e_{ij}^0) dv$	$EA \int_V \left\{ \begin{matrix} \delta w_{,z} \\ \delta v_{,z} \\ \delta v_{,zz} \end{matrix} \right\}^T \left[\begin{matrix} 1 & 0 & 0 \\ 0 & 0 & 0 \\ 0 & 0 & I/A \end{matrix} \right] \left\{ \begin{matrix} w_{,z} \\ v_{,z} \\ v_{,zz} \end{matrix} \right\} dz$	$=EA \int_V \left\{ \begin{matrix} \delta w_{,z} \\ \delta v_{,z} \\ \delta v_{,zz} \end{matrix} \right\}^T \left[\begin{matrix} 1 & \bar{v}_{,z} & 0 \\ 0 & 0 & 0 \\ 0 & 0 & I/A \end{matrix} \right] \left\{ \begin{matrix} w_{,z} \\ v_{,z} \\ v_{,zz} \end{matrix} \right\} dz$
$\int_V \sigma_{ij} \delta e_{ij}^{(1)} dv$	neglected in linear incremental formulation	
$\int_V \sigma_{ij} \delta e_{ij}^{(2)} dv$	neglected	
$\int_S t_i \delta u_i dS$	$EA \int_V \left\{ \begin{matrix} \delta w_{,z} \\ \delta v_{,z} \\ \delta v_{,zz} \end{matrix} \right\}^T \left[[\hat{k}_S] + [\hat{k}_G] \right] \left\{ \begin{matrix} w_{,z} \\ v_{,z} \\ v_{,zz} \end{matrix} \right\} dz$	$EA \int_V \left\{ \begin{matrix} \delta w_{,z} \\ \delta v_{,z} \\ \delta v_{,zz} \end{matrix} \right\}^T \left[[\hat{k}_S] + [\hat{n}_1] + [\hat{n}_2] \right] \left\{ \begin{matrix} w_{,z} \\ v_{,z} \\ v_{,zz} \end{matrix} \right\} dz$

Table B-1 (cont'd)

Case (a)		Case (b)	
Incremental matrices	Where	$[\hat{k}_S] = \begin{bmatrix} 1 & 0 & 0 \\ 0 & 0 & 0 \\ 0 & 0 & I/A \end{bmatrix}$	$[\hat{k}_S] = \begin{bmatrix} 1 & 0 & 0 \\ 0 & 0 & 0 \\ 0 & 0 & I/A \end{bmatrix}$
	and	$[\hat{k}_G] = \begin{bmatrix} 0 & 0 & 0 \\ 0 & \bar{w},z & 0 \\ 0 & 0 & 0 \end{bmatrix}$	$[\hat{n}_1] = \begin{bmatrix} 0 & \bar{v},z & 0 \\ \bar{v},z & \bar{w},z & 0 \\ 0 & 0 & 0 \end{bmatrix}$
			$[\hat{n}_2] = \begin{bmatrix} 0 & 0 & 0 \\ 0 & \frac{3}{2}\bar{v},z & 0 \\ 0 & 0 & 0 \end{bmatrix}$

TABLE B-2

COMPARISON OF BEAM-COLUMN SOLUTION BY VIRTUAL WORK AND POTENTIAL ENERGY APPROACHES

Axial load	Method 1				Method 2		
	Central deflection	[K _S] contribution	[N ₁] contribution	[N ₂] contribution	Central deflection	[K _S] contribution	[K _G] contribution
100	0.10324	5.261	- 0.2624	0.89D-03	0.1032	5.2617	- 0.2617
200	0.1134	5.5476	- 0.5732	0.117D-03	0.11465	5.577	- 0.5778
300	0.1260	5.8936	- 0.9496	0.1584D-02	0.1289	5.96856	- 0.9686
400	0.1418	6.322	- 1.416	0.222D-02	0.1473	6.466	- 1.4660
500	0.1717	7.122	- 2.12	0.3872D-02	0.1718	7.123	- 2.1238
600	0.20	7.806	- 2.96	0.606D-02	0.20628	8.039	- 3.039
700	0.2578	9.40	- 4.412	0.126D-01	0.25816	9.4066	- 4.40661
800	0.3443	11.66	- 6.69	0.2967D-01	0.34521	11.6862	- 6.6862
900	0.5169	16.16	-11.26	0.987D-01	0.52151	16.28	-11.280
1000	1.0032	28.84	-24.55	0.710	1.06885	30.485	-25.493
1050					2.254	61.243	-56.243
1100	2.6591	72.67	-80.90	13.23	-20.364	-525.0	530.0
1150					-1.843	-44.966	49.96
1200	4.635	127.07	-193.65	71.57	-0.9646	-22.1753	27.1753
1300	6.211	171.87	-342.31	175.47			
1400	7.532	209.87	-522.44	317.57			
1500	8.6912	243.15	-731.38	493.28			
1600	9.7335	272.84	-966.43	698.94			
1700	10.687	299.60	-1225.0	930.60			
1800	11.57	324.18	-1506.0	1187.0			
1900	12.40	346.70	-1807.0	1466.0			

$$[\bar{k}_S] = EA \begin{bmatrix} 0 & 0 & 0 & 0 & 0 & 0 \\ 0 & 1 & 0 & 0 & 0 & 0 \\ 0 & 0 & 0 & 0 & 0 & 0 \\ 0 & 0 & 0 & 0 & 0 & 0 \\ 0 & 0 & 0 & 0 & \frac{4I\ell}{A} & \frac{6I\ell^2}{A} \\ 0 & 0 & 0 & 0 & \frac{6I\ell^2}{A} & \frac{12I\ell^3}{A} \end{bmatrix}$$

Fig. B.1 FLEXURAL STIFFNESS (GENERALIZED COORDINATES)

$$[\bar{n}_1] = \begin{bmatrix} 0 & 0 & 0 & 0 & 0 & 0 \\ 0 & 0 & 0 & \bar{n}_1(2,4) & \bar{n}_1(2,5) & \bar{n}_1(2,6) \\ 0 & 0 & 0 & 0 & 0 & 0 \\ 0 & \bar{n}_1(4,2) & 0 & \bar{n}_1(4,4) & \bar{n}_1(4,5) & \bar{n}_1(4,6) \\ 0 & \bar{n}_1(5,2) & 0 & \bar{n}_1(5,4) & \bar{n}_1(5,5) & \bar{n}_1(5,6) \\ 0 & \bar{n}_1(6,2) & 0 & \bar{n}_1(6,4) & \bar{n}_1(6,5) & \bar{n}_1(6,6) \end{bmatrix}$$

$$\bar{n}_1(2,4) = \bar{n}_1(4,2) = EA(\beta_4 \ell + \beta_5 \ell^2 + \beta_6 \ell^3)$$

$$\bar{n}_1(2,5) = \bar{n}_1(5,2) = EA(\beta_4 \ell^2 + \frac{4}{3} \beta_5 \ell^3 + \frac{3}{2} \beta_6 \ell^4)$$

$$\bar{n}_1(2,6) = \bar{n}_1(6,2) = EA(\beta_4 \ell^3 + \frac{3}{2} \beta_5 \ell^4 + \frac{9}{5} \beta_6 \ell^5)$$

$$\bar{n}_1(4,4) = EA \ell \beta_2$$

$$\bar{n}_1(4,5) = \bar{n}_1(5,4) = EA \ell^2 \beta_2$$

$$\bar{n}_1(4,6) = \bar{n}_1(6,4) = EA \ell^3 \beta_2$$

$$\bar{n}_1(5,5) = \frac{4}{3} EA \ell^3 \beta_2$$

$$\bar{n}_1(5,6) = \bar{n}_1(6,5) = \frac{3}{2} EA \ell^4 \beta_2$$

$$\bar{n}_1(6,6) = \frac{9}{5} EA \ell^5 \beta_2$$

Fig. B.2 FIRST ORDER INITIAL DISPLACEMENT MATRIX

$$[\bar{n}_2] = \begin{bmatrix} 0 & 0 & 0 & 0 & 0 & 0 \\ 0 & 0 & 0 & 0 & 0 & 0 \\ 0 & 0 & 0 & 0 & 0 & 0 \\ 0 & 0 & 0 & \bar{n}_2(4,4) & \bar{n}_2(4,5) & \bar{n}_2(4,6) \\ 0 & 0 & 0 & \bar{n}_2(5,4) & \bar{n}_2(5,5) & \bar{n}_2(5,6) \\ 0 & 0 & 0 & \bar{n}_2(6,4) & \bar{n}_2(6,5) & \bar{n}_2(6,6) \end{bmatrix}$$

$$\bar{n}_2(4,4) = \frac{3}{2}(\beta_4^2 \ell + \frac{4}{3} \beta_5^2 \ell^3 + \frac{9}{5} \beta_6^2 \ell^5 + 2\beta_4 \beta_5 \ell^2 + 3\beta_5 \beta_6 \ell^4 + 2\beta_4 \beta_6 \ell^3)$$

$$\bar{n}_2(4,5) = 3(\frac{\beta_4^2 \ell^2}{2} + \beta_5^2 \ell^4 + \frac{9}{6} \beta_6^2 \ell^6 + \frac{4}{3} \beta_4 \beta_5 \ell^3 + \frac{12}{5} \beta_5 \beta_6 \ell^5 + \frac{6}{4} \beta_4 \beta_6 \ell^4)$$

$$\bar{n}_2(4,6) = \frac{9}{2}(\frac{\beta_4^2 \ell^3}{3} + \frac{4}{5} \beta_5^2 \ell^5 + \frac{9}{7} \beta_6^2 \ell^7 + \beta_4 \beta_5 \ell^4 + 2 \beta_5 \beta_6 \ell^6 + \frac{6}{5} \beta_4 \beta_6 \ell^5)$$

$$\bar{n}_2(5,5) = \frac{4}{3} \bar{n}_2(4,6)$$

$$\bar{n}_2(5,6) = 9(\frac{\beta_4^2 \ell^4}{4} + \frac{4}{6} \beta_5^2 \ell^6 + \frac{9}{8} \beta_6^2 \ell^8 + \frac{4}{5} \beta_4 \beta_5 \ell^5 + \frac{12}{7} \beta_5 \beta_6 \ell^7 + \beta_4 \beta_6 \ell^6)$$

$$\bar{n}_2(6,6) = \frac{27}{2}(\frac{\beta_4^2 \ell^5}{5} + \frac{4}{7} \beta_5^2 \ell^7 + \beta_6^2 \ell^9 + \frac{4}{6} \beta_4 \beta_5 \ell^6 + \frac{12}{8} \beta_5 \beta_6 \ell^8 + \frac{6}{7} \beta_4 \beta_6 \ell^7)$$

$$\bar{n}_2(5,4) = \bar{n}_2(4,5)$$

$$\bar{n}_2(6,4) = \bar{n}_2(4,6)$$

$$\bar{n}_2(6,5) = \bar{n}_2(5,6)$$

Fig. B.3 SECOND ORDER INITIAL DISPLACEMENT MATRIX

$$[T] = \begin{bmatrix} 0 & 0 & 1 & 0 & 0 & 0 \\ 0 & 0 & -\frac{1}{\ell} & 0 & 0 & \frac{1}{\ell} \\ 1 & 0 & 0 & 0 & 0 & 0 \\ 0 & 1 & 0 & 0 & 0 & 0 \\ -\frac{3}{\ell^2} & -\frac{2}{\ell} & 0 & \frac{3}{\ell^2} & -\frac{1}{\ell} & 0 \\ \frac{2}{\ell^3} & \frac{1}{\ell^2} & 0 & -\frac{2}{\ell^3} & \frac{1}{\ell^2} & 0 \end{bmatrix}$$

Fig. B.4 TRANSFORMATION MATRIX RELATING GENERALIZED
COORDINATES TO ELEMENT DISPLACEMENTS

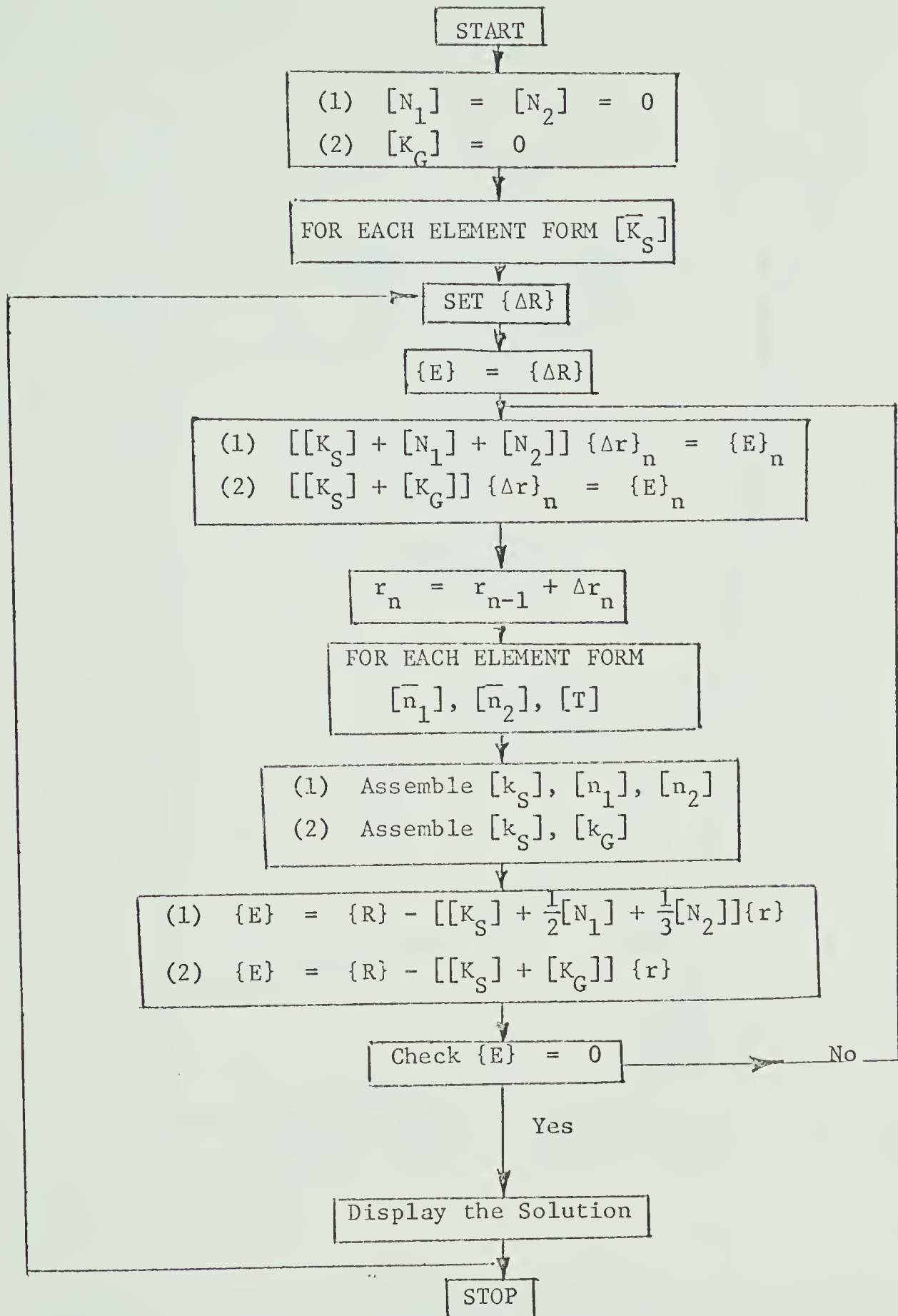


Fig. B.5 FLOW CHART EXPLAINING THE SOLUTION SCHEME
FOR BEAM-COLUMN PROBLEMS

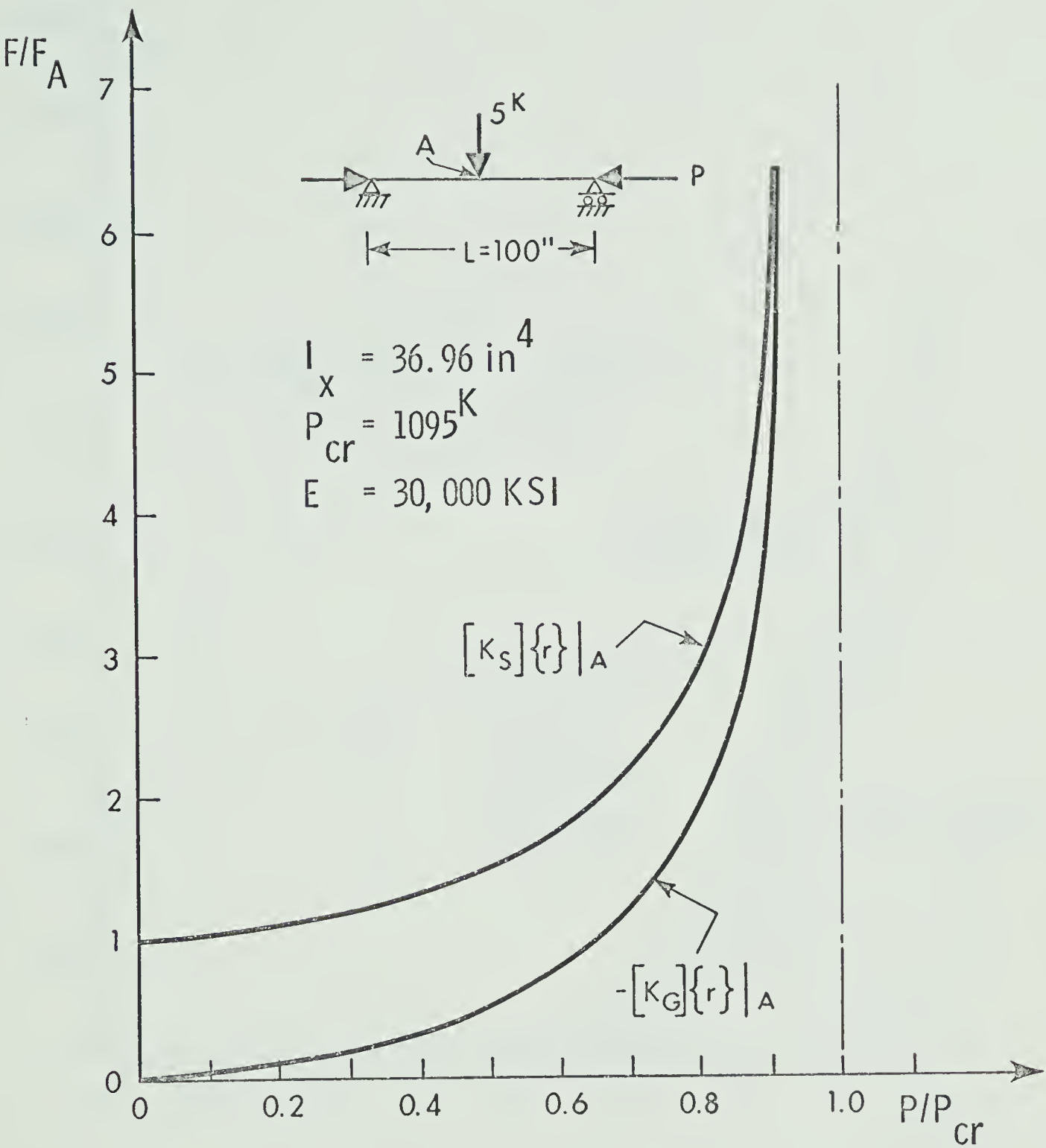


FIGURE B.6 EFFECT OF INCREMENTAL MATRICES IN SMALL DISPLACEMENT RANGE

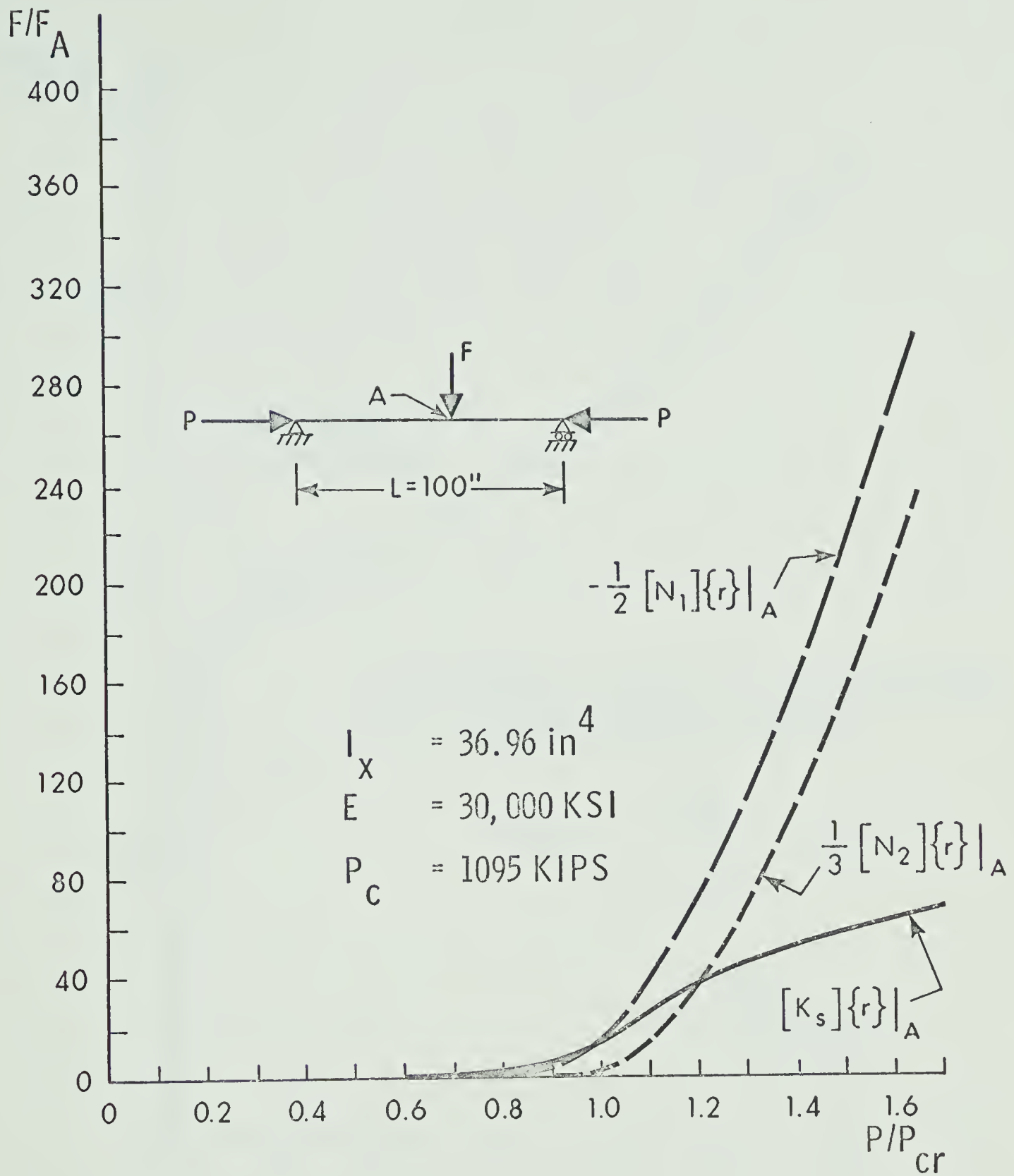


FIGURE B.7 EFFECT OF INCREMENTAL MATRICES IN LARGE DISPLACEMENT RANGE

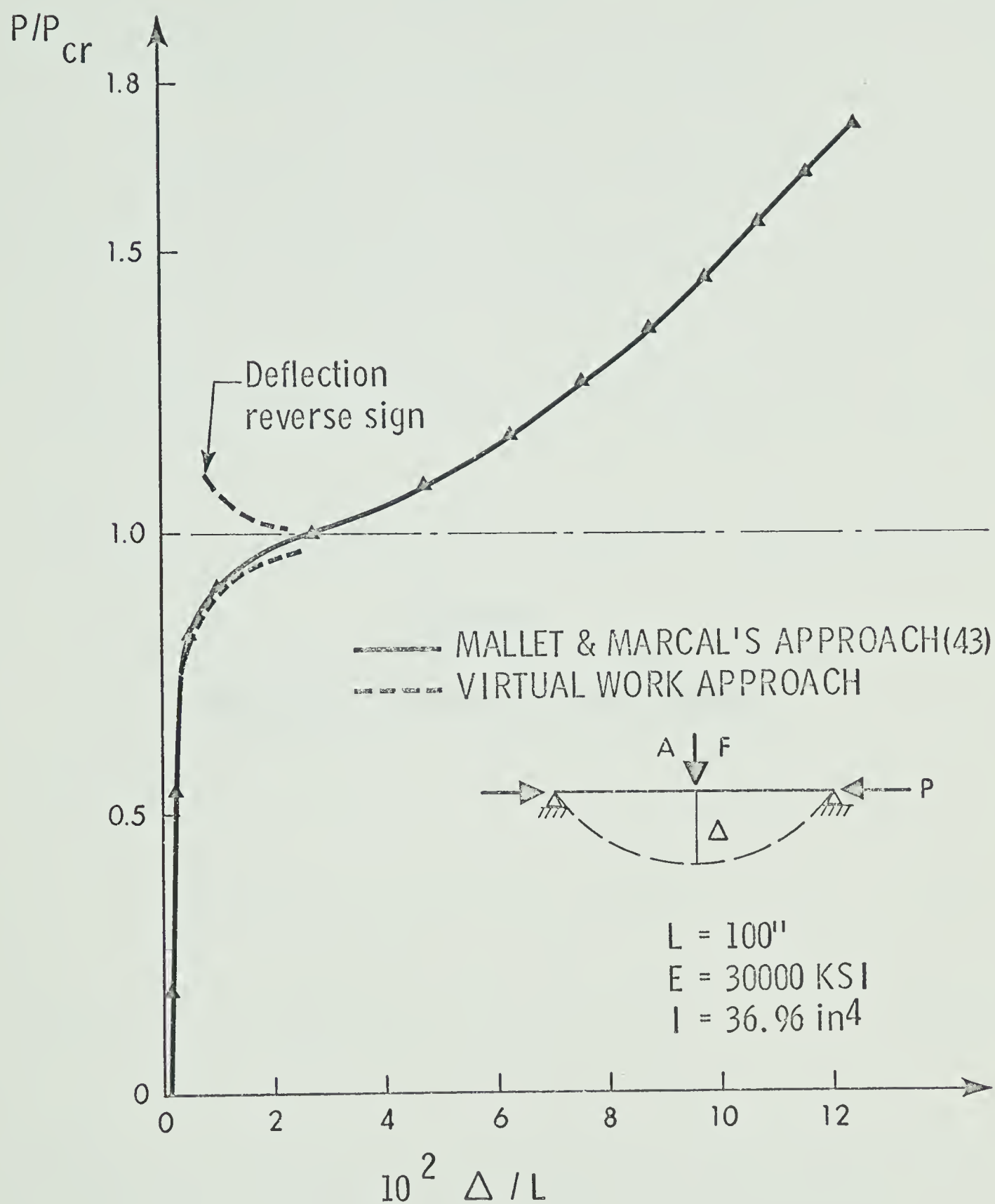


FIGURE B.8 PRE AND POST BUCKLING BEHAVIOUR OF BEAM-COLUMN

APPENDIX C

DERIVATION OF MATRICES FOR LOCAL BUCKLING

APPENDIX CDERIVATION OF MATRICES FOR LOCAL BUCKLING

The element stiffness matrices appearing in Equation 4-22 are obtained by substituting Equation 2-23, 4-17 and 4-21 into 4-14; integrating carrying out the variation; and grouping terms associated with each set of virtual nodal displacements. Assuming the moment is constant in an element length for the evaluation of the geometric stiffness of a plate segment, this results in the following set of equilibrium equations.

$$\begin{aligned} \frac{E I_y}{\ell^3} [K_{22}^3] \{\underline{u}\} + \frac{P}{\ell} [K_{11}^3] \{\underline{u}\} - \frac{M_{xi}}{\ell} [K_{11}^3] \{\underline{\phi}\} - v_y [K_{10}^3 + K_{11}^{31}] \{\underline{\phi}\} \\ + c_2 [K_{11}^3] \{\underline{v}_t^p\} + c_3 [K_{11}^3] \{\underline{v}_b^p\} = \{\underline{R}_u\} \end{aligned} \quad (C-1a)$$

$$\begin{aligned} \frac{E I_x}{\ell^3} [K_{22}^3] \{\underline{v}\} + \frac{P}{\ell} [K_{11}^3] \{\underline{v}\} + \frac{M_{yi}}{\ell} [K_{11}^3] \{\underline{\phi}\} + v_x [K_{10}^3 + K_{11}^{31}] \{\underline{\phi}\} \\ + c_1 [K_{11}^3] \{\underline{v}_t^p\} + c_1 [K_{11}^3] \{\underline{v}_b^p\} = \{\underline{R}_v\} \end{aligned} \quad (C-1b)$$

$$\frac{EA}{\ell} [K_{11}^1] \{\underline{w}\} = \{\underline{R}_w\} \quad (C-1c)$$

$$\begin{aligned} \frac{E I_\omega}{\ell^3} [K_{22}^3] \{\underline{\phi}\} + \frac{GK}{\ell} [K_{11}^3] \{\underline{\phi}\} + \frac{P I_p}{A\ell} [K_{11}^3] \{\underline{\phi}\} - \frac{M_{xi}}{\ell} [K_{11}^3] \{\underline{u}\} \\ - v_y [K_{01}^3 + K_{11}^{31}] \{\underline{u}\} + \frac{M_{yi}}{\ell} [K_{11}^3] \{\underline{v}\} + v_x [K_{01}^3 + K_{11}^{31}] \{\underline{v}\} \\ + c_4 [K_{11}^3] \{\underline{v}_t^p\} + c_5 [K_{11}^3] \{\underline{v}_b^p\} = \{\underline{R}_\phi\} \end{aligned} \quad (C-1d)$$

$$\begin{aligned}
& \left\{ \frac{D_t b_f}{3\ell^3} [K_{t1}] + \frac{2}{15} \frac{D_t (1-\nu)}{b_f \ell} [K_{t2}] + \left(\frac{P}{A} + \frac{M_x d_w}{2I_x} \right) \frac{t_f b_f}{90\ell} [G_t] \right. \\
& + \frac{D_b b_f}{3\ell^3} [K_{b1}] + \frac{2}{15} \frac{D_b (1-\nu)}{b_f \ell} [K_{b2}] + \left(\frac{P}{A} - \frac{M_x d_w}{2I_x} \right) \frac{t_f b_f}{90\ell} [G_b] \\
& + \frac{D_w \ell}{210 b_f^2 d_w} [A] + \frac{D_w d_w^3}{32 \times 105 \ell^3 b_f^2} [B] + \frac{D_w (1-\nu) d_w}{900 \ell b_f^2} [C] \\
& \left. + \frac{2 D_w \nu d_w}{225 \ell b_f^2} [D] + \frac{(\sigma_b + \sigma_t)}{64 \times 3150} \frac{t_w d_w^3}{b_f^2 \ell} [F] + \frac{(\sigma_b - \sigma_t)}{64 \times 3150} \frac{t_w d_w^3}{b_f^2 \ell} [H] \right\} \\
& \left\{ \frac{v_t^p}{v_b^p} \right\} + c_1 [M] \{ \underline{v} \} + c_2 [M] \{ \underline{u} \} + c_4 [M] \{ \underline{\phi} \} \\
& + c_1 [N] \{ \underline{v} \} + c_3 [N] \{ \underline{u} \} + c_5 [N] \{ \underline{\phi} \} = \{ \underline{R}_\ell \} \quad (C-1e)
\end{aligned}$$

where

$$[M] = \begin{bmatrix} [K_{11}^3] \\ [0] \end{bmatrix} \quad (C-2a)$$

$$[N] = \begin{bmatrix} [0] \\ [K_{11}^3] \end{bmatrix} \quad (C-2b)$$

$$c_1 = \frac{M_y}{b_f \ell} \quad (C-3a)$$

$$c_2 = \left(\frac{P}{6} \frac{d_w}{b_f} - \frac{A_w}{A} + \frac{M_x}{2b_f} \frac{I_{xw}}{I_x} \right) / \ell \quad (C-3b)$$

$$C_3 = \left(-\frac{P}{6} \frac{d_w}{b_f} \frac{A_w}{A} + \frac{M_x}{2b_f} \frac{I_{x_w}}{I_x} \right) / \ell \quad (C-3c)$$

$$C_4 = \left(\frac{P}{A} \frac{I_y}{b_f} - \frac{P}{2} \frac{I_{x_w}}{Ab_f} - \frac{M_x}{4} \frac{d_w}{b_f} \frac{I_{x_w}}{I_x} \right) / \ell \quad (C-3d)$$

$$C_5 = \left(\frac{P}{A} \frac{I_y}{b_f} - \frac{P}{2} \frac{I_{x_w}}{Ab_f} + \frac{M_x}{4} \frac{d_w}{b_f} \frac{I_{x_w}}{I_x} \right) / \ell \quad (C-3e)$$

$$\sigma_b + \sigma_t = \frac{2P}{A} ; \quad \sigma_b - \sigma_t = \frac{M_x d_w}{I_x} \quad (C-3f)$$

The matrices $[K_{11}^3]$, $[K_{22}^3]$, $[K_{10}^3]$, $[K_{11}^{31}]$ are the same as $[K_{11}^{330}]$, $[K_{22}^{330}]$, $[K_{10}^{330}]$, $[K_{11}^{331}]$ derived in Appendix A in Table A-2. The matrices $[K_{t1}]$, $[K_{t2}]$, $[K_{b1}]$, $[K_{b2}]$, $[G_t]$, $[G_b]$, $[A]$, $[B]$, $[C]$, $[D]$, $[F]$, $[H]$ are shown in Tables C-1, C-2, C-3, and C-4. The notation A_w designates the area of the web and I_{x_w} is the moment of inertia of the web.

TABLE C-1

$$[K_{t1}] = \begin{bmatrix} J & 0 \\ 0 & 0 \end{bmatrix} ; \quad [K_{t2}] = \begin{bmatrix} L & 0 \\ 0 & 0 \end{bmatrix} ;$$

$$[K_{b1}] = \begin{bmatrix} 0 & 0 \\ 0 & J \end{bmatrix} ; \quad [K_{b2}] = \begin{bmatrix} 0 & 0 \\ 0 & L \end{bmatrix} ;$$

$$[G_t] = \begin{bmatrix} Q & 0 \\ 0 & 0 \end{bmatrix} ; \quad [G_b] = \begin{bmatrix} 0 & 0 \\ 0 & Q \end{bmatrix} ;$$

$$[J] = \begin{bmatrix} 12 & 6 & -12 & 6 \\ 6 & 4 & -6 & 2 \\ -12 & -6 & 12 & -6 \\ 6 & 2 & -6 & 4 \end{bmatrix}$$

$$[L] = \begin{bmatrix} 72 & 6 & -72 & 6 \\ 6 & 8 & -6 & -2 \\ -72 & -6 & 72 & -6 \\ 6 & -2 & -6 & 8 \end{bmatrix}$$

$$[Q] = \begin{bmatrix} 36 & 3 & -36 & 3 \\ 3 & 4 & -3 & -1 \\ -36 & -3 & 36 & -3 \\ 3 & -1 & -3 & 4 \end{bmatrix}$$

TABLE C-2

$$[A] = \begin{bmatrix} 1248 & 176 & 432 & -104 & 624 & 88 & 216 & -52 \\ & 32 & 104 & -24 & 88 & 16 & 52 & -12 \\ & & 1248 & -176 & 216 & 52 & 624 & -88 \\ & & & 32 & -52 & -12 & -88 & 16 \\ & & & & 1248 & 176 & 432 & -104 \\ & \text{SYM.} & & & & 32 & 104 & -24 \\ & & & & & & 1248 & -176 \\ & & & & & & & 32 \end{bmatrix}$$

$$[B] = \begin{bmatrix} 1536 & 768 & -1536 & 768 & -1152 & -576 & 1152 & -576 \\ & 512 & -768 & 256 & -576 & -384 & 576 & -192 \\ & & 1536 & -768 & 1152 & 576 & -1152 & 576 \\ & & & 512 & -576 & -192 & 576 & -384 \\ & & & & 1536 & 768 & -1536 & 768 \\ & \text{SYM.} & & & & 512 & -768 & 256 \\ & & & & & & 1536 & -768 \\ & & & & & & & 512 \end{bmatrix}$$

TABLE C-3

$$[c] = \begin{bmatrix} 1152 & 96 & -1152 & 96 & -288 & -24 & 288 & -24 \\ & 128 & -96 & -32 & -24 & -32 & 24 & 8 \\ & & 1152 & -96 & 288 & 24 & -288 & 24 \\ & & & 128 & -24 & 8 & 24 & -32 \\ & \text{SYM.} & & & 1152 & 96 & -1152 & 96 \\ & & & & & 128 & -96 & -32 \\ & & & & & & 1152 & -96 \\ & & & & & & & 128 \end{bmatrix}$$

$$[D] = \begin{bmatrix} 144 & 72 & -144 & 72 & -36 & -18 & 36 & -3 \\ & 16 & -12 & -4 & -18 & -4 & 3 & 1 \\ & & 144 & -72 & 36 & 3 & -36 & 18 \\ & & & 16 & -3 & 1 & 18 & -4 \\ & & & & 144 & 72 & -144 & 12 \\ & \text{SYM.} & & & & 16 & -12 & -4 \\ & & & & & & 144 & -72 \\ & & & & & & & 16 \end{bmatrix}$$

TABLE C-4

$$[F] = \begin{bmatrix} 4608 & 384 & -4608 & 384 & -3456 & -288 & 3456 & -288 \\ & 512 & -384 & -128 & -288 & -384 & 288 & 96 \\ & & 4608 & -384 & 3456 & 288 & -3456 & 288 \\ & & & 512 & -288 & 96 & 288 & -384 \\ & & & & 4608 & 384 & -4608 & 384 \\ & \text{SYM.} & & & & 512 & -384 & -128 \\ & & & & & & 4608 & -384 \\ & & & & & & & 512 \end{bmatrix}$$

$$[H] = \begin{bmatrix} \begin{bmatrix} 1152 & 96 & -1152 & 96 \\ & 128 & -96 & -32 \\ & \text{SYM.} & 1152 & -96 \\ & & & 128 \end{bmatrix} & [0] \\ [0] & \begin{bmatrix} -1152 & -96 & 1152 & -96 \\ & -128 & 96 & 32 \\ & & -1152 & 96 \\ & & & -128 \end{bmatrix} \end{bmatrix}$$

APPENDIX D

CALCULATION OF SECTION PROPERTIES AND STRESS RESULTANTS

FOR THIN-WALLED SECTIONS

APPENDIX DCALCULATION OF SECTION PROPERTIES AND STRESS RESULTANTS
FOR THIN-WALLED SECTIONSD-1 Introduction

In the evaluation of the stiffness matrices for elastic sections, carried out in Appendix A, Section A-6, it is necessary to know the section properties. In the evaluation of the stiffness matrices for inelastic analysis, carried out in Appendix E, it is necessary to know the section properties of the transformed section. Once the transformed section has been determined, the evaluation of section properties is identical to that of any arbitrary elastic section. These section properties are always referred to the centroid, shear center and principal axes of the effective elastic (transformed) section.

In this appendix the method of determining the transformed section is discussed in Section D-2, and the equations for numerically evaluating section properties are specified in Section D-3. Equations for numerically evaluating stress resultants, which are required in the calculation of $[K_G]$ and in the evaluation of the unbalanced force vector for inelastic analysis, are given in Section D-4.

D-2 Determination of Transformed Section

The strain at any point of a thin-walled section is due to axial, bending and warping displacements, together with any residual strain, and for any set of nodal displacements may be evaluated from Equation A-36. If the residual strain distribution varies in some arbitrary manner, as shown in Fig. D.1b, then it can be approximated

by linear segments as shown in Fig. D.1c. For equilibrium

$$\int_A \sigma_R dA = 0 \quad (D-1a)$$

$$\int_A \sigma_R y dA = 0 \quad (D-1b)$$

$$\int_A \sigma_R x dA = 0 \quad (D-1c)$$

Considering any plate segment which has a linear variation of residual strain, by superposition, the total strain distribution will also be linear in the segment. The stress strain curve used is shown in Fig. D.1a. It is tri-linear, where the slopes of the three segments are designated as E = elastic modulus; E_p = plastic modulus; and E_s = strain hardening modulus. To approximate the idealized stress strain curve for mild steel, E_p may be set equal to zero.

Considering a segment under a linear variation of strain, as shown in Fig. D.2, when ϵ_A and ϵ_B have the same sign, ϵ_A and ϵ_B may be in any of the three strain ranges.

$$\epsilon_B > \epsilon_{st} \quad \epsilon_A > \epsilon_{st} \quad (D-2a)$$

$$\epsilon_y \leq \epsilon_B \leq \epsilon_{st} \quad \epsilon_y \leq \epsilon_A \leq \epsilon_{st} \quad (D-2b)$$

$$0 \leq \epsilon_B \leq \epsilon_y \quad 0 \leq \epsilon_A \leq \epsilon_y \quad (D-2c)$$

Hence there are nine combinations of strain distribution when ϵ_A and ϵ_B are of the same sign in a segment, and there will be nine other combinations of the strain distribution when ϵ_A and ϵ_B are of opposite signs. In each segment the incremental moduli are determined from the strain distribution, assuming no strain reversal. This divides the

plate segment into, at the most, five regions as shown in Fig. D.2. It is now possible to transform the section and evaluate section properties of the transformed area.

D-3 Evaluation of Section Properties

To determine the section properties, consider the segment of a plate of a thin-walled section under linear strain distribution as shown in Fig. D.2. As stated above, for any arbitrary segment, there are at most five possible regions in which moduli are different. The moment of inertia of the thin-wall about its y-axis is very small and hence in order to formulate tangent properties it is sufficiently accurate to modify the thickness between the corresponding regions by the modular ratio. Areas and moments of inertia of each region of the plate segment are calculated about the centroidal axis of the transformed segment. Moments of inertia of each plate segment are then transformed to the global axis orientation. A similar computation may now be performed to determine the centroid and moments of inertia of the total cross section by summing the properties for all the segments. Let \bar{C} be the centroid of the transformed area and 0 an arbitrary origin of coordinates X and Y. Referring to Fig. D.3b, we may write for the centroid

$$\hat{\bar{X}}_{\bar{C}} = \left(\sum_{k=1}^n A_k \hat{X}_k \right) / \left(\sum_{k=1}^n A_k \right) \quad (D-3a)$$

$$\hat{\bar{Y}}_{\bar{C}} = \left(\sum_{k=1}^n A_k \hat{Y}_k \right) / \left(\sum_{k=1}^n A_k \right) \quad (D-3b)$$

where A_k , \hat{X}_k , and \hat{Y}_k are the transformed area and distances to the

transformed centroid of the k^{th} plate segment, and there are n plate segments. The section properties with respect to the \hat{x} , \hat{y} axes of Fig. D.3b are

$$I_{\hat{x}} = \sum_{k=1}^n I_{xxk} + \sum_{k=1}^n A_k \hat{y}_k^2 \quad (\text{D-4a})$$

$$I_{\hat{y}} = \sum_{k=1}^n I_{yyk} + \sum_{k=1}^n A_k \hat{x}_k^2 \quad (\text{D-4b})$$

$$I_{\hat{x}\hat{y}} = \sum_{k=1}^n I_{xyk} + \sum_{k=1}^n A_k \hat{x}_k \hat{y}_k \quad (\text{D-4c})$$

$$\tan 2 \alpha = 2 I_{\hat{x}\hat{y}} / (I_{\hat{y}} - I_{\hat{x}}) \quad (\text{D-4d})$$

$$I_{\xi} = I_{\hat{x}} \cos^2 \alpha + I_{\hat{y}} \sin^2 \alpha - I_{\hat{x}\hat{y}} \sin 2 \alpha \quad (\text{D-4e})$$

$$I_{\eta} = I_{\hat{y}} \cos^2 \alpha + I_{\hat{x}} \sin^2 \alpha + I_{\hat{x}\hat{y}} \sin 2 \alpha \quad (\text{D-4f})$$

where α is the inclination of the principal axes, (ξ and η), with reference to the original axes and is positive if it is anticlockwise from the \hat{x} axis.

In order to locate the shear center, choose \bar{C} as the origin and \bar{CE} as the initial radius. For straight segments, sectorial area coordinates at the beginning and the end points of each region of the plate may be computed, from the definition of the sectorial coordinate in Equation A-13, as twice the sectorial area with respect to the initial radius, \bar{CE} . This is evaluated, see Fig. D.3b, as

$$\omega_j = \omega_i + \hat{x}_j \hat{y}_i - \hat{y}_j \hat{x}_i \quad (\text{D-5})$$

The sectorial static moment and the sectorial linear static moment about the \hat{x} and \hat{y} axes, with \bar{C} as the origin and \bar{CE} as the initial radius, are defined (see Equations A-29, A-30 and A-31) as

$$S_{\omega\bar{C}} = \int_E^F \omega \, dA \quad (D-6a)$$

$$S_{\omega\hat{x}\bar{C}} = \int_E^F \omega \, \hat{y} \, dA \quad (D-6b)$$

$$S_{\omega\hat{y}\bar{C}} = \int_E^F \omega \, \hat{x} \, dA \quad (D-6c)$$

The coordinates of the shear center, \bar{S} , of the transformed section may then be determined by the following equations, which are Equations A-30 for non-principal axes directions,

$$\bar{x}_S = (S_{\omega\hat{x}\bar{C}} I_{\hat{y}} - S_{\omega\hat{y}\bar{C}} I_{\hat{x}\hat{y}}) / (I_{\hat{x}} I_{\hat{y}} - I_{\hat{x}\hat{y}}^2) \quad (D-7a)$$

$$\bar{y}_S = -(S_{\omega\hat{y}\bar{C}} I_{\hat{x}} - S_{\omega\hat{x}\bar{C}} I_{\hat{x}\hat{y}}) / (I_{\hat{x}} I_{\hat{y}} - I_{\hat{x}\hat{y}}^2) \quad (D-7b)$$

Sectorial area coordinates, ω , are now calculated with respect to the shear center \bar{S} and with \bar{SE} as the initial radius, by a similar computation to that in Equation D-5.

A principal radius, $\bar{S} B'$, is defined as one for which the sectorial coordinates satisfy the following equation (see Equation A-31)

$$S_{\omega} = \int_A \bar{\omega} \, \bar{S} B' \, dA = 0 \quad (D-8a)$$

where

$$\bar{\omega}_{\bar{S}B'} = - \int_{B'}^A r \, ds \quad (D-8b)$$

becomes the principal sectorial coordinate of point A. Choosing $\bar{\omega}_{\bar{S}B'}$ as the principal sectorial coordinate with \bar{S} as the origin and $\bar{S}B'$ as the principal radius the principal sectorial static moment, S_{ω} , will therefore be zero. The quantity $\bar{\omega}_{\bar{S}B'}$ is usually called the normalized unit warping or the normalized warping coordinate, and designated as $\bar{\omega}_n$.

Now

$$\bar{\omega}_n = \bar{\omega}_{\bar{S}B'} = - \int_{B'}^A r \, ds \quad (D-9a)$$

$$= - \int_E^A r \, ds + C \quad (D-9b)$$

$$= - \omega + C \quad (D-9c)$$

Hence the normalized warping coordinate may be computed by subtracting the constant C from the ω values and changing sign.

Equation D-8a requires C to be

$$C = \frac{1}{A} \int_E^F \omega \, dA \quad (D-10)$$

The principal sectorial moment or simply sectorial moment of Inertia

$I_{\omega n}$ is now given by

$$I_{\omega n} = \int_E^F \bar{\omega}_n^2 \, dA \quad (D-11a)$$

which for the type of section shown in Fig. D.3b can be expressed as

$$I_{\omega n} = \sum_{k=1}^n \sum_{r=1}^5 b_r t_r (\bar{\omega}_i^2 + \bar{\omega}_i \bar{\omega}_j + \bar{\omega}_j^2) / 3 \quad (D-11b)$$

where $\bar{\omega}_i$ represents the normalized warping coordinate at junction i ; r indicates the region of the segment; and n is the number of segments.

If it is assumed that G is proportional to E , St. Venant's constant may be calculated by modifying the width. It is therefore

$$K_T = \frac{1}{3} \sum_{k=1}^n \sum_{r=1}^5 b_r^* t_k^3 \quad (D-12a)$$

where

$$b_r^* = E_t b_r / E \quad (D-12b)$$

Other properties which are necessary for the elastic analysis of the thin-walled structures, are those appearing in Equation 2-24 and are derived for elastic sections in Appendix A, Section A-2.

In these equations

$$I_P = I_{\hat{x}} + I_{\hat{y}} + A(\hat{x}_{\bar{S}}^2 + \hat{y}_{\bar{S}}^2) \quad (D-13)$$

where $\hat{x}_{\bar{S}}$ and $\hat{y}_{\bar{S}}$ are the coordinates of the shear centre with reference to centroidal axes, Fig. D.3; and,

$$C_{\hat{x}} = (H_{\hat{x}} I_{\hat{y}} - H_{\hat{y}} I_{\hat{x}\hat{y}}) / (I_{\hat{x}} I_{\hat{y}} - I_{\hat{x}\hat{y}}^2) - 2 \hat{y}_{\bar{S}} \quad (D-14a)$$

$$C_{\hat{y}} = (H_{\hat{y}} I_{\hat{x}} - H_{\hat{x}} I_{\hat{x}\hat{y}}) / (I_{\hat{x}} I_{\hat{y}} - I_{\hat{x}\hat{y}}^2) - 2 \hat{x}_{\bar{S}} \quad (D-14b)$$

$$C_{\omega} = H_{\omega} / I_{\omega n} \quad (D-14c)$$

By referring to Fig. D.4 the constant $H_{\hat{x}}$, $H_{\hat{y}}$ and H_{ω} may be

evaluated as

$$H_{\hat{y}} = \int_A \hat{x} (\hat{x}^2 + \hat{y}^2) dA = \sum_{k=1}^n \left[\frac{\hat{x}_j^{Lt}}{12} (2 \hat{\rho}_i^2 - L^2 + 4 \hat{\rho}_j^2) + \frac{\hat{x}_i^{Lt}}{12} (4 \hat{\rho}_i^2 - L^2 + 2 \hat{\rho}_j^2) \right] \quad (D-15a)$$

$$H_{\hat{x}} = \int_A \hat{y} (\hat{x}^2 + \hat{y}^2) dA = \sum_{k=1}^n \left[\frac{\hat{y}_j^{Lt}}{12} (2 \hat{\rho}_i^2 - L^2 + 4 \hat{\rho}_j^2) + \frac{\hat{y}_i^{Lt}}{12} (4 \hat{\rho}_i^2 - L^2 + 2 \hat{\rho}_j^2) \right] \quad (D-15b)$$

$$H_{\omega} = \int_A \bar{\omega}_n (\hat{x}^2 + \hat{y}^2) dA = \sum_{k=1}^n \left[\frac{\bar{\omega}_j^{Lt}}{12} (2 \hat{\rho}_i^2 - L^2 + 4 \hat{\rho}_j^2) + \frac{\bar{\omega}_i^{Lt}}{12} (4 \hat{\rho}_i^2 - L^2 + 2 \hat{\rho}_j^2) \right] \quad (D-15c)$$

For elastic sections the coordinates \hat{x} , \hat{y} are identical to x and y and \bar{C} , \bar{S} are the same as C and S (Fig. D.3a). The reference axes x and y through C of elastic section, the shear center S of the elastic section, the principal axes ξ and η through \bar{C} of transformed section, and the shear center \bar{S} of the transformed section, are shown in Fig. D.3c.

D-4 Evaluation of Stress Resultants

Assuming the strain is known, the stresses are calculated in each region of the plate segments. The stress resultants may then be evaluated numerically, in the C , S and x - y reference system, from their definition, as follows (see Fig. D.5)

$$P \equiv \int_A \sigma_z dA = \sum_{k=1}^n \sum_{r=1}^5 \frac{1}{2} b_r t_k (\sigma_{ir} + \sigma_{jr}) \quad (D-16a)$$

$$M_x \equiv \int_A \sigma_z y dA = \sum_{k=1}^n \sum_{r=1}^5 \frac{b_r t_k}{6} [\sigma_{ir} (y_{jr} + 2y_{ir}) + \sigma_{jr} (y_{ir} + 2y_{jr})] \quad (D-16b)$$

$$M_y \equiv \int_A \sigma_z x dA = \sum_{k=1}^n \sum_{r=1}^5 \frac{b_r t_k}{6} [\sigma_{ir} (x_{jr} + 2x_{ir}) + \sigma_{jr} (x_{ir} + 2x_{jr})] \quad (D-16c)$$

$$W_\omega \equiv \int_A \hat{\omega} \sigma_z dA = \sum_{k=1}^n \sum_{r=1}^5 \frac{b_r t_k}{6} [\sigma_{ir} (\hat{\omega}_{jr} + 2\hat{\omega}_{ir}) + \sigma_{jr} (\hat{\omega}_{ir} + 2\hat{\omega}_{jr})] \quad (D-16d)$$

where r = plate region; n = number of plate segments; k = plate segment index; t_k = plate segment thickness; b_r = plate region length; and $\hat{\omega}$ = the normalized warping coordinate with respect to S .

The quantity $M_{\rho\zeta}$ may be evaluated about \bar{S} as

$$M_{\rho\zeta} = \sum_{k=1}^n \sum_{r=1}^5 \frac{b_r t_k}{12} [\sigma_{ir} (4\rho_{ij}^{*2} + 2\rho_{jr}^{*2} - b_r^2) + \sigma_{jr} (4\rho_{jr}^{*2} + 2\rho_{ir}^{*2} - b_r^2)] \quad (D-17)$$

where ρ_{ir}^* and ρ_{jr}^* are the distances of the i^{th} and j^{th} nodal points of the region with respect to \bar{S} .

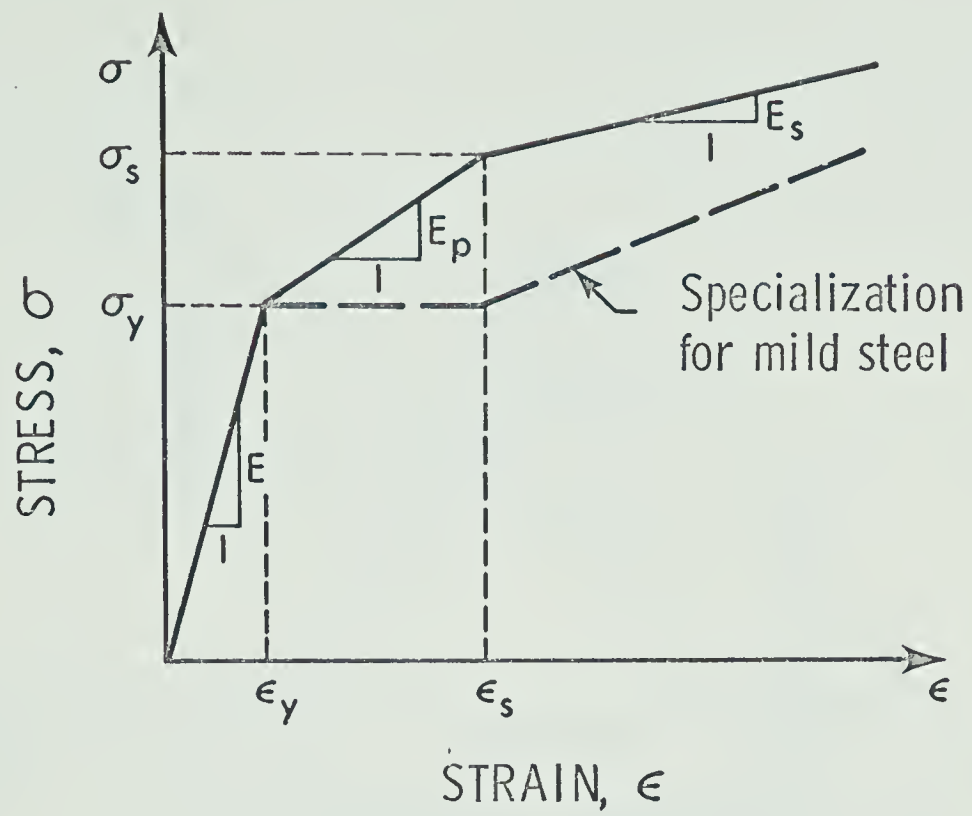


FIGURE D.1a TRI-LINEAR STRESS-STRAIN DIAGRAM

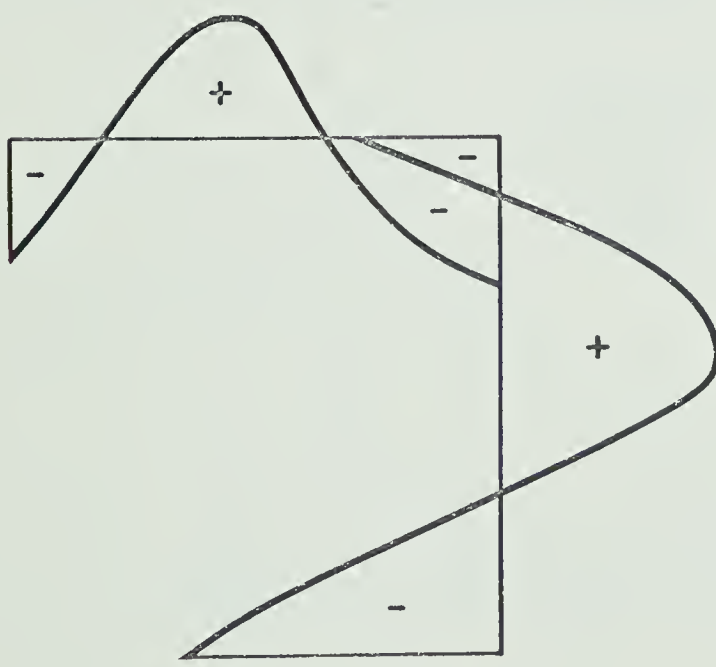


FIGURE 1.b ACTUAL RESIDUAL STRAIN DISTRIBUTION

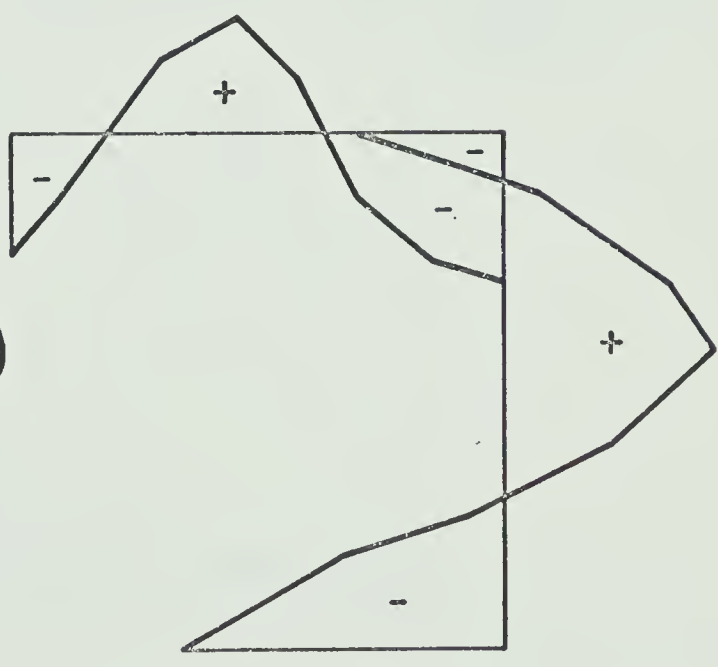


FIGURE D.1c ASSUMED RESIDUAL STRAIN DISTRIBUTION

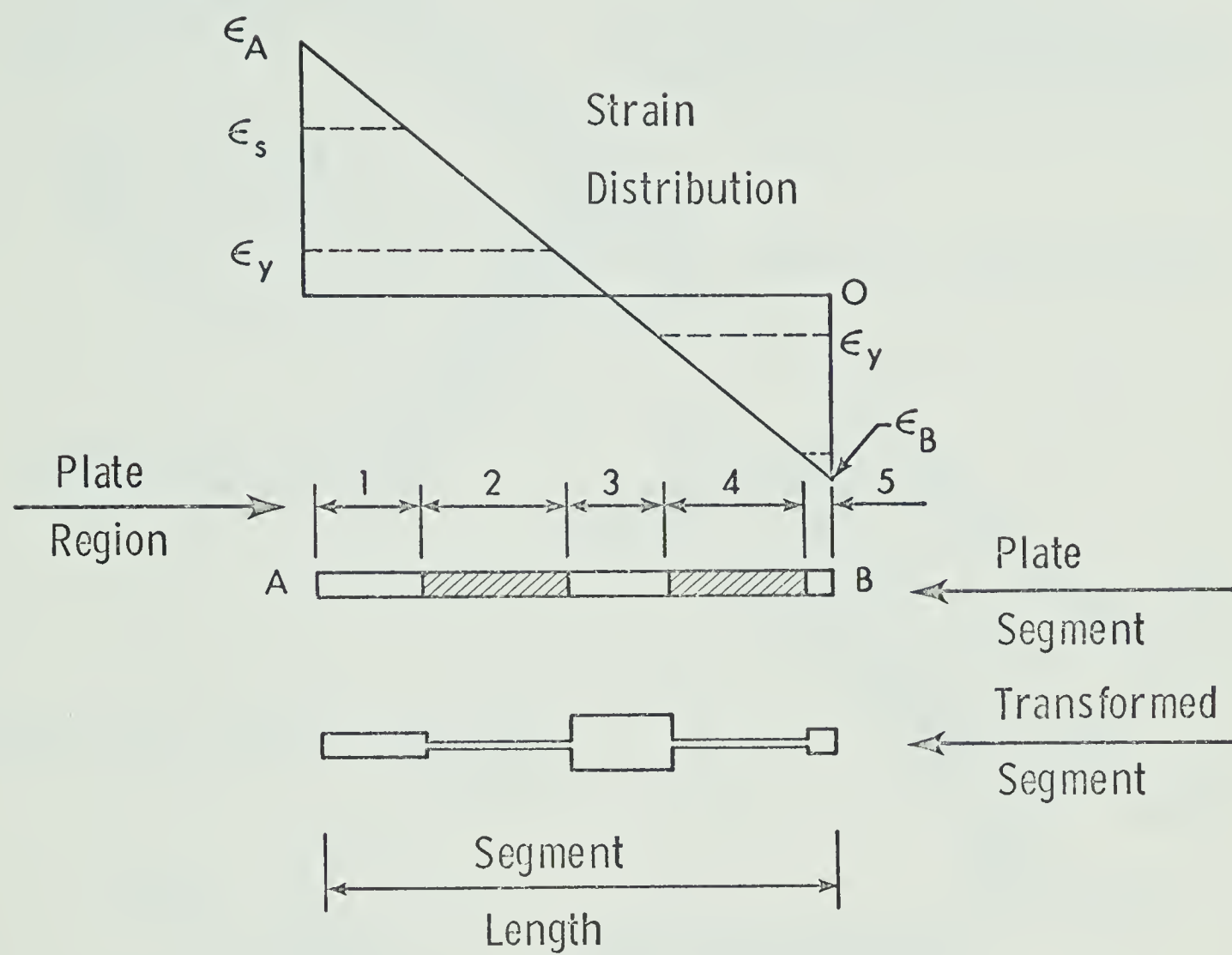


FIGURE D.2 TRANSFORMED SECTION OF A PLATE SEGMENT

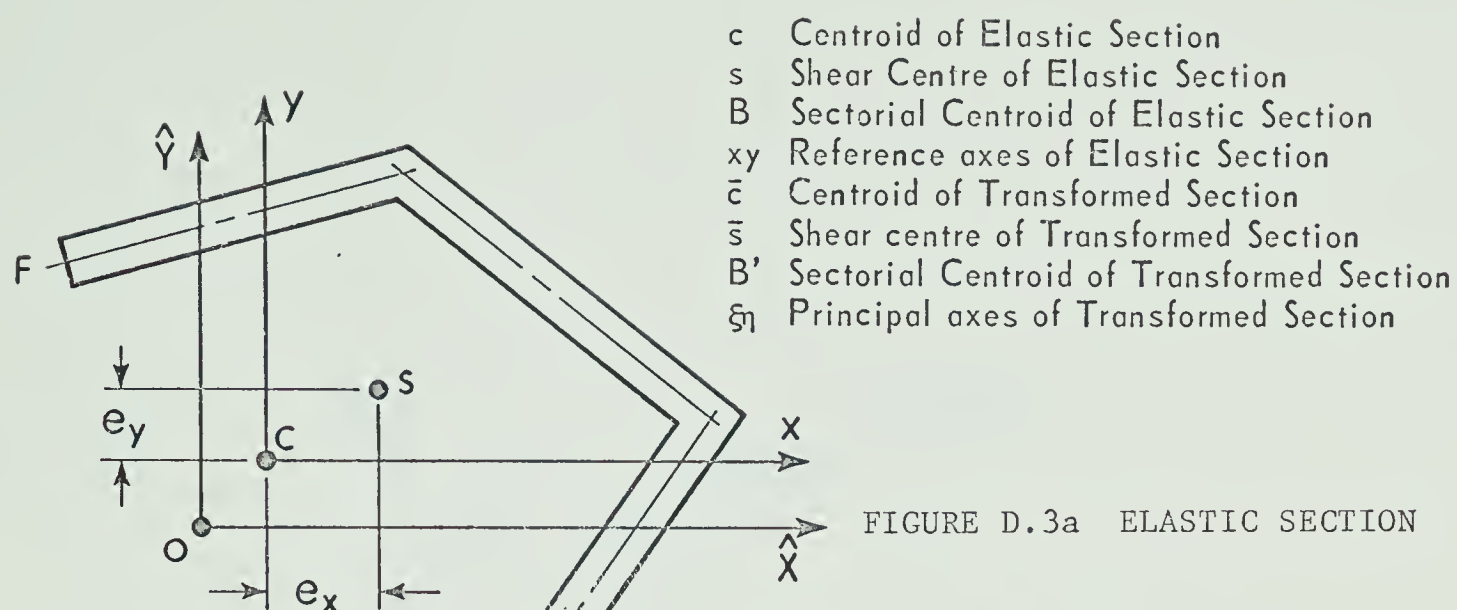
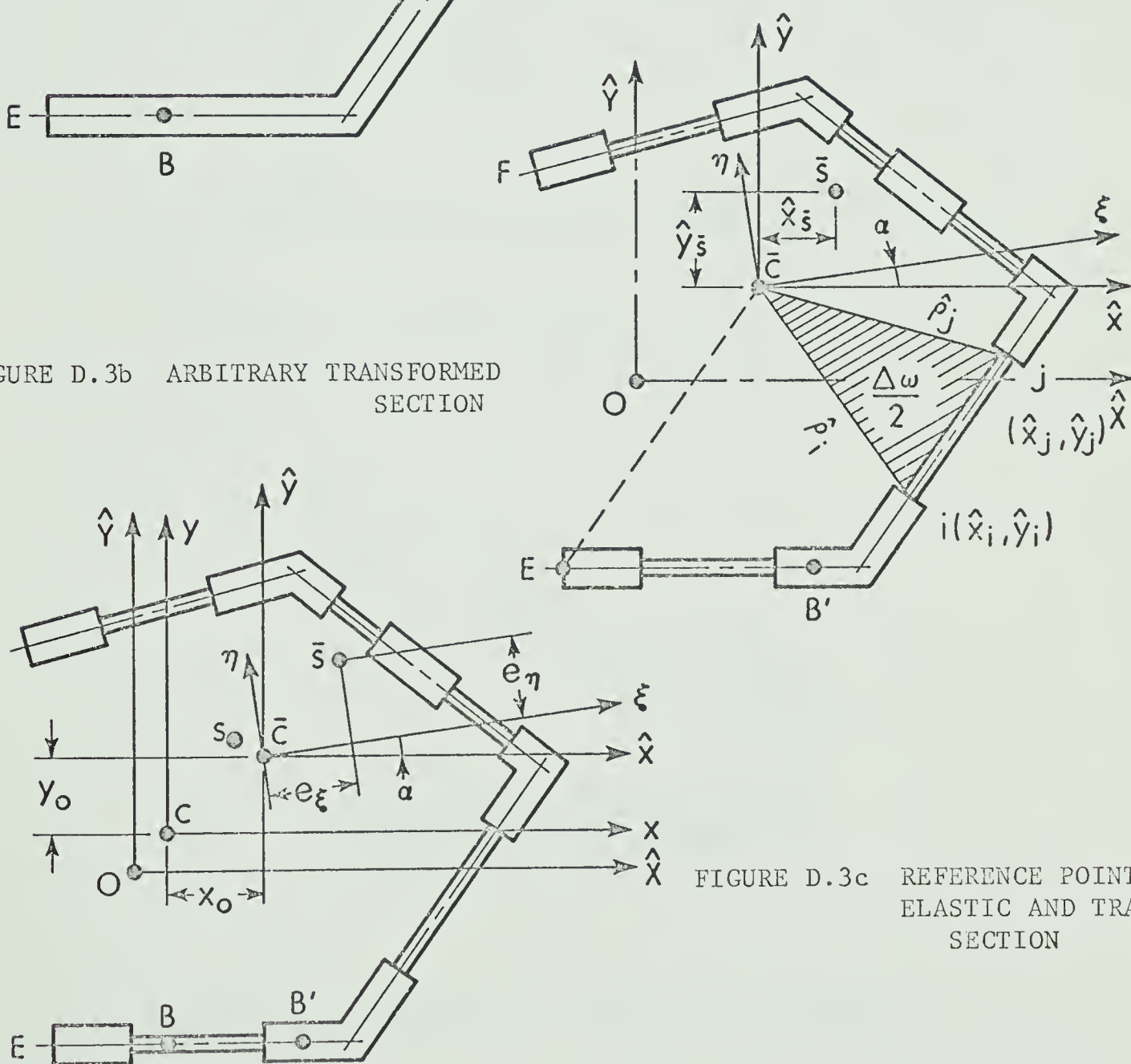


FIGURE D.3b ARBITRARY TRANSFORMED SECTION



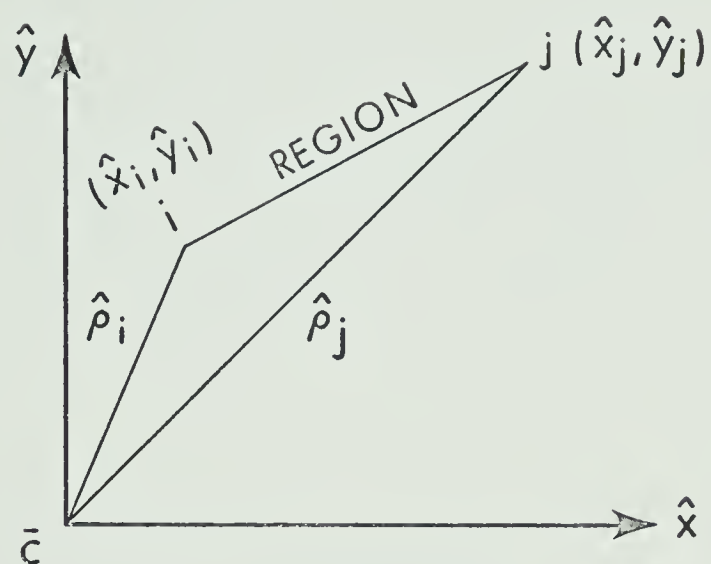


FIGURE D.4 TYPICAL REGION

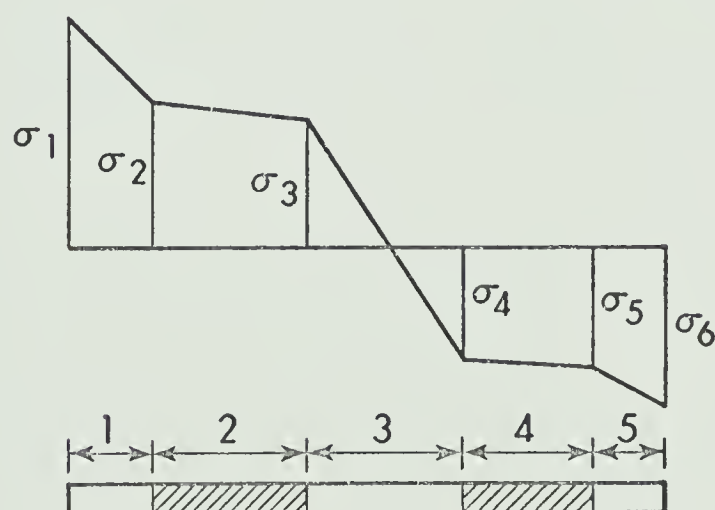


FIGURE D.5 STRESSES IN A TYPICAL PLATE SEGMENT

APPENDIX E

DETAILS OF INELASTIC FORMULATION

APPENDIX E

DETAILS OF INELASTIC FORMULATION

E-1 Introduction

In this appendix the tangent and geometric stiffness matrices are derived, in Section E-2, for 'Formulation 1' of Section 5.2.5, and in Section E-3, for 'Formulation 2' of Section 5.2.6. The section properties and stress resultants for the evaluation of tangent and geometric stiffness matrices have been determined as detailed in Appendix D.

E-2 Derivation of Tangent Stiffness and Geometric Stiffness Matrices For Formulation 1 (Section 5.2.5)

Since variations in incremental displacements are taken with respect to the reference points in the original undeformed configuration the tangent stiffness matrix contains coupled terms. The terms contributing to the tangent stiffness in the virtual work equation Equation 5-5 are given by

$$\begin{aligned}
 & \int_0^{\ell} [(EA^T w'_c \delta w'_c - EA^T y_o v''_s \delta w'_c - EA^T x_o u''_s \delta w'_c + ES^T_{\omega} \phi'' \delta w'_c \\
 & - EA^T y_o w'_c \delta v''_s + EI^T_x v''_s \delta v''_s + EI^T_{xy} u''_s \delta v''_s - ES^T_{\omega x} \phi'' \delta v''_s \\
 & - EA^T x_o w'_c \delta u''_s + EI^T_{xy} v''_s \delta u''_s + EI^T_y u''_s \delta u''_s - ES^T_{\omega y} \phi'' \delta u''_s \\
 & + ES^T_{\omega} w'_c \delta \phi'' - ES^T_{\omega x} v''_s \delta \phi'' - ES^T_{\omega y} u''_s \delta \phi'' + EI^T_{\omega} \phi'' \delta \phi'')] dz \quad (E-1)
 \end{aligned}$$

where

$$A^T = \int dA \quad (E-2a)$$

$$S_{\omega}^T = \int \hat{\omega} \, dA \quad (E-2b)$$

$$S_{\omega x}^T = \int \hat{\omega} \, y \, dA \quad (E-2c)$$

$$S_{\omega y}^T = \int \hat{\omega} \, x \, dA \quad (E-2d)$$

$$I_{\omega}^T = \int \hat{\omega}^2 \, dA \quad (E-2e)$$

$$I_x^T = \int y^2 \, dA \quad (E-2f)$$

$$I_y^T = \int x^2 \, dA \quad (E-2g)$$

$$I_{xy}^T = \int x \, y \, dA \quad (E-2h)$$

and all the integrals are computed over the transformed area. The quantity $\hat{\omega}$ is the normalized warping coordinate of the original elastic section with pole at S.

The same coupled terms in the tangent stiffness may be arrived at by using 'Formulation 2', Equations 5-7 and 5-8, and the transformation equations, Equations 5-17 and 5-22, where u_{ξ} , v_{η} and w_{ζ} are expressed as

$$u_{\xi} = u_s C_{\alpha} + v_x S_{\alpha} + \{(b_x - e_x)S_{\alpha} - (b_y - e_y)C_{\alpha}\}\phi \quad (5-17a)$$

$$v_{\eta} = -u_s S_{\alpha} + v_s C_{\alpha} + \{(b_y - e_y)S_{\alpha} + (b_x - e_x)C_{\alpha}\}\phi \quad (5-17b)$$

$$w_{\zeta} = w_c - y_o v'_s - x_o u'_s + \omega_{BB} \phi' \quad (5-21)$$

Then we can identify the following relationships

$$I_x^T = I_\xi^T C_\alpha^2 + I_\eta^T S_\alpha^2 + A^T y_o^2 \quad (E-3a)$$

$$I_y^T = I_\xi^T S_\alpha^2 + I_\eta^T C_\alpha^2 + A^T x_o^2 \quad (E-3b)$$

$$I_{xy}^T = (I_\eta^T - I_\xi^T) C_\alpha S_\alpha + A^T x_o y_o \quad (E-3c)$$

$$S_{\omega x}^T = (I_\eta^T y^* S_\alpha - I_\xi^T x^* C_\alpha + S_\omega^T y_o) \quad (E-3d)$$

$$S_{\omega y}^T = (I_\xi^T x^* S_\alpha + I_\eta^T y^* C_\alpha + S_\omega^T x_o) \quad (E-3e)$$

$$I_{\omega S}^T = I_{\omega S}^T + I_\xi^T x^{*2} + I_\eta^T y^{*2} + (S_\omega^T)^2 / A^T \quad (E-3f)$$

where

$$x^* = (b_x - e_x)C_\alpha + (b_y - e_y)S_\alpha \quad (E-4a)$$

$$y^* = (b_y - e_y)C_\alpha - (b_x - e_x)S_\alpha \quad (E-4b)$$

and $C_\alpha = \cos \alpha$; $S_\alpha = \sin \alpha$

By either of the above procedures, the incremental tangent stiffness matrix for an element may be written as

$$[k_S^T] = \begin{bmatrix} k_{uu}^T & k_{vv}^T & k_{u\phi}^T & k_{uw}^T \\ k_{vu}^T & k_{vv}^T & k_{v\phi}^T & k_{vw}^T \\ k_{\phi u}^T & k_{\phi v}^T & k_{\phi\phi}^T & k_{\phi w}^T \\ k_{wu}^T & k_{wv}^T & k_{w\phi}^T & k_{ww}^T \end{bmatrix} \quad (E-5)$$

where

$$\frac{\ell^3}{E} [k_{uu}^T] = I_{yp}^T [k_{22}^{330}] + (I_{yq}^T - I_{yp}^T) [k_{22}^{331}] \quad (E-6a)$$

$$\frac{\ell^3}{E} [k_{uv}^T] = I_{xy}^T [k_{22}^{330}] + (I_{xyq}^T - I_{xyp}^T) [k_{22}^{331}] \quad (E-6b)$$

$$\frac{\ell^3}{E} [k_{u\phi}^T] = -\{S_{\omega yp}^T [k_{22}^{330}] + (S_{\omega yq}^T - S_{\omega yp}^T) [k_{22}^{331}]\} \quad (E-6c)$$

$$\frac{\ell^2}{E} [k_{uw}^T] = -\{(A_{X_o}^T)_p [k_{21}^{320}] + ((A_{X_o}^T)_q - (A_{X_o}^T)_p) [k_{21}^{321}]\} \quad (E-6d)$$

$$\frac{\ell^3}{E} [k_{vv}^T] = I_{xp}^T [k_{22}^{330}] + (I_{xq}^T - I_{xp}^T) [k_{22}^{331}] \quad (E-6e)$$

$$\frac{\ell^3}{E} [k_{v\phi}^T] = -\{S_{\omega xp}^T [k_{22}^{330}] + (S_{\omega xq}^T - S_{\omega xp}^T) [k_{22}^{331}]\} \quad (E-6f)$$

$$\frac{\ell^2}{E} [k_{vw}^T] = -\{(A_{Y_o}^T)_p [k_{21}^{320}] + ((A_{Y_o}^T)_q - (A_{Y_o}^T)_p) [k_{21}^{321}]\} \quad (E-6g)$$

$$\frac{\ell^3}{E} [k_{\phi\phi}^T] = I_{\omega p}^T [k_{22}^{330}] + (I_{\omega q}^T - I_{\omega p}^T) [k_{22}^{331}] \quad (E-6h)$$

$$\frac{\ell^2}{E} [k_{\phi w}^T] = S_{\omega p}^T [k_{21}^{320}] + (S_{\omega q}^T - S_{\omega p}^T) [k_{21}^{321}] \quad (E-6i)$$

$$\frac{\ell}{E} [k_{ww}^T] = A_p^T [k_{11}^{220}] + (A_q^T - A_p^T) [k_{11}^{221}] \quad (E-6j)$$

$$[k_{vu}^T] = [k_{uv}^T]^T \quad (E-6k)$$

$$[k_{\phi u}^T] = [k_{u\phi}^T]^T \quad (E-6l)$$

$$[k_{\phi v}^T] = [k_{v\phi}^T]^T \quad (E-6m)$$

$$[k_{wu}^T] = [k_{uw}^T]^T \quad (E-6n)$$

$$[k_{wv}^T] = [k_{vw}^T]^T \quad (E-6o)$$

$$[k_{w\phi}^T] = [k_{\phi w}^T]^T \quad (E-6p)$$

The coefficient matrices in Equations 5-6 have been defined in Appendix A, Section A-6.

The matrix $[k_G]$ is the same as the geometric stiffness matrix of an element for the elastic case, i.e. Equation 2-28, except for the submatrix $[g_{\phi\phi}]$, which may now be expressed as

$$\frac{\ell}{G} [g_{\phi\phi}] = \bar{K}_p [k_{11}^{330}] + (\bar{K}_q - \bar{K}_p) [k_{11}^{331}] \quad (E-7a)$$

where

$$\bar{K}_p = K_p + (M_{\rho s})_p / G \quad (E-7b)$$

Hence the incremental equilibrium equation for an element may be written as

$$[[k_s^T] + [k_G]] \{\Delta r_E\} = \{\Delta R_E\} \quad (E-8)$$

which is Equation 5-9.

After transformation and assembly, Equation E-8 becomes

$$[[K_s^T] + [K_G]] \{\Delta r\} = \{\Delta R\} \quad (E-9a)$$

which is Equation 5-31. Grouping terms from these matrices we may write

$$[[K_1] + [K_2] + [K_3]] \{\Delta r\} + [K_G] \{\Delta r\} = \{\Delta R\} \quad (E-9b)$$

where $[K_1]$, $[K_2]$, and $[K_3]$ contain terms, dependent on the inverse of ℓ , ℓ^2 and ℓ^3 respectively and $[K_G]$ is linearly dependent on the inverse of ℓ .

E-3 Derivation of Tangent and Geometric Stiffness Matrices for 'Formulation 2' (Section 5.2.6)

When the incremental equilibrium equation, Equation 5-4, is expressed with respect to the instantaneous shear centre and sectorial centroid of the transformed area, Equation 5-7 will apply. Because of the form of Equations 5-8, the incremental tangent stiffness for an element may be written as

$$[k_s^T] = \begin{bmatrix} k_{uu}^T & & & \\ & k_{vv}^T & & \\ & & k_{\phi\phi}^T & \\ & & & k_{ww}^T \end{bmatrix} \quad (E-10)$$

where

$$\frac{\ell^3}{E} [k_{uu}^T] = I_{\eta p}^T [k_{22}^{330}] + (I_{\eta q}^T - I_{\eta p}^T) [k_{22}^{331}] \quad (E-11a)$$

$$\frac{\ell^3}{E} [k_{vv}^T] = I_{\xi p}^T [k_{22}^{330}] + (I_{\xi q}^T - I_{\xi p}^T) [k_{22}^{331}] \quad (E-11b)$$

$$\frac{\ell^3}{E} [k_{\phi\phi}^T] = I_{\omega sp}^T [k_{22}^{330}] + (I_{\omega sq}^T - I_{\omega sp}^T) [k_{22}^{331}] \quad (E-11c)$$

$$\frac{\ell}{E} [k_{ww}^T] = A_p^T [k_{11}^{220}] + (A_q^T - A_p^T) [k_{11}^{221}] \quad (E-11d)$$

The matrix $[k_G]$ is the same as in Equation 2-28 provided M_x , M_y are replaced by M_ξ , M_η and e_x , e_y by e_ξ and e_η . However, the submatrix $[g_{\phi\phi}]$ is now given by

$$\frac{\ell}{G} [g_{\phi\phi}] = \bar{K}_p [k_{11}^{330}] + (\bar{K}_q - \bar{K}_p) [k_{11}^{331}] \quad (E-12a)$$

where

$$\bar{K}_p = K_p + (M_{\rho s})_p / G \quad (E-12b)$$

The relationship between $M_{\rho s}$ in Equation E-7b and $M_{\rho s}$ in Equation E-12b is given by

$$\begin{aligned} M_{\rho s} = M_{\rho s} + 2M_y(b_x - e_x) + 2M_x(b_y - e_y) + P\{(b_x - e_x)^2 \\ + (b_y - e_y)^2 - 2(b_x - e_x)(x_o + \hat{x}_s) - 2(b_y - e_y)(y_o + \hat{y}_s)\} \end{aligned} \quad (E-13)$$

where x_o , y_o are the coordinates of the instantaneous centroid with respect to the original centroidal reference axes, and \hat{x}_s , \hat{y}_s are the coordinates of the instantaneous shear centre with respect to the instantaneous centroidal axes parallel to the original reference axes (see Fig. 5.3 and Fig. D.3b).

Hence the incremental equilibrium equation for an element is again written as

$$[[k_S^T] + [k_G]] \{\Delta r_E\}_L = \{\Delta R_E\}_L \quad (E-14a)$$

Using the transformation matrix, derived in Section 5.4.3 for 'Formulation 2', which is shown in Table 5-1, Equation E-14a becomes

$$[[T]^T [k_S^T] [T] + [T]^T [k_G] [T]] \{\Delta r_E\}_G = \{\Delta R_E\}_G \quad (E-14b)$$

After assembly, Equation E-14b becomes Equation 5-31, namely

$$[[K_S^T] + [K_G]] \{\Delta r\} = \{\Delta R\} \quad (E-15)$$

which is the incremental equilibrium equation for beam-column problems.

B30007